Bewerbung für den Promotionspreis der Medizinischen Fakultät der Universität Hamburg

Dr. med. Dr. Phil. Dong Wang

Irma-Keilhack-Ring 7
D-22145 Hamburg

email: dongw1990@gmail.com

Anhang:

- **Anschreiben**
- **Tabellarischer Lebenslauf**
- **Kopie der Promotionsurkunde**
- **Dissertationsschrift**

Universitäres Herzzentrum Hamburg
Ein Unternehmen des UKE

Klinik für Herz- und Gefäßchirurgie

Direktor:
Prof. Dr. Hermann Reichenspurner Ph. D.

Martinistraße 52
20246 Hamburg
Telefon: (040) 42803-2440
Telefax: (040) 42803-4931
Prof.Dr. Sonja Schrepfer
TSI-Lab

Dr. med. Dr. Phil. Dong Wang
Irma-Keilhack-Ring 7
22145 Hamburg, Germany

Hamburg, den 25.Juni 2021

Betreff: Bewerbung für den Volker Bay-Promotionspreis für Chirurgie

Sehr geehrter Herr Prof. Carstensen,

Mit diesem Schreiben möchte ich mich gerne für den „Volker Bay-Promotionspreis für Chirurgie“, ausgeschrieben durch den Freundes- und Förderkreis des Universitätsklinikums Hamburg-Eppendorf e.V., bewerben. Ich habe mich innerhalb meiner Promotionsarbeit an der Medizinischen Fakultät der Universität Hamburg mit moderner Grundlagenforschung der Chirurgie befasst.

Im Rahmen meiner Promotionsarbeit, die ich im MD/PhD Programm des Universitätsklinikum Hamburg Eppendorf durchgeführt und im Dezember 2020 mit „magna cum laude“ abgeschlossen habe, sind 5 Publikationen als Co-Autor und 1 Publikationen als Erstautor entstanden. Die Arbeiten wurden in den internationalen Journals „Nature Biotechnology“, „J Vis Exp“, und „Transplant International“ publiziert.

Die Arbeit ist unter der Leitung von Frau Prof. Dr. Sonja Schrepfer im „Transplantations- und Stammzellimmunbiologie“-Labor am UKE entstanden.

Ich habe Ihnen meinen Lebenslauf und Kopie der Promotionsurkunde, sowie die Dissertationsarbeit beigefügt.

Ich würde mich sehr freuen, wenn die Arbeit Ihren Kriterien entspricht und stehe Ihnen gerne für Rückfragen zur Verfügung.

Mit freundlichen Grüßen,

Dong Wang

Curriculum Vitae

Persönliche Daten:

Name:	Dong Wang
Telefon:	+49/17666338553
e-mail-Adresse:	dongw1990@gmail.com
Nationalität	Deutsch
Geburtsdatum:	26.08.1990

Ausbildung:

2020 - heute	Assistenzarzt an der Klinik für Kardiologie und Angiologie der Medizinischen Hochschule Hannover
2016 - 2020	PhD- Doktorarbeit im Rahmen des MD/PhD Programms an der Universität Hamburg im „Transplant and Stem Cell Immunobiology Lab“ AG Schrepfer *Magna cum laude*
2019	ECFMG Zertifikation (USMLE)
2009 – 2015	Medizinstudium an der Universität Hamburg *Note: 1,83*
2012 – 2015	Doktorarbeit im „Transplant and Stem Cell Immunobiology Lab“ AG Schrepfer *Summa cum laude*
2012 – 2013	Graduiertenkolleg „Individualized Cardiovascular Medicine“, des Cardiovascular Research Centers Hamburg am Universitätsklinikum Hamburg Eppendorf
2007 – 2009	Gymnasium Blankenese, Hamburg
2006 – 2007	Royalton High School, Royalton, MN, USA
2000 – 2006	Charlotte-Paulsen Gymnasium, Hamburg
1996 – 2000	Grundschule Schimmelmannstrasse, Hamburg

Wissenschaftlicher Werdegang:

2016-2020	Postdoktorand im „Transplant and Stem Cell Immunobiology Lab“ UCSF, San Francisco, USA
2017	Zusatzqualifikation „Grundlagen der Molekularen und Experimentellen Medizin“ der Medizinischen Fakultät Universität Hamburg
2015	Forschungsbesuch im „Marber Lab“ King’s College, London, England
2013 + 2014	Forschungsprojekt im Stanford University School of Medicine, Stanford, USA
2013 – 2015	Wissenschaftlicher Mitarbeiter im „Transplant und Stammzell

Immunbiologie Labor“, Universität Hamburg, Deutschland

Präsentationen:

2019 Posterpräsentation beim UCSF Cardiovascular Research Institute Retreat

2019 Präsentation beim NIH Tissue Chips Meeting („Chips in Space“)

2017 Präsentation beim Northern California Chapter, American College of Surgeons Meeting 2017
Thomas R. Russell Surgical Trainee Research Award Finalist

2017 Posterpräsentation bei International Society for Heart and Lung Transplantation (ISHLT) Meeting 2017

2015 Präsentation bei International Society for Heart and Lung Transplantation (ISHLT) Meeting 2015
Philip K. Caves Award Finalist

2014 Präsentation beim American Heart Association (AHA) Scientific Meeting 2014
Vivien Thomas Award Finalist

2013 Präsentation der Promotionsarbeit beim CVRC (Cardiovascular Research Center Hamburg) Seminar Oktober 2013

2013 Präsentation beim 1st UKE (University Medical Center Hamburg Eppendorf) Light Microscopy Symposium 2013

2013 Posterpräsentation beim “Cardiac Regeneration and Vascular Biology Conference 2013”
Posterpreis Kategorie: Clinical Trials and Translational Medicine

Preise und Stipendien:

2017 **Reisestipendium** des Universitätsklinikums Hamburg-Eppendorf

2017 **Forschungsstipendium** der Max-Kade-Stiftung (DFG) für einen Forschungsaufenthalt in den USA

2017 **Nachwuchsförderpreis** der Deutschen Gesellschaft für Thorax, Herz- und Gefäßchirurgie (DGTHG)

2017 **Promotionspreis** des Cardiovascular Research Center Hamburg

2015 Finalist in der **Philip K. Caves Award Session** der International Society for Heart and Lung Transplantation (ISHLT)

2015 **Scientific Meeting Travel Grant** des ISHLT für die Präsentation beim “ISHLT Scientific Meeting 2015”

2014 Finalist in der **Vivien Thomas Award Session** der American Heart Association (AHA) 2014

2014 **Abstract Travel Award** des AHA für die Präsentation bei “AHA Scientific

Sessions 2014"

2014 I**SHLT** (International Society for Heart and Lung Transplantation) **International Traveling Scholarship Award** 2014

2014 **Doktorandenstipendium** für fortgeschrittene Medizinpromovenden im DZHK (Deutsches Zentrum für Herz-Kreislauf-Forschung) Standort Hamburg

2013 **Reisestipendium des DZHK** für die Präsentation beim "Cardiac Regeneration and Vascular Biology Conference 2013"

2013 **Posterpreis** bei der "Cardiac Regeneration and Vascular Biology Conference 2013"

Publikationen:

1. Guihaire J, Deuse T, **Wang D**, Spin JM, Blankenberg FG, Fadel E, Reichenspurner H, Schrepfer S. Immunomodulation Therapy Using Tolerogenic Macrophages in a Rodent Model of Pulmonary Hypertension. **Stem Cells Dev. 2021** May 15;30(10):515-525. doi: 10.1089/scd.2021.0007. Epub 2021 Apr 16.
2. da Silveira WA, Fazelinia H, Rosenthal SB, Laiakis EC, Kim MS, Meydan C, Kidane Y, Rathi KS, Smith SM, Stear B, Ying Y, Zhang Y, Foox J, Zanello S, Crucian B, **Wang D**, Nugent A, Costa HA, Zwart SR, Schrepfer S, Elworth RAL, Sapoval N, Treangen T, MacKay M, Gokhale NS, Horner SM, Singh LN, Wallace DC, Willey JS, Schisler JC, Meller R, McDonald JT, Fisch KM, Hardiman G, Taylor D, Mason CE, Costes SV, Beheshti A. Comprehensive Multi-omics Analysis Reveals Mitochondrial Stress as a Central Biological Hub for Spaceflight Impact. **Cell. 2020** Nov 25;183(5):1185-1201.e20. doi: 10.1016/j.cell.2020.11.002.
3. Hu X, Kueppers ST, Kooreman NG, Gravina A, **Wang D**, Tediashvili G, Schlickeiser S, Frentsch M, Nikolaou C, Thiel A, Marcus S, Fuchs S, Velden J, Reichenspurner H, Volk HD, Deuse T, Schrepfer S. The H-Y Antigen in Embryonic Stem Cells Causes Rejection in Syngeneic Female Recipients. **Stem Cells Dev. 2020** Sep 15;29(18):1179-1189. doi: 10.1089/scd.2019.0299.
4. **Wang D**, Tediashvili G, Hu X, Gravina A, Marcus SG, Zhang H, Olgin JE, Deuse T, Schrepfer S. A Cryoinjury Model to Study Myocardial Infarction in the Mouse. **J Vis Exp. 2019** (151), e59958, doi:10.3791/59958 (2019)
5. Deuse T, Hu, X, Agbor-Enoh S, Koch M, Spitzer MH, Gravina A, Alawi M, Marishta A, Peters B, Kosaloglu-Yalcin Z, Yang Y, Rajalingam R, **Wang D**, Nashan B, Kiefmann R, Reichenspurner H, Valantine H, Weissman IL, Schrepfer S. De novo mutations in

mitochondrial DNA of iPSCs produce immunogenic neoepitopes in mice and humans. **Nat Biotechnol. 2019** Aug; doi: 10.1038/s41587-019-0227-7

6. Wang H, Cao H, Xu Z, **Wang D**, Zeng Y. SNP rs2596542 in MICA is associated with risk of hepatocellular carcinoma: a meta-analysis. **Biosci Rep. 2019** Apr 9. pii: BSR20181400. doi: 10.1042/BSR20181400.
7. Deuse T, Hu X, Gravina A, **Wang D**, Tediashvili G, De C, Thayer WO, Wahl A, Garcia JV, Reichenspurner H, Davis MM, Lanier LL, Schrepfer S. Hypoimmunogenic derivatives of induced pluripotent stem cells evade immune rejection in fully immunocompetent allogeneic recipients. **Nat Biotechnol. 2019** Mar;37(3):252-258. doi: 10.1038/s41587-019-0016-3.
8. Tediashvili G, **Wang D**, Reichenspurner H, Deuse T, Schrepfer S. Balloon-based Injury to Induce Myointimal Hyperplasia in the Mouse Abdominal Aorta. **J Vis Exp. 2018** Feb 7;(132). doi: 10.3791/56477.
9. Miller KK, **Wang D**, Hu X, Hua X, Deuse T, Neofytou E, Renne T, Velden J, Reichenspurner H, Schrepfer S, Bernstein D. Thalidomide treatment prevents chronic graft rejection after aortic transplantation in rats - an experimental study. **Transpl Int. 2017** Nov;30(11):1181-1189. doi: 10.1111/tri.13004
10. **Wang D**. Neue Mechanismen zur Verhinderung der myointimalen Hyperplasie. **Z Herz- Thorax- Gefäßchir 2017**. doi:10.1007/s00398-017-0153-2
11. **Wang D**, Tediashvili G, Pecha S, Reichenspurner H, Deuse T, Schrepfer S. Vein Interposition Model: A Suitable Model to Study Bypass Graft Patency. **J Vis Exp. 2017**;(119).
12. Guihaire J, Deuse T, **Wang D**, Fadel E, Reichenspurner H, Schrepfer S. Sex Differences in Immunology: More Severe Development of Experimental Pulmonary Hypertension in Male Rats Exposed to Vascular Endothelial Growth Factor Receptor Blockade. **Biomed Res Int. 2015**;2015:765292.
13. **Wang D**, Deuse T, Stubbendorff M, Chernogubova E, Erben RG, Eken SM, Jin H, Li Y, Busch A, Heeger CH, Behnisch B, Reichenspurner H, Robbins RC, Spin JM, Tsao PS, Maegdefessel L, Schrepfer S. Local MicroRNA Modulation Using a Novel Anti-miR-21-Eluting Stent Effectively Prevents Experimental In-Stent Restenosis. **Arterioscler Thromb Vasc Biol. 2015**;35(9):1945-53.
14. Schmidt-Lucke C, Zobel T, Schrepfer S, Kuhl U, **Wang D**, Klingel K, Becher PM, Fechner H, Pozzuto T, Van Linthout S, Lassner D, Spillmann F, Escher F, Holinski S, Volk HD, Schultheiss HP, Tschope C. Impaired Endothelial Regeneration Through Human

Parvovirus B19-Infected Circulating Angiogenic Cells in Patients With Cardiomyopathy. **J Infect Dis. 2015**. pii: jiv178.

15. Deuse T, **Wang D**, Stubbendorff M, Itagaki R, Grabosch A, Greaves LC, Alawi M, Gruenewald A, Hu X, Hua X, Velden J, Reichenspurner H, Robbins RC, Jaenisch R, Weissman IL, Schrepfer S. SCNT-derived ESCs with mismatched mitochondria trigger an immune response in allogeneic hosts. **Cell Stem Cell 2015**;16(1):33-8.
16. Deuse T, Hua X, **Wang D**, Maegdefessel L, Heeren J, Scheja L, Bolanos JP, Rakovic A, Spin J, Stubbendorff M, Ikeno F, Länger F, Zeller T, Schulte-Uentrop L, Stoehr A, Itagaki R, Haddad F, Eschenhagen T, Blankenberg S, Kiefmann R, Reichenspurner H, Velden J, Klein C, Yeung A, Robbins RC, Tsao PS, Schrepfer S. DCA prevents restenosis in preclinical animal models of vessel injury. **Nature 2014**;509(7502):641-4.

Sprachkenntnisse:

Deutsch:	Muttersprache
Englisch:	fließend in Wort und Schrift Cambridge Certificate of Proficiency
Chinesisch:	fließend in Wort und Schrift Hanyu Shuiping Kaoshi Advanced

Hannover, den 15.06.2021

UNIVERSITÄT HAMBURG

hereby confers under the presidency of

Professor Dr. Dr. h.c. Dieter Lenzen

through the

Faculty of Medicine

under the deanship of

Professor Dr. Blanche Schwappach-Pignataro

upon

Dr. med. Dong Wang

born 26 August 1990 in Beijing, China, Volksrepublik

the academic degree of

Doctor of Philosophy (PhD)

for the dissertation entitled:

„Developing new models, unveiling disease mechanisms and identifying novel therapeutic strategies for cardiovascular diseases"

and for the oral defense on 9 December 2020

Overall grade: „excellent (magna cum laude)"

Hamburg, 9 December 2020

i.V.

The President

Universität Hamburg (Siegel) 30c Fakultät Medizin

B. Schwappach-Pignataro

The Dean

- English translation of the original German document -

Addendum

UNIVERSITÄTSKLINIKUM HAMBURG-EPPENDORF

Universitäres Herzzentrum Hamburg (UHZ)
Klinik und Poliklinik für Herz- und Gefäßchirurgie
Transplantation und Stammzell Immunbiologie Labor (TSI)

Prof. Dr. Dr. Hermann Reichenspurner

Developing new models, unveiling disease mechanisms and identifying novel therapeutic strategies for cardiovascular diseases

Dissertation

zur Erlangung des Doktorgrades Doctor of Philosophy (PhD)
an der Medizinischen Fakultät der Universität Hamburg

vorgelegt von: Dong Wang aus Beijing, China

Hamburg 2020

Angenommen von der
Medizinischen Fakultät der Universität Hamburg am: 09.12.2020

Veröffentlicht mit der Genehmigung der
Medizinischen Fakultät der Universität Hamburg:

Prüfungsausschuss, der/die Vorsitzende: Prof. Dr. Sonja Schrepfer

Prüfungsausschuss, zweite/r Gutachter/in: Prof. Dr. Rainer Kiefmann

Die vorliegende kumulative Dissertation umfasst Arbeiten aus den folgenden sechs Publikationen:

1. **Wang D**, Tediashvili G, Pecha S, Reichenspurner H, Deuse T, Schrepfer S. *Vein Interposition Model: A Suitable Model to Study Bypass Graft Patency.* **J Vis Exp. 2017**;(119).
2. Tediashvili G, **Wang D**, Reichenspurner H, Deuse T, Schrepfer S. *Balloon-based Injury to Induce Myointimal Hyperplasia in the Mouse Abdominal Aorta.* **J Vis Exp. 2018** Feb 7;(132). doi: 10.3791/56477.
3. Guihaire J, Deuse T, **Wang D**, Fadel E, Reichenspurner H, Schrepfer S. Sex *Differences in Immunology: More Severe Development of Experimental Pulmonary Hypertension in Male Rats Exposed to Vascular Endothelial Growth Factor Receptor Blockade*. **Biomed Res Int. 2015**;2015:765292.
4. Miller KK, **Wang D**, Hu X, Hua X, Deuse T, Neofytou E, Renne T, Velden J, Reichenspurner H, Schrepfer S, Bernstein D. *Thalidomide treatment prevents chronic graft rejection after aortic transplantation in rats - an experimental study.* **Transpl Int. 2017** Nov;30(11):1181-1189. doi: 10.1111/tri.13004.
5. Deuse T, Hu X, Agbor-Enoh S, Koch M, Spitzer MH, Gravina A, Alawi M, Marishta A, Peters B, Kosaloglu-Yalcin Z, Yang Y, Rajalingam R, **Wang D**, Nashan B, Kiefmann R, Reichenspurner H, Valantine H, Weissman IL, Schrepfer S. *De novo mutations in mitochondrial DNA of iPSCs produce immunogenic neoepitopes in mice and humans*. **Nat Biotechnol**. 2019 Aug 19. doi: 10.1038/s41587-019-0227-7
6. Deuse T, Hu X, Gravina A, **Wang D**, Tediashvili G, De C, Thayer WO, Wahl A, Garcia JV, Reichenspurner H, Davis MM, Lanier LL, Schrepfer S. *Hypoimmunogenic derivatives of induced pluripotent stem cells evade immune rejection in fully immunocompetent allogeneic recipients*. **Nat Biotechnol. 2019** Mar;37(3):252-258. doi: 10.1038/s41587-019-0016-3.

Inhaltsangabe

1. Hintergrund

Kardiovaskuläre Erkrankungen sind die führenden Todesursachen weltweit, sowie in allen Regionen außer Afrika[1]. Allein in 2015 verstarben 17,9 Millionen Menschen an kardiovaskulären Erkrankungen und deren Folgen, ein Anstieg um 5,6 Millionen Menschen im Vergleich zu 1990[2, 3].

Ein großer Teil der Patienten erliegt den Folgen sogenannter vaskuloproliferativen Erkrankungen, wie Arteriosklerose, myointimale Hyperplasie oder pulmonale Hypertonie[4, 5]. Zu den Folgen vaskuloproliferativer Erkrankungen zählen unter anderem die koronare Herzerkrankung (KHK), Myokardinfarkt sowie Schlaganfall. Nach Schätzung der WHO wird im Jahr 2030 die Zahl der durch KHK bedingten Todesfälle auf 25 Millionen steigen[6].

In den meisten Fällen ist der Auslöser einer vaskuloproliferativen Erkrankung eine Verletzung der Gefäßwand. Die Verletzung führt zu einem überschießenden Reparaturvorgang mit Verlust der Gefäßfunktion und Einschränkung des Blutflusses[7]. Dabei kann die Gefäßverletzung durch mechanische, iatrogene oder auch immunologische Ursachen ausgelöst werden. Thrombozyten, Entzündungszellen und verletzte Gefäßzellen sezernieren Wachstumsfaktoren und Zytokine, die zu einer Aktivierung von glatten Gefäßmuskelzellen (VSMCs) führen[8]. Normalerweise befinden sich VSMCs in einem differenzierten kontraktilen Ruhezustand und sind in der Mediaschicht des Gefäßes lokalisiert. Kommt es im Rahmen der Gefäßverletzung zu einer Aktivierung der VSMCs, findet eine Dedifferenzierung der VSMCs zu einem synthetischen Phänotyp statt. Synthetische VSMCs sind charakterisiert durch eine gesteigerte Proliferation, Migration und Synthese von extrazellulären Matrixproteinen und lösen ein Remodeling des Gefäßes mit progredienter Einengung des Gefäßlumens aus[9]. Nach dem Gesetz von Hagen-Poiseuille verhält sich die Stromstärke proportional zur vierten Potenz des Gefäßradius. Kleine Abnahmen des Gefäßlumens führen zu einer starken Verminderung der Durchblutungssituation und einer Minderperfusion des dahinter geschalteten Organs.

Aktuelle Therapiestrategien zielen auf eine Wiederherstellung des Blutflusses durch Wiedereröffnen des Gefäßes oder das Anlegen eines Bypasses. Bei der perkutanen transluminalen Angioplastie (PTA) wird ein Draht über das Gefäßsystem bis zur Engstelle geschoben und die Verengung durch einen Ballon gedehnt. Im Anschluss kann ein zusätzlicher Stent in den dilatierten Gefäßabschnitt implantiert werden und schützt dadurch das Gefäß vor einem akuten elastischen Rückzug[10]. Ein ähnliches Verfahren ist die Endarteriektomie, bei der das Gefäß operativ geöffnet und die Gefäßablagerungen/Verengung chirurgisch beseitigt wird. Alternativ kann der Blutfluss durch Anlage eines Bypass- oder Interpositionsgraftes wiederhergestellt werden. Sind alle oben beschriebenen Therapiemöglichkeiten nicht praktikabel oder unwirksam und ist das Organ irreversibel beschädigt, bleibt als letzte Möglichkeit nur die Organtransplantation übrig.

Paradoxerweise lösen auch therapeutische Eingriffe eine Gefäßverletzung aus, die zur Entwicklung einer myointimalen Hyperplasie führt. Bei der PTA kommt es in 20 – 48 % der Fälle zur Restenose[11-14]. Trotz Einsatz eines Stents bleibt die Restenoserate über 30 %[15, 16]. Ursache hierfür ist eine andauernde Irritation des Gefäßes durch den Stent, was einen Proliferationsreiz für die VSMCs darstellt und zur Entwicklung einer myointimalen Hyperplasie führt[4, 17, 18]. Auch bei operativen Lösungen, wie die Endarteriektomie oder Bypass-Grafting, kommt es zur Restenose bzw. zum Bypassverschluss. So wird die Restenoserate bei der Karotisendarteriektomie mit 6 – 36 % beziffert und gründet auf einer Hyperplasie der VSMCs nach der Gefäßverletzung[19-22]. Bei dem koronaren Bypass-Grafting variiert die 10-Jahres-Verschlussrate zwischen 15 bis 40 % je nach Wahl des Graftes[23]. Ursache hierfür ist auch eine myointimale Hyperplasie, die getriggert wird durch die Gefäßverletzung bei der Graftentnahme. Zusätzliche Faktoren, wie eine Überdehnung beim Anschluss an das Kreislaufsystem oder eine Graftischämie, fördern die Entstehung der myointimalen Hyperplasie[24]. Auch bei der Organtransplantation kommt es zur Entstehung einer myointimalen Hyperplasie in den Gefäßen des transplantierten Organs und limitiert den therapeutischen Erfolg. So entwickelt sich bei 50 % der herztransplantierten Patienten nach zehn Jahren eine koronare Transplantatvaskulopathie (CAV)

im Graft[25]. CAV ist eine besonders aggressive Form der myointimalen Hyperplasie, die durch immun- und nicht-immun bedingte Reize ausgelöst wird[26].

Es bleibt festzuhalten, dass die myointimale Hyperplasie ein wichtiger pathobiologischer Mechanismus bei diversen kardiovaskulären Erkrankungen ist, wie die Restenose, das Bypass-Graftversagen und die CAV. Eine sorgfältige, fundierte Erforschung der myointimalen Hyperplasie ist von entscheidender Bedeutung und sollte parallel zur Entwicklung von neuen spezifischeren Medikamenten und Therapieoptionen erfolgen.

2. Zielsetzung

Trotz großer Fortschritte in der Versorgung von kardiovaskulären Patienten, bleiben die Pathomechanismen von vielen kardiovaskulären Erkrankungen noch immer ungeklärt. Um die pathobiologischen und –physiologischen Mechanismen zu untersuchen, sind Tiermodelle von essentieller Bedeutung. Ziel dieser Arbeit ist es, neue Tiermodelle zu entwickeln, um die Pathogenese und -mechanismen von vaskuloproliferativen Erkrankungen zu verstehen. Basierend auf dem dadurch gewonnenen Wissen und den Tiermodellen können neue Medikamente entwickelt werden, die spezifischer und nebenwirkungsärmer sind. Eine mögliche neue Therapie gegen die koronare Transplantationsvaskulopathie sind Immunmodulatoren, wie Thalidomid. In dieser Arbeit wird die therapeutische Wirksamkeit von Thalidomid bei der Prävention der koronaren Transplantationsvaskulopathie untersucht.

Neben der medikamentösen Therapie, stellt die regenerative Zelltherapie eine neue verheißungsvolle Therapieoption in der kardiovaskulären Medizin dar. Dabei verfolgt die regenerative Zelltherapie das Ziel, durch die Transplantation von Stammzellen oder deren differenzierten Derivaten, das bereits abgestorbene Gewebe zu regenerieren. Ziel meiner Arbeit auf diesem Gebiet ist es, ihre klinische Einsetzbarkeit aus immunbiologischer Sicht zu untersuchen und immunologische Lösungen zu entwickeln.

3. Die Entwicklung von Tiermodellen

3.1. Das Veneninterpositionsmodell

Vein Interposition Model: A Suitable Model to Study Bypass Graft Patency.

Neben der perkutanen transluminalen Koronarangioplastie (PTCA) und Stent-Implantation, ist die koronararterielle Bypass-Operation (CABG) eine etablierte Therapieoption zur Behandlung von KHK Patienten. Der Einsatz von Venenbypässen aus der Vene Saphena wurde erstmalig 1967 von Favalore beschrieben und über Jahre hinweg verfeinert[27]. Besonders in den komplexen Dreigefäßerkrankungen zeigen Studien eine Überlegenheit der CABG gegenüber der PTCA/Stent-Implantation[28].

Eine Einschränkung für den Langzeiterfolg von CABG Operationen ist die steigende Abnahme der Transplantatdurchgängigkeit. Besonders in Venengrafts kommt es vermehrt zur Abnahme der Graftdurchgängigkeit und zu Graftverschlüssen. Die Durchgängigkeit nach einem Jahr postoperativ liegt bei 85 %, und sinkt nach zehn Jahren auf 61 % [23, 29].

Um den Pathomechanismus beim Bypassverschluss besser zu verstehen, wurden unterschiedliche Tiermodelle in unterschiedlichen Spezies entwickelt. Großtiere wie Schweine[30], Schafe[31], Hunde[32] oder Primaten[33] haben menschenähnliche anatomische Strukturen und können eingesetzt werden, um komplexe therapeutische Strategien oder neue operative Techniken zu testen[34]. Allerdings sind spezielle Anforderungen nötig, wie besondere Haltungsanlagen, Ausrüstung und trainiertes Personal. Die damit verbundenen hohen Kosten limitieren eine breitere Nutzung von Großtiermodellen. Kleintiere, wie Ratten, sind einfacher zu handhaben, benötigen ferner keine speziellen Anlagen oder Ausstattungen, und sind kosteneffizient. Aus diesen Gründen entwickelten wir ein Rattenmodell für Gefäßbypass-Operationen. Hierbei wird ein Stück Vene aus der Vena Epigastrica inferior an die A. femoralis transplantiert. Das Modell ist reproduzierbar, einfach durchzuführen, zuverlässig und kostengünstig.

***Wang D**, Tediashvili G, Pecha S, Reichenspurner H, Deuse T, Schrepfer S. Vein Interposition Model: A Suitable Model to Study Bypass Graft Patency. **J Vis Exp. 2017**; (119).*

Zuerst wird ein Stück Vene der Vena epigastrica inferior von einer Donorratte entnommen. Die Vena epigastrica inferior kann durch eine Inzision entlang der Linea Inguinalis lokalisiert werden. Ein 0,5 bis 1 cm langes Segment von der Vene wird entnommen, mit Heparin durchspült und bis zur Transplantation in 1 % Lidocain auf Eis gelagert. An der Empfängerratte wird die A. Femoralis freigelegt und ein Segment exzidiert. Die entstandene Lücke sollte 1 – 2 mm länger sein als das Venentransplantat. Durch Einzelnähte werden Anastomosen zwischen dem Venengraft und der A. Femoralis hergestellt. Die anschließende Applikation von Fibrinkleber auf das Graft verhindert eine plötzliche Überdehnung des Venentransplantats nach Wiederherstellung des Blutflusses. Ein Puls sollte im Graft und distal des Gefäßes zu sehen sein. Nach der Blutstillung wird die Wunde am Bein vernäht und das Tier aus der Narkose geleitet.

Die Gefäßdurchgängigkeit und Blutfluss können mit Duplex Sonographie nicht-invasiv bestimmt werden. Die histologische Aufarbeitung des Venengrafts zeigt eine progressive myointimale Hyperplasie und damit einhergehend eine fortschreitende Abnahme des Gefäßlumens. So besteht bereits nach einer Woche eine Abnahme des Gefäßlumens um ca. 12 % und nach 4 Wochen um 40 %. Diese zeitliche Dynamik spiegelt den pathophysiologischen Aspekt beim Bypassverschluss wieder.

Wichtig bei der operativen Durchführung des Modells ist eine behutsame Handhabung des Venengrafts, sowohl bei der Graftentnahme als auch bei der Implantation. Die Schädigung des Grafts führt zur Entstehung von Thromben und einem akuten Gefäßverschluss. Zusätzlich ist es wichtig, eine Überdehnung des Grafts zu verhindern. Wird das Venengraft ohne Schutz dem arteriellen Drucksystem ausgesetzt, kommt es zu einer erhöhten Wandspannung und folglich zu einer Überdehnung und Veränderung des Blutflussprofils. Beide sind Auslöser von Thromben, Anastomoseninsuffizienzen und akutem Graftversagen. Der Einsatz von Fibrinkleber verhindert die unkontrollierte Überdehnung und schützt die

Intima- und Mediaschicht vor mechanischen Schäden. Alternativ können auch absorbierbare Kollagenmembrane um das Graft gewickelt werden, um den Venenbypass zu schützen.

Unterschiedliche Kleintiermodelle für Bypassversagen werden in der Literatur beschrieben. Die meisten bisherigen Modelle liefern jedoch nur eine geringe Menge an Gewebe für die Analysen[35]. Der Vorteil unserer Methode ist die vergleichbar große Gewebemenge. Ein Graft kann in mehrere Teile geteilt und in unterschiedlichen Assays untersucht werden. Damit reduziert sich die Anzahl der benötigten Tiere.

Zusammenfassend bildet unser Venenimplantationsmodell ein geeignetes Tiermodell zur Erforschung von Bypassverschlüssen nach CABG-Operationen. Die gute Reproduzierbarkeit, die einfache Etablierung und Handhabung und die geringen Kosten sind wichtige Vorteile dieses Tiermodells. Besonders für die Untersuchung von teuren therapeutischen Reagenzien, wie virale Vektoren für eine Gentherapie, ist dieses Modell geeignet. Erfolgreich getestete Behandlungsoptionen können im Anschluss in einem Großtiermodell bestätigt werden.

3.2. Das Aortendenudationsmodell

Balloon-based Injury to Induce Myointimal Hyperplasia in the Mouse Abdominal Aorta.

Neben der Bypassoperation sind die perkutane transluminale Koronarangioplastie (PTCA) und die Stent-Implantation etablierte Behandlungsmethoden für Patienten mit koronarer Herzerkrankung. Die erste PTCA wurde im Jahr 1977 von Andreas Grüntzig am Menschen durchgeführt. Nach den anfänglich positiven Ergebnissen, erkannte man bald die Komplikationen und Nebenwirkungen dieser Methode, wie ein akuter Gefäßverschluss oder eine Restenose. So zeigten sich bei 20 – 48 % der Patienten eine Restenose der dilatierten Gefäße[11-14]. Erst mit der Einführung von Stents durch Ulrich Sigward im Jahr 1987 konnte die Komplikationsrate gesenkt werden[36, 37]. Dennoch zeigten sich in Langzeitstudien, dass die Restenoserate nicht unter 30 % fiel[15, 16]. Ein wichtiger Fortschritt gelang um die Jahrhundertwende mit dem Einsatz von neuartigen Stents, die mit Medikamenten beschichtet sind. Diese sogenannten Drug-Eluting-Stents hemmen die Proliferation von Zellen und konnten die Restenoserate auf unter 10 % senken. Trotz der enormen Verbesserungen darf die Bedeutung der Restenose nicht unterschätzt werden, da die Anzahl der durchgeführten Perkutanen Kathetherinterventionen (PCI) deutlich zunahm. Allein in 2016 wurden in Deutschland mehr als 365.000 PCIs durchgeführt[38]. Aus diesem Grund ist es entscheidend, die pathophysiologischen und -biologischen Mechanismen bei der Restenose zu verstehen.

Unterschiedliche Tiermodelle werden in der Literatur für die Untersuchung der Restenose beschrieben. Die Großtiermodelle bieten den Vorteil, dass die arteriellen

anatomischen Strukturen den Menschen ähneln und besonders gut geeignet sind, um therapeutische Techniken, Prozeduren und Apparate zu testen[39, 40]. Die Nachteile liegen zum einen in den speziellen Anforderungen und zum anderen in den hohen Kosten. Nicht zu vernachlässigen sind auch die Spezies-bezogenen Besonderheiten jedes Modells. So haben Schweinmodelle den Nachteil einer erhöhten Thrombogenität[41] und Hundemodelle ein milderes Ansprechen auf Gefäßverletzungen[40]. Zu den

Kleintiermodellen zählen Maus- und Rattenmodelle. Im Vergleich zu Ratten haben Mausmodelle den Vorteil, dass es eine Reihe von Knock-out Stämmen gibt. Bisherige Modelle induzierten einen Gefäßschaden durch Drähte[42], Trocknung[43], Federdraht[44] oder Manschetten[45]. Da der Ursprung des Gefäßschadens einen Einfluss auf die Entwicklung und die Beschaffenheit der myointimalen Hyperplasie und Restenose hat, ist ein Gefäßschaden, ausgelöst durch einen Ballonkatheter, die beste Methode, um den klinischen Aufbau nachzuahmen. In der folgenden Studie entwickelten wir ein Restenosemodell für die Maus, das auf einer Ballonkatheterverletzung basiert.

*Tediashvili G, **Wang D**, Reichenspurner H, Deuse T, Schrepfer S. Balloon-based Injury to Induce Myointimal Hyperplasia in the Mouse Abdominal Aorta. **J Vis Exp. 2018** Feb 7; (132). doi: 10.3791/56477.*

Für dieses Modell werden Mäuse mit einem Gewicht von ca. 30 g verwendet. Dafür wird die infrarenale Aorta bis zur Bifurkation freigelegt und die kleinen Seitenäste werden ligiert. Es wird eine waagerechte Inzision in die Aorta vorgenommen und die Aorta von innen mit Heparin durchspült. An beiden Enden der Inzision wird jeweils eine Einzelknotennaht gelegt, um das Zerreißen des Gefäßes bei der Kathetereinführung zu verhindern. Mit einem Gefäßdilator wird die Aorta leicht vorgedehnt. Anschließend wird der Ballonkatheter in die Aorta eingeführt und retrograd ca. 2 cm bis zum Aortenbogen geführt. Wichtig dabei ist, dass der Ballon beim Hochführen im Gefäß aufgeblasen wird, damit eine Blutleckage verhindert und eine Gefäßverletzung ausgelöst wird. Nach Erreichen des Aortenbogens wird der Katheter herausgezogen und die Inzision mit Einzelnähten geschlossen. Absorbierbare blutstillende Einlagen werden auf die Inzision platziert, um die Blutstillung zu fördern. Wenn distal von der Inzision ein Puls zu sehen ist, kann die Bauchwunde verschlossen und das Tier aus der Narkose geleitet werden.
In dem verletzten Gefäßabschnitt entwickelt sich mit der Zeit eine myointimale Hyperplasie und Restenose, deren zelluläre Komponente aus glatten Muskelzellen und Myofibroblasten besteht. Zusätzlich finden sich vermehrt

extrazelluläre Matrixproteine, wie Kollagen III, in der Gefäßläsion wieder. Diese Zusammensetzung ähnelt humanen Restenose-Läsionen und bestätigt die Eignung unseres Tiermodells [46-48].

Der entscheidende und gleichzeitig anspruchsvollste Schritt bei der Durchführung ist die Denudierung der Aorta. Eine übermäßige Aufdehnung führt zur Bildung von Aneurysmen oder Dissektionen. Eine ungenügende Dilatation des Ballons führt zu unzureichenden Gefäßschäden und einer limitierten Ausbildung der myointimalen Hyperplasie.

Im Vergleich zu anderen Mausmodellen besitzt unser Modell den Vorteil, dass nicht nur die abdominelle Aorta, sondern auch die thorakale Aorta denudiert wird. Dadurch kann ein relativ großes Gewebestück für Analysen gewonnen werden. Zusätzlich kann dieses Modell an Knock-out Mäusen durchgeführt werden, um die Bedeutung von einzelnen Genen bei der Entstehung der myointimalen Hyperplasie und Restenose zu untersuchen.

Zusammenfassend haben wir in dieser Arbeit ein kostengünstiges, einfach durchzuführendes Kleintiermodell zur Erforschung von Restenose und myointimaler Hyperplasie entwickelt.

3.3. Das Pulmonale Hypertonie Modell

Sex Differences in Immunology: More Severe Development of Experimental Pulmonary Hypertension in Male Rats Exposed to Vascular Endothelial Growth Factor Receptor Blockade.

Die Pulmonale Hypertonie (PAH) ist eine vaskuloproliferative Erkrankung des pulmonalen Kreislaufs und wird definiert durch eine Erhöhung des mittleren pulmonal arteriellen Drucks (mPAP) ≥ 25 mmHg in der Rechtsherzkathetermessung[49]. Es wird charakterisiert durch eine fortschreitende Zunahme des pulmonalarteriellen Gefäßwiderstands, einhergehend mit einer Erhöhung des pulmonalarteriellen Drucks und einer Rechtsherzbelastung. Die Faktoren für die Zunahme des Gefäßwiderstandes sind: Endotheliale Dysfunktion, Thromben oder Inflammation, die letztendlich zu einem pulmonalvaskulären Remodeling führen[50, 51]. Das Remodeling basiert auf einer Proliferation von glatten Muskelzellen und Endothelzellen und In-situ-Mikrothromben, und geht in eine Fibrose des Gefäßes über[50, 51]. Interessanterweise ist die Prävalenz der PAH bei Frauen höher, doch die Schwere der Erkrankung ist gravierender bei männlichen Patienten[52].
Ähnliche geschlechtsspezifische Beobachtungen wurden auch in klassischen PAH Tiermodellen festgestellt, wie dem Hypoxie+Monocrotaline oder dem Hypoxie+Semaxanib Modell. Diese werden auf eine protektive Wirkung von Östrogen zurückgeführt[53, 54]. Um die bisherigen Beobachtungen zu erweitern, untersuchten wir die Rolle des Geschlechts bei der Pathogenese von PAH in einem neuen Tiermodell, dem Semaxanib-Monotherapie-Modell. Hierzu wurden männliche und weibliche T-Zell-defiziente Nude Ratten mit einer hohen Dosis von Semaxanib behandelt und die pulmonale Hypertonie sowie die Rechtsventrikuläre Funktion vier Wochen lang beobachtet.

*Guihaire J, Deuse T, **Wang D**, Fadel E, Reichenspurner H, Schrepfer S. Sex Differences in Immunology: More Severe Development of Experimental Pulmonary Hypertension in Male Rats Exposed to Vascular Endothelial Growth Factor Receptor Blockade. **Biomed Res Int. 2015**; 2015: 765292.*

Von den behandelten elf männlichen Tieren erreichten nur acht Tiere den Beobachtungsendpunkt von 28 Tagen, während alle weiblichen Tiere

überlebten. Funktionell echokardiographische Messungen des rechten Ventrikels zeigten eine deutliche Vergrößerung bei den männlichen Tieren mit einer gleichzeitigen Beeinträchtigung der rechtsventrikulären-pulmonalarteriellen Kopplung. Histologisch korrelierten die Ventrikelveränderungen mit hypertrophierten Kardiomyozyten. Ähnliche histologische Veränderungen waren auch in den Lungenarterien der männlichen Tiere zu sehen. Die Media-Schicht ist signifikant verdickt und es findet ein Phänotyp-Switch der glatten Muskelzellen vom kontraktilen zum dedifferenzierten Typ statt.

Zusammenfassend haben diese Versuche gezeigt, dass im Semaxanib-Monotherapie-Modell männliche Ratten deutlich schwerere PAH entwickeln als Weibliche. Eine mögliche Erklärung ist die protektive Einwirkung von Östrogen auf den Phenotyp-Switch von glatten Muskelzellen[55]. Östrogen verlangsamt den Phenotyp-Switch von kontraktilen glatten Muskelzellen zum dedifferenzierten Typ und verhindert eine übermäßige Proliferation[55, 56]. Weitere Versuche mit ovarektomierten Ratten könnten Aufschlüsse über den genauen protektiven Mechanismus geben.

Zusätzlich zeigt diese Studie auf, dass die Wahl des Tiergeschlechtes beim Tierversuch einen entscheidenden Einfluss auf das Ergebnis ausübt. Eine behutsame Auswahl und die genaue Angabe des Geschlechtes in wissenschaftlichen Publikationen unterstützt die Forschung um die strengen Standards der Wissenschaft zu erfüllen.

4. Die Therapie der Transplantatvaskulopathie

Thalidomide treatment prevents chronic graft rejection after aortic transplantation in rats - an experimental study.

Treten vaskuloproliferative Erkrankungen am Herzen auf, so kommt es langfristig zu einer Minderversorgung des Myokards und eine ischämische Kardiomyopathie entwickelt sich. Die ischämische Kardiomyopathie ist charakterisiert durch eine Dilatation des Ventrikels und einer Verminderung der Kontraktilität und führt zur Entwicklung einer Herzinsuffizienz[57]. Als einzige kausale Therapie gilt aktuell die Herztransplantation (HTX), die von Norman Shumway und Richard Lower entwickelt und als erstes 1967 durch Christiaan Barnard durchgeführt wurde.[58] Wie bei anderen allogenen Transplantationen, stellt die Abstoßungsreaktion eine entscheidende Einschränkung der Herztransplantation dar.

Während das mediane Überleben nach einer HTX in den 80er Jahren bei acht Jahren lag, ist es mittlerweile auf elf Jahre angestiegen [59]. Die Verbesserung basiert auf einer verbesserten Versorgung und Behandlung in der Frühphase nach HTX[60, 61]. Das Langzeitüberleben wird immer noch beeinträchtigt durch die chronische Abstoßungsreaktion, die sogenannte koronare Transplantatvaskulopathie (CAV). Die CAV stellt die Haupttodesursache in den ersten Jahren nach der Herztransplantation dar und ist bei 50 % der Patienten nach zehn Jahren Post-Transplantation detektierbar[25, 62]. Der zugrunde liegende pathobiologische Mechanismus ist eine besonders aggressive Form der myointimalen Hyperplasie, die charakterisiert wird durch eine diffuse, konzentrische, fibrinöse Intimahyperplasie, die vor allem die intramyokardialen Gefäße betreffen[63]. Von den wenigen gegenwärtigen Therapieoptionen sind die meisten in ihrer Effektivität limitiert und mit Nebenwirkungen belastet[64]. Aus diesem Grund ist es wichtig, neue, effektive, nebenwirkungsarme Therapiestrategien gegen die Entwicklung von CAV zu entwickeln.

Thalidomid wurde in den 50er Jahren gegen Schlaflosigkeit und Unruhe entwickelt. Aufgrund seiner teratogenen Nebenwirkung wurde es nach wenigen Jahren vom Markt genommen[65]. In den letzten Jahren erlebte Thalidomid eine Renaissance als Immunmodulator und erhielt die

Genehmigung für die Behandlung von unterschiedlichen Erkrankungen, wie Multiples Myelom oder Erythema Nodosum Leprosum[66-68]. Die immunmodulierende und anti-inflammatorische Wirkung von Thalidomid wirkt auch gegen eine Graft-versus-Host Disease nach Knochenmarktransplantation[69]. Diese Eigenschaften machen Thalidomid zu einer verlockenden Therapieoption für die Prävention von CAV.

*Miller KK, **Wang D**, Hu X, Hua X, Deuse T, Neofytou E, Renne T, Velden J, Reichenspurner H, Schrepfer S, Bernstein D. Thalidomide treatment prevents chronic graft rejection after aortic transplantation in rats - an experimental study.* ***Transpl Int. 2017*** *Nov; 30(11): 1181-1189. doi: 10.1111/tri. 13004*.

Um den Effekt von Thalidomid auf die Entstehung von CAV zu untersuchen, nutzten wir das etablierte orthotope Aortentransplantationsmodel[70]. Dazu wurde die Aorta einer Fischer 344 Ratte orthotop in eine Lewis Ratte transplantiert und das Tier mit Thalidomid behandelt. Als Kontrollgruppe dienten syngen transplantierte Gefäße von Lewis auf Lewis Ratten. Nach dreißig Tagen zeigten sich in den syngen transplantierten Gefäßen kaum Veränderungen, während sich in den allogen transplantierten Gefäßen eine Intimaverdickung entwickelte, die zu einer deutlichen Verminderung des Lumens führte. Die mit Thalidomid behandelten Tiere entwickelten deutlich weniger Hyperplasie mit minimaler Einengung des Lumens. Diese Ergebnisse deuten darauf hin, dass Thalidomid eine mögliche Präventionsstrategie für CAV darstellt.

Wichtig für die Entwicklung einer myointimalen Hyperplasie ist eine Dedifferenzierung von glatten Gefäßmuskelzellen. Um den Differenzierungsstatus von den VSMCs in den transplantierten Gefäßen zu untersuchen, bestimmten wir die Levels von Smooth-Muscle-Heavy-Chain (SMHC, Marker für differenzierte VSMCs) und embryonic smooth muscle heavy chain (SMemb, Marker für dedifferenzierte SMCs). In den allogenen Gefäßen der unbehandelten Tiere zeigten sich ein deutlich erhöhter Level von SMemb und eine Reduzierung von SMHC; beides Zeichen für einen Dedifferenzierungsprozess der VSMCs. Die Thalidomid Behandlung

verhinderte diesen Prozess und hielt die VSMCs in einen differenzierten Zustand.

Um den zugrundeliegende Mechanismus von Thalidomid zu erforschen, bestimmten wir den Cytokin- und Chemokin-Level in den transplantierten Gefäßen. In den allogenen Grafts detektierten wir deutlich höhere Mengen an MMP-8, TIMP-1, MCP-1 und ICAM-1. Interessanterweise verhinderte Thalidomid die Überexpression von MCP-1 und MMP-8. MCP-1 rekrutiert Monozyten, Lymphozyten und dendritische Zellen und spielt eine wichtige Rolle bei Entzündungsreaktionen nach Verletzungen oder Infektionen[71, 72]. MMPs sind Proteasen, die für den Abbau von extrazellulären Matrixproteinen verantwortlich sind und den Gewebeumbau fördern[73]. Unsere Ergebnisse deuten darauf hin, dass Thalidomid eine anti-inflammatorische und umbau-hemmende Wirkung besitzt und dadurch die Entwicklung der CAV verhindert.
Wichtig für den klinischen Einsatz sind geringe Nebenwirkungen und ein gutes Nebenwirkungsprofil. Besonders im Hinblick auf den Contergan-Skandal war es wichtig für uns, die potentiellen Nebenwirkungen von Thalidomid zu untersuchen. Die mit Thalidomid-behandelten Tiere zeigten keine Anzeichen von Unbehagen oder Beschwerden. Blutuntersuchungen, wie Nierenwerte, Leberwerte oder Blutbild, zeigten keine signifikanten Unterschiede zwischen unbehandelten oder behandelten Tieren.
Viele gegenwärtige Medikamente für CAV wirken über eine allgemeine Immunsuppression. Um zu klären, ob das auch für Thalidomid zutrifft, nutzten wir das heterotope Herztransplantationsmodell und untersuchten die Wirkung von Thalidomid auf die akute Abstoßung. Die akute Abstoßung bestimmten wir durch die Messung der T-Lymphozyten Aktivierung mittels ELISPOT und die Proliferation mittels MLR. Interessanterweise zeigte sich weder im ELISPOT noch im MLR Versuch Unterschiede zwischen der unbehandelten und der Thalidomid Gruppe. Diese Ergebnisse deuten darauf hin, dass Thalidomid die akute Abstoßung nicht beeinflusst und eine spezifische Therapie für CAV ist.
Zusammenfassend zeigte diese Studie, dass Thalidomid die Entwicklung von CAV verhindert, ohne signifikante Nebenwirkungen auszulösen. Durch die Beeinflussung des Zytokinmilieus und die Verhinderung der Dedifferenzierung

von glatten Muskelzellen verhindert Thalidomid die myointimale Hyperplasie und stellt eine neue Therapieoption gegen die CAV dar.

5. Die Stammzelltherapie

5.1. Immunbiologie von induzierten Pluripotenten Stammzellen (iPS)

De novo mutations in mitochondrial DNA of iPSCs produce immunogenic neoepitopes in mice and humans.

Trotz großer Fortschritte in der Versorgung von herztransplantierten Patienten ist die Herztransplantationstherapie noch mit vielen Einschränkungen und Nebenwirkungen behaftet. Dauerhafte Einnahmen von Immunsuppressiva führen zu Nebenwirkungen und Langzeitkomplikationen und schränken die Lebensqualität deutlich ein. Zu den wichtigsten medikamenten-induzierten Komplikationen zählen Nierenversagen, Tumore und Infektionen und sind mitverantwortlich für das befristete Überleben nach HTX.

Die größte Limitation der HTX stellt die geringe Anzahl an Spenderherzen dar. So wird bei jedem Spenderherz streng abgewogen, welchem Patienten das Organ verpflanzt wird. Allein in Deutschland starben 2014 mehr als 44000 Menschen an der Herzinsuffizienz, denen theoretisch durch eine HTX hätte geholfen werden können[38]. Bei lediglich 294 durchgeführten HTX-Operationen blieben den meisten Patienten diese Therapieoption versagt[74].

Aus diesem Grund ist es wichtig neue alternative Therapiestrategien für Patienten mit terminaler Herzinsuffizienz zu finden. Eine große Hoffnung wird auf die regenerative Medizin gesetzt, mit dem Ziel, das irreversibel geschädigte Gewebe durch Stammzellen zu ersetzen. Als besonders vielversprechend gelten induzierte Pluripotente Stammzellen (iPS), da diese aus adulten somatischen Zellen zurückprogrammiert werden und anschließend in die gewünschte Zellart differenziert werden können[75]. Der autologe Ursprung und die damit verbundene Immuntoleranz bei der Transplantation galten als entscheidender Vorteil von iPS Zellen. Nichtsdestotrotz wurde neuerdings mehrfach berichtet, dass differenzierte iPS-Zellen nach der Zelltransplantation abgestoßen werden[76]. Die zugrundeliegende Ursache für dieses Phänomen blieb bislang ungeklärt und könnte den Erfolg von iPS Zellen in der regenerativen Medizin gefährden.

Im Vergleich zur nukleären DNA ist die Mutationsrate von mitochondrialen DNA (mtDNA) um zehn bis zwanzigfach erhöht[77-79]. Gleichzeitig kann in einer Zelle sowohl mutierte als auch Wildtyp DNA vorhanden sein, ein Phänomen, das als Heteroplasmie bezeichnet wird[80]. Mutationen im mitochondrialen DNA können zu Störungen der metabolischen Funktion der Zelle führen[81] oder als Neoantigene wirken. In einer vorangegangenen Studie haben wir demonstriert, dass einzelne Einzelnukleotid-Polymorphismen (SNPs) des mitochondrialen DNAs für die Generierung eines immunologisch-relevanten Neoantigens ausreichend waren[82]. Aus diesem Grund stellten wir die Hypothese auf, dass Mutationen im mitochondrialen DNA zur Bildung von Neoantigenen in iPS Zellen führen und dadurch eine Abstoßungsreaktion im Host hervorrufen.

Deuse T, Hu X, Agbor-Enoh S, Koch M, Spitzer MH, Gravina A, Alawi M, Marishta A, Peters B, Kosaloglu-Yalcin Z, Yang Y, Rajalingam R, ***Wang D****, Nashan B, Kiefmann R, Reichenspurner H, Valantine H, Weissman IL, Schrepfer S. De novo mutations in mitochondrial DNA of iPSCs produce immunogenic neoepitopes in mice and humans.* ***Nat Biotechnol. 2019*** *Aug 19. doi: 10.1038/s41587-019-0227-7.*

Als erstes untersuchten wir die Reaktivität des murinen Immunsystems auf isolierte mtDNA SNPs. Dazu wurden BALB/c Mäuse mit Zellen immunisiert, die durch SNPs im mtDNA eine Aminosäuredifferenz (AA) in mitochondrial-kodierten Proteinen aufweisen. Immunisierte Splenozyten wurden nach fünf Tagen isoliert und für ELISPOT Versuche mit Fibrozyten stimuliert, die entweder das Protein mit oder ohne AA überexprimierten. Es zeigte sich, dass nur die Fibrozyten mit AA eine signifikante Immunantwort auslösen, die aus Th1 und Th2 Aktivierung bestand. Transplantierte man Fibrozyten mit AA in BALB/c Mäusen, zeigte sich eine B-Zell Aktivierung im Tier mit Bildung von spezifischen IgM Antikörpern und die Fibrozyten wurden abgestoßen. Um zu demonstrieren, dass die T-Zell Epitope die SNPs umfassen, wurden immunisierte Splenozyten mit SNP-gematched Peptiden stimuliert, die aus zwanzig Aminosäuren bestanden und die AA besaßen oder nicht. Ähnlich wie bei der Stimulation mit den Fibrozyten führten nur die Peptide mit AA im ELISPOT Versuch zu einer Aktivierung von Th1 und Th2 Zellen. Diese

Ergebnisse zeigen, dass isolierte mtDNA SNPs ausreichend sind, um eine umfangreiche systemische Immunantwort auszulösen.

Die Bedeutung eines mtDNA SNPs könnte bei einer allogenen Transplantation eine untergeordnete Rolle spielen, wenn zusätzlich noch weitere MHC (Major Histocompatibility Complex) Antigene vorhanden sind. Aus diesem Grund immunisierten wir BALB/c Mäuse mit Zellen, die zusätzlich zu den beiden mitochondrialen AA noch MHC-Mismatches besaßen. Splenozyten wurden aus diesen Tieren gewonnen und mit den oben beschriebenen Peptiden stimuliert. Es zeigte sich eine Immunaktivierung der T-Zellen durch Peptide mit AA, die von vergleichbarer Intensität war wie im vorrangegangenem Versuch. Dieser Versuch demonstrierte, dass mtDNA SNPs eine starke Immunantwort auslösen, ungeachtet ob noch weitere MHC Mismatches vorhanden sind.

Die Spezifität der Immunantwort wurde in zwei weiteren Versuchen belegt. Bei Tieren, die vorher nicht immunisiert wurden, lösten die Peptide keine Immunaktivierung aus. Zusätzlich führten Peptide mit fremden Sequenzen zu keiner Immunaktivierung.

Um die immunologische Relevanz von mtDNA SNPs für Menschen zu erforschen, wurden Patienten untersucht, die eine allogene Leber- oder Nierentransplantation erhielten. Dazu wurde die mtDNA von Empfängern und Spendern miteinander verglichen und nicht-synonyme SNPs identifiziert. Darauf basierend wurden Peptide um die SNPs hergestellt, die an der SNP Position eine autologe oder allogene Aminosäuresequenz besaßen. Drei Monate nach der Transplantation wurde Blut vom immunsupprimierten Empfänger entnommen und periphere mononukleäre Zellen (PBMCs) wurden isoliert. Diese Immunzellen wurden re-aktiviert und mit autologen oder allogenen Peptiden stimuliert. Bei den PBMCs, die mit dem allogenen Peptid stimuliert wurden, zeigte sich eine deutliche Immunaktivierung. Autologe Peptide hingegen lösten keine Immunaktivierung aus. Dies belegt die Antigenität von mtDNA SNPs bei Menschen und bestätigt die vorrangegangenen Versuche in der Maus.

Mutationen kommen besonders häufig in der mtDNA vor, da diese nicht von Histonen geschützt werden und ein ineffizientes DNA Reparationssystem besitzen. Gleichzeitig sind mtDNAs vermehrt mutagenen Reizen aus

Sauerstoffradikalen ausgesetzt[83]. Um das Auftreten von neuen Mutationen in iPS Zellen zu untersuchen, sequenzierten wir serienweise die mtDNA von C57BL/6 iPS Zellen während der Kultivierung. Wir beobachteten, dass der Heteroplasmiegrad von nicht-synonymen SNPs sich mit Dauer der Kultivierung in iPS Zellen veränderte.

Um die Bedeutung dieser Veränderungen zu untersuchen, transplantierten wir C57BL/6 iPS-Zellen einer frühen oder späten Passage in C57BL/6 Mäusen und bestimmten die Immunaktivierung und das Zellüberleben. Es fand nur eine Immunaktivierung gegen die iPS Zellen der späten Passage in den Tieren statt, mit einem verminderten Überleben der Zellen im Host. Die Differenzierung von iPS Zellen aus der späten Generation zu Endothelzellen verbesserte das Überleben im Host nicht. Diese Ergebnisse zeigen, dass eine langfristige Kultivierung von iPS Zellen zur Akkumulation von mtDNA SNPs führt und diese Neoantigene darstellen. Bei der Differenzierung zur reifen Zelle behält die Zelle die Antigenität bei.

Als nächstes untersuchten wir, ob dieses Phänomen auch bei humanen iPS Zellen auftritt. Vier humane iPS Zelllinien wurden aus Fibroblasten generiert und dessen mtDNA während der Kultivierung serienweise gescreent. Es zeigte sich, dass in allen vier Zelllinien Mutationen und Anreicherungen von SNPs beim Passagieren der Zellen auftreten. Neben Neumutationen beobachteten wir die Zu- und Abnahme des Heteroplasmiegrades bestimmter SNPs. Die Häufigkeit von Neumutationen und die Anreicherung von seltenen SNPs nahm mit der Höhe der Zellpassagen zu.

Die immunogene Bedeutung von Neoantigenen in humanen iPS Zellen untersuchten wir in einem anschließenden Versuch. Im ersten Schritt wurden iPS Zellen aus PBMCs generiert und bis zur Passage P35 kultiviert. Während der Kultivierung entwickelten sich in den iPS Zellen Neoantigene. Im zweiten Schritt wurden diese iPS Zellen zu Makrophagen differenziert und die Immunaktivierung in einem autologen ELISPOT Versuch untersucht. Aus iPS Zellen differenzierte Makrophagen besaßen Neoantigene und lösten eine Immunaktivierung aus. Kontroll- Makrophagen, die direkt aus den primären PBMCs differenziert wurden, lösten keine Immunaktivierung aus.

Zusammenfassend zeigte diese Studie, dass bei Mäusen und Menschen mutagene, nicht-synonyme mtDNA SNPs relevante Neoantigene darstellen,

die eine hoch spezifische Immunantwort auslösen. Eine ausgedehnte iPS-Zellkultur führt zu einer Ansammlung von mtDNA Neumutationen und zu einer Anreicherung von seltenen SNPs. Werden diese Zellen autolog transplantiert, kann es zu einer Immunreaktion im Empfänger kommen. Diese Immunogenität von autologen iPS Zellen sollte bei der Entwicklung von iPS-basierten Therapiestrategien beachtet werden.

5.2. Hypoimmunogene Stammzellen

Hypoimmunogenic derivatives of induced pluripotent stem cells evade immune rejection in fully immunocompetent allogeneic recipients.

Multipotente Stammzellen stellen eine verheißungsvolle Zellquelle für regenerative Therapiestrategien dar, da sie zu unterschiedlichen Zellarten differenziert und unendlich vermehrt werden können. Besonders iPS Zellen, die durch Reprogrammierung adulter somatischer Zellen hergestellt werden, sind vielversprechend, da sie patienten-spezifisch hergestellt und autolog eingesetzt werden können. Lange Zeit wurde davon ausgegangen, dass diese Zellen einer Immunantwort damit aus dem Weg gegangen werden können. Doch jüngste Studien von uns und anderen Gruppen zeigen, dass iPS Zellen immunologisch nicht inert sind und nach autologer Zelltransplantation abgestoßen werden (siehe oben). Weitere Einschränkungen einer iPS-basierten Zelltherapie sind zudem die hohen Kosten, ein extremer Zeitaufwand für die Generierung und eine ungewisse Ausbeute. Diese Einschränkungen führen dazu, dass eine iPS-basierte Therapie nur für chronische Erkrankungen einsatzfähig ist. Ökonomisch realisierbar, geeignet für eine breite Bevölkerung und in akuten Erkrankungen einsatzbereit gilt nur die allogene Zelltransplantation[84, 85]. Bisher stellte die immunologische Abstoßung jedoch ein entscheidendes Hindernis dar. Um diese Barriere zu überwinden, haben wir uns vorgenommen, hypoimmunogene pluripotente Stammzellen zu generieren, die keine Immunabstoßung auslösen und universell einsatzbar sind.

*Deuse T, Hu X, Gravina A, **Wang D**, Tediashvili G, De C, Thayer WO, Wahl A, Garcia JV, Reichenspurner H, Davis MM, Lanier LL, Schrepfer S. Hypoimmunogenic derivatives of induced pluripotent stem cells evade immune rejection in fully immunocompetent allogeneic recipients. **Nat Biotechnol. 2019** Mar; 37(3): 252-258. doi: 10.1038/s41587-019-0016-3.*

Dabei orientierten wir uns an einem Beispiel aus der Natur: Die Schwangerschaft. Bei einer Schwangerschaft kommt es zu keiner Immunabstoßung des Fötus, obwohl er allogene paternale Antigene besitzt.

Die Synzytiotrophoblasten stellen das Verbindungsstück zwischen maternalem Blut und fetalen Antigenen dar. Untersuchungen an Maus-Synzytiotrophoblasten zeigen, dass diese nur eine geringe Expression von Major Histocompatibility Complex (MHC) I und II aufweisen. Gleichzeitig wird CD47, ein Ig-ähnliches Membranprotein mit einer wichtigen Rolle bei der Phagozytose, vermehrt exprimiert. Wir ahmten dieses Muster nach und generierten iPS Zellen mit verminderter Expression von MHC-I und MHC-II und erhöhter Expression von CD47.

Zuerst generierten wir murine iPS Zellen (WT miPS) aus C57BL/6 Fibroblasten. Diese Zellen zeigten ein normales Mauskaryotyp, exprimierten pluripotenz-spezifische Gene und Proteine und bildeten Teratome in immundefizienten Scid-beige Mäusen. Um diese miPS Zellen immunologisch inert zu machen, führten wir ein dreistufiges Gen-Editing durch. Im ersten Schritt wurde das B2m Gen (codiert für β2-Mikroglobulin des MHC-I) mit der CRISPR/Cas Technik entfernt. B2m-/- Zellen wurden isoliert, expandiert und durchliefen eine weitere Geneditierung: Dem Knock out von Ciita (ein entscheidender Regulator für die MHC-II Expression). Im letzten Schritt wurde eine Überexpression von CD47 mit Lentiviren in den miPS Zellen induziert. Der erfolgreiche Knock-out von MHC-I und MHC-II und Überexpression von CD47 wurde mittels FACS konfirmiert.

Um die Antigenität von unserer genmodifizierten miPS Zelle zu untersuchen, transplantierten wir diese Zelle oder WT miPS Zellen in syngene C57BL/6 und allogene BALB/c Mäuse. WT miPS Zellen bildeten Teratome in syngenen C57BL/6 Tieren und wurden in allogenen BALB/c Mäusen abgestoßen. In den BALB/c Tieren kam es zur Aktivierung von Th1, Th2 Zellen und zur Bildung von IgM Antikörpern, die letztendlich zur Abstoßung der WT iPS Zellen führte. Im Gegensatz dazu lösten unsere genmodifizierten miPS Zellen (B2m-/- Ciita-/- Cd47 tg) nach Transplantation in allogenen BALB/c Mäusen keine Aktivierung des Immunsystems aus und bildeten Teratome in diesen Tieren.

Nach der „Missing-Self- Hypothese“ werden MHC-I defiziente Stammzellen von NK-Zellen eliminiert[86]. CD47 ist ein Molekül, dass eine inhibitorische Wirkung auf NK-Zellen ausübt[87]. Wir untersuchten, ob die Überexpression von CD47 miPS Zellen vor der NK-Zell Elimination schützt und verglichen dazu B2m-/- Ciita-/- Zellen mit B2m-/- Ciita-/- Cd47 tg Zellen. Im ELISPOT

Versuch mit NK-Zellen lösten B2m-/- Ciita-/- miPS Zellen eine Sekretion von IFN- γ in den Immunzellen aus, ein Zeichen für die Aktivierung des angeborenen Immunsystems. Im Gegensatz dazu führte die Stimulation mit B2m-/- Ciita-/- Cd47 tg Zellen zu keiner Aktivierung der NK- Zellen. Die ausbleibende Aktivierung vom angeborenen Immunsystem wurde in einem Tierversuch bestätigt. Unmodifizierte WT miPS Zellen wurden mit CFSE markiert und in einem Verhältnis von 50:50 mit B2m-/- Ciita-/- Zellen oder B2m-/- Ciita-/- Cd47 tg Zellen in die Bauchhöhle eines syngenen Tieres injiziert. Nach 48 Stunden wurde die Peritonealflüssigkeit aspiriert, und die aspirierten Zellen wurden analysiert. In der B2m-/- Ciita-/- Cd47 tg Gruppe blieb die Zellratio bei 50:50, da weder WT miPS noch B2m-/- Ciita-/- Cd47 tg Zellen abgestoßen werden. In der B2m-/- Ciita-/- Gruppe zeigte sich eine Verschiebung des Zellratios zugunsten von mehr WT miPS Zellen, da eine Elimination von B2m-/- Ciita-/- Zellen im Tier stattfand. Diese Versuche belegen, dass die Überexpression von CD47 die Aktivierung des angeborenen Immunsystems verhindert.

Im nächsten Schritt differenzierten wir aus der unmodifizierten WT miPS und 3-fach modifizierten B2m-/- Ciita-/- Cd47 tg miPS Zelle Herzgewebe-typische Zellen: Kardiomyozyten (iCM), Endothelzellen (iEC) und glatte Muskelzellen (iSMC). Alle differenzierten Zellen zeigten eine für die Zellart spezifische Zellmorphologie, Genexpression und Proteinexpression. Alle Zellderivate aus der unmodifierten Zelle exprimierten MHC-I und II Moleküle, jedoch in unterschiedlicher Menge. Wie erwartet war die Expression in den iECs am höchsten, da ECs als antigen-präsentierende Zellen fungieren und deutlich mehr MHC Moleküle exprimieren als CMs oder SMCs. Bei den Derivaten aus der B2m-/- Ciita-/- Cd47 tg miPS Zelle war die MHC-I und II Expression nicht vorhanden und CD47 deutlich überexprimiert.

Die Immunogenität der Zellderivate wurde im Anschluss untersucht. Nach Transplantation in ein allogenes BALB/c Tier verursachten die Derivate von der unmodifizierten miPS Zelle eine Immunaktivierung von Th1, Th2 und B-Zellen. Im Gegensatz dazu führten die Derivate von der B2m-/- Ciita-/- Cd47 tg miPS Zelle zu keiner Immunaktivierung des erworbenen Immunsystems. Auch das angeborene Immunsystem wurde nicht durch diese Zellen aktiviert.

Um das Überleben der Stammzellderivate in vivo zu verfolgen, wurden die Zellen mit Luciferase transfiziert, in ein Matrigel ins Tier injiziert und im Anschluss mittels Biolumineszenz Imaging beobachtet. Zellderivate von WT miPS Zellen überlebten den gesamten Beobachtungszeitraum (50 Tagen) im syngenen C57BL/6 Tier. Sie wurden aber in allogenen BALB/c Tieren abgestoßen. In der Umgebung der Zellen beobachteten wir infiltrierende T-Zellen, B-Zellen, Makropagen und NK-Zellen im Matrigel. Zudem ähnelte der Zytokinspiegel im Matrigel dem eines inflammatorischen Milieus. Im Gegensatz dazu zeigten Zellderivate von den B2m-/- Ciita-/- Cd47 tg miPS Zellen Langzeitüberleben in syngenen und allogenen Tieren. Diese Daten zeigen, dass nur die Zellderivate der B2m-/- Ciita-/- Cd47 tg miPS Zellen keine Immunaktivierung auslösen und im allogenen Tier nicht abgestoßen werden.

Basierend auf unseren murinen Ergebnissen strebten wir an, humane nicht-immunogene iPS Zellen zu generieren. Eine humane iPS (hiPS) Zelllinie wurde auf ihre Pluripotenz und Karyotyp getestet. Im Anschluss wurden Geneditierungen wie bei der oben beschriebenen murinen iPS Zelle durchgeführt. B2M und CIITA wurden mittels CRISPR/CAS Technologie ausgeknockt, und eine Überexpression von CD47 mittels Lentivirus induziert. Die erfolgreiche Modifikation wurde im FACS konfirmiert. Dreifach modifizierte B2M-/- CIITA-/- CD47 tg hiPS Zellen und unmodifizierte hiPS Zellen (WT-hiPS) wurden in endothel-ähnliche Zellen (hiEC) und kardiomyozyten-ähnliche Zellen (hiCM) differenziert und die erfolgreiche Differenzierung mit PCR und Immunfluoreszenzfärbungen konfirmiert. Wie bei den murinen iPS-Zellderivaten zeigten die Zellderivate aus den unmodifierten hiPS Zellen eine deutliche Expression von HLA-I und HLA-II und eine relativ geringe Expression von CD47. Besonders hiEC Zellen exprimieren als antigen-präsentierende Zellen viel HLA-I und HLA-II. Im Gegensatz dazu exprimierten die Derivate der B2M-/- CIITA-/- CD47 tg hiPS Zellen vermehrt CD47 und kein HLA-I und HLA-II.

Die Immunogenität der Zellen wurde in vivo an humanisierten NSG-SMG3 Mäusen getestet. Alle humanisierten Mäuse waren allogen zu den hiPS Zellen und deren Zellderivaten. Transplantation von unmodifizierten WT hiPS Zellen oder deren Derivate in NSG-SMG3 Mäusen riefen eine

Immunaktivierung der Th1, Th2 und B-Zellen hervor. Im Gegensatz dazu lösten B2M-/- CIITA-/- CD47 tg hiPS Zellen oder deren Derivate keine Immunantwort aus. NK-Zellen wurden auch nicht durch B2M-/- CIITA-/- CD47 tg hiPS Zellen oder deren Derivate aktiviert.

Wie bei den Mauszellversuchen untersuchten wir das Überleben der humanen Zellen in vivo mittels Biolumineszenz-Imaging. Wie erwartet überlebten die B2M-/- CIITA-/- CD47 tg hiPS Zellen in allogenen NSG-SMG3 Mäusen und bildeten Teratome. Auch modifizierten hiEC und hiCM Zellen überlebten in den Tieren und zeigten stabile Lumineszenz-Signale. Unmodifizierte WT hiPS Zellen und deren Derivate wurden hingegen abgestoßen.

Von den unterschiedlichen Zellderivaten sind hiECs am meisten immunogen. In einem letzten Versuch injizierten wir hiECs Derivate von WT hiPS oder B2M-/- CIITA-/- CD47 tg hiPS in humanisierte BLT Mäuse. Humanisierte BLT Mäuse besitzen ein humanes Immunsystem, das durch Implantation von humanen fetalen Leber- und Thymusgewebe und $CD34^+$ Zellen entstanden ist. WT hiEC Zellen lösten eine Immunaktivierung in den BLT Mäusen aus und wurden innerhalb kurzer Zeit abgestoßen. HiEC Zellen, die aus B2M-/- CIITA-/- CD47 tg hiPS differenziert wurden, riefen keine Immunaktivierung hervor und wurden nicht abgestoßen.

Zusammenfassend haben wir in dieser Studie gezeigt, dass eine kombinierte Genmodifikation mit dem Knockout von HLA-I und HLA-II und der Überexpression von CD47 die iPS Zellen und deren Zellderivate von derer Immunogenität befreit. Werden diese Zellen in allogene Empfänger transplantiert, kommt es zu keiner Immunantwort und Abstoßung. Der Einsatz von nicht-immunogenen Stammzellen kann dabei helfen, universelle Zellprodukte für die Therapie von irreversiblen kardiovaskulären Erkrankungen herzustellen.

6. Zusammenfassung

In meiner Doktorarbeit habe ich mich mit der Erforschung von vaskuloproliferativen kardiovaskulären Erkrankungen befasst. Dabei fokussierte ich mich auf die Entwicklung von geeigneten Tiermodellen, die möglichst dem klinischen Pathomechanismus und -biologie widerspiegeln. Das von mir entwickelte Veneninterpositionsmodel bietet mehrere Vorteile. Es ist einfach zu etablieren, kostengünstig, gut reproduzierbar und stellt ein passendes Tiermodel zur Erforschung von Bypassverschlüssen nach CABG-Operationen dar. Eine myointimale Hyperplasie entwickelt sich mit der Zeit und kann mittels Sonographie oder Histologie untersucht werden.

Eine weitere Erkrankung, die auf einer myointimalen Hyperplasie basiert, ist die Restenose nach Ballondilatation. Ein Aortendenudierungsmodell bei der Maus wurde erarbeitet, das die klinische Pathogenese weitgehend nachahmt. Durch Ballondilatation wird ein Gefäßschaden in der Mausaorta induziert, der zur Ausbildung einer myointimalen Hyperplasie führt. Diese setzt sich zusammen aus glatten Muskelzellen, Myofibroblasten und extrazellulären Matrixproteinen und entspricht Läsionen von restenotischen Gefäßen.

Pulmonale Hypertonie ist eine vaskuloproliferative Erkrankung, die kleine Pulmonalarterien betreffen. Diese Erkrankung ist beim Menschen gekennzeichnet durch geschlechtsspezifische Prävalenz und Mortalität. In unserer Studie haben wir festgestellt, dass diese Geschlechtsspezifität auch auf das Ratten-Semaxanib-Monotherapie-Modell zutrifft und männliche Ratten deutlich schwerere PAH entwickeln als weibliche Tiere. Die Wahl des Tiergeschlechts beim Tierversuch kann einen starken Einfluss auf das Ergebnis ausüben und sollte mit Bedacht gewählt und genau in wissenschaftlichen Arbeiten angegeben werden.

Kommt es im Rahmen von vaskuloproliferativen Erkrankungen zu einer ischämischen Kardiomyopathie mit Herzinsuffizienz, bleibt oftmals nur eine Herztransplantation als Therapie übrig. Jedoch ist der Langzeiterfolg der Herztransplantation durch die koronare Transplantatvaskulopathie limitiert. CAV ist eine Sonderform der myointimalen Hyperplasie, die durch eine chronische Immunreaktion ausgelöst wird und kaum therapierbar ist. In meiner Arbeit demonstrierte ich, dass Thalidomid ein effektiver

Immunmodulator ist und eine Dedifferenzierung von VSMCs inhibiert und damit die Entwicklung einer CAV verhindert. Der Einsatz von Thalidomid ist nebenwirkungsfrei und stellt somit eine aussichtsreiche zukünftige Therapieoption dar.

Durch den Organspendermangel ist die Herztransplantation als Therapieoption stark eingeschränkt. Als vielversprechende Alternative gilt die regenerative Zelltherapie, die das geschädigte Gewebe durch Stammzellen regeneriert und ersetzt. Autologe iPS Zellen können zu Kardiomyozyten differenziert werden und sind damit für eine Zelltransplantationstherapie geeignet. In meiner Arbeit untersuchte ich die Immunogenität von iPS Zellen und habe festgestellt, dass während der Langzeitzellkultur es zu Mutationen im mitochondrialen DNA der Zellen kommt. Dies führt zu einer Ansammlung von SNPs mit Bildung von Neoantigenen. Diese mitochondrialen Neoantigene lösen eine hoch spezifische Immunantwort aus, die zur Abstoßung des Zelltransplantats führt.

Eine Alternative zu autologen iPS Zellen ist die Generierung einer hypoimmunogenen Stammzelle, die bei allen Patienten eingesetzt werden kann. Genetischer Knock-out von HLA-I und HLA-II sowie eine Überexpression von CD47 führen zur Hypoimmunogenität der Stammzelle. Die Hypoimmunogenität bleibt auch nach Differenzierung zu Endothelzellen oder Kardiomyozyten erhalten. Die Transplantation von hypoimmunogenen Stammzellen oder deren Derivate in allogene Empfänger löste im Tiermodell keine Immunantwort aus, und die Zellen werden nicht abgestoßen. Hypoimmunogene Stammzellen stellen somit eine vielversprechende Ressource für die regenerative Zelltherapie dar.

Zusammenfassend eröffnen meine dargestellten Arbeiten neue Möglichkeiten, vaskuloproliferative Erkrankungen zu untersuchen und beinhalten neue Ansätze im Bereich der pharmako- und zellbasierten Therapie.

7. Abstract

I investigated in my PhD thesis vasculoproliferative diseases. Particularly, I focused on the development of suitable animals models that reflect the pathomechanisms and –biology of clinical disease. The vein interposition model has many advantages. It is inexpensive, reproducible and can be easily established. It is very well suited to investigate vein graft patency loss after venous coronary artery bypass grafting (CABG). Myointimal hyperplasia, which is the main cause of vein graft failure, develops rapidly over time and can be examined with duplex sonography or histopathology.
Another disease that bases on myointimal hyperplasia is vascular restenosis after balloon dilatation. An aortic denudation model was developed in the mouse that closely mimicked the clinical pathogenesis. A balloon catheter was inserted into the abdominal aorta and then dilated in order to induce vascular damage. Myointimal hyperplasia develops in the area of vascular damage and is composed of smooth muscle cells, myofibroblasts and extracellular matrix proteins. This corresponds to lesions of restenotic vessels.

Pulmonary hypertension is a vasculoproliferative disease affecting small pulmonary arteries. This disease is characterized by gender specific prevalence and mortality. In my study, I have found out that sex differences also apply to the rat semaxanib monotherapy model. Male rats develop significantly more severe PAH than female animals. The choice of animal sex in animal experiments can have a strong influence on the result. Therefore it should be chosen carefully and stated precisely in scientific papers.
If vasculoproliferative diseases remain untreated, it can lead to ischemic cardiomyopathy and heart failure. The only remaining treatment option is often heart transplantation. However, the long-term success of heart transplantation is limited by coronary graft vasculopathy. CAV is a special form of myointimal hyperplasia, which is triggered by a chronic immune reaction and is hardly treatable. In my work I have demonstrated that thalidomide is an effective immunomodulator and inhibits dedifferentiation of VSMCs and thus prevents the development of CAV. Thalidomide is free of

side effects and is therefore a promising new therapeutic strategy against CAV.

Due to the lack of donor organs, heart transplantation is a limited therapy option. A promising alternative is regenerative cell therapy, which replaces the damaged tissue with stem cells. Autologous iPS cells can be differentiated into cardiomyocytes and are therefore suitable for cell transplantation therapy. In my work, I have examined the immunogenicity of iPS cells and found out that mutations of mitochondrial DNA occur in cells during long-term cell culture. This leads to an accumulation of SNPs with the formation of neoantigens. These mitochondrial neoantigens trigger a highly specific immune response that leads to rejection of the cell graft.

An alternative to autologous iPS cells is the generation of a hypoimmunogenic stem cell that can be used for all patients. Genetic knock-out of HLA-I and HLA-II as well as overexpression of CD47 lead to hypoimmunogenicity of the stem cell. Hypoimmunogeneity is retained even after differentiation into endothelial cells or cardiomyocytes. Transplantation of hypoimmunogenic stem cells or their derivatives into allogeneic recipients does not trigger an immune response and the cells are not rejected. Hypoimmunogenic stem cells are therefore a promising resource for regenerative cell therapy.

In conclusion, my works open up new opportunities to investigate vasculoproliferative diseases and provide new therapeutic approaches in the field of pharmaco- and cell-based therapy.

8. Literaturverzeichnis

1. Mendis S, Puska P and Norrving B. *Global atlas on cardiovascular disease prevention and control*. Geneva: World Health Organization; 2011.
2. Mortality GBD and Causes of Death C. Global, regional, and national life expectancy, all-cause mortality, and cause-specific mortality for 249 causes of death, 1980-2015: a systematic analysis for the Global Burden of Disease Study 2015. *Lancet*. 2016;388:1459-1544.
3. Mortality GBD and Causes of Death C. Global, regional, and national age-sex specific all-cause and cause-specific mortality for 240 causes of death, 1990-2013: a systematic analysis for the Global Burden of Disease Study 2013. *Lancet*. 2015;385:117-71.
4. Dzau VJ, Braun-Dullaeus RC and Sedding DG. Vascular proliferation and atherosclerosis: new perspectives and therapeutic strategies. *Nat Med*. 2002;8:1249-56.
5. Schermuly R and Grimminger F. [Update in basic research in the therapy of pulmonary arterial hypertension]. *Dtsch Med Wochenschr*. 2008;133 Suppl 6:S170-2.
6. Mackay J, and George A. Mensah. *The atlas of heart disease and stroke.*: World Health Organization (WHO); 2004.
7. Denner LA and Dixon RAF. Chapter 7. Vascular Proliferative Disease. In: J. A. Bristol, ed. *Annual Reports in Medicinal Chemistry*: Academic Press; 1995(30): 61-70.
8. Charron T, Nili N and Strauss BH. The cell cycle: a critical therapeutic target to prevent vascular proliferative disease. *Can J Cardiol*. 2006;22 Suppl B:41B-55B.
9. Owens GK, Kumar MS and Wamhoff BR. Molecular regulation of vascular smooth muscle cell differentiation in development and disease. *Physiol Rev*. 2004;84:767-801.
10. Sigwart U, Puel J, Mirkovitch V, Joffre F and Kappenberger L. Intravascular stents to prevent occlusion and restenosis after transluminal angioplasty. *N Engl J Med*. 1987;316:701-6.
11. Poon M, Badimon JJ and Fuster V. Overcoming restenosis with sirolimus: from alphabet soup to clinical reality. *Lancet*. 2002;359:619-22.
12. Serruys PW, Luijten HE, Beatt KJ, Geuskens R, de Feyter PJ, van den Brand M, Reiber JH, ten Katen HJ, van Es GA and Hugenholtz PG. Incidence of restenosis after successful coronary angioplasty: a time-related phenomenon. A quantitative angiographic study in 342 consecutive patients at 1, 2, 3, and 4 months. *Circulation*. 1988;77:361-71.
13. Nobuyoshi M, Kimura T, Nosaka H, Mioka S, Ueno K, Yokoi H, Hamasaki N, Horiuchi H and Ohishi H. Restenosis after successful percutaneous transluminal coronary angioplasty: serial angiographic follow-up of 229 patients. *J Am Coll Cardiol*. 1988;12:616-23.
14. Sriram V and Patterson C. Cell cycle in vasculoproliferative diseases: potential interventions and routes of delivery. *Circulation*. 2001;103:2414-9.
15. Fischman DL, Leon MB, Baim DS, Schatz RA, Savage MP, Penn I, Detre K, Veltri L, Ricci D, Nobuyoshi M and et al. A randomized comparison of coronary-stent placement and balloon angioplasty in the treatment of coronary

artery disease. Stent Restenosis Study Investigators. *N Engl J Med*. 1994;331:496-501.
16. Elezi S, Kastrati A, Neumann FJ, Hadamitzky M, Dirschinger J and Schomig A. Vessel size and long-term outcome after coronary stent placement. *Circulation*. 1998;98:1875-80.
17. Hoffmann R, Mintz GS, Dussaillant GR, Popma JJ, Pichard AD, Satler LF, Kent KM, Griffin J and Leon MB. Patterns and mechanisms of in-stent restenosis. A serial intravascular ultrasound study. *Circulation*. 1996;94:1247-54.
18. Bennett MR. In-stent stenosis: pathology and implications for the development of drug eluting stents. *Heart*. 2003;89:218-24.
19. van Lammeren GW, Peeters W, de Vries JP, de Kleijn DP, De Borst GJ, Pasterkamp G and Moll FL. Restenosis after carotid surgery: the importance of clinical presentation and preoperative timing. *Stroke*. 2011;42:965-71.
20. Volteas N, Labropoulos N, Leon M, Kalodiki E, Chan P and Nicolaides AN. Risk factors associated with recurrent carotid stenosis. *Int Angiol*. 1994;13:143-7.
21. Zierler RE. Vascular surgery without arteriography: use of Duplex ultrasound. *Cardiovasc Surg*. 1999;7:74-82.
22. Yamada K, Kishiguchi T, Ito M, Otsuki H, Kohmura E, Taneda M and Hayakawa T. Restenosis following carotid endarterectomy--clinical profiles and pathological findings. *Neurol Med Chir (Tokyo)*. 1998;38 Suppl:284-8.
23. Goldman S, Zadina K, Moritz T, Ovitt T, Sethi G, Copeland JG, Thottapurathu L, Krasnicka B, Ellis N, Anderson RJ, Henderson W and Group VACS. Long-term patency of saphenous vein and left internal mammary artery grafts after coronary artery bypass surgery: results from a Department of Veterans Affairs Cooperative Study. *J Am Coll Cardiol*. 2004;44:2149-56.
24. Beijk M and Harskamp R. Treatment of Coronary Artery Bypass Graft Failure. In: W. S. Aronow, ed. *Artery Bypass* IntechOpen; March 13th 2013.
25. Lund LH, Edwards LB, Kucheryavaya AY, Benden C, Christie JD, Dipchand AI, Dobbels F, Goldfarb SB, Levvey BJ, Meiser B, Yusen RD, Stehlik J, International Society of H and Lung T. The registry of the International Society for Heart and Lung Transplantation: thirty-first official adult heart transplant report--2014; focus theme: retransplantation. *J Heart Lung Transplant*. 2014;33:996-1008.
26. Costello JP, Mohanakumar T and Nath DS. Mechanisms of chronic cardiac allograft rejection. *Tex Heart Inst J*. 2013;40:395-9.
27. Cooley DA. In memoriam. Tribute to Rene Favaloro, pioneer of coronary bypass. *Tex Heart Inst J*. 2000;27:231-2.
28. Guyton RA. Coronary artery bypass is superior to drug-eluting stents in multivessel coronary artery disease. *Ann Thorac Surg*. 2006;81:1949-57.
29. Fitzgibbon GM, Kafka HP, Leach AJ, Keon WJ, Hooper GD and Burton JR. Coronary bypass graft fate and patient outcome: angiographic follow-up of 5,065 grafts related to survival and reoperation in 1,388 patients during 25 years. *J Am Coll Cardiol*. 1996;28:616-26.
30. O'Brien JE, Jr., Shi Y, Fard A, Bauer T, Zalewski A and Mannion JD. Wound healing around and within saphenous vein bypass grafts. *J Thorac Cardiovasc Surg*. 1997;114:38-45.

31. El-Kurdi MS, Soletti L, Nieponice A, Abuin G, Gross C, Rousselle S, Greisler H and McGrath J. Ovine femoral artery bypass grafting using saphenous vein: a new model. *J Surg Res*. 2015;193:458-69.
32. Yuda A, Takai S, Jin D, Sawada Y, Nishimoto M, Matsuyama N, Asada K, Kondo K, Sasaki S and Miyazaki M. Angiotensin II receptor antagonist, L-158,809, prevents intimal hyperplasia in dog grafted veins. *Life Sci*. 2000;68:41-8.
33. McCann RL, Hagen PO and Fuchs JC. Aspirin and dipyridamole decrease intimal hyperplasia in experimental vein grafts. *Ann Surg*. 1980;191:238-43.
34. Thomas AC. Animal models for studying vein graft failure and therapeutic interventions. *Curr Opin Pharmacol*. 2012;12:121-6.
35. Yu P, Nguyen BT, Tao M, Campagna C and Ozaki CK. Rationale and practical techniques for mouse models of early vein graft adaptations. *J Vasc Surg*. 2010;52:444-52.
36. Serruys PW, de Bruyne B, Carlier S, Sousa JE, Piek J, Muramatsu T, Vrints C, Probst P, Seabra-Gomes R, Simpson I, Voudris V, Gurne O, Pijls N, Belardi J, van Es GA, Boersma E, Morel MA and van Hout B. Randomized comparison of primary stenting and provisional balloon angioplasty guided by flow velocity measurement. Doppler Endpoints Balloon Angioplasty Trial Europe (DEBATE) II Study Group. *Circulation*. 2000;102:2930-7.
37. Serruys PW, de Jaegere P, Kiemeneij F, Macaya C, Rutsch W, Heyndrickx G, Emanuelsson H, Marco J, Legrand V, Materne P and et al. A comparison of balloon-expandable-stent implantation with balloon angioplasty in patients with coronary artery disease. Benestent Study Group. *N Engl J Med*. 1994;331:489-95.
38. Hamm C and Fleck E. *Deutscher Herzbericht 2016*: Deutsche Herzstiftung e.V.; 2016.
39. Karas SP, Gravanis MB, Santoian EC, Robinson KA, Anderberg KA and King SB, 3rd. Coronary intimal proliferation after balloon injury and stenting in swine: an animal model of restenosis. *J Am Coll Cardiol*. 1992;20:467-74.
40. Lafont A and Faxon D. Why do animal models of post-angioplasty restenosis sometimes poorly predict the outcome of clinical trials? *Cardiovasc Res*. 1998;39:50-9.
41. Mason RG and Read MS. Some species differences in fibrinolysis and blood coagulation. *J Biomed Mater Res*. 1971;5:121-8.
42. Lindner V, Fingerle J and Reidy MA. Mouse model of arterial injury. *Circ Res*. 1993;73:792-6.
43. Simon DI, Dhen Z, Seifert P, Edelman ER, Ballantyne CM and Rogers C. Decreased neointimal formation in Mac-1(-/-) mice reveals a role for inflammation in vascular repair after angioplasty. *J Clin Invest*. 2000;105:293-300.
44. Sata M, Maejima Y, Adachi F, Fukino K, Saiura A, Sugiura S, Aoyagi T, Imai Y, Kurihara H, Kimura K, Omata M, Makuuchi M, Hirata Y and Nagai R. A mouse model of vascular injury that induces rapid onset of medial cell apoptosis followed by reproducible neointimal hyperplasia. *J Mol Cell Cardiol*. 2000;32:2097-104.
45. Moroi M, Zhang L, Yasuda T, Virmani R, Gold HK, Fishman MC and Huang PL. Interaction of genetic deficiency of endothelial nitric oxide, gender,

and pregnancy in vascular response to injury in mice. *J Clin Invest*. 1998;101:1225-32.
46. Krishnan P, Purushothaman KR, Purushothaman M, Turnbull IC, Tarricone A, Vasquez M, Jain S, Baber U, Lascano RA, Kini AS, Sharma SK and Moreno PR. Enhanced neointimal fibroblast, myofibroblast content and altered extracellular matrix composition: Implications in the progression of human peripheral artery restenosis. *Atherosclerosis*. 2016;251:226-233.
47. Karas SP, Santoian EC and Gravanis MB. Restenosis following coronary angioplasty. *Clin Cardiol*. 1991;14:791-801.
48. Chang C-C and Ong E-T. Coronary Restenosis. *Acta Cardiol Sin*. 2005;21:177-89.
49. Galie N, Humbert M, Vachiery JL, Gibbs S, Lang I, Torbicki A, Simonneau G, Peacock A, Vonk Noordegraaf A, Beghetti M, Ghofrani A, Gomez Sanchez MA, Hansmann G, Klepetko W, Lancellotti P, Matucci M, McDonagh T, Pierard LA, Trindade PT, Zompatori M and Hoeper M. 2015 ESC/ERS Guidelines for the diagnosis and treatment of pulmonary hypertension: The Joint Task Force for the Diagnosis and Treatment of Pulmonary Hypertension of the European Society of Cardiology (ESC) and the European Respiratory Society (ERS): Endorsed by: Association for European Paediatric and Congenital Cardiology (AEPC), International Society for Heart and Lung Transplantation (ISHLT). *Eur Respir J*. 2015;46:903-75.
50. Yaoita N, Satoh K and Shimokawa H. Novel Therapeutic Targets of Pulmonary Hypertension. *Arterioscler Thromb Vasc Biol*. 2016;36:e97-e102.
51. Schäfers H-J. *Pulmonale Hypertonie*. Blackwell Wissenschafts-Verlag Berlin Wien 2001.
52. Shapiro S, Traiger GL, Turner M, McGoon MD, Wason P and Barst RJ. Sex differences in the diagnosis, treatment, and outcome of patients with pulmonary arterial hypertension enrolled in the registry to evaluate early and long-term pulmonary arterial hypertension disease management. *Chest*. 2012;141:363-373.
53. Tofovic SP. Estrogens and development of pulmonary hypertension: interaction of estradiol metabolism and pulmonary vascular disease. *J Cardiovasc Pharmacol*. 2010;56:696-708.
54. Tofovic SP, Zhang X, Jackson EK, Dacic S and Petrusevska G. 2-Methoxyestradiol mediates the protective effects of estradiol in monocrotaline-induced pulmonary hypertension. *Vascul Pharmacol*. 2006;45:358-67.
55. Song J, Wan Y, Rolfe BE, Campbell JH and Campbell GR. Effect of estrogen on vascular smooth muscle cells is dependent upon cellular phenotype. *Atherosclerosis*. 1998;140:97-104.
56. Sivritas D, Becher MU, Ebrahimian T, Arfa O, Rapp S, Bohner A, Mueller CF, Umemura T, Wassmann S, Nickenig G and Wassmann K. Antiproliferative effect of estrogen in vascular smooth muscle cells is mediated by Kruppel-like factor-4 and manganese superoxide dismutase. *Basic Res Cardiol*. 2011;106:563-75.
57. Anversa P, Li P, Zhang X, Olivetti G and Capasso JM. Ischaemic myocardial injury and ventricular remodelling. *Cardiovasc Res*. 1993;27:145-57.
58. DiBardino DJ. The history and development of cardiac transplantation. *Tex Heart Inst J*. 1999;26:198-205.

59. Stehlik J, Edwards LB, Kucheryavaya AY, Benden C, Christie JD, Dipchand AI, Dobbels F, Kirk R, Rahmel AO, Hertz MI, International Society of H and Lung T. The Registry of the International Society for Heart and Lung Transplantation: 29th official adult heart transplant report--2012. *J Heart Lung Transplant*. 2012;31:1052-64.
60. Wilhelm MJ. Long-term outcome following heart transplantation: current perspective. *J Thorac Dis*. 2015;7:549-51.
61. Tonsho M, Michel S, Ahmed Z, Alessandrini A and Madsen JC. Heart transplantation: challenges facing the field. *Cold Spring Harb Perspect Med*. 2014;4.
62. Chih S, Chong AY, Mielniczuk LM, Bhatt DL and Beanlands RS. Allograft Vasculopathy: The Achilles' Heel of Heart Transplantation. *J Am Coll Cardiol*. 2016;68:80-91.
63. Ramzy D, Rao V, Brahm J, Miriuka S, Delgado D and Ross HJ. Cardiac allograft vasculopathy: a review. *Can J Surg*. 2005;48:319-27.
64. Schmauss D and Weis M. Cardiac allograft vasculopathy: recent developments. *Circulation*. 2008;117:2131-41.
65. Franks ME, Macpherson GR and Figg WD. Thalidomide. *Lancet*. 2004;363:1802-11.
66. Matthews SJ and McCoy C. Thalidomide: a review of approved and investigational uses. *Clin Ther*. 2003;25:342-95.
67. Sheskin J. Thalidomide in the Treatment of Lepra Reactions. *Clin Pharmacol Ther*. 1965;6:303-6.
68. Singhal S, Mehta J, Desikan R, Ayers D, Roberson P, Eddlemon P, Munshi N, Anaissie E, Wilson C, Dhodapkar M, Zeddis J and Barlogie B. Antitumor activity of thalidomide in refractory multiple myeloma. *N Engl J Med*. 1999;341:1565-71.
69. Lim SH, McWhannell A, Vora AJ and Boughton BJ. Successful treatment with thalidomide of acute graft-versus-host disease after bone-marrow transplantation. *Lancet*. 1988;1:117.
70. Stubbendorff M, Deuse T, Hammel A, Robbins RC, Reichenspurner H and Schrepfer S. Orthotopic aortic transplantation: a rat model to study the development of chronic vasculopathy. *J Vis Exp*. 2010.
71. Carr MW, Roth SJ, Luther E, Rose SS and Springer TA. Monocyte chemoattractant protein 1 acts as a T-lymphocyte chemoattractant. *Proc Natl Acad Sci U S A*. 1994;91:3652-6.
72. Xu LL, Warren MK, Rose WL, Gong W and Wang JM. Human recombinant monocyte chemotactic protein and other C-C chemokines bind and induce directional migration of dendritic cells in vitro. *J Leukoc Biol*. 1996;60:365-71.
73. Suzuki J, Isobe M Fau - Kawauchi M, Kawauchi M Fau - Endoh M, Endoh M Fau - Amano J, Amano J Fau - Takamoto S and Takamoto S. Altered expression of matrix metalloproteinases and tissue inhibitors of metalloproteinases in acutely rejected myocardium and coronary arteriosclerosis in cardiac allografts of nonhuman primates.
74. Welz A, Cremer J and Gummert J. Grundlegende Informationen zum Thema Herztransplantation.
75. Hirschi KK, Li S and Roy K. Induced pluripotent stem cells for regenerative medicine. *Annu Rev Biomed Eng*. 2014;16:277-94.

76. Liu X, Li W, Fu X and Xu Y. The Immunogenicity and Immune Tolerance of Pluripotent Stem Cell Derivatives. *Front Immunol*. 2017;8:645.
77. Yakes FM and Van Houten B. Mitochondrial DNA damage is more extensive and persists longer than nuclear DNA damage in human cells following oxidative stress. *Proc Natl Acad Sci U S A*. 1997;94:514-9.
78. Brown WM, George M, Jr. and Wilson AC. Rapid evolution of animal mitochondrial DNA. *Proc Natl Acad Sci U S A*. 1979;76:1967-71.
79. Zastawny TH, Dabrowska M, Jaskolski T, Klimarczyk M, Kulinski L, Koszela A, Szczesniewicz M, Sliwinska M, Witkowski P and Olinski R. Comparison of oxidative base damage in mitochondrial and nuclear DNA. *Free Radic Biol Med*. 1998;24:722-5.
80. He Y, Wu J, Dressman DC, Iacobuzio-Donahue C, Markowitz SD, Velculescu VE, Diaz LA, Jr., Kinzler KW, Vogelstein B and Papadopoulos N. Heteroplasmic mitochondrial DNA mutations in normal and tumour cells. *Nature*. 2010;464:610-4.
81. Kang E, Wang X, Tippner-Hedges R, Ma H, Folmes CD, Gutierrez NM, Lee Y, Van Dyken C, Ahmed R, Li Y, Koski A, Hayama T, Luo S, Harding CO, Amato P, Jensen J, Battaglia D, Lee D, Wu D, Terzic A, Wolf DP, Huang T and Mitalipov S. Age-Related Accumulation of Somatic Mitochondrial DNA Mutations in Adult-Derived Human iPSCs. *Cell Stem Cell*. 2016;18:625-36.
82. Deuse T, Wang D, Stubbendorff M, Itagaki R, Grabosch A, Greaves LC, Alawi M, Grunewald A, Hu X, Hua X, Velden J, Reichenspurner H, Robbins RC, Jaenisch R, Weissman IL and Schrepfer S. SCNT-derived ESCs with mismatched mitochondria trigger an immune response in allogeneic hosts. *Cell Stem Cell*. 2015;16:33-8.
83. Miyazono F, Schneider PM, Metzger R, Warnecke-Eberz U, Baldus SE, Dienes HP, Aikou T and Hoelscher AH. Mutations in the mitochondrial DNA D-Loop region occur frequently in adenocarcinoma in Barrett's esophagus. *Oncogene*. 2002;21:3780-3.
84. Smith DM. Assessing commercial opportunities for autologous and allogeneic cell-based products. *Regen Med*. 2012;7:721-32.
85. Lipsitz YY, Bedford P, Davies AH, Timmins NE and Zandstra PW. Achieving Efficient Manufacturing and Quality Assurance through Synthetic Cell Therapy Design. *Cell Stem Cell*. 2017;20:13-17.
86. Wang D, Quan Y, Yan Q, Morales JE and Wetsel RA. Targeted Disruption of the beta2-Microglobulin Gene Minimizes the Immunogenicity of Human Embryonic Stem Cells. *Stem Cells Transl Med*. 2015;4:1234-45.
87. Kim MJ, Lee JC, Lee JJ, Kim S, Lee SG, Park SW, Sung MW and Heo DS. Association of CD47 with natural killer cell-mediated cytotoxicity of head-and-neck squamous cell carcinoma lines. *Tumour Biol*. 2008;29:28-34.

9. Erklärung des Eigenanteiles an der Publikation

1. **Wang D**, Tediashvili G, Pecha S, Reichenspurner H, Deuse T, Schrepfer S. *Vein Interposition Model: A Suitable Model to Study Bypass Graft Patency*. **J Vis Exp. 2017**;(119).

Folgende Arbeiten wurden von mir in der obengenannten Publikation geleistet:

- Planung und Design der Studie in Verständigung mit Prof. Sonja Schrepfer
- Durchführung und Auswertung der histopathologischen Versuche
- Statistische Auswertung
- Erstellung der Abbildungen
- Verfassung des Manuskripts

Folgende Anteile wurden von den Co-Autoren und Mitarbeitern geleistet:

- Durchführung der Operation am Tier
- Durchführung der Duplex Sonographie und Biolumineszenz Imaging
- Korrektur und Einreichung des Manuskripts beim Journal

2. Tediashvili G, **Wang D**, Reichenspurner H, Deuse T, Schrepfer S. *Balloon-based Injury to Induce Myointimal Hyperplasia in the Mouse Abdominal Aorta.* **J Vis Exp. 2018** Feb 7;(132). doi: 10.3791/56477.

Folgende Arbeiten wurden von mir in der obengenannten Publikation geleistet:

- Durchführung und Auswertung der histopathologischen und Immunfluoreszenz Versuche
- Erstellung der Abbildungen
- Überarbeitung und fachliche Revision des Manuskripts

Folgende Anteile wurden von den Co-Autoren und Mitarbeitern geleistet:

- Design und Planung der Studie

- Durchführung der Operation am Tier
- Erstellung des Manuskripts und Einreichung beim Journal

3. Guihaire J, Deuse T, **Wang D**, Fadel E, Reichenspurner H, Schrepfer S. Sex *Differences in Immunology: More Severe Development of Experimental Pulmonary Hypertension in Male Rats Exposed to Vascular Endothelial Growth Factor Receptor Blockade*. **Biomed Res Int. 2015**;2015:765292.

Folgende Arbeiten wurden von mir in der obengenannten Publikation geleistet:

- Durchführung und Auswertung der Immunfluoreszenz und Konfokalmikroskop Versuche
- Überarbeitung und Korrektur des Manuskripts

Folgende Anteile wurden von den Co-Autoren und Mitarbeitern geleistet:

- Design, Planung und Finanzierung der Studie
- Durchführung der Tierversuche
- Erstellung des Manuskripts und Einreichung beim Journal

4. Miller KK, **Wang D**, Hu X, Hua X, Deuse T, Neofytou E, Renne T, Velden J, Reichenspurner H, Schrepfer S, Bernstein D. *Thalidomide treatment prevents chronic graft rejection after aortic transplantation in rats - an experimental study.* **Transpl Int. 2017** Nov;30(11):1181-1189. doi: 10.1111/tri.13004.

Folgende Arbeiten wurden von mir in der obengenannten Publikation geleistet:

- Durchführung und Auswertung der Immunfluoreszenz und Konfokalmikroskop Versuche
- Statistische Auswertung und Erstellung der Abbildungen zum Aspekt der Dedifferenzierung von glatten Muskelzellen

- Überarbeitung und Korrektur des Manuskripts

Folgende Anteile wurden von den Co-Autoren und Mitarbeitern geleistet:

- Design, Planung und Finanzierung der Studie
- Durchführung der Tier- und Immunbiologischen Versuche
- Erstellung des Manuskripts und Einreichung beim Journal

5. Deuse T, Hu X, Agbor-Enoh S, Koch M, Spitzer MH, Gravina A, Alawi M, Marishta A, Peters B, Kosaloglu-Yalcin Z, Yang Y, Rajalingam R, **Wang D**, Nashan B, Kiefmann R, Reichenspurner H, Valantine H, Weissman IL, Schrepfer S. *De novo mutations in mitochondrial DNA of iPSCs produce immunogenic neoepitopes in mice and humans*. **Nat Biotechnol**. 2019 Aug 19. doi: 10.1038/s41587-019-0227-7

Folgende Arbeiten wurden von mir in der obengenannten Publikation geleistet:

- Durchführung und Auswertung der Immunfluoreszenz und Konfokalmikroskop Versuche
- Überarbeitung und Korrektur des Manuskripts

Folgende Anteile wurden von den Co-Autoren und Mitarbeitern geleistet:

- Design, Planung und Finanzierung der Studie
- Durchführung der immunbiologischen, molekularbiologischen, Biolumineszenz- und Sequenzierungsversuche
- Erstellung des Manuskripts und Einreichung beim Journal

6. Deuse T, Hu X, Gravina A, **Wang D**, Tediashvili G, De C, Thayer WO, Wahl A, Garcia JV, Reichenspurner H, Davis MM, Lanier LL, Schrepfer S. *Hypoimmunogenic derivatives of induced pluripotent stem cells evade immune rejection in fully immunocompetent allogeneic recipients*. **Nat Biotechnol. 2019** Mar;37(3):252-258. doi:

10.1038/s41587-019-0016-3.

Folgende Arbeiten wurden von mir in der obengenannten Publikation geleistet:

- Durchführung und Auswertung der histopathologischen Versuche
- Durchführung und Auswertung der Immunfluoreszenz und Konfokalmikroskop Versuche
- Durchführung und Auswertung der immunzytologischen Versuche
- Überarbeitung und Korrektur des Manuskripts

Folgende Anteile wurden von den Co-Autoren und Mitarbeitern geleistet:

- Design, Planung und Finanzierung der Studie
- Durchführung der immunbiologischen, molekularbiologischen, Biolumineszenz- und Sequenzierungsversuche
- Erstellung des Manuskripts und Einreichung beim Journal

10. Appendix

10.1. Abkürzungen

glatte Gefäßmuskelzellen (VSMC)
Koronare Herzerkrankung (KHK)
Perkutane transluminale Angioplastie (PTA)
Perkutanen transluminalen Koronarangioplastie (PTCA)
Perkutane Kathetherintervention (PCI)
Koronararterielle Bypass-Operation (CABG)
Pulmonale Hypertonie (PAH)
mittleren pulmonal arteriellen Drucks (mPAP)
Herztransplantation (HTX)
Periphere mononukleäre Zellen (PBMC)
Einzelnukleotid-Polymorphismus (SNP)
Induzierte Pluripotente Stammzelle (iPS)
Murine induzierte Pluripotente Stammzellen (miPS)
Humane induzierte Pluripotente Stammzellen (hiPS)
Aminosäuredifferenze (AA)
Mitochondriale DNA (mtDNA)
Major Histocompatibility Complex (MHC)
Koronare Transplantatvaskulopathie (CAV)

10.2. Publikationen

1. **Wang D**, Tediashvili G, Hu X, Gravina A, Marcus SG, Zhang H, Olgin JE, Deuse T, Schrepfer S. A Cryoinjury Model to Study Myocardial Infarction in the Mouse. **J Vis Exp. 2019** (151), e59958, doi:10.3791/59958 (2019)
2. Deuse T, Hu X, Agbor-Enoh S, Koch M, Spitzer MH, Gravina A, Alawi M, Marishta A, Peters B, Kosaloglu-Yalcin Z, Yang Y, Rajalingam R, **Wang D**, Nashan B, Kiefmann R, Reichenspurner H, Valantine H, Weissman IL, Schrepfer S. De novo mutations in mitochondrial DNA of iPSCs produce immunogenic neoepitopes in mice and humans. **Nat Biotechnol**. 2019 Aug 19. doi: 10.1038/s41587-019-0227-7
3. Deuse T, Hu X, Gravina A, **Wang D**, Tediashvili G, De C, Thayer WO, Wahl A, Garcia JV, Reichenspurner H, Davis MM, Lanier LL, Schrepfer S. Hypoimmunogenic derivatives of induced pluripotent stem cells evade immune rejection in fully immunocompetent allogeneic recipients. **Nat Biotechnol. 2019** Mar;37(3):252-258. doi: 10.1038/s41587-019-0016-3.
4. Tediashvili G, **Wang D**, Reichenspurner H, Deuse T, Schrepfer S. Balloon-based Injury to Induce Myointimal Hyperplasia in the Mouse Abdominal Aorta. **J Vis Exp. 2018** Feb 7;(132). doi: 10.3791/56477.
5. Miller KK, **Wang D**, Hu X, Hua X, Deuse T, Neofytou E, Renne T, Velden J, Reichenspurner H, Schrepfer S, Bernstein D. Thalidomide treatment prevents chronic graft rejection after aortic transplantation in rats - an experimental study. **Transpl Int. 2017** Nov;30(11):1181-1189. doi: 10.1111/tri.13004.
6. **Wang D**. Neue Mechanismen zur Verhinderung der myointimalen Hyperplasie. **Z Herz- Thorax- Gefäßchir 2017**. doi:10.1007/s00398-017-0153-2
7. **Wang D**, Tediashvili G, Pecha S, Reichenspurner H, Deuse T, Schrepfer S. Vein Interposition Model: A Suitable Model to Study Bypass Graft Patency. **J Vis Exp. 2017**;(119).
8. Guihaire J, Deuse T, **Wang D**, Fadel E, Reichenspurner H, Schrepfer S. Sex Differences in Immunology: More Severe Development of Experimental Pulmonary Hypertension in Male Rats Exposed to Vascular Endothelial Growth Factor Receptor Blockade. **Biomed Res Int. 2015**;2015:765292.
9. **Wang D**, Deuse T, Stubbendorff M, Chernogubova E, Erben RG, Eken SM, Jin H, Li Y, Busch A, Heeger CH, Behnisch B, Reichenspurner H, Robbins RC, Spin JM, Tsao PS, Maegdefessel L, Schrepfer S. Local MicroRNA Modulation Using a Novel Anti-miR-21-Eluting Stent Effectively Prevents Experimental In-Stent Restenosis. **Arterioscler Thromb Vasc Biol. 2015**;35(9):1945-53.

10. Schmidt-Lucke C, Zobel T, Schrepfer S, Kuhl U, **Wang D**, Klingel K, Becher PM, Fechner H, Pozzuto T, Van Linthout S, Lassner D, Spillmann F, Escher F, Holinski S, Volk HD, Schultheiss HP, Tschope C. Impaired Endothelial Regeneration Through Human Parvovirus B19-Infected Circulating Angiogenic Cells in Patients With Cardiomyopathy. **J Infect Dis. 2015**. pii: jiv178.
11. Deuse T, **Wang D**, Stubbendorff M, Itagaki R, Grabosch A, Greaves LC, Alawi M, Gruenewald A, Hu X, Hua X, Velden J, Reichenspurner H, Robbins RC, Jaenisch R, Weissman IL, Schrepfer S. SCNT-derived ESCs with mismatched mitochondria trigger an immune response in allogeneic hosts. **Cell Stem Cell 2015**;16(1):33-8.
12. Deuse T, Hua X, **Wang D**, Maegdefessel L, Heeren J, Scheja L, Bolanos JP, Rakovic A, Spin J, Stubbendorff M, Ikeno F, Länger F, Zeller T, Schulte-Uentrop L, Stoehr A, Itagaki R, Haddad F, Eschenhagen T, Blankenberg S, Kiefmann R, Reichenspurner H, Velden J, Klein C, Yeung A, Robbins RC, Tsao PS, Schrepfer S. DCA prevents restenosis in preclinical animal models of vessel injury. **Nature 2014**;509(7502):641-4.

11. Lebenslauf

Lebenslauf wurde aus datenschutzrechtlichen Gründen entfernt.

12. Danksagung

An dieser Stelle möchte ich mich bei allen Personen bedanken, die mich bei der Erstellung dieser Arbeit unterstützt haben.

Mein besonderer Dank gilt dabei Prof. Dr. Sonja Schrepfer für die Überlassung des spannenden Themas, der exzellenten Betreuung und umfangreiche Unterstützung. In diesem Rahmen möchte ich mich bei ihr auch für die persönliche und berufliche Förderung bedanken.

Gleichzeitig gilt mein Dank Prof. Dr. Tobias Deuse für seine Unterstützung während meiner Arbeit, seiner Diskussionsbereitschaft und seinen wissenschaftlichen Rat.

Ebenso möchte ich mich bei Christiane Pahrmann, Grigol Tediashvilli, Xiaomeng Hu und Alessia Gravina und allen Mitarbeitern des Transplantation- und Stammzell- Immunbiologie Labors für ihre Unterstützung, Anleitung und Hilfeleistung bei meiner Arbeit bedanken.

Meinen Eltern danke ich von ganzem Herzen für ihre immerwährende Liebe, Unterstützung und ihren Rückhalt wahrend des Entstehungsprozesses und der Fertigstellung dieser Arbeit. Auch möchte ich mich bei meinem Bruder bedanken für seine Anregungen, Kritik und Geduld. Ohne den starken familiären Rückhalt wäre dieses Projekt so nicht möglich gewesen.

13. Eidesstattliche Erklärung

Hiermit versichere ich, dass ich die Arbeit selbstständig und ohne fremde Hilfe Verfasst habe, andere als die von mir angegebenen Quellen und Hilfsmittel nicht benutzt und die aus den benutzten Werken wörtlich oder inhaltlich entnommenen Stellen einzeln nach Ausgabe (Auflage und Jahr des Erscheinens), Band und Seite des benutzten Werkes kenntlich gemacht habe. Ferner versichere ich, dass ich die Dissertation bisher nicht einem Fachvertreter an einer anderen Hochschule zur Überprüfung vorgelegt oder mich anderweitig um Zulassung zur Promotion beworben habe.
Ich erkläre mich einverstanden, dass meine Dissertation vom Dekanat der Medizinischen Fakultät mit einer gängigen Software zur Erkennung von Plagiaten überprüft werden kann.

Hamburg, den 12.01.2020

Dong Wang

Video Article

Vein Interposition Model: A Suitable Model to Study Bypass Graft Patency

Dong Wang[1,2,3,4], Grigol Tediashvili[1,2,3], Simon Pecha[4], Hermann Reichenspurner[4], Tobias Deuse[1,2,3,4], Sonja Schrepfer[1,2,3,4]

[1]Transplant and Stem Cell Immunobiology Lab, University Heart Center Hamburg

[2]Department of Surgery, Transplant and Stem Cell Immunobiology Lab, University of California San Francisco (UCSF)

[3]Cardiovascular Research Center (CVRC) and DZHK German Center for Cardiovascular Research), partner site Hamburg/Kiel/Luebeck

[4]Cardiovascular Surgery, University Heart Center Hamburg

Correspondence to: Sonja Schrepfer at Sonja.Schrepfer@ucsf.edu

URL: https://www.jove.com/video/54839
DOI: doi:10.3791/54839

Keywords: Medicine, Issue 119, Bypass graft failure, myointimal hyperplasia, rat model

Date Published: 1/15/2017

Citation: Wang, D., Tediashvili, G., Pecha, S., Reichenspurner, H., Deuse, T., Schrepfer, S. Vein Interposition Model: A Suitable Model to Study Bypass Graft Patency. *J. Vis. Exp.* (119), e54839, doi:10.3791/54839 (2017).

Abstract

Bypass grafting is an established treatment method for coronary artery disease. Graft patency continues to be the Achilles heel of saphenous vein grafts. Research models for bypass graft failure are essential for a better understanding of pathobiological and pathophysiological processes during graft patency loss. Large animal models, such as pigs or sheep, resemble human anatomical structures but require special facilities and equipment. This video describes a rat vein interposition model to investigate vein graft patency loss. Rats are inexpensive and easy to handle. Compared to mouse models, the convenient size of rats permits better operability and enables a sufficient amount of material to be obtained for further diverse analysis. In brief, the inferior epigastric vein of a donor rat is harvested and used to replace a segment of the femoral artery. Anastomosis is conducted via single stitches and sealed with fibrin glue. Graft patency can be monitored non-invasively using duplex sonography. Myointimal hyperplasia, which is the main cause for graft patency loss, develops progressively over time and can be calculated from histological cross sections.

Video Link

The video component of this article can be found at https://www.jove.com/video/54839/

Introduction

Coronary artery diseases and their complications are among the leading causes of death worldwide. Current therapeutic strategies focus on re-establishing the blood flow, either by dilating the narrowed vessel or by creating a bypass. Coronary artery bypass grafting (CABG) using vein autografts was first described in 1968 and has been refined over the years. Apart from the revascularization of the left anterior descending coronary artery, saphenous vein conduits are most commonly used[1]. However, graft patency remains the Achilles heel of saphenous vein grafts (SVG). One year after surgery, graft patency is 85%, dropping to 61% after ten years[2,3]. Unveiling the pathophysiological mechanisms and causes of SVG patency loss is therefore an important task.

This video demonstrates a rat vein interposition model to investigate vein graft loss. The overall goals of this method are to explore the underlying pathobiological and -physiological processes during disease progression and to develop a suitable model for drug or therapeutic option testing. By transplanting the superficial epigastric vein into the arterial system, this model closely mimics the clinical setting of coronary artery bypass grafting. Surgical trauma, ischemia, and wall stress are important triggers of pathological vascular changes and are imitated in the model described.

Different models and species are available to investigate vein graft patency loss. Large animal models, such as pigs[4], sheep[5], dogs[6], and monkeys[7], resemble human vessel and anatomical structures and thus enable complex therapeutic strategies, such as bypass stenting or new surgical techniques, to be tested[8]. However, special housing, equipment, and staff are required. In addition, high costs and the need for an additional anesthetist during surgery impede their broader application. Small animals, including rats, are easy to handle, do not require special housing, and have manageable costs. Compared to mouse models[9,10], rat models have the advantage of better operability and therefore less variability in the outcome. Rats are physiologically and genetically more similar to humans than mice[11,12]. In addition, most wild-type mice only develop limited myointima[13], which make mouse models prone to type II errors. The histology of the main mouse veins, such as the inferior vena cava, only consists of a few cell layers and renders early evaluation difficult[13]. A further disadvantage is the small amount of tissue available for subsequent analysis after graft recovery.

The model described in this video is reproducible, inexpensive, and easy to perform, and it can be established quickly and reliably. It is especially suitable for evaluating expensive experimental therapeutic agents, such as viral vectors for gene therapy, in an economical fashion.

Protocol

Animals received humane care in compliance with the Guide for the Principles of Laboratory Animals, prepared by the Institute of Laboratory Animal Resources and published by the National Institutes of Health. All animal protocols were approved by the responsible local authority ("Amt für Gesundheit und Verbraucherschutz, Hansestadt (Office for Health and Consumer Protection) Hamburg").

1. Animal Care

1. Obtain Lewis rats (LEW/Crl) rats and ROSA/luciferase-LEW transgenic rats weighing 300-350 g from the Institute of Laboratory Animals.
2. Keep the rats under conventional conditions in ventilated cabinets and feed them standard rat chow and autoclaved water ad libitum.
3. Perform a graft transplantation using the ROSA/luciferase-LEW transgenic rats as the donors and the syngenic LEW/Crl rats as the recipients.

2. Preparation of the Donor Rat

1. Use an induction chamber to anaesthetize a rat with isoflurane (2.5-3%).
2. Place the rat on its back and maintain the anesthesia with a facemask covering the mouth and nose. Check for sufficient depth of anesthesia by pinching the hind feet and verifying the absence of reflexes. Apply some vet ointment to the eyes to prevent dryness while under anesthesia.
3. Spread the hind legs and fix their position using tape.
4. Shave the inguinal hair with a hair trimmer and disinfect the entire area using povidone-iodine followed by 80% ethanol. Repeat the disinfection step twice.
   NOTE: The surgical area, gauze, and surgical instruments should be sterilized. Maintain a sterile field throughout the procedure and wear single-use, sterile surgical gloves, masks, and caps.
5. Under a microscope, perform a vertical incision along the linea inguinalis. Use two forceps to gently separate the subcutaneous tissues and expose the superficial epigastric vein from its origin on the femoral vein. Carefully isolate the superficial epigastric vein from the surrounding tissues.
6. Stop blood flow in the superficial epigastric vein using two micro clamps.
7. Harvest an approximately 0.5 to 1 cm segment of the vein by carefully lifting the isolated vein with forceps and cutting through the vessel with microscissors. Leave the micro clamps on the vessel stump to prevent the loss of blood. Place the removed piece of vein on sterile gauze. Carefully place a 30 G needle inside one end of the harvested vein and flush the vessel with heparin (50 units/ml).
   NOTE: Handle the vein with care and avoid damage during lifting, cutting, and flushing. Make sure to flush the graft with the proper amount of heparin.
8. Keep the vessel segment in 1% lidocaine on ice until transplantation into the recipient rat to prevent a vessel spasm.
9. Euthanize the donor rat by increasing the anesthesia to 5% isoflurane. After 2-3 min, open the abdomen along the linea alba, cut through the diaphragm, and remove the heart to stop circulation.

3. Preparation of the Recipient Rat

1. Anesthetize and fix the recipient rat in the same way as the donor rat.
2. Shave the medial side of the legs with a hair trimmer and disinfect three times using povidone-iodine and 80% ethanol.
3. Monitor the depth of anesthesia and ensure that it is sufficient by verifying the absence of reflexes when pinching the hind feet.
4. Perform a median femoral incision from the knee to the inguinal fold. Under a microscope, use 2 forceps to separate the femoral artery from its surroundings.
5. Use micro clamps to stop the flow of blood. Place the proximal clamp first, followed by the distal clamp.
6. Cut out a short segment of the clamped femoral artery with microscissors and discard it. Shorten the remaining arterial stump with microscissors, creating a gap that is 1-2 mm larger than the vein graft. Flush the arterial stump with heparin using a 30 G needle.
   NOTE: If the adventitia protrudes slightly beyond the vessel stump, use forceps to pull it slightly over the end of the vessel and remove a piece.
7. Place the harvested vein from step 2.8 between the arterial stumps and adjust the length so that it fits suitably into the gap. Note the direction of the vein.
8. Perform the proximal anastomosis first using a 10-0 prolene suture. Conduct single stitches in the order shown (**Figure 1D**). Start with a suture on each lateral side before adding three more sutures on the ventral side. Afterwards, place three stitches on the dorsal side of the vessel to complete the anastomosis.
9. Connect the distal vessels with the graft using the same technique as for the proximal anastomosis described in step 3.8. Again, start with a suture on each lateral side, and then place three sutures on the ventral side and the dorsal side.
10. Load two 1-mL syringes with fibrin glue component 1 and 2. Carefully lift the graft with forceps and drop approximately 100 µl of fibrin glue component 1 under the graft, followed by component 2.
    NOTE: Make sure that components 1 and 2 are applied in a 1:1 ratio.
11. Place the graft back in its position and drop an additional 100 µl of components 1 and 2 on top of the graft. Be sure that the glue covers both the graft and the anastomosis in order to prevent anastomotic insufficiency and over-distension of the vein graft.
12. Carefully open the distal clamp, followed by the proximal.
13. Confirm a successful surgery by checking for a visible pulse in the transplanted vein and distal artery of the graft.
14. Remove excessive glue, which impedes skin closure. Use forceps to lift the cured glue and remove the excess with microscissors. Close the skin layers with 5-0 prolene sutures.

15. Inject 4-5 mg/kg Carprofen subcutaneously before allowing the rat to wake up. Do not leave the animal unattended until it has regained sufficient consciousness to maintain sternal recumbency. Keep the animal in a single cage until it is fully recovered.
16. Add Metamizole to the drinking water (50 mg Metamizole per 100 ml) as pain medication for the following 3 days and monitor the animal daily.

4. Duplex Sonography

NOTE: Use duxplex sonography to visualize blood flow non-invasively in rats[14].

1. Anaesthetize a rat in an induction chamber (isoflurane 2%). Place the rat on its back and maintain anesthesia with a facemask covering the nose.
2. Use hair clippers and hair removal cream to remove the hair around the area of the thigh.
3. Apply ultrasound gel to the thigh. Make sure that there are no air bubbles. Acquire duplex sonography images using an MS 400 transducer (center frequency: 30 MHz) with a frame rate of 230-400 frames/sec.

5. Histopathology

NOTE: Harvest and stain the vessel with Masson's trichrome staining for morphometric analysis[15].

1. Fix the harvested vessel in 4% paraformaldehyde overnight and dehydrate it in increasing concentrations of ethanol. Embed the sample in paraffin and cut it into 5 µm thick slices using a microtome.
   NOTE: Paraformaldehyde is toxic and should be handled with special care.
2. Deparaffinize the slides before staining them with trichrome staining solution. Dehydrate the stained slides, clear them with xylene, and mount them in mounting medium. After drying the slides, view the samples with a microscope.

6. Bioluminescence Imaging (BLI)

NOTE: The postoperative graft was tracked over time in vivo by measuring bioluminescent signal[16].

1. Dissolve 1 g of D-Luciferin potassium salt in 22 ml of PBS and inject it intraperitoneally into the rat (375 mg/kg body weight). Wait 15 min for the luciferin to circulate in the animal.
2. Place the rat into a real-time bioluminescent quantification system and access the bioluminescence signal.

Representative Results

The rat vein interposition model is suitable to study the development of myointima hyperplasia and vein graft failure. Animals recover well from the surgery and show excellent physical condition post-operation. **Figure 1** shows the key surgical steps. After the skin incision along the linea inguinalis, the epigastric superficial vein and femoral artery are identified (**Figure 1A**). Harvesting of the graft should be performed carefully, without damaging the graft (**Figure 1B**), as this can lead to early graft failure and patency loss. After positioning the graft in the recipient animal (**Figure 1C**), anastomosis stitches are performed in the order shown in **Figure 1D**. The completed venous interposition graft appears pale (**Figure 1E**) and should become red and show pulsation after reperfusion (**Figure 1F**).

The successful integration of the vein into the femoral artery and graft patency after transplantation can be confirmed non-invasively using duplex sonography (**Figure 2A**). By transplanting the vein of a Luc-positive rat into a syngeneic Luc-negative rat, bioluminescence imaging can be used to monitor graft presence over time (**Figure 2B**).

Myointima hyperplasia develops progressively in the graft over time. Histological staining with Masson's trichrome demonstrates myointima formation inside the internal elastic lamina (**Figure 2C**). The calculation of luminal obliteration, (dividing the cross-sectional area of the lumen by the area within the internal elastic lamina) revealed a gradual loss of graft patency from day 7 to day 28 post-surgery, thus confirming the reproducible dynamics of myointima hyperplasia in this rat model (**Figure 2D**).

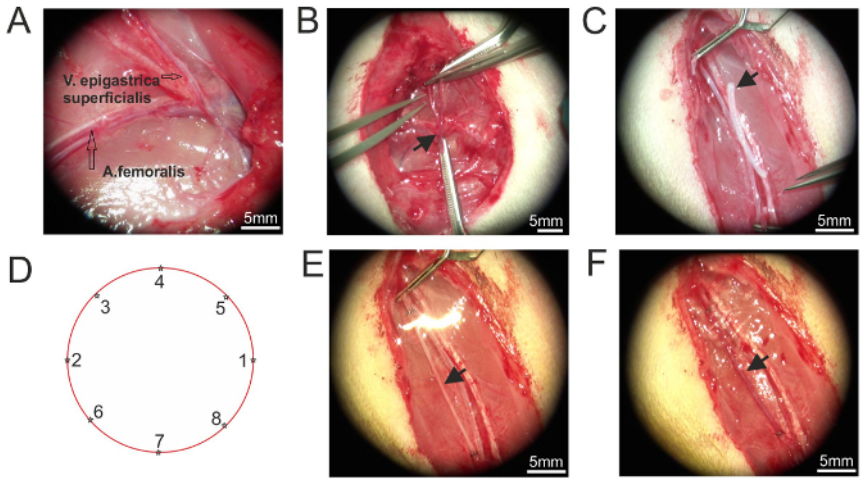

Figure 1: Detailed Scheme of the Surgical Procedure. (A) Anatomy of the inguinal region. (B) Harvesting the epigastric superficial vein graft. (C) Placing the vein graft between the arterial stumps of the recipient animal. (D) Order of anastomosis stitches. (E) Site after the venous graft construction. (F) Site after the reperfusion of the venous interposition graft. Black arrows mark the epigastric superficial vein. The Scale bar = 5 mm. Please click here to view a larger version of this figure.

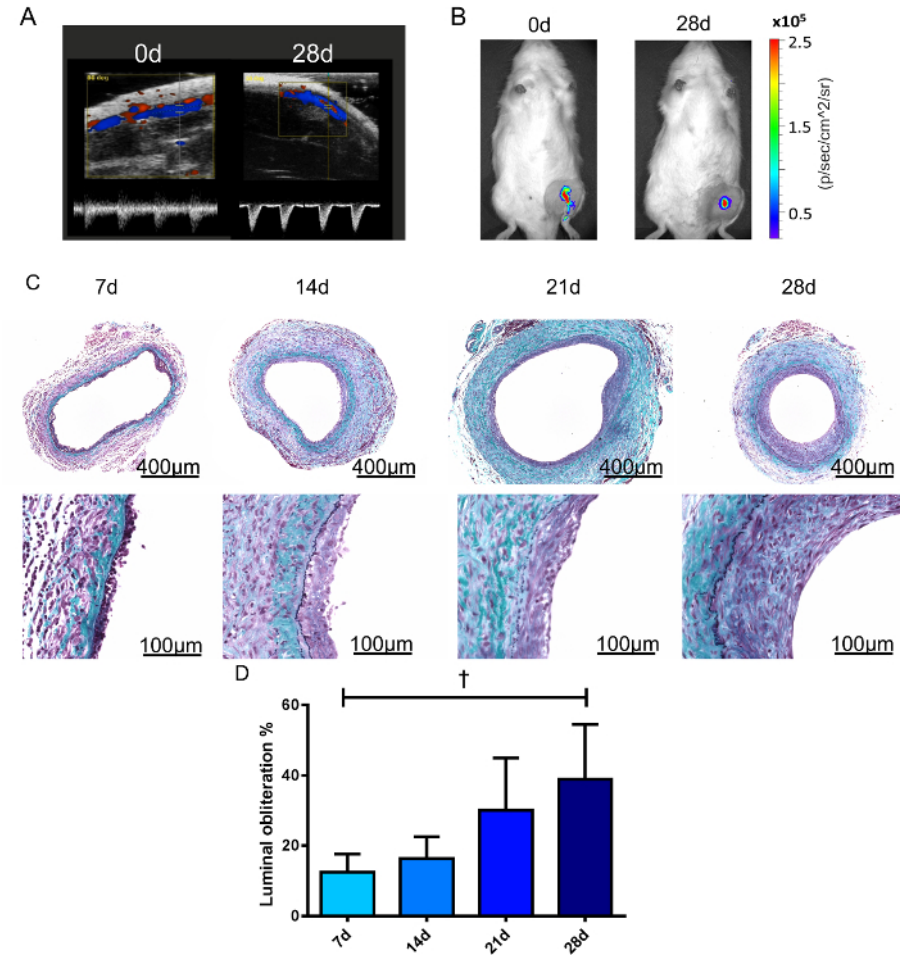

Figure 2: Characterization of the Animal Model. (**A**) Duplex sonography of a venous interposition graft immediately after transplantation (0d) and 28 days post-operation (28d). (**B**) BLI from Luc-positive grafts transplanted into Luc-negative rats at 0 days and 28 days after surgery. (**C**) Representative graft cross sections harvested after days 7, 14, 21, and 28 and stained with Masson's trichrome. (Upper panel: the Scale bar = 400 µm; Lower panel: the Scale bar = 100 µm) (**D**) Luminal obliteration in percentage is calculated by dividing the new inner lumen from the former lumen. Intergroup differences were assessed by one-way analysis of variance (ANOVA) with Bonferroni's post-Hoc test. $p < 0.01$. The error bars are the standard deviation (SD). Please click here to view a larger version of this figure.

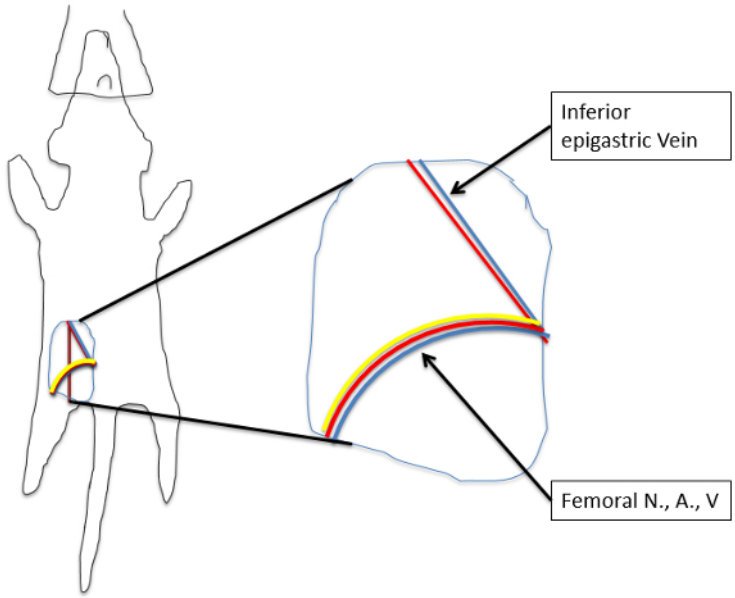

Supplemental File 1: Schematic Illustration of the Surgical Procedure. A vertical incision along the linea inguinalis is performed on the donor rat, exposing the inferior epigastric vein. Blood flow is stopped with two micro clamps, and a vein segment 0.5-1.0 cm long is harvested. In the recipient rat, a median femoral incision is performed, exposing the femoral vein, artery, and nerve. After clamping the femoral artery, a vessel segment is removed and replaced by the harvested vein graft. Please click here to view Supplemental File 1 (or right-click to download).

Discussion

This video demonstrates a rat vein interposition model to investigate vein graft loss and to allow for the exploration of the underlying pathological processes and the testing of new drugs or therapeutic options.

Anesthesia is a crucial aspect of surgical procedures. A continuous inhalative anesthesia system is recommended, as this is a safe and easy method, especially during prolonged operations. This can be of great importance during the training phase, when the operation takes more than 1 hr.

With respect to the surgical procedure, it is critical not to damage the vein graft during harvest and implantation[17]. Gripping the adventitia of the vessel can prevent damage to the vein graft and avoid subsequent thrombus formation and graft failure. Graft patency can be determined immediately after vein graft construction through the observation of blood flow and of pulsation in the vein graft or distal artery, as well as through duplex sonography.

Another critical aspect of the procedure is to prevent the over-distension of the vein graft. Sudden exposure of the vein graft to the arterial pressure system leads to increased wall tension, subsequent over-distension, and changes in flow pattern. These are sources of thrombosis, anastomotic insufficiency, and early graft failure. Supporting the vein graft with fibrin glue can prevent uncontrolled ballooning and protect the intima and media from mechanical destruction. Absorbable collagen covers are an alternative to fibrin glue and can be used as perivenous covers[18].

The most critical step within this protocol is undoubtedly the anastomosis between the vein graft and the artery. Care must be taken not to pierce the two walls of the vessel, as this will lead to the narrowing of the anastomosis, which may result in early failure of the graft. In addition, special attention must be paid to the localization of sutures. Congruency of the suture positions in the artery and vein ensures graft patency and prevents insufficiency. To facilitate this, sutures can be performed in the order shown in **Figure 1D**.

The degree of technical difficulty can be viewed as a limitation of the technique, because a novice must first become familiar with the microsurgical equipment and the small sizes of the anatomical structures. However, other models used exhibit the same difficulties, and we believe that this video will help novice surgeons to master this technique within a short time.

Numerous small animal models for venous graft failure have been described in the literature. However, most models only provide very small amounts of tissue for analysis[13]. An advantage of this method is the comparatively large amount of tissue that can be obtained. One graft can be divided into multiple parts and used for different assays, thereby reducing the number of experimental animals required.

Recent advances in zinc-finger nuclease technology enabled the generation of knockout rats[19]. By selecting suitable knock-out rats, graft patency loss can be studied in different disease conditions. For example, renin knockout rats can be utilized to study hypertension[20]. These genetic backgrounds can be combined with this animal model to glean information on the mechanisms of vein graft failure in different settings or on the impact of certain genes in the development of myointima hyperplasia.

In conclusion, the model described in this video is reproducible, inexpensive, and easy to perform, and it can be established quickly and reliably. Myointima hyperplasia, which is the main cause of vein graft failure, developed rapidly over four weeks, resulting in progressive luminal obliteration. Successfully tested treatment options in this model can be further confirmed in large animal models.

Disclosures

The authors have nothing to disclose.

Acknowledgements

The authors thank Christiane Pahrmann for her technical assistance. This study was funded by the Deutsche Stiftung fuer Herzforschung (F/28/14). D.W. was supported by the travel award from the International Society for Heart and Lung Transplantation. T.D. received the Else Kröner Excellence Stipend from the Else-Kröner-Fresenius-Stiftung (2012_EKES.04). S.S. received research grants from the Deutsche Forschungsgemeinschaft (DFG; DE2133/2-1, T.D. and SCHR992/3- 1, SCHR992/4-1, S.S.).

References

1. Sabik, J. F., 3rd. Understanding saphenous vein graft patency. *Circulation.* **124**, 273-275, (2011).
2. Goldman, S. *et al.* Long-term patency of saphenous vein and left internal mammary artery grafts after coronary artery bypass surgery: results from a Department of Veterans Affairs Cooperative Study. *J Am Coll Cardiol.* **44**, 2149-2156 (2004).
3. Fitzgibbon, G. M. *et al.* Coronary bypass graft fate and patient outcome: angiographic follow-up of 5,065 grafts related to survival and reoperation in 1,388 patients during 25 years. *J Am Coll Cardiol.* **28**, 616-626 (1996).
4. Brien, J. E., Jr. *et al.* Wound healing around and within saphenous vein bypass grafts. *J Thorac Cardiovasc Surg.* **114**, 38-45 (1997).
5. El-Kurdi, M. S. *et al.* Ovine femoral artery bypass grafting using saphenous vein: a new model. *J Surg Res.* **193**, 458-469 (2015).
6. Yuda, A. *et al.* Angiotensin II receptor antagonist, L-158,809, prevents intimal hyperplasia in dog grafted veins. *Life Sci.* **68**, 41-48 (2000).
7. McCann, R. L., Hagen, P. O., & Fuchs, J. C. Aspirin and dipyridamole decrease intimal hyperplasia in experimental vein grafts. *Ann Surg.* **191**, 238-243, http://journals.lww.com/annalsofsurgery/abstract/1980/02000/aspirin_and_dipyridamole_decrease_intimal.18.aspx (1980).
8. Thomas, A. C. Animal models for studying vein graft failure and therapeutic interventions. *Curr Opin Pharmacol.* **12**, 121-126 (2012).
9. Hu, Y., & Xu, Q. New mouse model of vein bypass graft atherosclerosis. *Heart Lung Circ.* **11**, 182-188 (2002).
10. Salzberg, S. P. *et al.* Increased neointimal formation after surgical vein grafting in a murine model of type 2 diabetes. *Circulation.* **114**, I302-307 (2006).
11. Abbott, A. Laboratory animals: the Renaissance rat. *Nature.* **428**, 464-466 (2004).
12. Lindblad-Toh, K. Genome sequencing: three's company. *Nature.* **428**, 475-476 (2004).
13. Yu, P., Nguyen, B. T., Tao, M., Campagna, C., & Ozaki, C. K. Rationale and practical techniques for mouse models of early vein graft adaptations. *Journal of vascular surgery.* **52**, 444-452 (2010).
14. Olver, D. T., Lacefield, J. C., & Shoemaker, K. J. Evidence of bidirectional flow in the sciatic vasa nervorum. *Microvascular research.* **94**, 103-105 (2014).
15. Stubbendorff, M. *et al.* Inducing myointimal hyperplasia versus atherosclerosis in mice: an introduction of two valid models. *Journal of visualized experiments : JoVE.* (2014).
16. Conradi, L. *et al.* Immunobiology of fibrin-based engineered heart tissue. *Stem cells translational medicine.* **4**, 625-631 (2015).
17. Dashwood, M. R., & Tsui, J. C. 'No-touch' saphenous vein harvesting improves graft performance in patients undergoing coronary artery bypass surgery: A journey from bedside to bench. *Vascular Pharmacology.* **58**, 240-250 (2013).
18. Bekler, H. I., Rosenwasser, M. P., Akilina, Y., & Bulut, G. The use of an absorbable collagen cover (NeuraWrap) improves patency of interpositional vein grafts. *Acta orthopaedica et traumatologica turcica.* **44**, 157-161 (2010).
19. Geurts, A. M. *et al.* Knockout rats via embryo microinjection of zinc-finger nucleases. *Science.* **325**, 433 (2009).
20. Moreno, C. *et al.* Creation and characterization of a renin knockout rat. *Hypertension.* **57**, 614-619 (2011).

Video Article

Balloon-based Injury to Induce Myointimal Hyperplasia in the Mouse Abdominal Aorta

Grigol Tediashvili[1,2,3], Dong Wang[1,2,3,4], Hermann Reichenspurner[4], Tobias Deuse[1,2,3,4], Sonja Schrepfer[1,2,3,4]

[1]Transplant and Stem Cell Immunobiology Lab, University Heart Center

[2]Department of Surgery, Transplant and Stem Cell Immunobiology Lab, University of California San Francisco (UCSF)

[3]Cardiovascular Research Center (CVRC) and DZHK German Center for Cardiovascular Research

[4]Cardiovascular Surgery, University Heart Center

Correspondence to: Sonja Schrepfer at Sonja.Schrepfer@ucsf.edu

URL: https://www.jove.com/video/56477
DOI: doi:10.3791/56477

Keywords: Medicine, Issue 132, Myointimal hyperplasia, mouse, denudation model, balloon injury, smooth muscle cell, vasculopathy

Date Published: 2/7/2018

Citation: Tediashvili, G., Wang, D., Reichenspurner, H., Deuse, T., Schrepfer, S. Balloon-based Injury to Induce Myointimal Hyperplasia in the Mouse Abdominal Aorta. *J. Vis. Exp.* (132), e56477, doi:10.3791/56477 (2018).

Abstract

The use of animal models is essential for a better understanding of MH, one major cause for arterial stenosis.In this article, we demonstrate a murine balloon denudation model, which is comparable with established vessel injury models in large animals. The aorta denudation model with balloon catheters mimics the clinical setting and leads to comparable pathobiological and physiological changes. Briefly, after performing a horizontal incision in the *aorta abdominalis*, a balloon catheter will be inserted into the vessel, inflated, and introduced retrogradely. Inflation of the balloon will lead to intima injury and overdistension of the vessel. After removing the catheter, the aortic incision will be closed with single stiches. The model shown in this article is reproducible, easy to perform, and can be established quickly and reliably. It is especially suitable for evaluating expensive experimental therapeutic agents, which can be applied in an economical fashion. By using different knockout-mouse strains, the impact of different genes on MH development can be assessed.

Video Link

The video component of this article can be found at https://www.jove.com/video/56477/

Introduction

Arterial stenosis in coronary and peripheral arteries has a large effect on the morbidity and mortality of patients[1]. One underlying pathological mechanism is myointima hyperplasia (MH), which is characterized by increased proliferation, migration, and synthesis of extracellular matrix proteins from vascular smooth muscle cells (SMC)[2]. SMC are located in the media layer of the vessel and migrate upon stimulation to the surface of the lumen. Stimulatory signals include growth factors, cytokines, cell-cell contact, lipids, extracellular matrix components, and mechanical shear and stretch forces[3,4,5,6]. Injuries of the vessel wall, pathological or iatrogenic, cause endothelial cell and smooth muscle cell damage and stimulate inflammatory reactions, and thus lead to MH[7].

Different animal models are currently available to study arterial injury and myointima hyperplasia. Large animals like pigs or dogs have the advantage of sharing a similar artery and coronary anatomy with humans and are especially suitable for studies investigating angioplasty techniques, procedure, and devices[8]. However, pig models have the drawback of higher thrombogenicity[9,10], while dogs only have a mild response to vessel injury[11]. In addition, all large animal models require special housing, equipment, and staff, which are connected with high costs and are not always available at an institution. Small animal models include rats and mice. Compared to rats, mice have the advantages of lower cost and the existence of a variety of knock out models. The model described in this video can be combined with ApoE-/- mice fed with a western diet to closely mimic the clinical setting of angioplasty in atherosclerotic vessels[12]. Previous models induced vascular injury via wire injury[13], fluid desiccation[14], spring[15], or cuff injury[16]. Since the nature of the injury will greatly impact the development and constitution of MH, using a balloon catheter to induce vessel injury is the best way to mimic the clinical setting.

In this article we describe a novel method to induce MH with a balloon catheter in mice. The use of a balloon catheter (1.2 mm x 6 mm) with a RX-Port (**Figure 1A**) allows the scraping of the intimal layer and, at the same time, the induction of an overdistension of the vessel. Both of these factors are important triggers for the development of MH. The observation time for this model is 28 days[17].

Protocol

Animals received humane care in compliance with the Guide for the Principles of Laboratory Animals, prepared by the Institute of Laboratory Animal Resources, and published by the National Institutes of Health. All animal protocols were approved by the responsible local authority ("Amt für Gesundheit und Verbraucherschutz, Hansestadt (Office for Health and Consumer Protection) Hamburg").

1. Catheter Preparation

NOTE: Refer to the **Table of Materials** for information regarding the catheter.

1. Take catheter from the catheter holder.
2. Pull the guidewire from the lumen through the distal port out.
3. Put in a drop of cyanoacrylate adhesive on the distal end of catheter.
   Caution: Wear latex or nitrile gloves.
4. Place the guidewire at the RX port of the catheter and advance it through the lumen to the distal port. Afterwards, pull the guidewire back slightly to leave a space of ~5 mm to the end.
5. Wait 5 min to allow the adhesive to dry.
6. Move the guidewire, it should be fixed. If it is still mobile, repeat steps 1.3 - 1.6.
7. Fill a 3-mL syringe with 1.5 mL 0.9% saline and connect it to the balloon inflation port.
8. Push the syringe plunger to test balloon inflation. Leave 0.6 mL saline in the syringe.

2. Mouse preparation

1. Obtain male mice at the age of 14 weeks weighing approximately 30 g.
   NOTE: We used animals obtained from the Institute of Laboratory Animals. We used C57BL/6J here.
2. Use an induction chamber to anaesthetize the mouse with 2.0-2.5% isofurane (500 mL/min oxygen flow rate).
3. Place the mouse on its back on a heating pad and maintain anesthesia with a facemask covering the mouth and nose of the mouse. Check for sufficient depth of anesthesia by pinching the hind feet and tail to verify an absence of reflexes.
4. Remove the abdominal hair using a hair trimmer.
5. Spread the hind legs and fix their position using tape.
6. Disinfect the abdominal area using povidone-iodine, followed by 80% ethanol. Repeat this step two more times.
7. Use a surgical drape to ensure surgical site does not get contaminated. Open the skin and muscle layers along the *linea alba* with a scissor (or scalpel) to expose the abdominal organs.
8. Lay the intestines in a 0.9% saline moisturized glove and wrap to keep them moist.
9. Use two fine forceps to remove the fatty tissue above the abdominal aorta.
10. Using an insulin syringe (30G), inject 250 µL of heparin solution (50 U/mL) into the Inferior Vena Cava (IVC) and wait 3 min for its systemic distribution. Heparin will suppress hemostasis and prevent undesired clotting during surgery.
11. Using two forceps, dissect the infrarenal aorta down to its bifurcation and its outgoing branch vessels.
12. Ligate the side vessels, which are expected to be placed in the clamped area, with a high temperature cauterizer.
13. Stop blood flow by clamping the infrarenal aorta directly beneath the renal arteries.
14. Place a second clamp at a distal position just above the aortic bifurcation.
15. Perform a small horizontal incision using scissors at the midpoint between the clamps along the vessel.
    NOTE: The size of the incision should be equivalent to 1/3 of the circumference of the vessel.
16. Insert a syringe with a (30G) needle into the incision and flush the aorta with 250 µL heparin solution (50 U/mL).
17. Using 10-0 sutures, place one single knot on each side of the incision.
18. Dilate the aorta by inserting a vessel dilator into the incision and spread the vessel slightly. Repeat the dilation 2 to 3 times.
19. Moisturize the balloon-catheter with 0.9% saline.
20. Insert the flattened balloon-catheter into the aorta and advance it towards the proximal clamp on the aorta.
21. When reaching the proximal clamp, carefully open the proximal clamp and inflate the balloon to prevent blood leakage, by injecting ~0.6 mL of saline.
    NOTE: The ratio of the inflated balloon to vessel is 1.5:1.
22. Advance the catheter retrograde for approximately 2 cm.
23. Pull the expanded catheter back, while deflating the balloon slightly by releasing the syringe.
24. Reattach the proximal clamp when the catheter reaches the incision of the aorta. Deflate the balloon completely and remove it.
25. Rinse the aorta with 250 µL heparin solution (50 U/mL) using a 30G syringe.
26. Close the aortic incision using 10-0 sutures. Place interrupted stitches on each lateral side, followed by one or two stitches on the ventral side.
27. Open the distal clamp. In case of bleeding, close the clamp again and place additional stitches.
28. Open the proximal clamp carefully.
29. Place two swabs on the suture to support it and stop any bleeding.
30. Place absorbable hemostats on the suture to sustain it.
    NOTE: An aortic pulse should be visible distally from the incision.
31. Place the intestines back into the abdomen.
32. Rinse the abdominal cavity with sterile 0.9% saline, which has been pre-warmed to 37 °C.
33. Close the abdominal muscle layer using 6-0 running sutures.
34. Close the skin with 5-0 running sutures.
35. Inject 4-5 mg/kg Carprofen subcutaneously before allowing the mouse to wake up. Monitor the animal until it has gained consciousness, maintain sternal recumbency. Keep the animal alone in a cage until complete recovery.
36. Add Metamizole to the drinking water (50 mg/100 mL) as pain medication for 3 days and monitor the animal daily. Usually mice like the sweet taste of metamizole and start drinking immediately after the surgery. If preferred, sustained-release injectable agents can be used instead of metamizole.
    NOTE: The observation period for this model is 28 days.

3. Histopathology

1. Harvest the balloon-injured aorta after 28 days by preparing the mice as described in steps 2.2 to 2.9.
2. Use scissors to remove the balloon-injured aorta (between the bifurcation and 0.3 mm above the renal vessels) and euthanize the mouse by cutting out its heart.
3. Flush the lumen of the vessel with 0.9% NaCl.
4. Fix the harvested vessel in 4% paraformaldehyde (PFA) overnight and dehydrate it in increasing concentrations of ethanol, starting with 70% ethanol for 2 hours, 80% ethanol for 1 hour, 95% ethanol for 2 hours, and 100% ethanol for 5 hours. Then, incubate the samples in xylene for 2 hours 3 times, before infiltrating the samples with paraffin.
   NOTE: Instead of flushing the harvested vessel with 0.9% NaCl, it can be flushed with 4% PFA.
   Caution: PFA and xylene are toxic and should be handled with special care.
5. Embed the sample in paraffin and cut into slices of 5 µm thickness using a microtome.
6. Deparaffinize the slides with xylene 3 times for 5 minutes.
7. Rehydrate tissue slides using a decreasing series of ethanol. Start with 100% ethanol 2 times for 5 min, followed by 3 minutes of 95%, 80% and 70% ethanol.
8. Stain the slides with Masson's trichrome staining as described[18].
9. Dehydrate stained slides in 100% ethanol 2 times for 10 min each. Clear with xylene 2 times for 10 min each and mount in mounting medium.
10. View the slides with a bright field microscope. Use a lens with 5x magnification and a numerical aperture of 0.12 for an overview picture or a lens with 20x magnifications with a numerical aperture of 0.35 for detailed observation.

4. Immunofluorescence Microscopy

1. Rehydrate tissue slides using a decreasing series of ethanol. Start with 100% ethanol 2 times for 5 min, followed by 3 min of 95%, 80% and 70% ethanol.
2. Perform antigen-retrieval by heating the slides in antigen-retrieval solution in a steamer for 20 min.
3. Let the slides cool down to room temperature.
4. After washing the slides for three times with phosphate buffered saline (PBS), apply antigen blocking solution on sections for 30 min.
5. Wash slides three times for 5 min with PBS.
6. Incubate sections with primary antibody diluted in primary antibody diluent.
   NOTE: The right concentration and incubation time should be chosen separately for each antibody.
7. Wash slides three times for 5 min with PBS to remove unbound antibody.
8. Incubate sections with a pre-conjugated secondary antibody diluted in secondary antibody diluent.
   NOTE: The right concentration and incubation time should be chosen separately for each antibody.
9. Remove unbound antibodies by washing the slides for 5 min three times.
10. Counterstain the cell nuclei using 4',6-diamidino-2-phenylindole (DAPI) for 15 min; the final DAPI concentration should be 350 nM.
11. Mount slides in immunofluorescence compatible mounting solution.
    NOTE: Using the wrong mounting solution can obscure the fluorescence signal.
12. View slides with a fluorescence microscope. Use a 40x magnification lens with a numerical aperture of 1.3.

Representative Results

Balloon denudation is a suitable model to study the development of MH in mice. Animals recover well from the surgery and show an excellent physical condition post-operation. We established this model in 50 mice with less than 3% death rate due to the surgical procedure. **Figures 1B-C** show the key surgical steps. After a skin incision along the *linea alba*, identify the *aorta abdominalis*. Place microsurgical clamps (**Figure 1B**). Make a small incision in the middle of aorta, set a balloon catheter into the vessel and slide it retrograde, against the direction of blood flow (**Figure 1C**). Movement of the inflated balloon leads to scraping of intima and, at the same time, overdistension of the vessel. The aortic incision will be closed with single stiches. An aortic pulse should be visible distally from the incision.

MH develops progressively in the graft over time. Histological staining with Masson's trichrome demonstrates myointima formation inside the internal elastic lamina (**Figure 2A**). Myointimal lesions consisted mainly of cellular components positive for SM22 and some extracellular matrix components (**Figure 2B**). Myointimal cells are further evaluated by immunofluorescence staining. The main population in the myointima consists of smooth muscle (smooth muscle actin (SMA) positive) cells and myofibroblasts (fibroblast activation protein (FAP) positive) cells (**Figure 2B**).

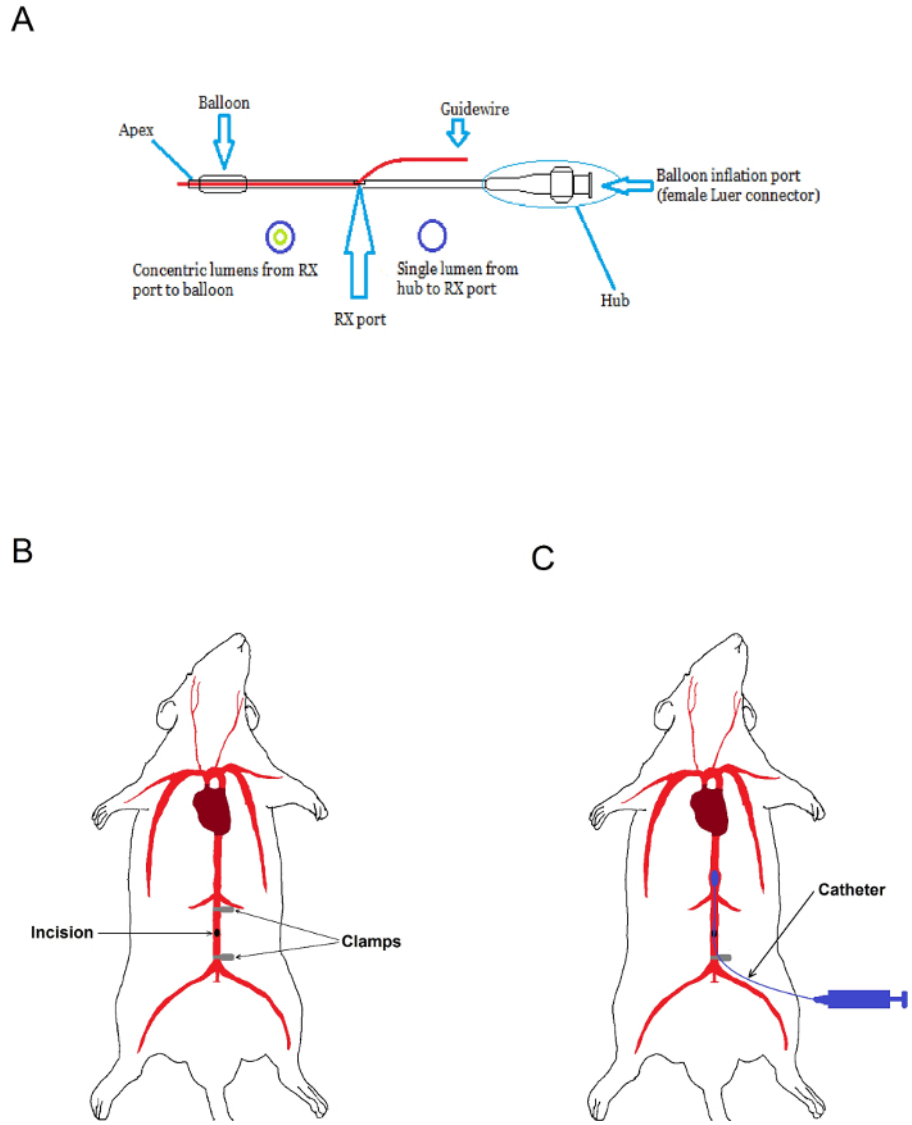

Figure 1. Schematics of the catheter and its implantation. (A) Detailed schematic of the catheter. Distal port, balloon, rapid exchange port (RX-port), guidewire, single lumen to RX-port, double lumens from RX-Port to balloon, hub, balloon inflation port. **(B)** Schematic illustration of surgical procedure. Blood flow of the *Aorta abdominalis* is stopped with two micro clamps and a small incision is performed. C. Inflated catheter inside *aorta abdominalis*. Please click here to view a larger version of this figure.

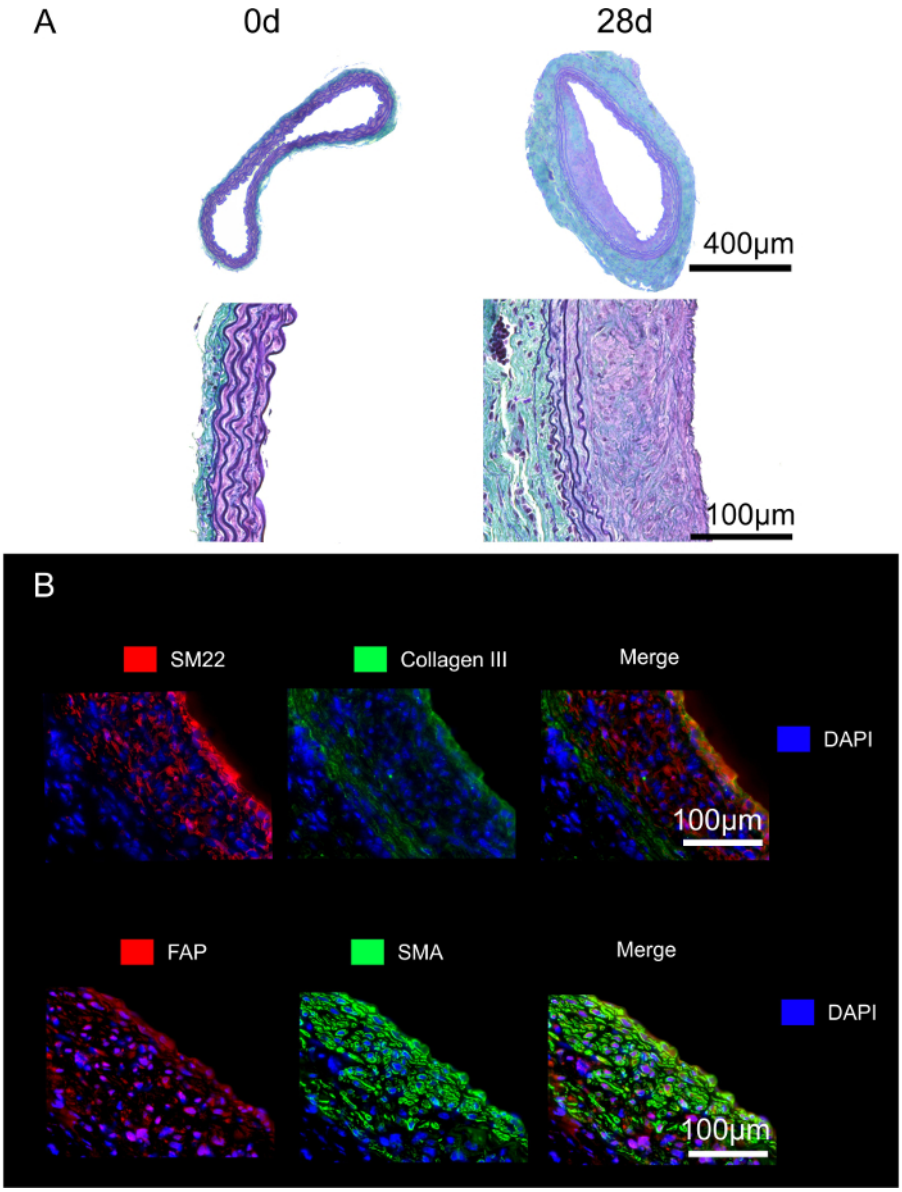

Figure 2. Myointima formation inside the internal elastic lamina. (A) Denuded mouse aortas are harvested, paraffin embedded, and a representative cross section is shown in trichrome staining. **(B)** Double immunofluorescence staining of balloon-denuded aortae is shown. The upper row depicts myointimal lesions stained for SM22 and collagen III. In the bottom row, vessels are stained for SMA and FAP. Please click here to view a larger version of this figure.

Discussion

This article demonstrates a murine model to study the development of myointimal hyperplasia and allows the exploration of the underlying pathological processes and the testing of new drugs or therapeutic options.

The most critical step in this protocol is the denudation of the aorta. Special care should be paid during this step as excessive denudation will lead to aneurysm formation and model failure. On the other hand, if denudation is performed insufficiently, too little myointima will develop. Therefore, the intensity of the denudation step is crucial for the outcome and success of this animal model.

With respect to the surgical procedure, it is critical the two walls of the vessel are not pierced by setting the stiches, which might result in early failure of the vessel patency. We have previously described a mouse model in which we induced vessel stenosis in the abdominal aorta of mice[18]. However, this and most other models only provide very small amounts of tissue for analysis. An advantage of this method is the comparatively large amount of tissue obtained (~1 cm vessel segment). A single vessel graft can thus be divided into multiple parts and used for various analyses, effectively reducing the number of experimental animals required.

Furthermore, suitable knock-out animals can be used to study the development of myointima hyperplasia in different disease conditions. The genetic backgrounds can also be combined with this animal model to understand the mechanisms of myointimal hyperplasia in a variety of settings or the impact of certain genes.

In summary, the model described here is reproducible, easy to perform, and can be established quickly and reliably. Successfully tested treatment options in this model can be further confirmed in large animal models[19].

Disclosures

The authors have nothing to disclose.

Acknowledgements

The authors thank Christiane Pahrmann for her technical assistance.

D.W. was supported by the Max Kade Foundation. T.D. received grants from the Else Kröner Fondation (2012_EKES.04) and the Deutsche Forschungsgemeinschaft (DE2133/2-1_. S. S. received research grants from the Deutsche Forschungsgemeinschaft (DFG; SCHR992/3- 1, SCHR992/4-1).

References

1. Kochanek, K. D., Xu, J., Murphy, S. L., Minino, A. M., & Kung, H. C. Deaths: final data for 2009. *Natl Vital Stat Rep.* **60**(3), 1-116 (2011).
2. Austin, G. E., Ratliff, N. B., Hollman, J., Tabei, S., & Phillips, D. F. Intimal proliferation of smooth muscle cells as an explanation for recurrent coronary artery stenosis after percutaneous transluminal coronary angioplasty. *J Am Coll Cardiol.* **6**(2), 369-375 (1985).
3. Greenwald, S. E., & Berry, C. L. Improving vascular grafts: the importance of mechanical and haemodynamic properties. *J Pathol.* **190**(3), 292-299 (2000).
4. Majesky, M. W., & Schwartz, S. M. Smooth muscle diversity in arterial wound repair. *Toxicol Pathol.* **18**(4 Pt 1), 554-559 (1990).
5. Owens, G. K. Regulation of differentiation of vascular smooth muscle cells. *Physiol Rev.* **75**(3), 487-517 (1995).
6. Owens, G. K., Kumar, M. S., & Wamhoff, B. R. Molecular regulation of vascular smooth muscle cell differentiation in development and disease. *Physiol Rev.* **84**(3), 767-801 (2004).
7. Kleemann, R., Zadelaar, S., & Kooistra, T. Cytokines and atherosclerosis: a comprehensive review of studies in mice. *Cardiovasc Res.* **79**(3), 360-376 (2008).
8. Karas, S. P. *et al.* Coronary intimal proliferation after balloon injury and stenting in swine: an animal model of restenosis. *J Am Coll Cardiol.* **20**(2), 467-474 (1992).
9. Ip, J. H. *et al.* The role of platelets, thrombin and hyperplasia in restenosis after coronary angioplasty. *J Am Coll Cardiol.* **17**(6 Suppl B), 77B-88B (1991).
10. Mason, R. G., & Read, M. S. Some species differences in fibrinolysis and blood coagulation. *J Biomed Mater Res.* **5**(1), 121-128 (1971).
11. Lafont, A., & Faxon, D. Why do animal models of post-angioplasty restenosis sometimes poorly predict the outcome of clinical trials? *Cardiovasc Res.* **39**(1), 50-59 (1998).
12. Matter, C. M. *et al.* Increased balloon-induced inflammation, proliferation, and neointima formation in apolipoprotein E (ApoE) knockout mice. *Stroke.* **37**(10), 2625-2632 (2006).
13. Lindner, V., Fingerle, J., & Reidy, M. A. Mouse model of arterial injury. *Circ Res.* **73**(5), 792-796 (1993).
14. Simon, D. I. *et al.* Decreased neointimal formation in Mac-1(-/-) mice reveals a role for inflammation in vascular repair after angioplasty. *J Clin Invest.* **105**(3), 293-300 (2000).
15. Sata, M. *et al.* A mouse model of vascular injury that induces rapid onset of medial cell apoptosis followed by reproducible neointimal hyperplasia. *J Mol Cell Cardiol.* **32**(11), 2097-2104 (2000).
16. Moroi, M. *et al.* Interaction of genetic deficiency of endothelial nitric oxide, gender, and pregnancy in vascular response to injury in mice. *J Clin Invest.* **101**(6), 1225-1232 (1998).
17. Painter, T. A. Myointimal hyperplasia: pathogenesis and implications. 2. Animal injury models and mechanical factors. *Artif Organs.* **15**(2), 103-118 (1991).
18. Stubbendorff, M. *et al.* Inducing myointimal hyperplasia versus atherosclerosis in mice: an introduction of two valid models. *J Vis Exp.* (87), 51459 (2014).
19. Deuse, T. et al. Dichloroacetate prevents restenosis in preclinical animal models of vessel injury. *Nature.* 509 (7502), 641-644 (2014).

Hindawi Publishing Corporation
BioMed Research International
Volume 2015, Article ID 765292, 7 pages
http://dx.doi.org/10.1155/2015/765292

Research Article

Sex Differences in Immunology: More Severe Development of Experimental Pulmonary Hypertension in Male Rats Exposed to Vascular Endothelial Growth Factor Receptor Blockade

Julien Guihaire,[1] Tobias Deuse,[1,2,3] Dong Wang,[1,2] Elie Fadel,[4] Hermann Reichenspurner,[2,3] and Sonja Schrepfer[1,2,3,5]

[1]*TSI Laboratory, University Heart Center Hamburg, 20246 Hamburg, Germany*
[2]*Cardiovascular Research Center Hamburg (CVRC) and DZHK (German Center for Cardiovascular Research), Partner Site Hamburg/Kiel/Lübeck, 20246 Hamburg, Germany*
[3]*Cardiovascular Surgery, University Heart Center Hamburg, 20246 Hamburg, Germany*
[4]*Thoracic and Vascular Surgery and Heart-Lung Transplantation, Marie Lannelongue Hospital, University of Paris-Sud, 92350 Le Plessis-Robinson, France*
[5]*Department of Cardiothoracic Surgery and Stanford Cardiovascular Institute, Stanford University, Stanford, CA 94305, USA*

Correspondence should be addressed to Sonja Schrepfer; schrepfer@stanford.edu

Received 25 May 2015; Accepted 5 August 2015

Academic Editor: Rei Shibata

Background. The epidemiology of pulmonary hypertension (PH) is characterized by a female preponderance, whereas males share higher severity of the disease. *Objective.* To compare the severity of experimental PH between male and female athymic rats. *Methods.* PH was induced in 11 male and 11 female athymic rats (resp., SU_M and SU_F groups) using an inhibitor of VEGF-receptors I and II, semaxanib (40 mg/kg). After 28 days, right ventricular (RV) remodeling, systolic function, and hemodynamics were measured using echocardiography and a pressure-volume admittance catheter. Morphometric analyses of lung vasculature and RV myocardium were performed. *Results.* Four weeks after semaxanib injection, RV end-systolic pressure was higher in SU_M than in SU_F. Males developed marked RV enlargement and systolic dysfunction compared to females. Impairment of RV-PA coupling efficiency was observed only in SU_M. The smooth muscle cells of the pulmonary arteries switched from a contractile state to a dedifferentiated state only in males. *Conclusions.* Female athymic rats were protected against the development of severe PH. RV-PA coupling was preserved in females through limitation of pulmonary artery muscularization. Control of smooth muscle cells plasticity may be a promising therapeutic approach to reverse established vascular remodeling in PH patients.

1. Introduction

Pulmonary hypertension (PH) is a disabling disease characterized by higher prevalence in females [1]. Considering the independent predictors of mortality, male gender is however one of the strongest [2]. Since few males are included in clinical trials investigating PH, there is lack of data regarding the precise role of estrogens in the development and progression of pulmonary vascular disorders. Experimentally, estrogens exhibit protective effects on the pulmonary vasculature in classical models of PH in rodents including the chronic hypoxia and monocrotaline models [3, 4]. Sweeney et al. suggested in 2009 that female gender may protect against semaxanib/hypoxia related angioproliferative PH, possibly by preventing semaxanib-induced pulmonary endothelial apoptosis [5]. In the present study, we induced PH in male and female rats to investigate the influence of gender difference on the development and severity of PH. We did not use the classical model of angioproliferative PH which combines semaxanib with chronic hypoxia because of the lack of hypoxic chambers in our animal facilities. However we injected the double dose of semaxanib in athymic nude

rats since T-cell deficiency has been demonstrated to increase semaxanib toxicity in the pulmonary vasculature [6].

2. Methods

Thirty eight 6-week-old athymic RNU-rats (Crl:NIH-*Foxn1*^{rnu}) rats including 19 males and 19 females were purchased (Charles River, Sulzfeld, Germany). The mean body weight was 213 ± 67 gr. The research protocol was approved by our Institutional Committee on Animal Welfare. Experimental PAH was induced using the tyrosine kinase inhibitor semaxanib (SU5416, SUGEN Inc., Sigma-Aldrich, Saint Louis, MO) suspended in CMC (0.5% (w/v) carboxymethylcellulose sodium, 0.9% (w/v) sodium chloride, 0.4% (v/v) polysorbate 80, and 0.9% (v/v) benzyl alcohol in deionized water) [4]. Eleven males (SU_M group) and 11 females (SU_F group) received a single subcutaneous injection of semaxanib (40 mg/kg;), while 8 males (RNU_M group) and 8 females (RNU_F group) only received an injection of CMC vehicle. Animals received humane care in compliance with the "Principles of Laboratory Animal Care" formulated by the National Society for Medical Research and the "Guide for the Care and Use of Laboratory Animals" prepared by the Institute of Laboratory Animal Resources and published by the National Institutes of Health (NIH Publication number 86-23, revised 1996) and were housed under normoxic conditions (animal facilities of the University Hospital Eppendorf, Hamburg, Germany).

All procedures were performed under general anesthesia combining buprenorphine (0.5 mg/kg, SC) with inhaled isoflurane (2% mixed with 0.5 L/min 100% oxygen for induction, 1% to 1.5% for maintenance). Rats were then placed in the supine position (head up) onto a warmed plate to help maintain the rat core temperature at 37°C.Cardiac echography (Vevo 2100 system, VisualSonics, Toronto, Canada) was performed 21 days after PH induction to assess the mid-right-ventricular end-diastolic diameter (RVEDD) and the tricuspid annular plane systolic excursion (TAPSE). The ultrasound transducer (13–24 MHz, MS250, VisualSonics) was manually immobilized on the shaved area overlying the heart with a 45° angle. A complete two-dimensional (2D) 4-chamber view was obtained by adjusting the position of the probe parasternally over the cardiac apex. TAPSE was measured as the maximal motion toward the apex of the lateral tricuspid annulus (Figure 1). A 1.2 Fr–4.5 mm electrode spacing admittance catheter (Scisence, Ontario, Canada) was introduced in the right ventricle through the apex via an open-chest approach at day 28. The probe was connected to the ADVantage admittance pressure-volume system (Scisence) for real-time assessment of absolute right ventricular (RV) volume and pressure. Pressure-volume loops were recorded under general anesthesia (inhaled isoflurane 2% and buprenorphine 0.5 mg/kg, SC) and the RV end-systolic pressure-volume relationship was assessed during transient external occlusion of the inferior vena cava using nontoothed DeBakey forceps. TheRV end-systolic elastance (E_{es}) was defined as the slope of the end-systolic pressure-volume relationship (Figure 2). The pulmonary arterial elastance (E_a) was defined as follows: RV end-systolic pressure/RV stroke volume. Right ventricular-pulmonary arterial (RV-PA) coupling efficiency was quantified by the E_{es}/E_a ratio.

Animals were sacrificed at day 28 for heart and lung procurement. To assess RV hypertrophy, the Fulton index was calculated as the weight ratio of the right ventricle and left ventricle + septum. After one-day fixation in 4% buffer formalin solution, 5 μm sections were performed on paraffin-embedded tissues. Medial thickness of the pulmonary arteries (50 to 100 μm of maximal diameter adjacent to bronchioles) was calculated as the percentage of medial layer as compared with the cross-sectional diameter of the artery from one external elastic lamina to the opposed external elastic lamina (Elastica von Gieson staining; Thermo Fisher Scientific, Schwerte, Germany; magnification ×400) [7]. To quantify RV hypertrophy, the cross-sectional area of 20 randomized cardiomyocytes was measured in the subepicardial layer of the RV free wall (Hematoxylin-eosin staining; Sigma-Aldrich; magnification ×400).

To study gender differences in smooth muscle cells (SMCs) plasticity, paraffin-embedded lungs underwent heat-induced antigen retrieval with Dako antigen retrieval solution (Dako, Glostrup, Denmark) in a steamer for 20 min. After blocking with Image-iT FX signal enhancer (Invitrogen, Carlsbad, Ca) for 30 minutes, slides were incubated with primary antibodies against smooth-muscle-heavy-chain (SM heavy chain; EPR5335, Abcam, Cambridge, UK) and embryonic smooth muscle myosin heavy chain (SMemb; 3H2, Yamasa, Tokyo, Japan) for 16 h at 4°C. After washing with PBS, sections were incubated for 1 h at 37°C with the corresponding secondary antibody conjugated with Alexa Fluor 488 or Alexa Fluor 555 (Invitrogen). DAPI was used to counterstain cell nuclei. Images were obtained by a Nikon Eclipse TiE microscope (Nikon, Tokyo, Japan) equipped with the Perkin Elmer UltraVIEW VoX confocal imaging system (Perkin Elmer, Waltham, MA).

All variables were reported as mean value ± standard deviation. One-way analysis of variance was performed for between-group comparisons with a 95% confidence interval using the Prism software (GraphPad, La Jolla, CA). Only animals who survived until day 28 were included in the statistical analysis.

3. Results

Among the 11 semaxanib-treated males, 3 died before day 28 (on days 21, 21, and 26) and 3 developed marked pleuropericardial effusion. All females survived until day 28 without any thoracic effusion. Induction of experimental PH resulted in a significant enlargement of the right ventricle after 3 weeks in males compared to females (RVEDD: 5.6 ± 0.7 versus 2.5 ± 0.4 mm, $P < 0.01$). In addition, TAPSE was lower in the SU_M group (1.28 ± 0.15 versus 2.09 ± 0.35 mm, $P < 0.01$). Hemodynamic parameters after 28 days are listed in Table 1. In response to semaxanib injection, athymic males showed significant RV pressure overload during systole, with an average of 66.3 mm Hg. Increased E_a combined to altered E_{es} in male rats resulted in impairment of RV-PA coupling efficiency, while ventricular-arterial coupling was preserved

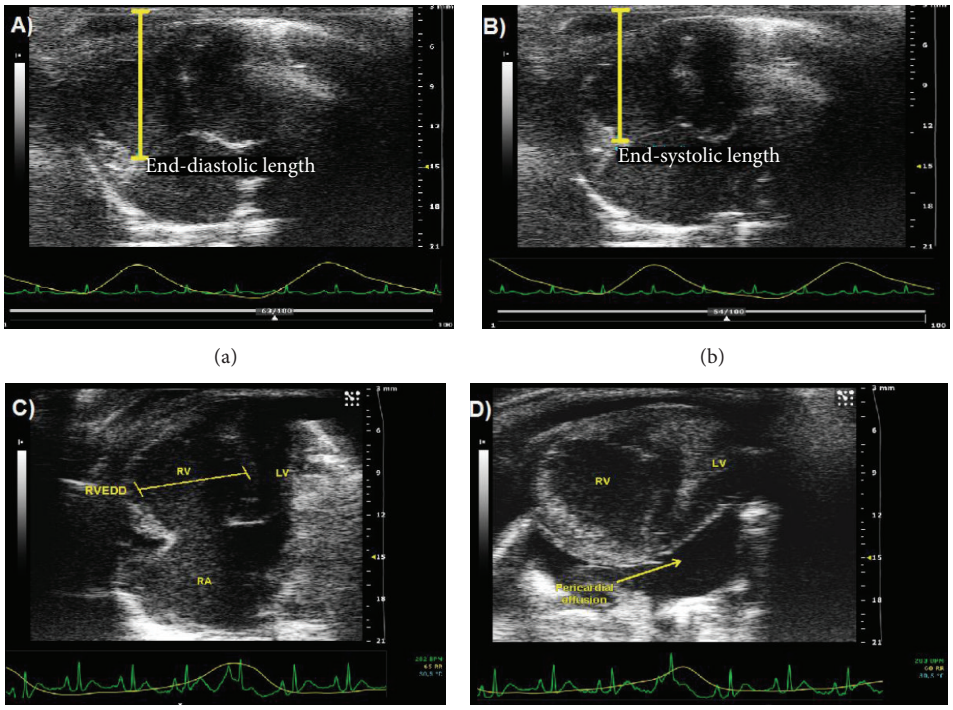

(a) (b) (c) (d)

Figure 1: Representative cardiac echo imaging in rats at 3 weeks. The tricuspid annular plane systolic excursion (TAPSE) is measured on a 4-chamber apical view (2D-mode) as the difference in length between the tricuspid annulus and a fixed point at the end-diastolic (a) and end-systolic times (b). On the same view, the right ventricular end-diastolic diameter (RVEDD) is measured transversally from the midinterventricular septum to the mid-right-ventricular free wall (c, 2D-mode). In SU_M at 3 weeks, pericardial effusion can be observed (d, parasternal short axis, 2D-mode). RV: right ventricle; RA: right atrium; LV: left ventricle.

Table 1: Right heart hemodynamics at 4 weeks.

Group (n)	RNU_M (8)	RNU_F (8)	SU_M (8)	SU_F (11)
Semaxanib (mg/kg)	0	0	40	40
Heart rate (beat/min)	269 ± 37	311 ± 35	296 ± 48	280 ± 73
RVESP (mm Hg)	21 ± 2.5	24.3 ± 8.1	$66.3 \pm 8.9^{*\#\S}$	29.5 ± 13.4
RVEDP (mm Hg)	1.5 ± 3.5	3 ± 3.6	$6.2 \pm 2.8^{\S}$	2.1 ± 4.3
CO (mL/min)	134 ± 4	122 ± 5	$58 \pm 24^{*\#\S}$	89 ± 17
PVR (dyn·s·cm^{-5})	0.013 ± 0.002	0.016 ± 0.006	$0.103 \pm 0.06^{*\#\S}$	0.027 ± 0.01
dP/dt max (mm Hg/s)	1173 ± 161	1311 ± 414	$2636 \pm 495^{*\#\S}$	1374 ± 320
dP/dt min (mm Hg/s)	−1318 ± 37	−871 ± 232	$-2370 \pm 912^{*\#\S}$	−1072 ± 415
E_{es} (mm Hg/μL)	0.19 ± 0.05	0.21 ± 0.15	$0.12 \pm 0.06^{*\#\S}$	0.18 ± 0.05
E_a (mm Hg/μL)	0.04 ± 0.01	0.06 ± 0.03	$0.33 \pm 0.12^{*\#\S}$	0.09 ± 0.02
E_{es}/E_a	4.75 ± 0.63	3.5 ± 0.45	$0.36 \pm 0.17^{*\#\S}$	2.1 ± 0.34

RVESP: right ventricular end-systolic pressure; RVEDP: right ventricular end-diastolic pressure; CO: cardiac output; PVR: pulmonary vascular resistance; dP/dt max: right ventricular maximal isovolumic rate of development of ventricular pressure; dP/dt min: right ventricular minimal isovolumic rate of development of ventricular pressure. Other abbreviations are in text. $*$ explains $P < 0.05$ for comparison with SU_F; # explains $P < 0.05$ for comparison with RNU_M; § explains $P < 0.05$ for comparison with RNU_F.

in the SU_F group. Morphometric analysis of the lung vasculature showed a very small rate of intimal remodeling and plexiform lesions were not remarkable among semaxanib-treated animals. Hypertrophy of the pulmonary medial layer was significantly higher in SU_M group (25.9% ± 4.5% versus 14.6% ± 2.8%, $P < 0.001$). RV pressure overload was associated with RV hypertrophy as illustrated by the higher Fulton ratio in SU_M compared to SU_F (0.57 ± 0.07 versus 0.29 ± 0.07, $P < 0.001$; Figure 3). Similarly cardiomyocytes hypertrophy was only observed in athymic males

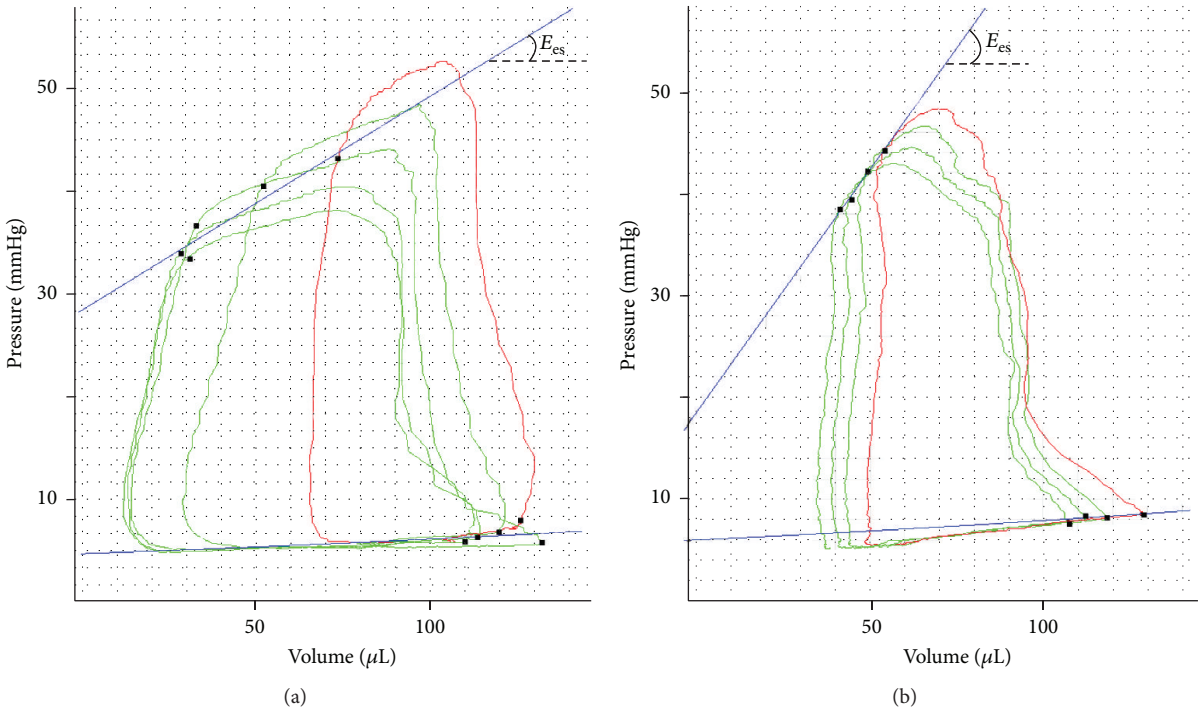

Figure 2: Representative pressure-volume loops from SU_M and RNU_M at 4 weeks. At baseline, the pressure-volume loop is in red. During occlusion of the inferior vena cava, the right ventricular end-diastolic volume decreases, shifting the following loops (green) toward the left. Similarly the right ventricular end-systolic pressure decreases, shifting the loops to the bottom. The linear end-systolic relationship is represented in blue, linking all end-systolic points from the successive pressure-volume loops during transient occlusion of the inferior vena cava. The slope of this line defines the end-systolic elastance of the ventricle (E_{es}).

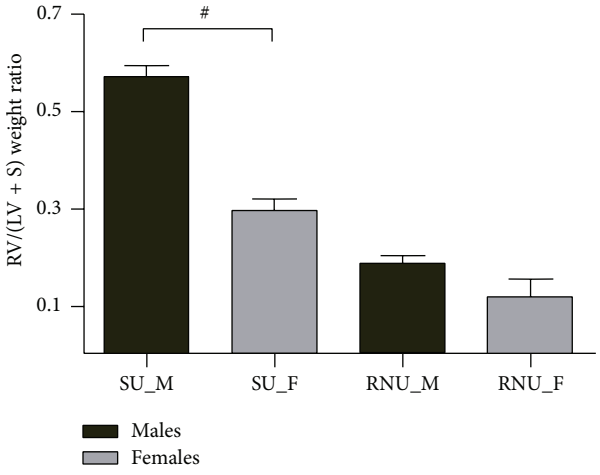

Figure 3: Fulton index (RV/(LV + S)) in rats at 4 weeks. The right ventricle of Su_M was significantly hypertrophied compared to Su_F, RNU_F, and RNU_M, as illustrated by the elevated Fulton index in this group. # explains $P < 0.001$.

(273 ± 48 versus $168 \pm 24\,\mu m^2$, $P < 0.001$) (Figure 4). Both Fulton index and cardiomyocytes area were not significantly different between RNU_M and RNU_F. The SMC-phenotype switch in pulmonary arteries from a contractile (SM heavy chain-positive) to a dedifferentiated (SMemb-positive) state after induction of PH was only observed in male rats (Figure 5).

4. Discussion

Athymic female rats developed less severe PH in response to vascular endothelial growth factor (VEGF) receptor blockade. As a consequence, RV function and RV-PA coupling were preserved only in females in this experimental descriptive study. We hypothesize a protective role of endogenous estrogens against PH in semaxanib-treated rats under normoxic conditions. Our findings are in accordance with previous experimental studies showing that ovariectomized rats develop more severe PH in response to chronic hypoxia or to monocrotaline [3]. *In vitro*, estrogens effects on the pulmonary circulation include increase in prostacyclin release, upregulation of the endothelial nitric oxide synthase, and downregulation of endothelin-1 expression [8]. However, the effects of steroid hormones and their analogues in PH patients are controversial [9]. Estrogens exhibit proangiogenic properties through the upregulation of VEGF receptors. Since VEGF is a key regulator of endothelial cell survival in the lung, estrogen-therapy may interfere with the development of the pulmonary vascular lesions in PH patients [10]. Protective effects of estrogens might thus concern hyperproliferative SMCs rather than phenotypically altered endothelial cells. This is in agreement with the present results, since

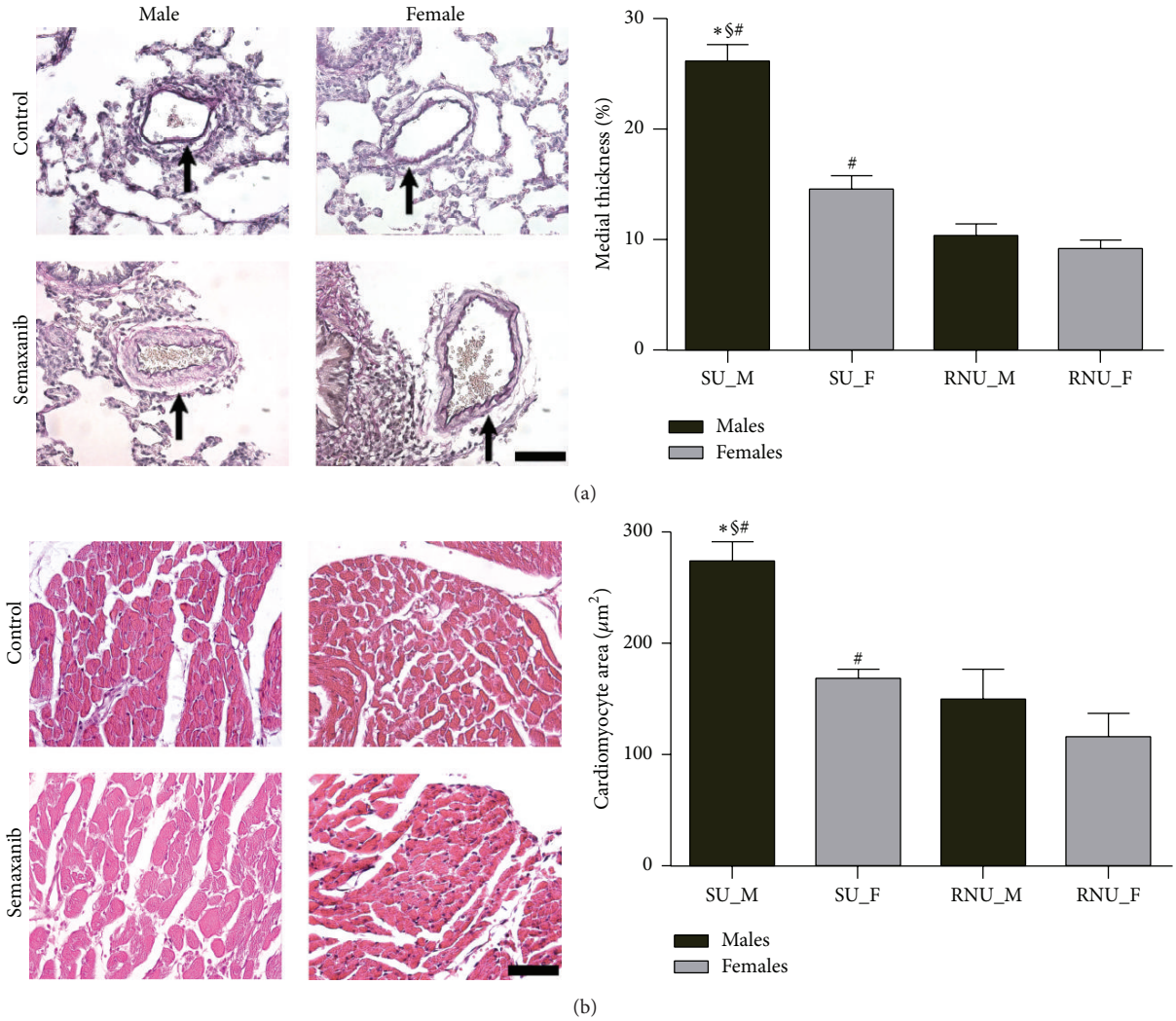

Figure 4: Morphometry of the pulmonary arteries and of the right ventricle at 4 weeks. (a) Pulmonary artery muscularization, defined by medial thickening over 10% of the cross-sectional diameter, was remarkable in male rats, while females did not develop significant medial hypertrophy in response to semaxanib injection (black arrows show the medial layer). (b) Similarly, cardiomyocytes hypertrophy was lower among females exposed to experimental PAH. Scale bars represent 50 μm. Abbreviations are in the text. ∗ § and # explain $P < 0.05$, respectively, compared to SU_F, RNU_M, and RNU_F (one-way ANOVA).

isolated hypertrophy of the medial layer was the hallmark of PA narrowing in our athymic rat model. Since we used a modified model of angioproliferative PH combining semaxanib injection in athymic nude rats under normoxic conditions [6], animals were thus exposed to a strong angioproliferative stress resulting in impairment of ventricular-arterial coupling efficiency, pleuropericardial effusion, and sudden death in males. Taraseviciene-Stewart et al. reported that T-cell deficiency is associated with severe PH after semaxanib injection under normoxic conditions [6]. In this modified angioproliferative PH model, animals share a progressive RV remodeling and dysfunction, with various ranges of severity, which was relevant for between-group comparisons.

Effects of estrogens on the pulmonary vasculature are complex and not clearly understood. Sex differences have been poorly investigated in PH. Jacobs et al. recently reported in a retrospective clinical study worse outcome in men, suggesting gender difference in cardiac adaptation to chronic PH [11]. The present study shows that female rats are experimentally protected against the development of severe PH and that the phenotype switch of SMCs from contractile to a dedifferentiated state occurs only in male rats after PH induction. The lack of major intimal damage in our model suggests that endogenous estrogens preserved RV-PA coupling through limitation of medial muscular thickening. We did not study ovariectomized females to prove whether PH severity was only related to the absence of estrogens in males or whether the gender differences observed here were only determined by a genetic predisposition between male and female rats. Further studies are necessary to investigate the potential of estrogen-therapy to reverse established pulmonary vascular remodeling in PH patients.

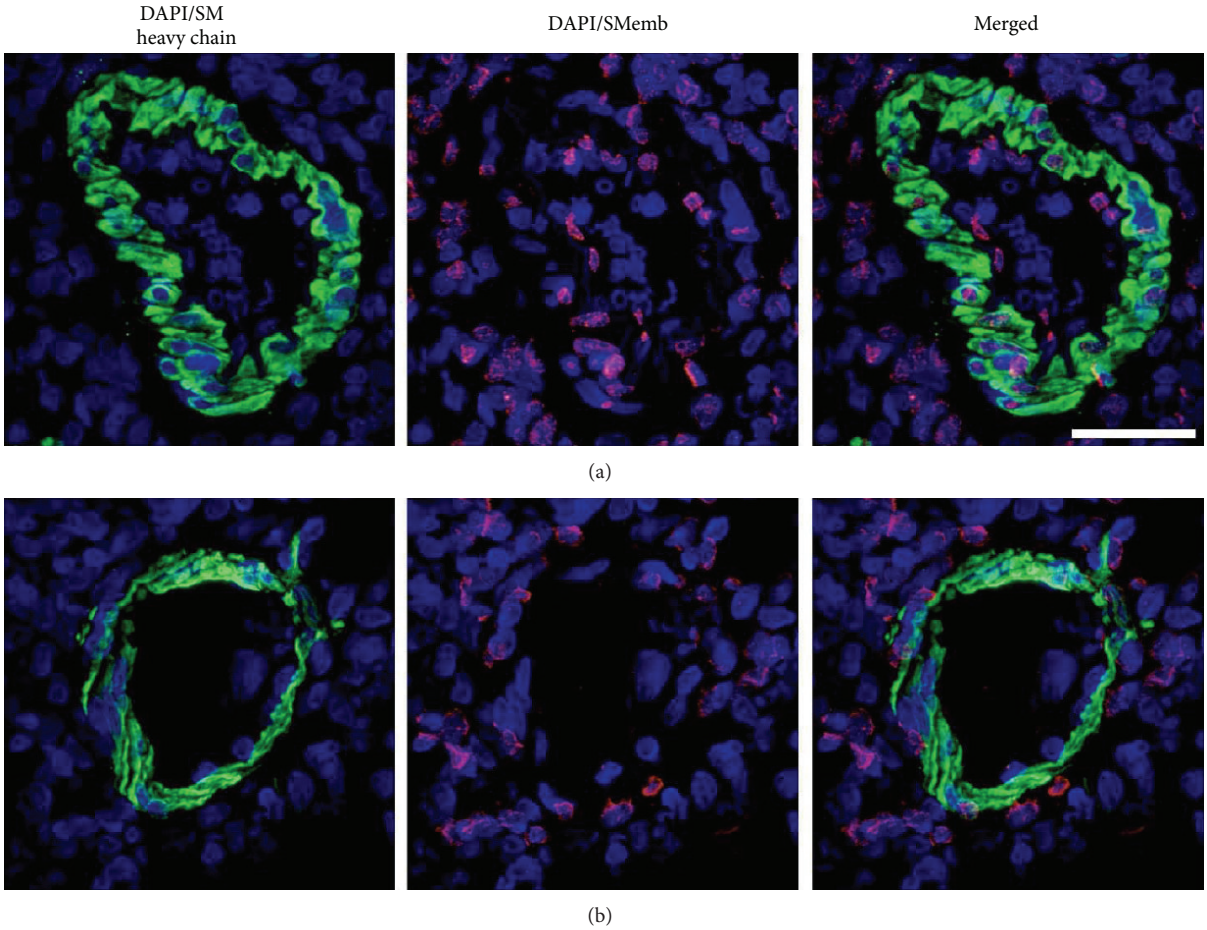

Figure 5: Immunofluorescence analysis of the pulmonary arteries at 4 weeks. (a) In male rats, SMemb, the embryonic form of smooth muscle myosin heavy chain and a marker for dedifferentiated SMCs, was increased within the pulmonary arteries, indicating SU-induced SMC-phenotype switch. (b) In contrast, confocal immunofluorescence revealed differentiated SMC-phenotype in female pulmonary arteries. (Blue: nucleus staining with DAPI; green: smooth-muscle-heavy-chain (SM heavy chain); pink: embryonic smooth muscle myosin heavy chain (SMemb); scale bars represent 33 μm).

5. Conclusions

Female athymic rats developed less severe pulmonary vascular damage as males in response to angioproliferative stress. Moderate pulmonary artery muscularization and the lack of phenotype switch of smooth muscle cells from contractile to dedifferentiated state was associated with preserved ventricular-arterial coupling and RV efficiency in semaxanib-treated females. Control of smooth muscle cells plasticity may be a promising therapeutic approach to reverse established vascular remodeling in PH patients.

Abbreviation

PAH: Pulmonary hypertension.

Conflict of Interests

The authors have no conflict of interests.

Authors' Contribution

Julien Guihaire performed the experiments, analyzed the data, and wrote the paper. Tobias Deuse designed the studies and wrote the paper. Dong Wang performed the experiments related to gender differences in SMC plasticity and edited the paper. Elie Fadel and Hermann Reichenspurner designed the studies and edited the paper. Sonja Schrepfer designed the studies, secured the funding, analyzed the data, and wrote the paper.

Acknowledgments

The authors thank Christiane Pahrmann for her technical assistance. They also thank UKE Imaging Facility (UMIF, Bernd Zobiak) and the UKE Animal Facility. This study was funded by the "Fédération Française de Cardiologie" (Paris, France: Julien Guihaire), the "Association Chirurgicale pour le Développement et l'Amélioration des Techniques de Dépistage et de Traitement des Maladies Cardiovasculaires" (Suresnes, France: Julien Guihaire), the German

Research Foundation (Deutsche Forschungsgemeinschaft; DFG: SCHR992/3-1 and SCHR992/4-1; Sonja Schrepfer), and the International Society for Heart and Lung Transplantation (ISHLT; Dong Wang and Sonja Schrepfer).

References

[1] S. Shapiro, G. L. Traiger, M. Turner, M. D. McGoon, P. Wason, and R. J. Barst, "Sex differences in the diagnosis, treatment, and outcome of patients with pulmonary arterial hypertension enrolled in the registry to evaluate early and long-term pulmonary arterial hypertension disease management," *Chest*, vol. 141, no. 2, pp. 363–373, 2012.

[2] M. Humbert, O. Sitbon, A. Chaouat et al., "Survival in patients with idiopathic, familial, and anorexigen-associated pulmonary arterial hypertension in the modern management era," *Circulation*, vol. 122, no. 2, pp. 156–163, 2010.

[3] S. P. Tofovic, "Estrogens and development of pulmonary hypertension: interaction of estradiol metabolism and pulmonary vascular disease," *Journal of Cardiovascular Pharmacology*, vol. 56, no. 6, pp. 696–708, 2010.

[4] S. P. Tofovic, X. Zhang, E. K. Jackson, S. Dacic, and G. Petrusevska, "2-Methoxyestradiol mediates the protective effects of estradiol in monocrotaline-induced pulmonary hypertension," *Vascular Pharmacology*, vol. 45, no. 6, pp. 358–367, 2006.

[5] L. B. Sweeney, H. J. Bogaard, R. Natarajan, D. Kraskauskas, and N. F. Voelkel, "Female gender protects against angioproliferative pulmonary hypertension induced by VEGF receptor inhibition and hypoxic exposure," in *Proceedings of the American Thoracic Society International Conference*, Abstract A1826, San Diego, Calif, USA, May 2009.

[6] L. Taraseviciene-Stewart, M. R. Nicolls, D. Kraskauskas et al., "Absence of T cells confers increased pulmonary arterial hypertension and vascular remodeling," *American Journal of Respiratory and Critical Care Medicine*, vol. 175, no. 12, pp. 1280–1289, 2007.

[7] B. Rondelet, F. Kerbaul, S. Motte et al., "Bosentan for the prevention of overcirculation-induced experimental pulmonary arterial hypertension," *Circulation*, vol. 107, no. 9, pp. 1329–1335, 2003.

[8] R. Paulin and E. D. Michelakis, "The estrogen puzzle in pulmonary arterial hypertension," *Circulation*, vol. 126, no. 9, pp. 1016–1019, 2012.

[9] K. M. Mair, A. K. Z. Johansen, A. F. Wright, E. Wallace, and M. R. Maclean, "Pulmonary arterial hypertension: basis of sex differences in incidence and treatment response," *British Journal of Pharmacology*, vol. 171, no. 3, pp. 567–579, 2014.

[10] H.-P. Gerber, A. McMurtrey, J. Kowalski et al., "Vascular endothelial growth factor regulates endothelial cell survival through the phosphatidylinositol 3′-kinase/Akt signal transduction pathway: requirement for Flk-1/KDR activation," *The Journal of Biological Chemistry*, vol. 273, no. 46, pp. 30336–30343, 1998.

[11] W. Jacobs, M. C. van de Veerdonk, P. Trip et al., "The right ventricle explains sex differences in survival in idiopathic pulmonary arterial hypertension," *Chest*, vol. 145, no. 6, pp. 1230–1236, 2014.

Published in final edited form as:

Transpl Int. 2017 November ; 30(11): 1181–1189. doi:10.1111/tri.13004.

THALIDOMIDE TREATMENT PREVENTS CHRONIC GRAFT REJECTION AFTER AORTIC TRANSPLANTATION IN RATS

Katharine K. Miller, PhD[a,b,c,d], **Dong Wang, MD**[a,b,c,d], **Xiaomeng Hu**[a,b,c,d], **Xiaoqin Hua, MD**[a,c,d], **Tobias Deuse, MD**[a,b,c,d,e], **Evgenios Neofytou, MD**[f,g], **Thomas Renne, MD, PhD**[h,i], **Joachim Velden, MD**[j], **Hermann Reichenspurner, MD, PhD**[c,d,e], **Sonja Schrepfer, MD, PhD**[a,b,c,d,e,*], and **Daniel Bernstein, MD**[k,l,*]

[a]University Heart Center Hamburg, Transplant and Stem Cell Immunobiology (TSI)-Lab, Hamburg, Germany

[b]Department of Surgery, Transplant and Stem Cell Immunobiology (TSI)-Lab, University California San Francisco (UCSF), San Francisco, California

[c]Cardiovascular Research Center (CVRC), University Medical Center Hamburg-Eppendorf, Hamburg, Germany

[d]German Centre for Cardiovascular Research (DZHK) e.V., University Medical Center Hamburg-Eppendorf, Hamburg, Germany

[e]Department of Cardiovascular Surgery, University Heart Center Hamburg, Hamburg, Germany

[f]Stanford Cardiovascular Institute, Stanford University School of Medicine, Stanford, California

[g]Division of Cardiology, Department of Medicine, Stanford University School of Medicine, Stanford, California

[h]Department of Clinical Chemistry, University Medical Center Hamburg, Hamburg, Germany

[i]Department of Molecular Medicine and Surgery, Karolinska Institute, Stockholm, Sweden

[j]Evotec AG, Manfred Eigen Campus, Hamburg, Germany

[k]Stanford Cardiovascular Institute, Stanford University School of Medicine, Stanford, California

[l]Department of Pediatrics (Cardiology) and the Cardiovascular Institute, Stanford University, Stanford, California

Abstract

Correspondence author contact Information: Prof. Dr. med. Sonja Schrepfer, University Heart Center Hamburg, Transplant and Stem Cell Immunobiology Lab (TSI), Campus Research (N27), Martinistr. 52, 20246 Hamburg, Germany, Phone: +49-40-7410-59982, sonja.schrepfer@ucsf.edu.

*shared last authorship

DR. SONJA SCHREPFER (Orcid ID : 0000-0002-7696-6229)

Authorship:

The concept was incepted by D.B. and S.S., project development and experiments were overseen by S.S., the manuscript was prepared by K.K.M. and E.N., additional scientific input and analysis was given by K.K.M., experiments were performed by D.W., X.H., X.H., T.D., T.R., and J.V., further scientific guidance was given by H.R., and final manuscript review was performed by D.B. and S.S.

Conflict of interest statement:

None of the authors has a conflict of interest.

Background—Cardiac allograft vasculopathy (CAV) affects approximately 30% of cardiac transplant patients at five years post-transplantation. To date there are few CAV treatment or prevention options, none of which are highly effective. The aim of the study was to investigate the effect of thalidomide on the development of CAV.

Methods—The effect of thalidomide treatment on chronic rejection was assessed in rat orthotopic aortic transplants in allogeneic F344 or syngeneic Lew rats (n=6/group). Animals were left untreated or received thalidomide for 30 days post-transplant, and evidence of graft CAV was determined by histology (trichrome and immunohistochemistry) and intragraft cytokine measurements.

Results—Animals that received thalidomide treatment post-transplant showed markedly reduced luminal obliteration, with concomitant rescue of smooth muscle cells (SMCs) in the aortic media of grafts. Thalidomide counteracted neointimal hyperplasia by preventing dedifferentiation of vascular SMCs. Measurement of intragraft cytokine levels after thalidomide treatment revealed down-regulation of matrix metalloproteinase 8 (MMP-8) and monocyte chemotactic protein 1 (MCP-1), cytokines involved in tissue remodeling and inflammation, respectively. Importantly, no negative side effects of thalidomide were observed.

Conclusions—Thalidomide treatment prevents CAV development in a rodent model and is therefore potentially useful in clinical applications to prevent post-transplant heart rejection.

Keywords

Cardiac allograft vasculopathy; rats; thalidomide

INTRODUCTION

Over the past several decades, patient survival after heart transplantation has improved; however, most of this benefit has accrued during the early period post-transplantation while long-term survival is still compromised by complications such as chronic cardiac allograft rejection, otherwise known as cardiac allograft vasculopathy (CAV). This form of chronic rejection – occurring months to years post-transplant – affects more than 30% of patients at 5 years post-transplant[1–3]. CAV is a highly aggressive form of coronary artery disease[4] caused by a combination of immune and non-immune responses that result in characteristic narrowing of donor coronary arteries, although the exact mechanisms remain unclear. Of the few treatment options available for CAV, most focus on prevention and none are particularly effective[5]. To this date, the only treatment option for patients with CAV associated with longer lifespan is re-transplantation, which carries a higher risk compared to the original transplant[6].

Thalidomide was originally introduced as a therapy for morning sickness in pregnant women, but was soon removed from the market due to its teratogenic effects[7]. However, thalidomide has since been repurposed as an immunomodulator, and has been approved for use as a treatment for multiple diseases, including multiple myeloma and erythema nodosum leprosum[8–10]. Thalidomide's anti-inflammatory and immunomodulatory functions as well as its beneficial effect on chronic graft-versus host disease after bone marrow transplantation make it an ideal candidate for preventing graft rejection[11]. Indeed, thalidomide alone or low

levels of thalidomide and cyclosporine can be used to reduce rejection of cardiac allografts in rabbits[12], and thalidomide has been found to lessen neotintimal thickness after aortic graft transplantation[13]. However, the mechanism by which thalidomide reduces rejection rates remains unknown, with reports conflicting regarding its effects on inflammatory cells, vascular pericytes, and SMCs.

Here we show effects of thalidomide treatment in a chronic rat orthotopic (Male Fischer 344:Male Lewis) aortic transplantation model. Thalidomide dramatically reduces the development of intimal thickening by rescuing SMC numbers, differentiation, and localization. Intragraft cytokine levels were measured to further determine thalidomide's possible mechanisms of action.

MATERIALS AND METHODS

Animals

All animals were purchased from Charles River Laboratories, Germany, and received care in compliance with the Guide for the Care and Use of Laboratory Animals prepared by the Institute of Laboratory Animal Resources and published by the National Institutes of Health (NIH Publication No. 86-23, revised 1996). Studies were approved by the local ethical committee "Hamburg Amt für Gesundheit und Verbraucherschutz".

Orthotopic Aortic Transplantation (Chronic CAV Study)

Orthotopic aortic transplantation was performed as previously described[14]. Briefly, a section of the thoracic aorta from F344 (allogeneic) or Lew (syngeneic) was orthotopically transplanted into the infra-renal abdominal aorta of Lew rats via an end-to-end anastomosis. Three groups (n=6 animals per group) were randomly assigned to receive either 100mg/kg/d of thalidomide p.o., or vehicle control.

Heterotopic Heart Transplantation (Acute Study)

Heterotopic heart transplantation was performed as previously described[15]. Briefly, BN (allogeneic) and Lew (syngeneic) hearts were heterotopically transplanted to the abdominal great vessels of Lew rats. Three groups (n=6 animals per group) were randomly assigned to receive either 100mg/kg/d of thalidomide p.o., or vehicle control. Six days post transplant, animals were euthanized, the apical half of the graft was snap frozen for cytokine quantification, and the caudal part was fixed (4% paraformaldehyde) for further tissue processing.

Histopathology

Harvested grafts were fixed (4% paraformaldehyde), dehydrated and embedded in paraffin. Each block was sectioned into five-micrometer sections followed by trichrome staining using the manufacturer's protocol (Sigma Aldrich) for evaluating luminal occlusion and immunofluorescence. Luminal obliteration was quantified, using Image J (Bethesda, MD) as follows: Vascular occlusion (%)=[Area of intima/(Area of intima+Vascular lumen)]×100. Three sections were analyzed from each aortic allograft, and results were averaged.

Immunofluorescence Staining

Paraffin sections underwent heat-induced antigen retrieval with Dako antigen retrieval solution (Dako, Glostrup, Denmark) followed by blocking with Image-iT FX signal enhancer (Invitrogen). Primary antibodies were used as appropriate: Smooth Muscle Actin (SMA) (ab5694), Smooth Muscle Heavy Chain (SMHC) (ab124679), or embryonic smooth muscle heavy chain (SmemB) (Yamasa 7602). A mouse irrelevant IgG1 (Abcam) was used as negative control. Secondary antibodies were Alexa Fluor 488 or Alexa Fluor 555 (Invitrogen). Imaging was performed using a Nikon Eclipse TiE microscope equipped with the Perkin Elmer UltraVIEW VoX confocal imaging system. Analysis was carried out with Volocity 6.1.1 (Perkin Elmer).

Side Effect Screening

Serum was obtained prior to animal sacrifice in order to investigate the effect of thalidomide on blood cholesterol, triglycerides, kidney, liver, and blood count.

Cytokine Antibody Array

Cytokine antibody arrays of homogenized grafts were performed according to the manufacturer's protocol (Raybiotech, Norcross, Georgia, USA). Membranes were digitized using bioluminescence imaging and quantified using Image J (Bethesda, Maryland). Cytokine concentrations are expressed in arbitrary units (AU).

Unidirectional ELISpot Assay

Recipient splenocytes (responder cells) were isolated from fresh spleen six days after heart transplantation. $1x10^6$ donor stimulator cells were incubated with $1x10^6$ responder cells for 24h. IFNγ spot frequencies were assessed in quadruplicate using an automatic counted ELISpot plate reader (CTL, Cincinnati, OH).

CFSE-MLR Proliferation Assay

The carboxyfluorescein succinimidyl ester–mixed lymphocyte reaction (CFSE-MLR) was performed with the acute heterotopic transplantation study animals. Briefly, Responder and stimulator cells were co-cultured at equal ratios ($3 x10^6$/ml) in a 48 well plate for five days at 37°C, 5% CO_2 in RPMI 1640 medium (Gibco) supplemented with 1% penicillin/streptomycin solution, 10% FCS and 50μM β-mercaptoethanol (Millipore, ES-007-E). Cells were harvested and analyzed by flow cytometry, gating for intensity of CFSE fluorescence. Stimulation index (SI) was calculated based on the mean value of each animal.

Statistics

Data are presented as mean ± standard deviation. Comparisons within groups used analysis of variance with Bonferroni or LSD Post-hoc tests, as appropriate. Probability values (*P*) less than 0.05 were considered significant. Statistical analysis was performed using SPSS statistical software package 15.0 for Windows (SPSS Inc., Chicago, IL).

RESULTS

Thalidomide treatment reduces luminal obliteration in chronic rejection model

We measured the effect of thalidomide on intimal thickening in a chronic low responder model using an accepted orthotopic aortic transplantation model for CAV[14,16]. Syngeneic transplants were performed as a procedural control. Allogeneic transplants were given either vehicle control or 100mg/kg thalidomide by oral gavage for 30 days post-transplant (Figure 1A).

As expected, syngeneic grafts showed no signs of cellular rejection in histology and exhibited minimal levels of luminal obliteration (1.32%) as compared to vehicle-treated allogeneic grafts (21.27%). Strikingly, animals treated with thalidomide showed marked reduction in luminal occlusion (6.76%, $p<0.001$) (Figure 1B/C), suggesting that thalidomide may be a viable option for preventing CAV.

SMCs of the aortic media are maintained by thalidomide in CAV model

Staining for smooth muscle actin (SMA) confirms that the aortic media of syngeneic grafts is largely comprised of mature SMCs (Figure 2A). A strong reduction in medial SMA intensity was found in vehicle-treated allogeneic grafts, an effect that was prevented by thalidomide-treatment. Quantification of immunohistochemical images confirmed these observations (Figure 2C).

To clarify SMC differentiation levels in each model, we compared smooth muscle cell heavy chain (SMHC; marker for differentiated SMCs) and embryonic smooth muscle heavy chain (SMemb; marker for dedifferentiated SMCs) intensities (Figure 2B/C). Our images visually and quantifiably revealed that syngeneic transplants have organized differentiated medial SMCs and low levels of dedifferentiated intimal SMCs. In contrast, vehicle-treated allogeneic transplants had decreased differentiated SMC levels and increased dedifferentiated SMCs. Thalidomide treatment strongly attenuated these effects, reducing dedifferentiated intimal cells to control levels with a corresponding increase in differentiated medial SMCs.

Thalidomide treatment alters intra-graft cytokine release profile

To investigate the mechanism by which thalidomide affects the proliferative and pathological features of CAV, we examined expression of key cytokines/chemokines induced in allogeneic graft transplantation (Figure 3). Cytokine protein arrays showed that several cytokines, including MMP-8, TIMP-1, MCP-1, and ICAM-1, were significantly upregulated in the vehicle-treated allogeneic group vs. controls. Thalidomide reduced expression levels of MMP-8 ($p<0.05$) and MCP-1 ($p<0.01$), cytokines associated with tissue remodeling and inflammation, respectively. Reduction of these cytokines may be indicative of thalidomide's mechanism of action: decreased tissue remodeling, as seen in our histological results, as well as reduced post-transplant inflammation.

No significant side effects caused by thalidomide treatment in rats

We tested the safety of thalidomide after allogeneic orthotopic aortic transplants. Animals treated with thalidomide showed no obvious signs of discomfort or distress. Blood samples from vehicle (n=3) or thalidomide (n=7) treated animals showed no significant differences in biomarkers of kidney function (BUN, creatinine), serum cholesterol and tryglyceride levels (cholesterol, triglyceride, LDL, HDL), liver function (ALT, AST), or whole blood count (RDW, Leukocyte, PLT, Hb, Hct, RBC, MCV, MCH, MCHC) (Supplementary Figure 1).

Thalidomide treatment does not attenuate lymphocyte activity in acute transplant rejection model

Since our data supports thalidomide as a potential therapy for CAV, we aimed to clarify whether the success of thalidomide treatment was due to a general reduction in graft rejection or whether it was specific to chronic rejection. Thus, we tested the effect of thalidomide treatment in heterotopic heart transplantation, an accepted rodent model for acute transplant rejection[15]. Syngeneic (Lew:Lew) or allogeneic (BN:Lew) transplantation was performed (Supplementary Figure 2A). Allogeneic transplant recipients received either vehicle control or thalidomide post-transplant. At six days post-operation (POD6), splenocytes were collected for ELISpot and mixed lymphocyte reaction (MLR) assays.

IFNγ levels – a proxy for systemic lymphocyte activation – were measured by ELISpot. In contrast to the dramatic effects of thalidomide in our chronic rejection model, thalidomide treatment did not appear to affect IFNγ production in our acute rejection model (Supplementary Figure 2B). Similarly, no alterations in lymphocyte proliferation were found by our MLR assay (Supplementary Figure 2C). These data suggest that thalidomide may be a specific treatment for chronic rejection, as it does not appear to be beneficial for reduction of acute rejection.

The primary pathology in CAV is coronary vessel intimal thickening; thus, reducing luminal obliteration would be highly advantageous to the long-term survival of transplant recipients.

DISCUSSION

CAV is a leading cause of late death for cardiac transplant recipients, and has remained resistant to therapeutic interventions. The identification of thalidomide as an immunomodulatory agent suggests its potential use in preventing graft rejection. Thalidomide has been described as having anti-cytokine, anti-integrin, and anti-angiogenic properties[17], and has beneficial effects in other proliferative diseases, including as a treatment for idiopathic pulmonary fibrosis, bone marrow transplantation, skin allograft transplantation, and heterotopic heart transplantation[12,18,19]. Since thalidomide's complete mechanism of action is yet unclear, we have investigated the pathophysiological effects of thalidomide in a rat aortic model of CAV. In this model, analysis of histopathological specimens is drastically facilitated since transplant vasculopathy may be examined in one single vessel of a sole defined diameter instead of the exploration of numerous small cardiac vessels showing a vast variety in size in the heterotopic heart transplant model. Indeed, the

immune response generated by an aortic allograft is sufficient to trigger chronic alterations in the transplant[20].

Our data suggest that thalidomide dramatically reduces luminal narrowing in an established rat model of CAV. Immunohistochemical analysis showed that loss of medial differentiated SMCs – a hallmark of CAV – was prevented by thalidomide treatment. Furthermore, thalidomide prevented dedifferentiation and intimal proliferation of SMCs. Our results are supported by recent literature showing beneficial effects of thalidomide in rat models of transplant arteriosclerosis and hereditary hemorrhagic telangiectasia[13,21].

Because the molecular mechanism of thalidomide is not yet clear, we generated an intragraft cytokine profile, showing that thalidomide significantly reduced expression of MMP-8 and MCP-1. Zhang et al. used immunohistochemistry and western blot to suggest that thalidomide alters VEGF, PDGF, and ICAM-1 levels, whereas we found no significant alteration in these molecules using the more accurate ELISpot and MLR assays[13]. This difference in observation is likely due to the fact that Zhang et al. used a high responder transplantation model (BN:Lew) in their assays, which does not accurately represent CA, while we used a more appropriate low responder model (F344:Lew) to simulate chronic rejection.

Matrix metalloproteases (MMPs) are zinc enzymes involved in extracellular matrix turnover. Interestingly, increased MMP expression levels have been connected with intimal thickening[22] and increased levels of MMP-2 and MMP-9 have been associated with chronic graft rejection[22]. MMP-8 itself appears to largely be produced by neutrophils, and is upregulated within the first few weeks post-transplantation[23]. Furthermore, general inhibition of MMPs prevents migration and proliferation of SMCs in CAV[24]. An MMP inhibitor that has been shown to reduce levels of MMP-8, was also linked to attenuation of CAV[24]. This is consistent with our findings, which show downregulation of MMP-8 associated with thalidomide treatment and reduced SMC proliferation and dedifferentiation.

Intragraft cytokine MCP-1 levels were also significantly reduced by thalidomide treatment. The literature surrounding MCP-1's function supports this data. Monocyte chemotactic protein-1 (MCP-1) is associated with inflammatory responses, namely recruiting monocytes, memory T cells, and dendritic cells to places of inflammation. Reduced levels of MCP-1 have been correlated with reduction of neointimal hyperplasia[25,26] and decreased chronic cardiac rejection[27].

Because of thalidomide's previously identified teratogenic effects[7], it was vital that we examine the potential side effects of thalidomide treatment. As seen with previous approval of thalidomide for treatment of erythema nodosum leprosum, we found no significant side effects to our thalidomide treatment in rats. However, the study period was only 28 days, thus lacking long-term data for safety and toxicity of thalidomide.

Finally, to further elucidate thalidomide's function, we wanted to clarify whether the effect we saw was specific to CAV or due to general immunogenic suppression. We examined whether thalidomide affected the pathogenic pathways associated with acute transplant rejection, namely T lymphocyte activation and proliferation. In contrast to the dramatic

effects seen on CAV pathophysiology, we did not see significant inhibition of lymphocyte activation or proliferation. This leads us to conclude that thalidomide likely does not reduce CAV via prevention of generalized immune activation, but rather through a different, more specific mechanism of action on the vascular wall.

In conclusion, we demonstrate that thalidomide treatment dramatically reduces CAV in a well-established rat model of chronic rejection, preventing the intimal proliferation and the loss of medial differentiated SMCs that are hallmarks of CAV. Thalidomide is therefore potentially useful in clinical applications to prevent CAV after human heart transplantation.

Supplementary Material

Refer to Web version on PubMed Central for supplementary material.

Acknowledgments

Funding sources:

This study was funded by the German Research Foundation (Deutsche Forschungsgemeinschaft; DFG: SCHR992/3-1 and SCHR992/4-1; S.S. and DE2133/2-1; T.D.), the International Society for Heart and Lung Transplantation (ISHLT; K.K.M., D.W. and S.S.), the Else Kröner Excellence Stipend from the Else-Kröner-Fresenius-Stiftung (2012_EKES.04), and the National Institutes of Health (NIH) grant R21 HL123655 (D.B.).

We thank Christiane Pahrmann for her technical assistance.

References

1. Taylor DO, Edwards LB, Boucek MM, et al. Registry of the International Society for Heart and Lung Transplantation: twenty-fourth official adult heart transplant report--2007. J Heart Lung Transplant. 2007; 26(8):769–781. [PubMed: 17692781]
2. Colvin-Adams M, Agnihotri A. Cardiac allograft vasculopathy: current knowledge and future direction. Clin Transplant. 2011; 25(2):175–184. [PubMed: 21457328]
3. Lindenfeld J, Miller GG, Shakar SF, et al. Drug therapy in the heart transplant recipient: part I: cardiac rejection and immunosuppressive drugs. Circulation. 2004; 110(24):3734–3740. [PubMed: 15596559]
4. Costello JP, Mohanakumar T, Nath DS. Mechanisms of chronic cardiac allograft rejection. Tex Heart Inst J. 2013; 40(4):395–399. [PubMed: 24082367]
5. Schmauss D, Weis M. Cardiac allograft vasculopathy: recent developments. Circulation. 2008; 117(16):2131–2141. [PubMed: 18427143]
6. Johnson MR, Aaronson KD, Canter CE, et al. Heart retransplantation. Am J Transplant. 2007; 7(9): 2075–2081. [PubMed: 17640316]
7. Franks ME, Macpherson GR, Figg WD. Thalidomide. Lancet. 2004; 363(9423):1802–1811. [PubMed: 15172781]
8. Singhal S, Mehta J, Desikan R, et al. Antitumor activity of thalidomide in refractory multiple myeloma. N Engl J Med. 1999; 341(21):1565–1571. [PubMed: 10564685]
9. Sheskin J. Thalidomide in the Treatment of Lepra Reactions. Clin Pharmacol Ther. 1965; 6:303–306. [PubMed: 14296027]
10. Matthews SJ, McCoy C. Thalidomide: a review of approved and investigational uses. Clin Ther. 2003; 25(2):342–395. [PubMed: 12749503]
11. Lim SH, McWhannell A, Vora AJ, Boughton BJ. Successful treatment with thalidomide of acute graft-versus-host disease after bone-marrow transplantation. Lancet. 1988; 1(8577):117.

12. Carvalho JB, Petroianu A, Travolo E, de Oliveira BH, Duarte AB, Alberti LR. Effects of immunosuppression induced by thalidomide and cyclosporine in heterotopic heart transplantation in rabbits. Transplant Proc. 2007; 39(5):1640–1641. [PubMed: 17580207]
13. Zhang Y, Yang M, Yang Y, et al. Thalidomide attenuates graft arteriosclerosis of aortic transplant in a rat model. Transplant Proc. 2011; 43(5):2022–2026. [PubMed: 21693319]
14. Stubbendorff M, Deuse T, Hammel A, Robbins RC, Reichenspurner H, Schrepfer S. Orthotopic aortic transplantation: a rat model to study the development of chronic vasculopathy. J Vis Exp. 2010; (46)
15. Deuse T, Hua X, Taylor V, et al. Significant reduction of acute cardiac allograft rejection by selective janus kinase-1/3 inhibition using R507 and R545. Transplantation. 2012; 94(7):695–702. [PubMed: 22971540]
16. Deuse T, Hoyt G, Koyanagi T, Robbins RC, Schrepfer S. Prevention and inhibition but not reversion of chronic allograft vasculopathy by FK778. Transplantation. 2008; 85(6):870–877. [PubMed: 18360270]
17. Peuckmann V, Fisch M, Bruera E. Potential novel uses of thalidomide: focus on palliative care. Drugs. 2000; 60(2):273–292. [PubMed: 10983733]
18. Ye Q, Chen B, Tong Z, et al. Thalidomide reduces IL-18, IL-8 and TNF-alpha release from alveolar macrophages in interstitial lung disease. Eur Respir J. 2006; 28(4):824–831. [PubMed: 16837501]
19. Chaves DN, Petroianu A, Alberti LR, Pereira WA. Effects of thalidomide, cyclosporine, and diclofenac on skin allograft survival in rabbits. Transplant Proc. 2004; 36(4):1018–1020. [PubMed: 15194354]
20. Mennander A, Tiisala S, Halttunen J, Yilmaz S, Paavonen T, Hayry P. Chronic rejection in rat aortic allografts. An experimental model for transplant arteriosclerosis. Arterioscler Thromb. 1991; 11(3):671–680. [PubMed: 2029505]
21. Lebrin F, Srun S, Raymond K, et al. Thalidomide stimulates vessel maturation and reduces epistaxis in individuals with hereditary hemorrhagic telangiectasia. Nat Med. 2010; 16(4):420–428. [PubMed: 20364125]
22. Suzuki J, Isobe M, Kawauchi M, Endoh M, Amano J, Takamoto S. Altered expression of matrix metalloproteinases and tissue inhibitors of metalloproteinases in acutely rejected myocardium and coronary arteriosclerosis in cardiac allografts of nonhuman primates. Transpl Int. 2000; 13(2):106–113. [PubMed: 10836646]
23. Aharinejad S, Krenn K, Zuckermann A, et al. Serum matrix metalloprotease-1 and vascular endothelial growth factor--a predict cardiac allograft rejection. Am J Transplant. 2009; 9(1):149–159. [PubMed: 19067665]
24. Hariya A, Takazawa K, Yamamoto T, Amano A. ONO-4817, a novel matrix metalloproteinase inhibitor, attenuates allograft vasculopathy in a rat cardiac transplant. J Heart Lung Transplant. 2004; 23(10):1163–1169. [PubMed: 15477110]
25. Ge S, Zhou G, Cheng S, et al. Anti-atherogenic effects of montelukast associated with reduced MCP-1 expression in a rabbit carotid balloon injury model. Atherosclerosis. 2009; 205(1):74–79. [PubMed: 19110249]
26. Ishihara T, Haraguchi G, Konishi M, et al. Effect of adiponectin on cardiac allograft vasculopathy. Circ J. 2011; 75(8):2005–2012. [PubMed: 21737957]
27. Itoh S, Nakae S, Axtell RC, et al. IL-17 contributes to the development of chronic rejection in a murine heart transplant model. J Clin Immunol. 2010; 30(2):235–240. [PubMed: 20130970]

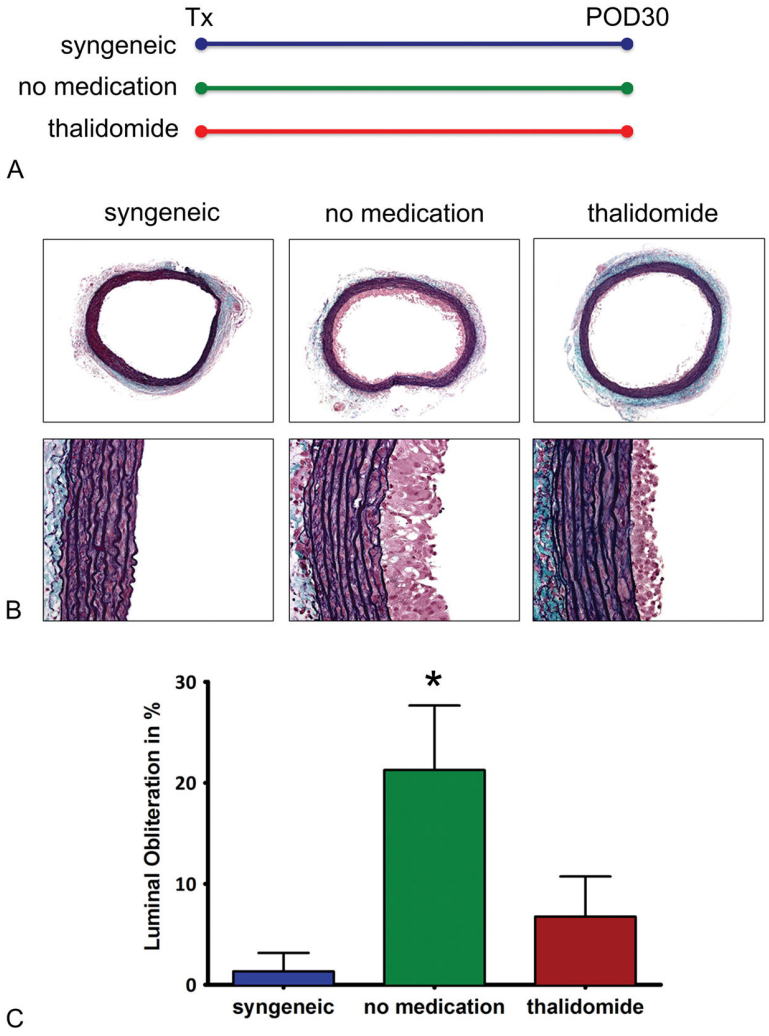

Figure 1. Treatment with thalidomide reduces luminal obliteration

(A) Overview of experimental protocol. Rats underwent either syngeneic (blue) or allogeneic (green and red) orthotopic aortic transplants. Allogeneic transplant recipients received either no medication (vehicle control, green) or thalidomide (100 mg/kg; red) by oral gavage for 30d post-transplant. (B) Representative Masson's trichrome-stained images of aortic luminae after treatment regime show that the increased luminal obliteration after allogeneic transplant is drastically reduced by thalidomide treatment. (Top row: 50x magnification; Bottom row: 400x magnification). (C) Quantification of luminal obliteration confirms levels of hyperplasia. The syngeneic model shows low base levels of obliteration (mean=1.34%), which is strongly increased in the allogeneic no medication control (mean=21.27%) and strikingly mitigated upon treatment with thalidomide (mean=6.76%; $p<0.001$). Error bars indicate mean ± SD. *$P<0.05$.

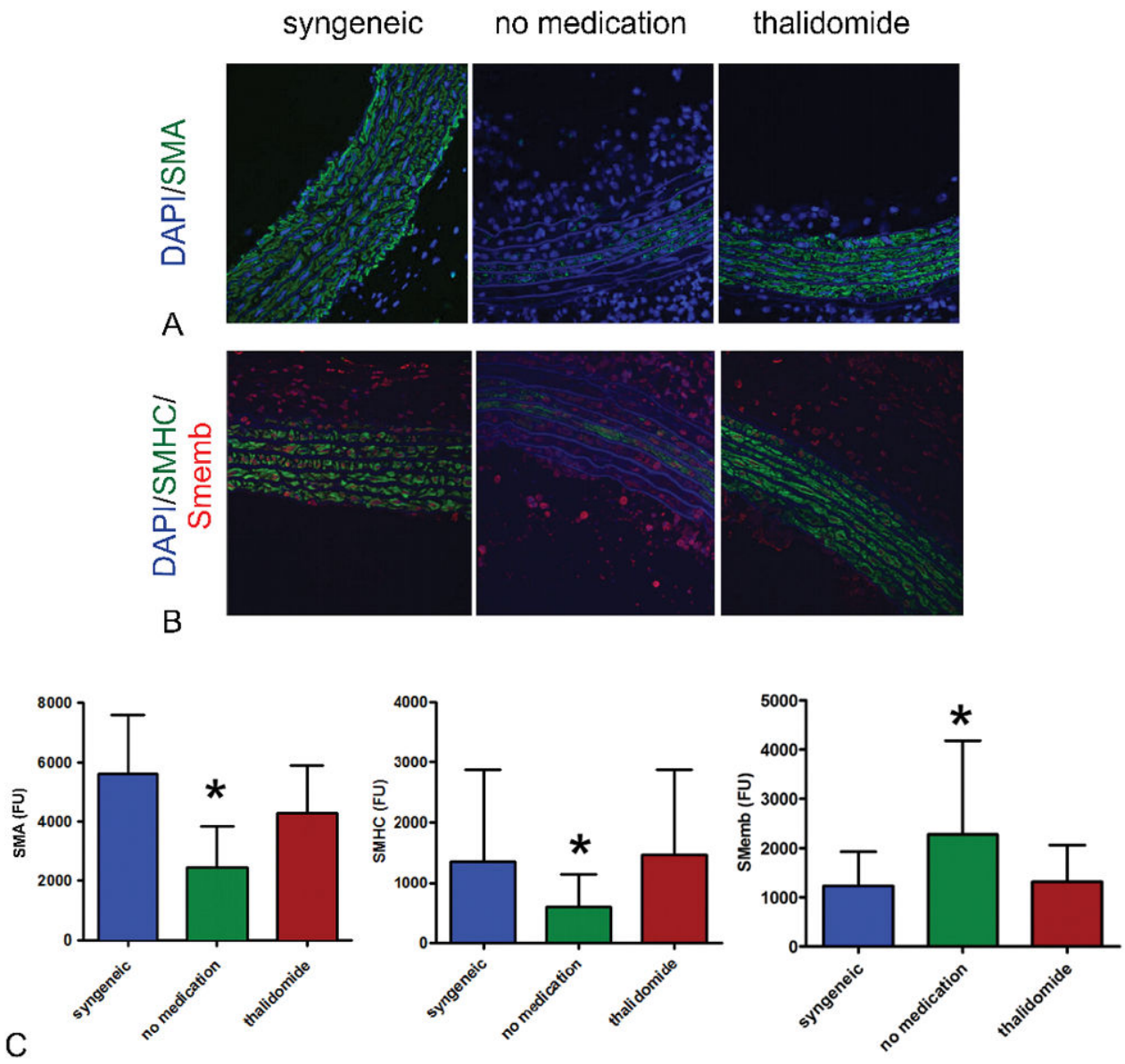

Figure 2. SMC number, differentiation, and localization are maintained by thalidomide treatment

(A) Mature SMCs stained with SMA (green) are shown organized at the aortic media in syngeneic model. While allogeneic no medication control treated animals show a disorganized media with a reduction in the number of SMCs, treatment with thalidomide shows a clear retention of both number and localization of SMCs (400x magnification). (B) Allogeneic transplant shows an increase in dedifferentiated SMCs (Smemb; Red) which correlates with a parallel loss of differentiated SMCs (SMHC; Green). Thalidomide treatment maintains differentiation and localization of SMCs. (400x magnification). (C) Quantification of fluorescence further confirms the retention of mature SMC by thalidomide treatment (SMA, SMHC) and dedifferentiated SMC (SMemb) levels. Error bars indicate mean ± SD. *P<0.05.

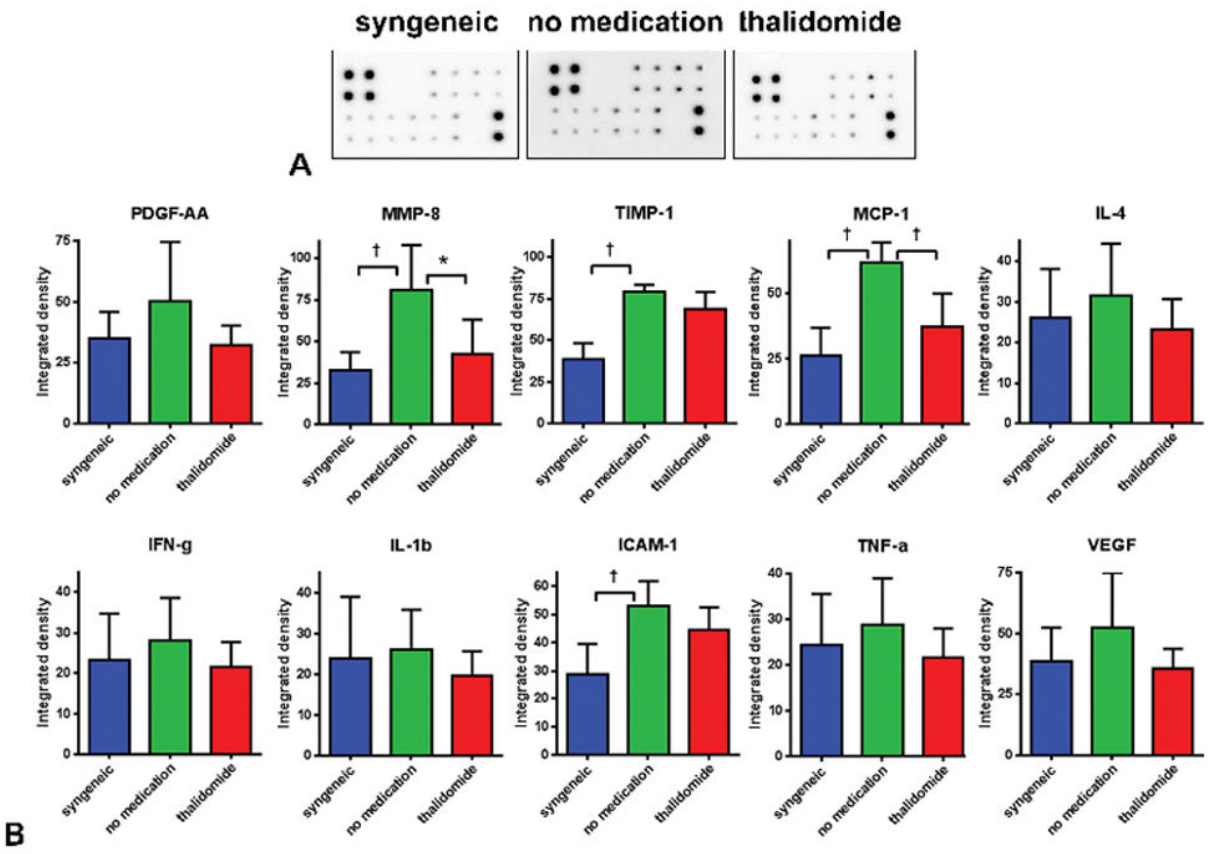

Figure 3. Cytokine profiles of grafts show thalidomide treatment reduces levels of specific cytokines

(A) Representative images of intragraft cytokine profiles for each graft type. (B) Quantification of cytokine profiles reveals that expression levels of MMP-8, TIMP-1, MCP-1 and ICAM-1 are upregulated after allogeneic transplant with no medication. MMP-8 and MCP-1 expression are reduced in the thalidomide treatment model. Error bars indicate mean ± SD. *P<0.05. †P<0.01.

nature biotechnology

LETTERS

https://doi.org/10.1038/s41587-019-0227-7

De novo mutations in mitochondrial DNA of iPSCs produce immunogenic neoepitopes in mice and humans

Tobias Deuse[1,16], Xiaomeng Hu[1,2,3,16], Sean Agbor-Enoh[4,5], Martina Koch[6], Matthew H. Spitzer[7,8,9], Alessia Gravina[1,3], Malik Alawi[10], Argit Marishta[5], Bjoern Peters[11], Zeynep Kosaloglu-Yalcin[11], Yanqin Yang[5], Raja Rajalingam[12], Dong Wang[1,2,3], Bjoern Nashan[6], Rainer Kiefmann[13], Hermann Reichenspurner[2,3], Hannah Valantine[5], Irving L. Weissman[14] and Sonja Schrepfer[1,2,3,15]*

The utility of autologous induced pluripotent stem cell (iPSC) therapies for tissue regeneration depends on reliable production of immunologically silent functional iPSC derivatives. However, rejection of autologous iPSC-derived cells has been reported, although the mechanism underlying rejection is largely unknown. We hypothesized that de novo mutations in mitochondrial DNA (mtDNA), which has far less reliable repair mechanisms than chromosomal DNA, might produce neoantigens capable of eliciting immune recognition and rejection. Here we present evidence in mice and humans that nonsynonymous mtDNA mutations can arise and become enriched during reprogramming to the iPSC stage, long-term culture and differentiation into target cells. These mtDNA mutations encode neoantigens that provoke an immune response that is highly specific and dependent on the host major histocompatibility complex genotype. Our results reveal that autologous iPSCs and their derivatives are not inherently immunologically inert for autologous transplantation and suggest that iPSC-derived products should be screened for mtDNA mutations.

iPSC-derived grafts can be immunogenic and rejected by the host even though they are derived from host cells. Several factors relating to the reprogramming of somatic cells, expansion of iPSCs in culture and differentiation of iPSCs into tissue cells are thought to contribute. Suppression[1] and overexpression[2] of pluripotency factors are known to establish de novo antigenicity that diminishes with differentiation[1,3,4]. However, differentiation of iPSCs can lead to the expression of immunogenic antigens not usually expressed in corresponding somatic cells causing rejection.[5] In addition, mutations acquired during reprogramming and expansion may generate mutant proteins that can act as neoantigens.

Mutation rates during reprogramming have been reported to be up to ninefold higher than the background mutation rate in culture.[6] Furthermore, the mutation rate for mtDNA is 10- to 20-fold higher than that of nuclear DNA[7–9]. Both mutated and wild-type mtDNA can coexist in the same cell, a phenomenon called heteroplasmy[10]. Nonsynonymous mtDNA mutations can impact both the function of proteins[11] and its antigenicity. mtDNA-encoded mitochondrial minor antigens[12] have been described as transplant barriers[13], and our group has shown that individual single nucleotide polymorphisms (SNPs) are sufficient to create immunogenic neoantigens[14]. However, the extent to which neoantigenic SNP enrichments affect autologous immune responses are not known. Here we sought to characterize the immunogenicity of mtDNA SNPs and assess their immunologic relevance for iPSC-based regenerative therapies.

First, we assessed the sensitivity and specificity of the mouse immune system to respond to isolated mtDNA SNPs. Using the technique of somatic cell nucleus transfer, embryonic stem cells (ESCs) with BALB/c (B/c) nuclear DNA and C57BL/6 (B6) mtDNA were generated (these cells are referred to as NT-ESCs throughout). In comparison to B/c, these NT-ESCs showed only two homoplasmic nonsynonymous SNPs in the *mt-Co3* and *mt-Cytb* genes, and generate cytochrome C oxidase III (Co3) or cytochrome b (Cytb) proteins with one amino acid substitution each (Supplementary Table 1). NT-ESCs were used for immunization against these two epitopes in B/c mice (Fig. 1a). To confirm that mitochondrial proteins with a single amino acid substitution can function as neoantigens, B/c fibroblasts were transfected to transiently overexpress either the B/c or B6 forms of Co3 or Cytb (Fig. 1a,b). Splenocytes recovered after 5 d were used for enzyme-linked immunospot (ELISpot) assays against either of the four fibroblast preparations. ELISpot assays for interferon-γ (IFN-γ) and interleukin-4 (IL-4) were performed. Spot

[1]Department of Surgery, Division of Cardiothoracic Surgery, Transplant and Stem Cell Immunobiology Lab, University of California, San Francisco, San Francisco, CA, USA. [2]Department of Cardiovascular Surgery, University Heart Center Hamburg, Hamburg, Germany. [3]Cardiovascular Research Center Hamburg and German Center for Cardiovascular Research, partner site Hamburg/Kiel/Luebeck, Hamburg, Germany. [4]Division of Pulmonary and Critical Care Medicine, The Johns Hopkins School of Medicine, Baltimore, MD, USA. [5]Laboratory of Transplantation Genomics, Division of Intramural Research, National Heart, Lung, and Blood Institute, Bethesda, MD, USA. [6]Department of Hepatobiliary and Transplant Surgery, University Medical Center Hamburg-Eppendorf, University Transplant Center, Hamburg, Germany. [7]Departments of Otolaryngology, Head and Neck Surgery and Microbiology and Immunology, Helen Diller Family Comprehensive Cancer Center, University of California, San Francisco, San Francisco, CA, USA. [8]Parker Institute for Cancer Immunotherapy, San Francisco, CA, USA. [9]Chan Zuckerberg Biohub, San Francisco, CA, USA. [10]Bioinformatics Core, University Medical Center Hamburg-Eppendorf, Hamburg, Germany. [11]Division of Vaccine Discovery, La Jolla Institute for Allergy and Immunology, La Jolla, CA, USA. [12]Immunogenetics and Transplantation Laboratory, Department of Surgery, University of California, San Francisco, San Francisco, CA, USA. [13]Department of Anaesthesia, University Medical Center Hamburg-Eppendorf, Hamburg, Germany. [14]Department of Developmental Biology, Stanford Institute for Stem Cell Biology and Regenerative Medicine, Stanford University School of Medicine, Stanford, CA, USA. [15]Sana Biotechnology Inc., South San Francisco, CA, USA. [16]These authors contributed equally: Tobias Deuse, Xiaomeng Hu. *e-mail: Sonja.Schrepfer@ucsf.edu

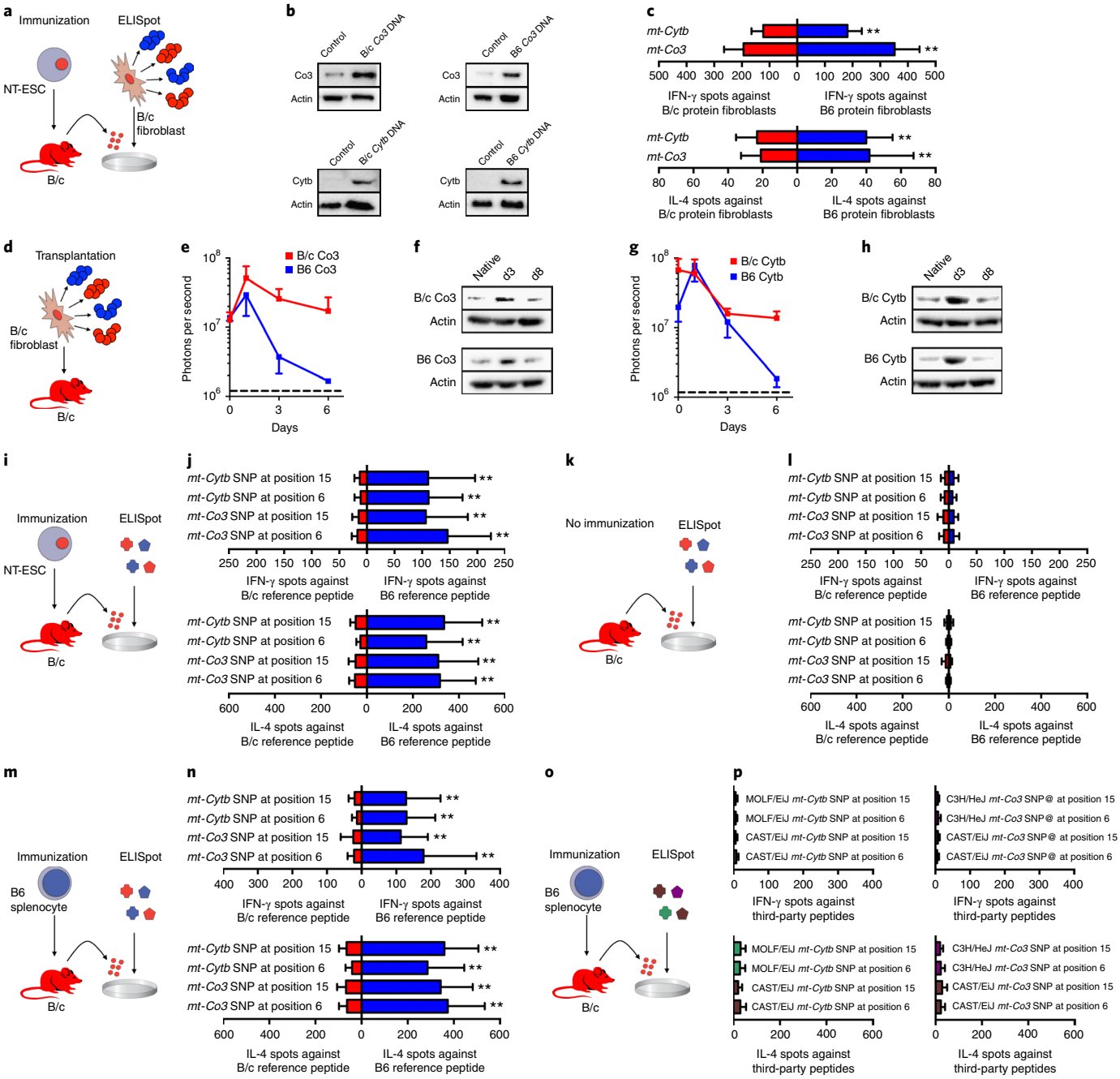

Fig. 1 | Immune response to allogeneic mtDNA-derived proteins in mice. a, B/c mice were immunized with NT-ESCs, which were generated by somatic cell nucleus transfer. NT-ESCs were suspended in saline and injected into the thigh muscle. NT-ESCs express two homoplasmic nonsynonymous mtDNA SNPs in the *mt-Co3* and *mt-Cytb* genes as compared to the B/c strain. **b**, We confirmed overexpression of the B/c or B6 forms of Co3 or Cytb protein in B/c fibroblasts using immunoblotting (pictures are representative of two replicates). **c**, Splenocytes were recovered after 5 d and their response against B/c fibroblasts expressing B/c (red) or B6 protein (blue) was assessed by IFN-γ and IL-4 ELISpot assay. Data are mean ± s.d. of quadruplicates from six animals per protein. **d**, B/c fibroblasts overexpressing B6 or B/c forms of Co3 or Cytb were suspended in saline and transplanted subcutaneously into B/c mice. **e**–**h**, Cell survival was assessed by bioluminescence imaging (BLI) and followed for 6 d. **e**,**g**, Cells were considered rejected when their BLI signals fell to background levels (dashed lines indicate background). Data are mean ± s.d. from five animals per group. **f**,**h**, Overexpression of B6 or B/c forms of Co3 or Cytb was confirmed over the 6-d study period by immunoblot. Blots are representative of two replicates. **i**, To confirm that the immunogenic epitope involves the SNP region, splenocytes of B/c mice immunized with NT-ESCs were tested against the B6-specific (blue) or B/c-specific (red) 20-residue oligomers with an amino acid variation at position 6 or 15. **j**, The immune responses were measured by ELISpot assay. Data are mean ± s.d. of quadruplicates from eight animals per 20-residue oligomer. **k**,**l**, The response of splenocytes derived from naive B/c mice and tested against the same B6-specific 20-residue oligmers (**k**) was assessed by ELISpot (**l**). Data are mean ± s.d. of quadruplicates from six (IFN-γ) or five (IL-4) animals per 20-residue oligomer. Significance was tested by two-tailed Student's *t* test. **m**, B/c mice were immunized with fully allogeneic B6 splenocytes that were MHC mismatched in addition to their mtDNA mismatch. **n**, IFN-γ and IL-4 spot frequencies were assessed in ELISpot assays. Data are mean ± s.d. of quadruplicates from eight animals per 20-residue oligomer. **o**,**p**, Splenocytes from B/c mice immunized with B6 cells (**o**) were tested against 20-residue oligomers derived from unconnected third-party strains (**p**). Data are mean ± s.d. of quadruplicates from five animals per 20-residue oligmer. Blue shades correspond to B6, red shades to B/c. **c**,**j**,**n**, $^{**}P < 0.01$, two-tailed Student's *t* test.

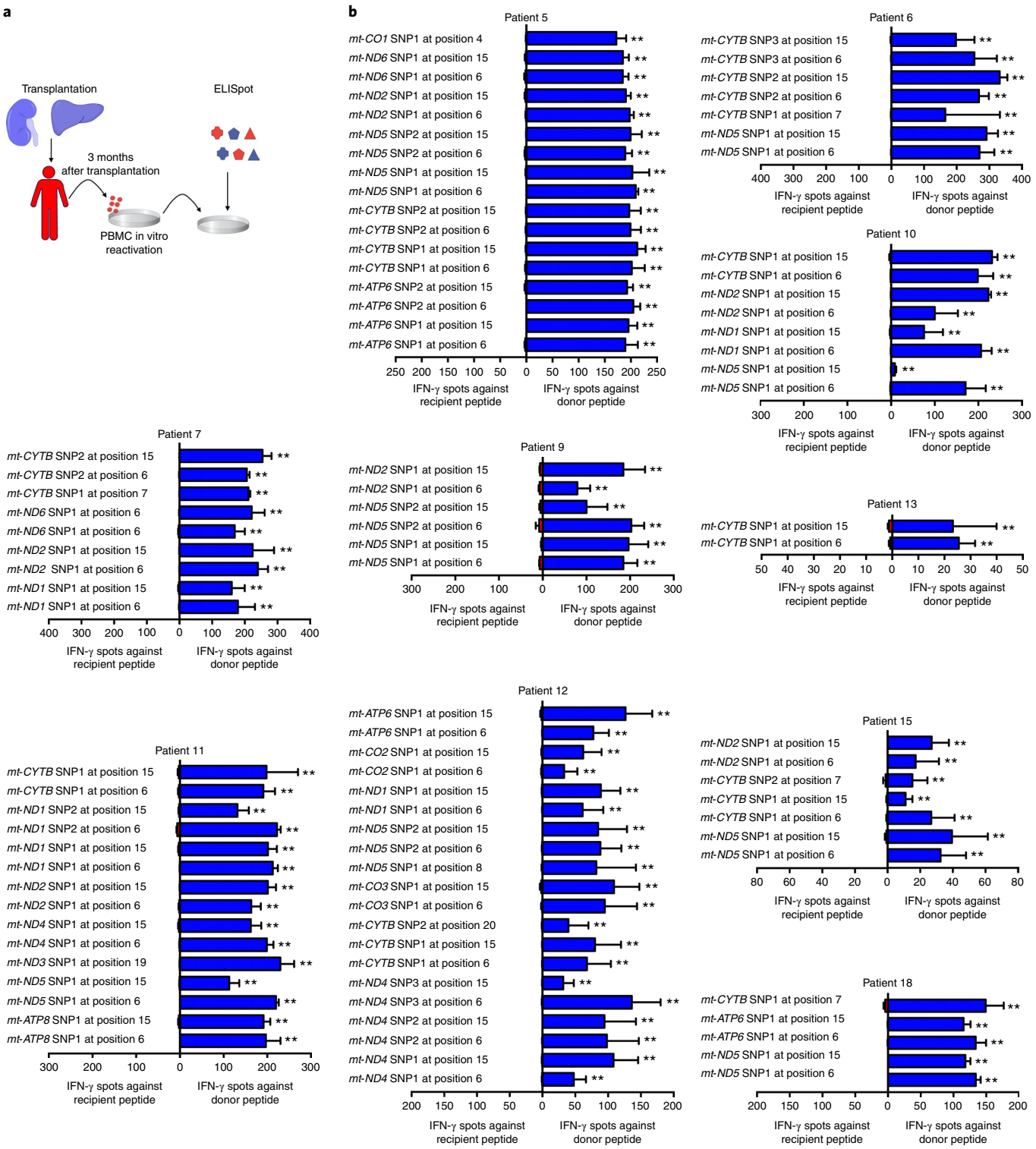

Fig. 2 | Immune response to allogeneic mtDNA-derived proteins in human transplant recipients. a, Patients underwent allogeneic kidney or liver transplantation. Donor–recipient pairs were screened for homoplasmic nonsynonymous mtDNA SNPs. After 3 months, recipient PBMCs were isolated, reactivated in vitro and incubated with 20-residue oligomer peptides covering the donor- or recipient-specific amino acid variation. **b**, PBMC responses were measured by ELISpot IFN-γ spot frequencies against the donor (blue) and recipient (red) 20-residue oligomers are shown for ten patients. Data are mean ± s.d. of quadruplicates per 20-residue oligomer and patient. Significance was assessed by two-tailed Student's *t* test, $^{**}P < 0.01$.

frequencies are presented to directly compare the immune response against the allogeneic B6 protein with that of the syngeneic B/c protein (Fig. 1c). Only the two fibroblasts overexpressing allogeneic B6 protein evoked a substantial T cell response. When transplanted into B/c recipients (Fig. 1d), only those two fibroblast grafts underwent rejection (Fig. 1e,g) during the time period of protein overexpression (Fig. 1f,h). Mass cytometry of splenocytes recovered after 5 d revealed remodeling of the T and B cell compartments as

well as alterations to natural killer cells and dendritic cells in animals challenged with allogeneic Co3 or Cytb (Supplementary Figs. 1 and 2). Taken together, these results are consistent with the notion that single mtDNA SNPs are sufficient to trigger a broad systemic immune response.

To verify that the T cell epitopes span the SNP, B/c mice were again immunized with NT-ESC grafts, but this time, splenocytes were directly challenged with 20-residue oligomer peptides designed around the SNP (Fig. 1i). Two 20-residue oligomer peptides per epitope were generated with the amino acid variation from the SNP at position 6 or 15 (thus, overlapping by 11 residues; Supplementary Table 1). Splenocytes specifically recognized all four allogeneic 20-residue oligomers and showed marked IFN-γ and IL-4 release (Fig. 1j). No immune activation was observed in non-immunized B/c animals (Fig. 1k,l). To assess the possibility of cross-reactivity against fetal nuclear-gene-derived antigens present in ESCs, B/c mice were immunized with B/c ESCs (Supplementary Fig. 3). Splenocytes did not recognize any of the four allogeneic 20-residue oligomers, confirming the specificity of the immune response and identifying the sequence covering the SNP as minor histocompatibility antigens (MiHAs).

The relevance of MiHAs may weaken in the allogeneic transplant context in the presence of multiple major histocompatibility complex (MHC) antigens owing to antigen competition. To test this, we immunized B/c mice ($H2^d$) with fully allogeneic B6 splenocytes ($H2^b$), which carry the same B6 mitochondria as the NT-ESCs but are MHC mismatched. Recipient splenocytes were challenged with the same peptides representing the four syngeneic and allogeneic 20-residue oligomers (Fig. 1m), and the observed immune responses (Fig. 1n) were similar in intensity to those obtained after NT-ESC immunization (see Fig. 1j). Twenty-residue oligomers designed on the basis of allogeneic Co3 and Cytb from unconnected third-party strains (Supplementary Table 2 and Fig. 1o) did not evoke an immune response (Fig. 1p). This highlights the strong antigenicity of mitochondrial MiHAs, which elicited strong and specific immune activation despite abundant competing mismatched MHC burden.

We wanted to assess the immunologic relevance of mtDNA SNPs in human allogeneic transplantation. Patients undergoing allogeneic kidney or liver transplantation were screened for homoplasmic mtDNA differences to their donors (>99% heteroplasmy; Supplementary Fig. 4a). In 15 donor–recipient pairs, we found a total of 81 nonsynonymous SNPs, varying from 1–12 per pair with higher numbers between more distant ethnic groups (Supplementary Fig. 4b–d). Twenty-residue oligomer peptides were again designed around the autologous and allogeneic SNP (Supplementary Table 3). Three months after transplantation, blood was drawn from the 15 immunosuppressed recipients and peripheral blood mononuclear cells (PBMCs) were isolated and underwent in vitro reactivation (Supplementary Fig. 5). Thereby, PBMCs from recipients with adequate immunosuppression (mean tacrolimus trough level = 9.6 ± 2.7 ng ml^{-1}) regained their activity within 24 h. Reactivated PBMCs were challenged with autologous or allogeneic 20-residue oligomers (Fig. 2a) and immune responses were observed for every allogeneic 20-residue oligomer in all patients (Fig. 2b and Supplementary Fig. 6). To confirm the specificity of these results, we studied samples from patients ($n = 6$) with blood drawn 6 months after transplantation. Reactivated PBMCs were challenged with autologous and allogeneic 20-residue oligomers from both their organ donor and an unconnected donor (Supplementary Fig. 7 and Supplementary Table 4). Again, immune responses were observed against 20-residue oligomers from every donor. Immune responses were not observed against 20-residue oligomers from unconnected donors, but when SNPs were also present in the patient's donor immune responses were observed. However, despite the specificity, we noticed that the degree of immune activation varied between patients and between 20-residue oligomers.

We next assessed whether the strength of the immune response to mutated mtDNA-derived MiHAs depended on the ability of the mitochondrial epitope to bind to host human leukocyte antigens (HLAs). Two volunteers underwent four-digit HLA typing, and in silico antigenicity prediction was performed for proteins harboring one of 232 annotated human missense SNPs from Ensembl[15] (Supplementary Table 5). Twenty-residue oligomers were generated for the five top and the five bottom SNPs based on the HLA type of each individual, as well as for the corresponding autologous epitope (Supplementary Table 6). PBMCs from those volunteers were then used in extended 14-d naive in vitro immunization ELISpot assays, allowing in vitro antigen presentation and lymphocyte priming (Supplementary Fig. 8a). As predicted, the five top SNPs were markedly more immunogenic than the five bottom SNPs (Supplementary Fig. 8b), confirming that the antigenicity of mtDNA SNPs depends on the host HLA repertoire for presentation.

To screen for the occurrence of de novo mutations or SNP enrichments, we generated B6 and FVB iPSCs from fibroblasts and serially sequenced their mtDNA during culture (Fig. 3a,b and Supplementary Tables 7 and 8). On the basis of our sequencing depth of 4,000–10,000 per base pair, we defined the threshold for detection at 1% variant heteroplasmy. De novo mutations were regarded as candidates for neoantigens when the non-dominant SNP heteroplasmy increased from <1% to >5%, which corresponds to a drop from >99% to <95% in positions where the dominant SNP differs from the reference genome. SNP enrichments were regarded as potential neoantigens when low-level heteroplasmies of <5% in the source parental cell increased to >15% (or heteroplasmies >95% dropped below 85%) during cell culture. Both high-passage iPSC

Fig. 3 | Antigenicity of low- and high-passage iPSCs and their iEC derivatives in mice. a,**b**, B6 (**a**) and FVB (**b**) iPSCs were generated from fibroblasts and expanded in vitro. The source fibroblasts, low-passage iPSCs and high-passage iPSCs underwent mtDNA sequencing, and the variant SNP heteroplasmy according to the GRCm38 mouse reference genome is shown in heat maps. Automated clustering of nonsynonymous SNPs with >1% variation in heteroplasmy over time is shown with the corresponding amino acid substitutions. SNPs that increased in heteroplasmy from <1% in fibroblasts (below the detection threshold) to >1% in iPSCs were defined as de novo mutations and are marked in green. SNPs that were present in the parental fibroblast (>1% heteroplasmy) and were diluted or enriched over time are marked in black. Candidate SNPs for neoantigens are outlined (mutagenic SNPs increasing in heteroplasmy from <1% to >5% or enriched SNPs increasing from <5% to >15%; alternatively, SNPs decreasing in heteroplasmy from >99% to <95% or from >95% to <85% in positions where the dominant SNP differs from the reference genome). **c**–**e**, B6 mice received different amounts of autologous low-passage (P7) or high-passage (P37) iPSCs grafts injected into the thigh muscle and were followed for immune response and teratoma development (**c**). **d**, After 5 d, splenocytes were recovered for ELISpot assays. Data are mean ± s.d. of quadruplicates from five animals per group, two-tailed Student's *t*-test. **e**, Teratoma growth is shown for every animal and the percentage of teratoma formation for each group is shown in a separate bar graph. Data are from five mice per cell amount and iPSC group. **f**–**h**, iECs derived from P7 or P37 iPSCs were transplanted into B6 mice and cell survival was followed by BLI (**f**). **g**, After 5 d, splenocytes were recovered for ELISpot assays. Data are mean ± s.d. of quadruplicates from five animals per group. Significance was assessed by two-tailed Student's *t* test. **h**, The survival of iEC (P7) and iEC (P37) grafts was assessed by BLI and the percentage of graft survival for each group is shown in a separate bar graph. Cells were considered rejected when their BLI signals fell to background levels. Individual animals are shown, $n = 5$ per iEC group; dashed lines indicate background.

lines from B6 and FVB revealed potential neoantigens. Single-cell sequencing of B6 cells showed that the heteroplasmies obtained in bulk sequencing accurately reflected the average of more heterogeneous heteroplasmies in individual cells (Supplementary Table 9).

The MHC binding affinities of the B6 neoantigen candidates were modeled using in silico prediction (Supplementary Fig. 8c and Supplementary Table 10), which showed that the mutant SNP in *mt-Co1* generated peptides with decent MHC binding affinities whereas the affinity of the mutant Nd3 peptide was very low. Twenty-residue oligomers were synthesized from a sequence carrying the neoantigenic or reference SNP (Supplementary Table 11). Mice were immunized with low-passage or high-passage iPSCs and splenocytes were

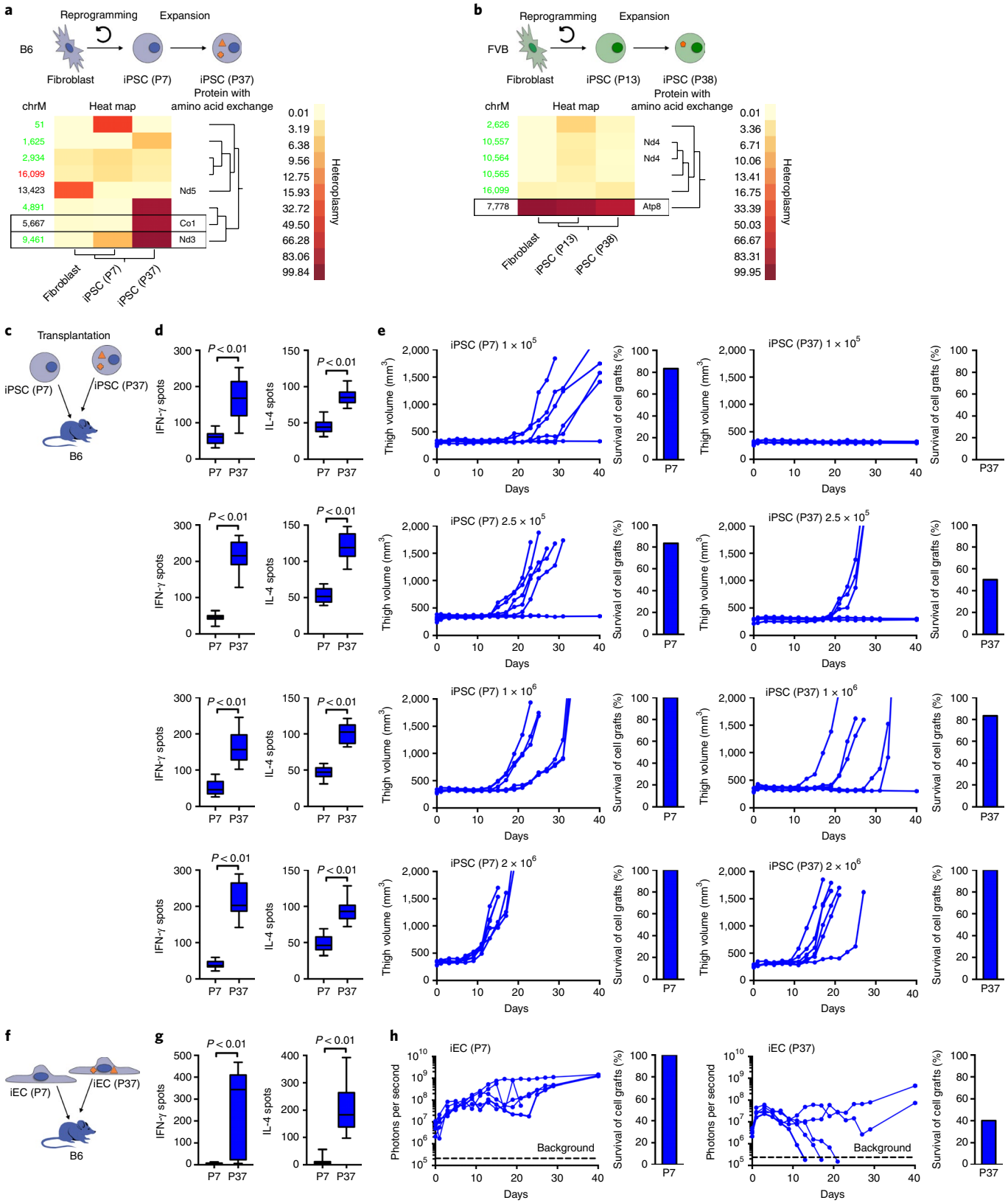

challenged with 20-residue oligomers 5 d later (Supplementary Fig. 8d–f). As predicted, in B6 mice we observed IFN-γ and IL-4 responses against the Co1 neoantigen but not the mutant Nd3. Immunogenicity was also demonstrated for the 20-residue oligomer of the Atp8 neoantigen in FVB (Supplementary Fig. 8g–i).

B6 (Fig. 3c–e) and FVB mice (Supplementary Fig. 9) then received subcutaneous grafts of either low-passage or high-passage iPSCs to assess whether the neoantigens could provoke an immune response and diminish cell survival in vivo. Varying cell numbers were used, as the survival and teratoma formation of pluripotent cell grafts depends on the overall cell load[16]. Across graft sizes, we observed an increased immune response and a correspondingly reduced survival of high-passage iPSC grafts.

Next, we sought to confirm the immunogenic nature of the reduced survival of B6 passage 37 (P37) iPSCs as compared to P7 iPSCs. Both P7 and P37 iPSCs showed similar proliferative capacity in vivo and in vitro (Supplementary Fig. 10 and Supplementary Video 1). P37 grafts showed more dense immune cell infiltrations than P7 in immunocompetent B6 mice (Supplementary Fig. 11a–d). Transplantation of low-dose P37 iPSCs in immunosuppressed or immunocompromised recipients did not cause substantial immune activation and resulted in 100% survival (Supplementary Fig. 11e–j). To assess whether this newly developed immunogenicity would persist after differentiation into functional tissue cells, B6 P7 and P37 iPSCs were differentiated into endothelial cells (iECs). We observed immune activation and markedly reduced survival of iEC P37 grafts, demonstrating that the acquired antigenicity persists after differentiation and is not associated with the pluripotency state (Fig. 3f–h).

We next aimed to assess whether MHC presentation of mtDNA neoantigens is required for T cell activation. We inactivated *B2m* and *Ciita* genes in P7 iPSCs using CRISPR–Cas9 and the derived MHC double knockout (dKO) iECs lacked expression of MHC class I and II, both of which were expressed in P7 iECs (Supplementary Fig. 12a–c). P7 and dKO iECs were then transfected to overexpress either B/c or B6 forms of Co3 and Cytb and used to immunize B6 mice (Supplementary Fig. 12d). Overexpression of syngeneic B6 Co3 and Cytb did not induce an IFN-γ response against either iEC population (Supplementary Fig. 12e). Overexpression of allogeneic B/c Co3 and Cytb induced an IFN-γ response in P7 iECs expressing MHC but did not induce a response in dKO iECs (Supplementary Fig. 12f). These results thus show that immunogenicity of mtDNA neoantigens requires MHC presentation.

Next, we evaluated the emergence of neoantigens during reprogramming and extended culture of human iPSCs (Fig. 4a). Four human iPSCs created from fibroblasts were sequentially sequenced up to ≥P60 (Fig. 4b–e and Supplementary Table 12). For nonsynonymous SNPs, the protein harboring the amino acid variation is listed. In all cases, unsupervised clustering automatically arranged the passages in the correct ascending order. The data show that, while the heteroplasmy of variant SNPs can drift in cell culture over time, the likelihood for de novo mutations and enrichment of rare SNPs increases with an increase in passages. The heteroplasmies quantified in bulk culture represent the mean of a more heterogeneic clonal distribution of cells with different degrees of heteroplasmy revealed by single-cell sequencing (Supplementary Table 13). Applying our previous definition, two of the four cell lines developed candidates for neoantigens (boxed SNPs). To assess whether mtDNA neoantigens similarly occur in vivo, blood was taken from six healthy volunteers over a 6- to 12-month period and PBMCs, a cell type with high turnover, were sequenced (Supplementary Table 14). Of note, all heteroplasmic SNPs in protein-coding regions were maintained at a relatively constant level in vivo, and we did not find a single neoantigen candidate (Supplementary Fig. 13). We assume mechanisms to scavenge neoantigenic cells are effective in vivo but ineffective in vitro, potentially owing to the lack of immune surveillance in cell culture.

To assess whether neoantigens in autologous human iPSC derivatives could induce rejection, PBMCs from healthy volunteers were reprogrammed to iPSCs, differentiated into endothelial cells (iECs) and expanded in culture to P35 (Fig. 4f). mtDNA sequencing revealed one neoantigen candidate mutation each in two of the three iECs (Fig. 4g and Supplementary Table 15). Extended naive in vitro immunization ELISpot assays with 20-residue oligomers for the predominant and non-dominant proteins (Fig. 4h) showed a specific immune response against the two neoantigenic non-dominant peptides, but not any of the other peptides (Fig. 4i). To test whether these mtDNA neoantigens were immunogenic on a cellular level, parental PBMCs and iPSCs were differentiated into macrophages, a possible target cell type for both PBMCs and iPSCs (Fig. 4f). Autologous ELISpot assays (Fig. 4j) confirmed that only neoantigen-carrying iPSC-derived macrophages induced an immune response (Fig. 4k). To examine whether such an immune response would suffice to reject autologous iEC grafts, fresh volunteer PBMCs were primed with iECs in vitro for 7 d (Fig. 4l) and then transferred to iEC layers for real-time impedance measurements. Primed PBMCs killed neoantigen-expressing autologous iECs from volunteers 1 and 2, but not the iECs from volunteer 3 (Fig. 4m). This suggests that autologous iPSC-based cell products expressing mtDNA neoantigens can be subject to rejection.

Fig. 4 | Occurrence and antigenicity of mtDNA-derived neoantigens in human iPSCs and iECs. a, Human iPSCs were generated from adult fibroblasts and were culture expanded over >60 passages. **b**–**e**, During this process, serial mtDNA sequencing was performed and heat maps showing the heteroplasmies of the variant SNPs versus the Cambridge reference sequence are presented. SNPs in the non-coding D loop are marked in red. Non-dominant SNPs with <1% heteroplasmy in parental fibroblasts that increased to >1% in iPSCs were considered de novo mutations and are marked in green. SNPs that were present in the fibroblasts and changed their heteroplasmy >1% over time are marked in black. Candidate SNPs for neoantigens are boxed (mutagenic SNPs increasing in heteroplasmy from <1% to >5% or enriched SNPs increasing from <5% to >15%; alternatively, SNPs decreasing in heteroplasmy from >99% to <95% or from >95% to <85% in positions where the dominant SNP differs from the reference genome). For nonsynonymous SNPs, the protein with the amino acid substitution is listed. **f**, PBMCs from three volunteers were reprogrammed to iPSCs, differentiated to iECs and culture expanded to P35. PBMCs and iPSCs were also differentiated into macrophages (a cell type that both source cells can reliably be differentiated into) to assess the immunogenicity of mtDNA neoantigens on a cellular level. **g**, mtDNA from PBMCs, iPSCs and iECs was sequenced and in two of three volunteers iPSCs and iECs showed one neoantigenic SNP candidate. **h**, For all coding SNPs that changed their heteroplasmy by >1% over time, fresh PBMCs from volunteers were incubated with 20-residue oligomers from the volunteer's predominant (blue) or non-dominant mtDNA SNPs (yellow). **i**, IFN-γ and IL-5 responses were assessed in extended naive in vitro immunization ELISpot assays. Data are mean ± s.d. of quadruplicates per 20-residue oligomer. Significance was assessed by two-tailed Student's *t* test. **j**, Fresh PBMCs from volunteers were incubated with the autologous PBMC-derived macrophages (PBMC-Mac) or iPSC-derived macrophages (iPSC-Mac) generated in **f**. **k**, The autologous IFN-γ and IL-5 immune responses were assessed in extended in vitro immunization ELISpot assays. Data are mean ± s.d. from eight replicates per group. Significance was tested by two-tailed Student's *t* test. **l**, Fresh PBMCs from volunteers were incubated with the autologous P35 iECs generated in **f** to immunize T cells in vitro for 7 d. PBMCs were then collected and transferred to P35 iEC layers grown on electrodes for a real-time in vitro impedance cytotoxicity assay. **m**, The integrity of the autologous iEC layers over 48 h was expressed as normalized cell index. Data are mean ± s.d. from triplicates per group. Subsequently, the iECs were collected and the percentage of living cells was assessed by flow cytometry. Data are mean ± s.d. of quadruplicates per group. $^{**}P < 0.01$.

Although the compact circular 16,569-base-pair human mtDNA only encodes 13 protein subunits of the electron transport chain, it may contribute to almost 30% of total mRNA in certain tissues[17]. Nonsynonymous SNPs may thus generate a high amount of mutant peptide. In our study, the immune system of both mice and humans was able to recognize and respond to every mtDNA

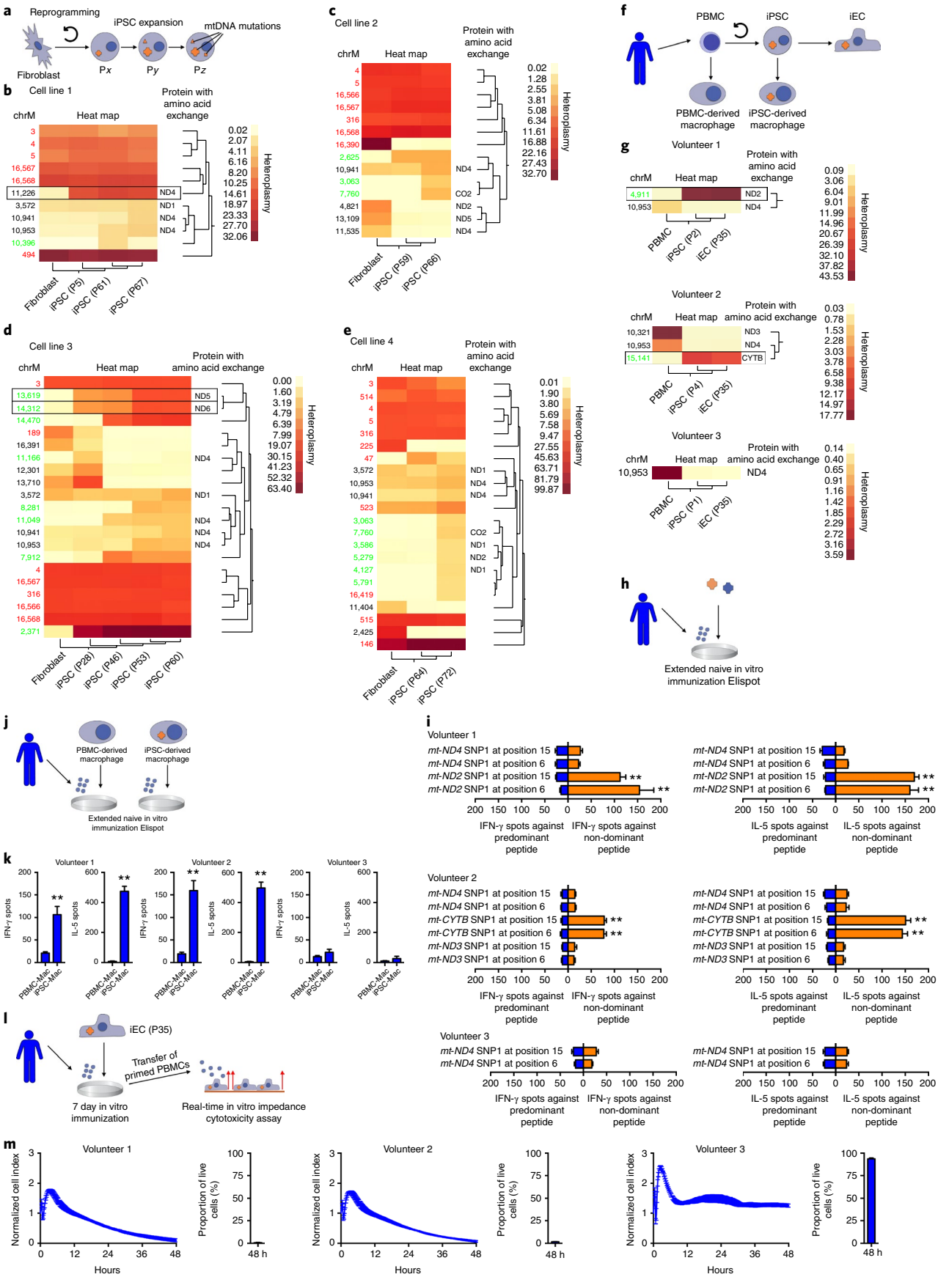

SNP-derived peptide (or the corresponding 20-residue oligomer) if it became sufficiently enriched to meet our definition of a neoantigen. Although the thresholds for changes in SNP heteroplasmy to qualify as neoantigen were set arbitrarily, we assumed the immune system would require a certain burden of mutant peptide to induce a response. A signaling threshold for the magnitude and duration of T cell-receptor signaling required for T cell activation has recently been described[18]. If an immune response was induced, it depended on MHC presentation, and we were able to predict immunogenicity on the basis of the host MHC genotype.

Presumably, most mtDNA heteroplasmies found in healthy tissue in vivo have been present since embryogenesis, and mtDNA SNP enrichments or de novo mutations are not regularly observed[10]. We believe that this phenomenon is due to constant immune surveillance. Malignant tumors, which evade immune clearance, show a much higher incidence of cancer-specific somatic mtDNA mutations in protein-coding or RNA-coding regions[10]. Long-term in vitro iPSC expansion resembles tumor growth, as it takes place in the absence of immune regulation and cell clones with growth advantage, whether attributed to their mtDNA or not, will promote their mtDNA composition within the overall expanding cell population. Reprogramming eliteness and clonal fitness have been shown to drive such cellular dynamics and poised clones are destined to dominate[19]. Most DNA[6,20–23], as well as mtDNA, mutations[11] found in iPSCs were shown to be derived from pre-existing mutations in donor cells, while de novo mutations were rather uncommon. However, no connection has so far been made with neoantigenicity of enriched SNPs. Extended iPSC culture, as shown herein, increases the risk of amplifying neoantigenic SNPs on a large scale. This acquired immunological barrier may become an inherent shortcoming of autologous iPSC-based regenerative strategies. Screening and assessment of neoantigenic mtDNA SNPs in industrial processes will be challenging. For the near future, unless such screening and assessments have been done, immunosuppression protocols for 'near match' iPSC products may be warranted.

Online content

Any methods, additional references, Nature Research reporting summaries, source data, statements of code and data availability and associated accession codes are available at https://doi.org/10.1038/s41587-019-0227-7.

Received: 13 November 2017; Accepted: 16 July 2019;
Published online: 19 August 2019

References

1. de Almeida, P. E. et al. Transplanted terminally differentiated induced pluripotent stem cells are accepted by immune mechanisms similar to self-tolerance. *Nat. Commun.* **5**, 3903 (2014).
2. Zhao, T., Zhang, Z. N., Rong, Z. & Xu, Y. Immunogenicity of induced pluripotent stem cells. *Nature* **474**, 212–215 (2011).
3. Araki, R. et al. Negligible immunogenicity of terminally differentiated cells derived from induced pluripotent or embryonic stem cells. *Nature* **494**, 100–104 (2013).
4. Guha, P., Morgan, J. W., Mostoslavsky, G., Rodrigues, N. P. & Boyd, A. S. Lack of immune response to differentiated cells derived from syngeneic induced pluripotent stem cells. *Cell Stem Cell* **12**, 407–412 (2013).
5. Zhao, T. et al. Humanized mice reveal differential immunogenicity of cells derived from autologous induced pluripotent stem cells. *Cell Stem Cell* **17**, 353–359 (2015).
6. Ji, J. et al. Elevated coding mutation rate during the reprogramming of human somatic cells into induced pluripotent stem cells. *Stem Cells* **30**, 435–440 (2012).
7. Brown, W. M., George, M. Jr. & Wilson, A. C. Rapid evolution of animal mitochondrial DNA. *Proc. Natl Acad. Sci. USA* **76**, 1967–1971 (1979).
8. Yakes, F. M. & Van Houten, B. Mitochondrial DNA damage is more extensive and persists longer than nuclear DNA damage in human cells following oxidative stress. *Proc. Natl Acad. Sci. USA* **94**, 514–519 (1997).
9. Zastawny, T. H. et al. Comparison of oxidative base damage in mitochondrial and nuclear DNA. *Free Radic. Biol. Med.* **24**, 722–725 (1998).
10. He, Y. et al. Heteroplasmic mitochondrial DNA mutations in normal and tumour cells. *Nature* **464**, 610–614 (2010).
11. Kang, E. et al. Age-related accumulation of somatic mitochondrial DNA mutations in adult-derived human iPSCs. *Cell Stem Cell* **18**, 625–636 (2016).
12. Loveland, B., Wang, C. R., Yonekawa, H., Hermel, E. & Lindahl, K. F. Maternally transmitted histocompatibility antigen of mice: a hydrophobic peptide of a mitochondrially encoded protein. *Cell* **60**, 971–980 (1990).
13. Hanekamp, J. S. et al. Cytoplasmic inheritance of transplantation antigens in animals produced by nuclear transfer. *Transplantation* **88**, 30–37 (2009).
14. Deuse, T. et al. SCNT-derived ESCs with mismatched mitochondria trigger an immune response in allogeneic hosts. *Cell Stem Cell* **16**, 33–38 (2015).
15. Yates, A. et al. Ensembl 2016. *Nucleic Acids Res.* **44**, D710–716 (2016).
16. Lee, A. S. et al. Effects of cell number on teratoma formation by human embryonic stem cells. *Cell Cycle* **8**, 2608–2612 (2009).
17. Mercer, T. R. et al. The human mitochondrial transcriptome. *Cell* **146**, 645–658 (2011).
18. Au-Yeung, B. B. et al. A sharp T-cell antigen receptor signaling threshold for T-cell proliferation. *Proc. Natl Acad. Sci. USA* **111**, E3679–3688 (2014).
19. Shakiba, N. et al. Cell competition during reprogramming gives rise to dominant clones. *Science* **364**, eaan0925 (2019).
20. Young, M. A. et al. Background mutations in parental cells account for most of the genetic heterogeneity of induced pluripotent stem cells. *Cell Stem Cell* **10**, 570–582 (2012).
21. Quinlan, A. R. et al. Genome sequencing of mouse induced pluripotent stem cells reveals retroelement stability and infrequent DNA rearrangement during reprogramming. *Cell Stem Cell* **9**, 366–373 (2011).
22. Laurent, L. C. et al. Dynamic changes in the copy number of pluripotency and cell proliferation genes in human ESCs and iPSCs during reprogramming and time in culture. *Cell Stem Cell* **8**, 106–118 (2011).
23. Sugiura, M. et al. Induced pluripotent stem cell generation-associated point mutations arise during the initial stages of the conversion of these cells. *Stem Cell Reports* **2**, 52–63 (2014).

Acknowledgements

We thank C. Pahrmann for cell culture work, assistance with experiments and immunoblots; G. Tediashvili for assistance with the in vivo experiments; and M.S. Mahadevan for computer assistance. Special thanks to R. Jaenisch (MIT, Department of Biology, MIT, Cambridge, MA) for providing the NT-ESCs and to J. Wu (Stanford Cardiovascular Institute, Stanford, CA) and P.-L. So (Stem Cell Core, Gladstone Institutes, San Francsico, CA) for providing the mouse and human iPSCs. Special thanks to D. Sun and X. Wu for their help in developing the targeted mtDNA sequencing and droplet digital PCR assays. We thank R. Nelson and K. Copeland for their support with in vivo imaging and M. Lewis for his support with the Xcelligence experiments. S.S. received research grants from the Deutsche Forschungsgemeinschaft (DFG; grants SCHR992/3-1, SCHR992/4-1), the Fondation Leducq (CDA 2013-2015) and the DZHK (German Center for Cardiovascular Research; grant FKZ 81Z2710105). D.W. was supported by the Max-Kade-Foundation (DFG). M.H.S. received an NIH shared instrumentation grant (1S10OD018040-01). B.P. and Z.K.-Y. were supported by the NIH (grant 1R21AI134127-01). S.A.-E., A. M., Y. Y. and H. V. were supported by National Heart Lung and Blood Institute (NHLBI) Intramural Research Program.

Author contributions

T.D. and S.S. designed the experiments, supervised the project and wrote the manuscript. X.H. performed the immunobiology experiments, molecular biology, imaging studies, cell culture work and analyzed the data. S.A.E., A.M., Y.Y. and H.V. performed the mtDNA sequencing and analysis. M.H.S. performed cytometry by time of flight experiments. A.G. did imaging studies and cell culture work. M.A. performed bioinformatics analyses. B.P. and Z.K.-Y. performed epitope predictions and designed 20-residue oligomers. R.R. performed HLA typing. D.W. performed the in vivo and immunofluorescence imaging studies (confocal microscopy). M.K., B.N. and R.K. performed the human kidney and liver transplant study. H.R. and I.L.W. gave technical support and conceptual advice. All authors contributed to editing the manuscript.

Competing interests

The authors declare no competing interests.

Additional information

Supplementary information is available for this paper at https://doi.org/10.1038/s41587-019-0227-7.

Reprints and permissions information is available at www.nature.com/reprints.

Correspondence and requests for materials should be addressed to S.S.

Publisher's note: Springer Nature remains neutral with regard to jurisdictional claims in published maps and institutional affiliations.

Methods

Mice. Male 6- to 8-week-old BALB/c (BALB/cAnNCrl, $H2^d$), C57BL/6 (C57BL/6 J, $H2^b$), FVB (FVB/NCrl), SCID-beige (CB17.Cg-*Prkdc*^{scid}*Lyst*$^{bg\text{-}J}$/Crl), and CD4-knockout (B6.129S2-*Cd4*^{tm1Mak}/J) mice were purchased from Charles River Laboratories or Jackson Laboratory, received humane care in compliance with the Guide for the Principles of Laboratory Animals, and experiments have complied with all relevant ethical regulations. Mouse studies were approved by the Hamburg Amt für Gesundheit und Verbraucherschutz or the University of California, San Francisco Institutional Animal Care and Use Committee. Some B6 animals were immunosuppressed with tacrolimus (Prograf, Astella Pharma) at a concentration of 0.5 mg kg^{-1} d^{-1}.

Generation and culture of ESCs. NT-ESCs were generated as previously described using F1 enucleated BDF1 oocytes (C57BL/6J × DBA/2NCrl) and somatic cell nucleus from BALB/c (B/c) fibroblasts[14]. NT-ESCs were cultured on γ-irradiated CF1 feeders (Millipore) using standard ESC medium (Gibco) containing leukemia inhibitory factor (LIF; Millipore). Before being used in experiments, NT-ESCs were cultured on gelatin (Millipore) without feeders using standard medium containing LIF. Cell cultures were regularly screened for mycoplasma infections (Lonza).

Mouse iPSC reprogramming and modification. FVB iPSCs were a gift from J. Wu (Stanford University, Stanford, CA). C57BL/6 iPSCs were generated by reprogramming mouse-tail-tip fibroblasts using a codon-optimized minicircle (CoMiC) construct as previously described[24]. CRISPR–Cas9 technology was used for the generation of B6 *B2m*$^{-/-}$*Ciita*$^{-/-}$ iPSCs[25]. Please see Supplementary Note 1 for details.

Mouse iPSC-derived iECs. For endothelial cell differentiation, mouse iPSCs were plated on gelatin in six-well plates. After the cells arrived at 60% confluence, the differentiation was started and medium was changed to RPMI-1640 containing 2% B-27 minus insulin (both Gibco) and 5 μM CHIR-99021 (Selleckchem). On day 2, the medium was changed to reduced RPMI-1640 containing 2% B-27 minus insulin and 2 μM CHIR-99021 (Selleckchem). From day 4 to day 7, cells were exposed to RPMI-1640 containing 2% B-27 minus insulin plus 50 ng ml^{-1} mouse vascular endothelial growth factor (mVEGF; R&D Systems), 10 ng ml^{-1} mouse fibroblast growth factor (mFGF; R&D Systems), 10 μM Y-27632 (Sigma Aldrich) and 1 μM SB 431542 (Sigma Aldrich). Endothelial cell clusters were visible from day 7 and cells were maintained in EGM-2 SingleQuots medium (Lonza) plus 10% heat-inactivated FCS (Gibco), 25 ng ml^{-1} mVEGF, 2 ng ml^{-1} mFGF, 10 μM Y-27632 (Sigma Aldrich) and 1 μM SB 431542. The differentiation process was completed after 21 d and undifferentiated cells detached during the differentiation process. For purification, cells went through MACS purification according to the manufactures' protocol using anti-CD15 monoclonal-antibody-coated magnetic microbeads (Miltenyi) for negative selection.

Human iPSC reprogramming. PBMCs were isolated from healthy volunteers and iPSCs were generated by the Yale University stem cell core laboratory using Sendai viral expression of *OCT4*, *SOX2*, *KLF4* and *MYC* genes. The experiments were approved by the University of California, San Francisco Institutional Review Board. Human iPSCs were plated on diluted Matrigel (356231, Corning) in six-well plates and maintained in Essential 8 Flex medium (Thermo Fisher Scientific). All human iPSC culture was feeder-layer free and cultures were clump passaged every 2–3 d. Cell cultures were regularly screened for mycoplasma infections (Lonza).

Human iPSC-derived iECs. For the differentiation to endothelial cells, iPSC cultures were grown to 60% confluence and medium was changed to RPMI-1640 containing 2% B-27 minus insulin and 5 μM CHIR-99021 (Selleckchem). On day 2 of the differentiation, the medium was changed to reduced RPMI-1640 containing 2% B-27 minus insulin and 2 μM CHIR-99021 (Selleckchem). From day 4 to day 7, cells were exposed to RPMI-1640 containing 2% B-27 minus insulin plus 50 ng ml^{-1} human vascular endothelial growth factor (VEGF; R&D Systems), 10 ng ml^{-1} human fibroblast growth factor (FGF; R&D Systems), 10 μM Y-27632 (Sigma Aldrich) and 1 μM SB 431542 (Sigma Aldrich). Endothelial cell clusters were visible from day 7 and cells were maintained in EGM-2 SingleQuots medium (Lonza) plus 10% heat-inactivated FCS (Gibco), 25 ng ml^{-1} VEGF, 2 ng ml^{-1} FGF, 10 μM Y-27632 (Sigma Aldrich) and 1 μM SB 431542 (Sigma Aldrich). The differentiation process was completed after 14 d and undifferentiated cells detached during the differentiation process. For purification, cells were treated with 20 μM PluriSln-1 (StemCell Technologies) for 48 h. The highly enriched iECs were cultured in EGM-2 SingleQuots medium (Lonza) plus supplements and 10% heat-inactivated FCS (Gibco). TrypLE was used for passaging the cells at a 1:3 ratio every 3–4 d.

Human fibroblast-derived iPSCs. Human iPSCs and their parental fibroblasts from four different individuals were provided by the Cardiovascular Institute at Stanford School of Medicine and the Stem Cell Core at the Gladstone Institutes. HLA typing confirmed that the cell lines had no common origin.

Human iPSC-derived macrophages. To differentiate iPSC-derived macrophages, 2×10^6 iPSCs were resuspended in DMEM 11965, supplemented with 10% KO-serum, 1% glutamine, 0.1 mM 2-mercaptoethanol and 1% RevitaCells (all Gibco) and were cultured in six-well low-attachment plates (Corning) for 4 d for embryoid body formation. Embryoid bodies were transferred to gelatin-coated six-well plates in macrophage medium containing DMEM 11965, supplemented with 10% heat-inactivated FCS, 1% glutamine, 0.1 mM 2-mercaptoethanol (all Gibco), 50 ng ml^{-1} human macrophage colony-stimulating factor (M-CSF) and 25 ng ml^{-1} human IL-3 (both Peprotech). Medium was changed every second day and non-adherent macrophages were collected on day 8. Macrophages were replated in macrophage medium with 100 ng ml human M-CSF for another 24 h before the cells were used for assays.

Human PBMC-derived macrophages. PBMCs were isolated by Ficoll separation (GE Healthcare) from fresh blood from healthy volunteers and were resuspended in RPMI-1640 with 10% heat-inactivated FCS, 1% penicillin–streptomycin (all Gibco) and 10 ng ml^{-1} human M-CSF (Peprotech). Cells were plated in 24-well plates at a concentration of 1×10^6 cells per milliliter (1 milliliter per 24-well plate) and medium was changed every second day until day 6. Macrophages were stimulated from day 6 with 1 μg ml^{-1} human IL-2 (Peprotech) for 24 h before the cells were used for assays.

Protein overexpression in fibroblasts or endothelial cells for Co3 and Cytb. For transfection experiments, 1.5×10^5 B/c fibroblasts or B6 iECs were plated per well into six-well plates and incubated overnight at 37 °C in a cell incubator. Next day, transfection experiments were performed using Fugene (Promega) and 6.6 μg of *Co3* DNA or *Cytb* DNA (Eurofins) in a 3:2 ratio. The transfection reagent solution was pipetted to OptiMEM (Gibco), mixed and incubated for 10 min at room temperature. The DNA transfection complex was added to 2 ml of cell medium. After 24 h, the transfection was stopped and cells were grown for another 48 h in cell-specific medium until they were used for experiments. Successful transfection was confirmed by immunoblots. Proteins were separated on SDS–PAGE gels (Invitrogen) and immunoblots were conducted with specific antibodies to Cytb (ab81215, Abcam), Co3 (ABIN223366, antikoerper-online.de) or actin (ab3280, Abcam). Membranes were digitized using BLI and quantified using the NIH ImageJ software v.1.46r. Actin served as a housekeeping control.

Human transplant study. Patients listed for kidney or liver transplantation gave consent to participate in this study. The study was approved by the External Review Board of the Ärztekammer Hamburg (PV5100) and complied with all relevant ethical regulations. A total of nine patients underwent kidney transplantation (patients 4, 7, 9, 10, 12, 13, 14, 15 and 16) and six patients underwent liver transplantation (patients 5, 6, 11, 17, 18 and 21). During the transplant operation, a blood sample from the recipient and some discarded fat tissue from the donor organ was collected and mtDNA sequencing was performed. Homoplasmic mismatches (heteroplasmy >99%) were identified. Twenty-residue oligomer peptides were designed and generated to cover the donor SNP and the recipient's own autologous SNP, respectively. Patients received standard immunosuppression, which included tacrolimus, cyclosporine A or co-stimulation blockers according to center-specific protocols. At 3 and 6 months after the transplantation (only at 6 months for patient 4), blood was drawn from the recipients during regular follow-up visits.

Ethylenediaminetetraacetic-acid-treated blood was drawn and tacrolimus was quantified using liquid chromatography–mass spectrometry (AescuLabor).

To verify the in vitro PBMC reactivation protocol, PBMCs from kidney or liver transplant recipients were isolated with Ficoll centrifugation (GE Healthcare). These PBMCs then served as responder cells either directly after cell isolation or after 24 h of in vitro cell culture with 1 μg ml^{-1} anti-CD3 and anti-CD28 antibodies (Sanquin) in IMEM medium supplemented with 1% penicillin–streptomycin (all Gibco) (Supplementary Fig. 4). Recipient responder PBMCs (5×10^5 cells) were incubated with phorbol myristate acetate (PMA; 1 ng ml^{-1}) and ionomycin (500 ng ml^{-1}) (both Sigma Aldrich) for 24 h and IFN-γ spot frequencies were automatically enumerated using an ELISpot plate reader (AID).

For quantitative PCR analysis of IL-2, PBMCs from patients after kidney or liver transplantation were isolated as described above and were stimulated either directly after cell isolation or after 24 h in vitro culture with 1 μg ml^{-1} anti-CD3 and anti-CD28 antibodies (Sanquin) with PMA (1 ng ml^{-1}) and ionomycin (500 ng ml^{-1}) (both Sigma Aldrich) for 4 h (Supplementary Fig. 4). Total RNA was isolated with a TRIzol-based RNA isolation protocol (Invitrogen). RNA was quantified by NanoDrop (Agilent Technologies). Samples required 260/280 ratios of >1.8. RNA was reverse-transcribed with the high-capacity cDNA reverse transcription kit (Applied Biosystems) according to the manufacturer's instructions. Quantitative determination of cDNA was performed by quantitative PCR with reverse transcription with SYBR Premix Ex taq II (Takara Bio), according to the manufacturer's instructions. IL-2 RNA was amplified using the following primers: forward, 5′-GTCACAAACAGTGCACCTAC-3′; and reverse, 5′-CCCTGGGTCTTAAGTGAAAG-3′. Experiments were performed on the Mx3000p (Agilent Technologies). The RNA amount was estimated according to the comparative C_t method using the $2^{-\Delta\Delta C_t}$ formula.

For the human ELISpot assays, PBMCs were isolated using Ficoll centrifugation (GE Healthcare), washed to eliminate immunosuppressive agents and cultured in

the presence of anti-CD3 and anti-CD28 antibodies (Sanquin) in IMEM medium supplemented with 1% penicillin–streptomycin (all Gibco) to reactivate their responsiveness. IFN-γ ELISpot assays were performed against the recipient and donor 20-residue oligomers. One hundred thousand responder PBMCs were incubated with each peptide at a concentration of 40 μg ml^{-1} for 48 h and IFN-γ spot frequencies were automatically enumerated as described before.

mtDNA sequencing and analysis. For human kidney or liver transplant donor–recipient pairs, genomic DNA was extracted from adipose tissue or 1×10^6 cells (Qiagen DNeasy Blood and Tissue kit, Qiagen). mtDNA was enriched by depletion of nuclear genomic DNA (depletion of methylated genomic DNA using anti-methylated-DNA-coated beads (Next Microbiome DNA Enrichment kit, New England Biolabs) and exonuclease digestion to remove the linear genomic DNA (New England Biolabs)) and targeted amplification of mtDNA sequences using mtDNA-specific primers and multiple-displacement technology (REPLI-g Mitochondrial DNA kit, Qiagen). Enzymatic fragmentation and tagmentation were used to prepare the mtDNA libraries (Nextera XT DNA Library Prep kit, Illumina). The quality of mtDNA libraries was analyzed by electrophoresis (Bioanalyzer 2100 High Sensitivity DNA, Agilent) before sequencing (HiSeq 2500, 2×50, Illumina). Raw sequencing data were cleaned up by Trimmomatic[26] (v.0.36) to remove Illumina adaptor sequences and unpaired reads. The trimmed paired reads were aligned to the revised Cambridge reference sequence (rCRS; accession number NC_012920)[27] using Bowtie2 (v.2.2.9)[28]. After marking PCR duplication reads in Picard (v.2.9.0; http://broadinstitute.github.io/picard/), the paired donor and recipient mapped reads were piled up by Samtools (v.1.4)[29]. The variants between each pair of donor and recipient samples were called in Varscan (v.2.4.3)[30] with the following customized parameters: --min coverage 500 --min reads 10 --min avg-qual 26 --min var-freq 0.02 --min freq-for-hom 0.95. The differences in mutation frequency between donor and recipient were computed for selection. A mismatched homoplasmy was selected if the difference in paired frequencies was greater than 95%. Differences in the frequencies in the range of 5% to 95% were grouped as mismatched heteroplasmy mutations. The annotation of variants was performed using ANNOVAR[31] and the UniProt IDs of nonsynonymous mutations were input into the UniProtKB database[32] to retrieve their amino acid sequence in fasta format.

The same pipeline and parameter settings were applied for analyzing mouse iPSC mitochondrial sequencing data referencing the chrMT genome retrieved from the GRCm38 mouse genome. Residual genetic material originating from mouse embryonic feeder cells (Supplementary Table 16) was excluded from further analysis. For sequential sequencing data of human and mouse mtDNA, SNPs were filtered out if their change in heteroplasmy was <1%. Heat maps showing the heteroplasmy of the variant SNP were generated. Our mtDNA sequencing method was confirmed using two established techniques (targeted sequencing and digital droplet quantitative PCR) focusing on individual SNP positions (Supplementary Table 17). For targeted sequencing, we designed primer sets to amplify both alleles of the SNP of interest. Using DNA from iPSC passages, the region of interest was amplified by PCR. Amplified sequences were used to make DNA libraries that were then pooled and sequenced on the Illumina MiSeq platform. Sequence reads were then aligned to the reference genome sequence to identify individual alleles. The percentage of the alleles were then computed and compared to the percentage derived from unbiased mtDNA sequencing. For single-cell targeted mtDNA sequencing, please see Supplementary Note 2.

Design of 20-residue oligomers. The amino acid sequences around the SNPs were obtained from the NCBI protein database (https://blast.ncbi.nlm.nih.gov/Blast.cgi). Peptides were synthesized as crude material on a small (1-mg) scale (A and A) and were prepared at 20 mg ml^{-1} in 100% DMSO for assays. Two 20-residue oligomer peptides per epitope were generated with the amino acid variation of the SNP at position 6 or 15, thus overlapping by 11 residues. If the amino acid corresponding to the SNP was located 8–14 positions from the start or end of the peptide, then the SNP in one of the 20-residue oligomers was displaced accordingly. If it was located less than 8 positions from the start or end of the peptide, then only one 20-residue or 21-residue oligomer was generated. The peptide sequences are provided in Supplementary Tables 1–4, 6, 11 and 15.

ELISpot assays. Human IFN-γ ELISpot assays (BD Bioscience) were performed against 20-residue oligomers using 10^5 responder PBMCs incubated with 40 μg ml^{-1} peptide for 48 h and IFN-γ spot frequencies were automatically enumerated using an ELISpot plate reader (AID).

When using non-stimulated responder cells, extended naive in vitro immunization ELISpot assays were performed. One hundred thousand PBMCs from human volunteers were incubated in vitro for 14 d in IMEM medium supplemented with 10% heat-inactivated FCS with 40 μg ml^{-1} of peptide and 1 μl ml^{-1} of anti-CD3 and anti-CD28 antibodies (Sanquin). If macrophages were used as stimulator cells, 10^5 responder PBMCs were incubated with 10^5 macrophages in RPMI medium containing 10% heat-inactivated FCS (Gibco). Macrophages were inhibited with mitomycin. Medium was changed on days 3, 7 and 10. IFN-γ (BD Bioscience) and IL-5 (Mabtech) spot frequencies were analyzed as described before.

For mouse ELISpot assays, recipient splenocytes were isolated from fresh spleen 5 d after cell injection and used as responder cells. When cells were used as stimulators, they were mitomycin-inhibited. One hundred thousand stimulator cells were incubated with 5×10^5 recipient responder splenocytes for 24 h and IFN-γ and IL-4 spot frequencies (both BD Bioscience) were automatically enumerated using an ELISpot plate reader (AID). When peptides were used as stimulators, isolated splenocytes from fresh spleen 5 d after cell injection or from untreated mice were preincubated in vitro for 24 h with 40 μg ml^{-1} peptide in RPMI medium containing 10% heat-inactivated FCS (all Gibco). Peptide (40 μg ml^{-1}) was incubated with 10^6 recipient responder splenocytes for 48 h and IFN-γ spot frequencies were automatically analyzed using an ELISpot plate reader (AID).

When using non-stimulated responder cells, extended naive in vitro immunization ELISpot assays were performed. One million splenocytes were incubated in vitro for 14 d in RPMI-1640 medium supplemented with 10% heat-inactivated FCS with 40 μg ml^{-1} peptide or 10^6 cells. Medium was changed on days 3, 7 and 10. IFN-γ spot frequencies were analyzed as described before.

ELISpot frequencies are displayed in bar graphs directly comparing two experimental conditions. The positive *x* axis shows the allogeneic or neoantigenic condition and the negative *x* axis shows the autologous, reference or control condition.

In vitro T cell-mediated rejection. T cell-mediated rejection was assessed with the real-time in vitro impedance XCelligence SP platform (ACEA BioSciences). Fresh PBMCs from volunteers and autologous iECs derived from the same volunteer were co-cultured with 1 μl ml^{-1} anti-CD3 and anti-CD28 antibodies (Sanquin) in six-well plates at a 1:1 ratio for 7 d. PBMCs were collected while iECs were discarded. In parallel, 96-well E-plates (ACEA BioSciences) were coated with gelatin (Millipore) and 4×10^5 iECs were plated in 100 μl of cell-specific medium. After the cell index value reached 0.7, PBMCs were transferred to the E-plates at an effector cell:target cell ratio of 1:1. As a control, iECs were grown in the absence of PBMCs. Data were standardized and analyzed with the RTCA software (ACEA).

After 90 h, iECs were collected and stained for the live/dead assay (LifeTechnologies). In brief, cells were stained with 2 μl of 50 μM calcein AM and 4 μl of 2 mM ethidium homodimer-1 for 45 min at 4 °C. The analysis was performed by flow cytometry (BD Bioscience) and results were expressed as a percentage of live cells. Please see Supplementary Note 3 for details on gating.

Mass cytometry (cytometry by time of flight). A summary of all mass cytometry antibodies, reporter isotopes and concentrations used for analysis can be found in Supplementary Table 18. Please see Supplementary Note 4 for details.

Teratoma development of mouse iPSCs in vivo. Before transplantation, iPSCs were cultured off-feeder for two passages to avoid contamination with feeder cells. Cells were trypsinated, resuspended in sterile saline and directly injected into the thigh muscles using a 27-gauge syringe (cell numbers as indicated in the figures). Cell survival leading to teratoma formation was monitored using a digimatic caliper (Mitutoyo). Animals were killed once the thigh volume exceeded 1,500 mm^3.

Bioluminescence imaging of iECs and fibroblasts. Luciferase-expressing iECs (5×10^5) were injected into the right thigh muscle of B6 animals using a 27-gauge syringe. Imaging was performed on days 0 and 1, every second day until day 30 and on day 40. Luciferase-expressing fibroblasts (5×10^5) overexpressing Co3 and Cytb were mixed at a 1:1 ratio with BD Matrigel high concentration (BD Biosciences) and 500 μl was injected subcutaneously into the right lower abdomen of B/c mice using a 23-gauge syringe. Imaging of the animals was performed on days 0, 3 and 6. BLI was performed on the amiHT bioimaging platform (Spectral Instruments Imaging). D-Luciferin potassium salt (Biosynth AG) dissolved in PBS, pH 7.4 (Gibco) was injected intraperitoneally (375 mg kg^{-1}) into anesthetized mice (2% isoflurane). Region of interest (ROI) bioluminescence was quantified in units of maximum photons per second per square centimeter per steradian. The maximum ROI signal was measured using AmiView Image Analysis Software (Spectral Instruments).

iPSC graft infiltration. A total of 1×10^6 B6 P7 or P37 iPSCs were injected below the kidney capsule of syngeneic B6 mice. After 5 d, the kidneys were recovered, embedded in paraffin and the injection sites were sectioned at 5-μm thickness. Slides were stained with antibodies against CD3 (Ab16669, Abcam), CD335 (16-3351-81, Thermo Fisher Scientific) and F4/80 (ab6640, Abcam) and were counterstained with DAPI (Thermo Fisher Scientific).

Epitope prediction. The Immune Epitope Database (IEDB) analysis resource[33,34], was used to perform predictions of MHC class I and MHC class II binding. We used the standalone versions of the MHC class I and MHC class II predictors with the default setting 'IEDB_recommended', which is usually a consensus method combining different prediction methods[33], and performed predictions for each MHC–peptide combination.

For the human prediction based on the volunteers' HLA type (see Supplementary Note 5), only the 232 annotated human missense SNPs with SIFT

prediction listed as 'tolerated' in Ensembl were used. For HLA class I peptides, we took lengths 8–11 into account, while for HLA class II peptides we considered 15-residue oligomers. The predicted percentile ranks were used to rank and select peptides for further evaluation. Based on the predicted percentile ranks, five peptides with the highest predicted immunogenicity and five peptides with the lowest predicted immunogenicity were picked for testing.

Mouse predictions are possible for B6, which express H-2 K^b and H-2 D^b for MHC class I and H2 IAb for MHC class II. For MHC class I, we considered less than second percentile rank a possible binder, less than first percentile a likely binder, and less than a half percentile a likely high-affinity binder. For MHC class II, we considered less than 20th percentile rank a reasonable threshold to identify candidates.

Statistics. In box plots, the median is shown, the edges of the box are the 25th and 75th percentiles and the whiskers extend to the most extreme data points. Bar graphs show the mean ± s.d. Intergroup differences were appropriately assessed by either unpaired Student's *t* test or one-way analysis of variance (ANOVA) with Bonferroni's post hoc test. $P < 0.01$ is represented by asterisks if space is restricted.

Reporting Summary. Further information on research design is available in the Nature Research Reporting Summary linked to this article.

Data availability

All epitope sequences and 20-residue oligomer sequences are presented in the paper. All data supporting the findings of this study are available in the paper and its supplementary information files. Sequencing data are available from the Sequence Read Archive under accession code PRJNA544330.

References

24. Diecke, S. et al. Novel codon-optimized mini-intronic plasmid for efficient, inexpensive, and xeno-free induction of pluripotency. *Sci. Rep.* **5**, 8081 (2015).
25. Deuse, T. et al. Hypoimmunogenic derivatives of induced pluripotent stem cells evade immune rejection in fully immunocompetent allogeneic recipients. *Nat. Biotechnol.* **37**, 252–258 (2019).
26. Bolger, A. M., Lohse, M. & Usadel, B. Trimmomatic: a flexible trimmer for Illumina sequence data. *Bioinformatics* **30**, 2114–2120 (2014).
27. Andrews, R. M. et al. Reanalysis and revision of the Cambridge reference sequence for human mitochondrial DNA. *Nat. Genet.* **23**, 147 (1999).
28. Langmead, B. & Salzberg, S. L. Fast gapped-read alignment with Bowtie 2. *Nat. Methods* **9**, 357–359 (2012).
29. Li, H. et al. The Sequence Alignment/Map format and SAMtools. *Bioinformatics* **25**, 2078–2079 (2009).
30. Koboldt, D. C. et al. VarScan 2: somatic mutation and copy number alteration discovery in cancer by exome sequencing. *Genome Res.* **22**, 568–576 (2012).
31. Wang, K., Li, M. & Hakonarson, H. ANNOVAR: functional annotation of genetic variants from high-throughput sequencing data. *Nucleic Acids Res.* **38**, e164 (2010).
32. The UniProt Consortium UniProt: the universal protein knowledgebase. *Nucleic Acids Res.* **45**, D158–D169 (2017).
33. Fleri, W. et al. The immune epitope database and analysis resource in epitope discovery and synthetic vaccine design. *Front. Immunol.* **8**, 278 (2017).
34. Kim, Y. et al. Immune epitope database analysis resource. *Nucleic Acids Res.* **40**, W525–530 (2012).

nature research

Corresponding author(s): Sonja Schrepfer

Last updated by author(s): Jul 11, 2019

Reporting Summary

Nature Research wishes to improve the reproducibility of the work that we publish. This form provides structure for consistency and transparency in reporting. For further information on Nature Research policies, see Authors & Referees and the Editorial Policy Checklist.

Statistics

For all statistical analyses, confirm that the following items are present in the figure legend, table legend, main text, or Methods section.

n/a	Confirmed	
☐	☒	The exact sample size (*n*) for each experimental group/condition, given as a discrete number and unit of measurement
☐	☒	A statement on whether measurements were taken from distinct samples or whether the same sample was measured repeatedly
☐	☒	The statistical test(s) used AND whether they are one- or two-sided *Only common tests should be described solely by name; describe more complex techniques in the Methods section.*
☐	☒	A description of all covariates tested
☐	☒	A description of any assumptions or corrections, such as tests of normality and adjustment for multiple comparisons
☐	☒	A full description of the statistical parameters including central tendency (e.g. means) or other basic estimates (e.g. regression coefficient) AND variation (e.g. standard deviation) or associated estimates of uncertainty (e.g. confidence intervals)
☐	☒	For null hypothesis testing, the test statistic (e.g. *F*, *t*, *r*) with confidence intervals, effect sizes, degrees of freedom and *P* value noted *Give P values as exact values whenever suitable.*
☒	☐	For Bayesian analysis, information on the choice of priors and Markov chain Monte Carlo settings
☐	☒	For hierarchical and complex designs, identification of the appropriate level for tests and full reporting of outcomes
☒	☐	Estimates of effect sizes (e.g. Cohen's *d*, Pearson's *r*), indicating how they were calculated

Our web collection on statistics for biologists contains articles on many of the points above.

Software and code

Policy information about availability of computer code

Data collection	FlowJo7 was used to analyze flow cytometric data. HLA genotyping was assigned using TwinTM version 2.0.1 (Omixon). Western Blot membranes were digitized using bioluminescence imaging and quantified using the NIH ImageJ software version 1.46r. Raw mtDNA sequencing data were cleaned up by Trimmomatic (v0.36) to remove Illumina adapter sequences and unpaired reads. The trimmed paired reads were aligned to the revised Cambridge Reference Sequence (rCRS, accession number NC_012920) by Bowtie2 (v2.2.9). The maximum ROI signal in BLI imaging was measured using AmiView Image Analysis Software (Spectral Instruments).
Data analysis	Prism7 was used for graphing and statistical analysis. Elispots were enumerated by Immunospot software.

For manuscripts utilizing custom algorithms or software that are central to the research but not yet described in published literature, software must be made available to editors/reviewers. We strongly encourage code deposition in a community repository (e.g. GitHub). See the Nature Research guidelines for submitting code & software for further information.

Data

Policy information about availability of data

All manuscripts must include a data availability statement. This statement should provide the following information, where applicable:

- Accession codes, unique identifiers, or web links for publicly available datasets
- A list of figures that have associated raw data
- A description of any restrictions on data availability

All epitope sequences and 20mer sequences are presented in the paper. All data supporting the findings of this study are available in the paper and its Supplementary Information files. Sequence Read Archive accession code for sequencing files: PRJNA544330.

Field-specific reporting

Please select the one below that is the best fit for your research. If you are not sure, read the appropriate sections before making your selection.

☒ Life sciences ☐ Behavioural & social sciences ☐ Ecological, evolutionary & environmental sciences

For a reference copy of the document with all sections, see nature.com/documents/nr-reporting-summary-flat.pdf

Life sciences study design

All studies must disclose on these points even when the disclosure is negative.

Sample size	The sample size for the in vivo studies to achieve statistical significance was not calculated before the studies as the survival of cell grafts with and without expression of neoantigens and in different cell amounts was unknown. It was reasoned that 5-10 mice per group in individual experiments would indicate valid efficacy. Experiments with inbred strains usually produce very consistent results so that an animal number < 10 is frequently sufficient. For in vitro studies, triplicates and quadruplicates were mostly used for comparisons between groups, followed by the statistical test.
Data exclusions	No detailed pre-established data exclusion method was used, but data from experiments where control samples failed to produce the expected effect were excluded.
Replication	The experimental findings can be reliably reproduced. Some key data generated by one co-author were repeated by other co-authors. Repeat experiments were done on other days and frequently different batch numbers of reagents to minimize external bias.
Randomization	All samples were number coded until the readout was finalized. The numbers were assigned prior to the experiment and determined the group/ treatment/ condition. Animals were number coded and assigned to a group prior to the surgical procedure.
Blinding	The investigators doing the readouts were not blinded, but frequently not familiar with the experimental setup of another co-worker. Readouts like impedance and spot frequency, the most frequently utilized readout in this paper, are generated by automated machines and not biased.

Reporting for specific materials, systems and methods

We require information from authors about some types of materials, experimental systems and methods used in many studies. Here, indicate whether each material, system or method listed is relevant to your study. If you are not sure if a list item applies to your research, read the appropriate section before selecting a response.

Materials & experimental systems

n/a	Involved in the study
☐	☒ Antibodies
☐	☒ Eukaryotic cell lines
☒	☐ Palaeontology
☐	☒ Animals and other organisms
☐	☒ Human research participants
☒	☐ Clinical data

Methods

n/a	Involved in the study
☒	☐ ChIP-seq
☐	☒ Flow cytometry
☒	☐ MRI-based neuroimaging

Antibodies

Antibodies used	Flow cytometry antibodies: MHC class I (clone AF6-88.5.5.3, PerCP-eFlour710, catalog# 46-5958-82, eBioscience), IgG2b isotype-matched control antibody (clone eB149/10H5, PerCP-eFlour710, catalog# 50-160-39, eBioscience), MHC class II (clone M5/114.15.2, PerCP-eFlour710, catalog# 50-160-63, eBioscience), IgG2a isotype-matched control antibody (clone eBM2a, PerCP-eFlour710, catalog# 50-113-0808, eBioscience). Antibody concentrations were chosen according to the manufacturer's

protocol.

Western Blots: Cytb (polyclonal, catalog# ab81215, Abcam), Co3 (polyclonal, catalog# ABIN223366, antikoerper-online.de), Actin (clone ACTN05 (C4), catalog# ab3280, Abcam). Antibody concentrations were chosen according to the manufacturer's protocol.

Mass cytometry: Ter119 (clone TER119, In-113, catalog# 116241, Biolegend), CD45 (clone 30-F11, In-115, catalog# 103102, Biolegend), Ly6G (clone 1A8, La-139, catalog# 127637, Biolegend), IgD (clone 11-26c.2a, Ce-140, catalog# 553438, BD), CD16/32 (clone 2.4G2, Pr-141, catalog# 560539, BD), CD49b (clone HMα2, Nd-142, catalog# 103513, Biolegend), CD11c (clone HL3, Nd-143, catalog# 550283, BD), CD27 (clone LG.3A10, Nd-145, catalog# 124202, Biolegend), CD138 (clone 281-2, Nd-146, catalog# 142502, Biolegend), PD-L1 (clone 10F.9G2, Sm-147, catalog# 124307, Biolegend), CD103 (clone 2E7, Nd-148, catalog# 121407, Biolegend), SiglecF (clone E50-2440, Sm-149, catalog# 552125, BD), PDCA-1 (clone 120g8, Nd-150, catalog# DDX0390-HD05, Imgenex), Ly6C (clone HK1.4, Eu-151, catalog# 128002, Biolegend), Ki67 (clone SolA15, Sm-151, catalog# 50245564, eBioscience), CD11b (clone M1/70, Eu-153, catalog# 101202, Biolegend), c-Kit (clone 2B8, Sm-154, catalog# 105829, Biolegend), CD8 (clone 53-6.7, Gd-155, catalog# 100716, Biolegend), CD4 (clone RM4-5, Gd-156, catalog# 100520, Biolegend), CD3 (clone 17A2, Gd-157, catalog# 555273, BD), PD-1 (clone 29F.1A12, Gd-158, catalog# 135202, Biolegend), B220 (clone RA3-6B2, Tb-159, catalog# 561880, BD), NK1.1 (clone PK136, Gd-160, catalog# 108743, Biolegend), T-bet (clone 04-46, Dy-161, catalog# 564141, BD), TCRgd (clone GL3, Dy-162, catalog# 118101, Biolegend), CD62L (clone MEL-14 - FITC, catalog# 104406, Biolegend; followed by anti-FITC, clone FIT-22, Dy-163, catalog# 408301, Biolegend), CD86 (clone GL-1, Dy-164, catalog# 105002, Biolegend), CD69 (clone H1.2F3, Ho-165, catalog# 104502, Biolegend), FcER1a (clone MAR-1, Er-166, catalog# 134313, Biolegend), Foxp3 (clone NRRF-30, Er-167, catalog# 14-4771-80, eBioscience), RORgt (clone B2D, Er-168, catalog# 12-6981-82, eBioscience), F4/80 (clone BM8, Tm-169, catalog# 123102, Biolegend), CD115 (clone AFS98, Er-170, catalog# 135535, Biolegend), CD64 (clone X54-5/7.1, Yb-171, catalog# 139303, Biolegend), GATA3 (clone L50-823, Yb-172, catalog# 558686, BD), CD19 (clone 6D5, Yb-173, catalog# 115502, Biolegend), IgM (clone RMM-1, Yb-174, catalog# 406502, Biolegend), CD44 (clone IM7, Lu-175, catalog# 550538, BD), CD90 (clone G7, Yb-176, catalog# 105202, Biolegend), MHC II (clone M5/114.15.2, Bi-209, catalog# 107601, Biolegend). Each antibody clone and lot was titrated to optimal staining concentrations using primary murine samples. One antibody cocktail was prepared for the staining of all samples for mass cytometry analysis.

Immunofluorescence stainings: CD3 (clone SP7, catalog# ab16669, Abcam), CD335 (clone 29A1.4, catalog# 16-3351-81, Thermo Fisher Scientific), and F4/80 (clone CI:A3-1, catalog# ab6640, Abcam). Antibody concentrations were chosen according to the manufacturer's protocol.

Magnetic-activated cell sorting (MACS): For purification of mouse iPSC-derived iECs, cells went through MACS purification according the manufactures' protocol using anti-CD15 mAb-coated magnetic microbeads (catalog# 130-094-530, Miltenyi) for negative selection. Antibody concentration was chosen according to the manufacturer's protocol.

In vitro lymphocyte reactivation: anti-CD3 (clone CLB-T3/4.E, 1XE, catalog# M1654, Sanquin) and anti-CD28 (CLB-CD28/1, 15E8, catalog# M1650, Sanquin) were used. Antibody concentrations were chosen according to the manufacturer's protocol.

Validation

All antibodies were validated with the recommended positive control samples.

Eukaryotic cell lines

Policy information about cell lines

Cell line source(s)

NT-ESCs were generated using enucleated BDF1 oocytes (C57BL/6J × DBA/2NCrl) F1 and somatic cell nucleus from BALB/c (B/c) fibroblasts.

FVB iPSCs were a kind gift from Dr. Joseph Wu (Stanford University, Stanford, CA). C57BL/6 iPSCs were generated by reprograming mouse-tail tip fibroblasts using a codon-optimized minicircle (CoMiC) construct.

From healthy volunteers, PBMCs were isolated and iPSCs were generated by the Yale University stem cell core lab (New Haven, CT) using Sendai viral expression of OCT4, SOX2, KLF4, and MYC genes. The experiments were approved by the University of California San Francisco Institutional Review Board.

Human iPSCs and their parental fibroblasts from 4 different individuals were provided by the Cardiovascular Institute, Stanford School of Medicine (Stanford, CA), the Stem Cell Core, Gladstone Institutes (San Francisco, CA).

NT-ESCs were cultured on γ-irradiated CF1 feeders (catalog# ASF-1216, Millipore).

Authentication

No cell line authentication was used.

Mycoplasma contamination

All cell lines have been tested for mycoplasma contamination and all cells tested negative.

Commonly misidentified lines
(See ICLAC register)

N/A

Animals and other organisms

Policy information about studies involving animals; ARRIVE guidelines recommended for reporting animal research

Laboratory animals

Male 6 - 8 week-old BALB/c (BALB/cAnNCrl, H2d), C57BL/6 (C57BL/6J, H2b), FVB (FVB/NCrl), SCID-beige (CB17.Cg-PrkdcscidLystbg-J/Crl), and CD4-knockout (B6.129S2-Cd4tm1Mak/J) mice were purchased from Charles River Laboratories

	(Sulzfeld, Germany) or Jackson Laboratory (Sacramento, CA), received humane care in compliance with the Guide for the Principles of Laboratory Animals, and experiments have complied with all relevant ethical regulations. Some B6 animals were immunosuppressed with tacrolimus (Prograf, Astella Pharma, Northbrook, IL) in a concentration of 0.5 mg/kg/d).
Wild animals	N/A
Field-collected samples	N/A
Ethics oversight	Mouse studies were approved by the Hamburg "Amt für Gesundheit und Verbraucherschutz" or the University of California San Francisco (UCSF) Institutional Animal Care and Use Committee.

Note that full information on the approval of the study protocol must also be provided in the manuscript.

Human research participants

Policy information about studies involving human research participants

Population characteristics	Patients listed for kidney or liver transplantation were consented to participate in this study. A total of 9 patients underwent kidney transplantation (patients 4, 7, 9, 10, 12, 13, 14, 15, 16) and 6 patients underwent liver transplantation (patients 5, 6, 11, 17, 18, 21). During the transplant operation, a blood sample from the recipient and some discarded fat tissue from the donor organ was collected and mtDNA sequencing was performed. Homoplasmic mismatches (heteroplasmy >99%) were identified. 20mer peptides were designed and generated to cover the donor SNP and the recipient's own autologous SNP, respectively. Patients received standard immunosuppression, which included tacrolimus, cyclosporine A, or co-stimulation blockers according to center-specific protocols. At 3 and 6 months after the transplantation (only at 6 months for patient 4), blood was drawn from the recipients during regular follow-up visits. Healthy volunteers agreed to provide PBMCs for mtDNA sequencing and iPSC generation.
Recruitment	Patients listed for kidney or liver transplantation at Hamburg University were asked to participate in this study. The patients who consented to participate and underwent transplantation during the time period of data collection were included. Healthy volunteers were recruited on a voluntary basis.
Ethics oversight	The transplant study was approved by the External Review Board of the Ärztekammer Hamburg (PV5100) and complied with all relevant ethical regulations. The use of volunteer PBMCs was approved by the UCSF Institutional Review Board.

Note that full information on the approval of the study protocol must also be provided in the manuscript.

Flow Cytometry

Plots

Confirm that:

☒ The axis labels state the marker and fluorochrome used (e.g. CD4-FITC).

☒ The axis scales are clearly visible. Include numbers along axes only for bottom left plot of group (a 'group' is an analysis of identical markers).

☒ All plots are contour plots with outliers or pseudocolor plots.

☒ A numerical value for number of cells or percentage (with statistics) is provided.

Methodology

Sample preparation	For the detection of MHC class I and II surface molecules, cells were plated on gelatin-coated 6-well plates in medium containing 100 ng/ml IFNγ. After harvesting, cells were labeled with antibodies. For MHC class I: PerCP-eFlour710-labeled anti-MHC class I antibody (clone AF6-88.5.5.3, eBioscience, Santa Clara, CA) or PerCP-eFlour710-labeled mouse IgG2b isotype-matched control antibody (clone eB149/10H5, eBioscience). For MHC class II: PerCP-eFlour710-labeled anti-MHC class II antibody (clone M5/114.15.2, eBioscience) or PerCP-eFlour710-labeled mouse IgG2a isotype-matched control antibody (clone eBM2a, eBioscience). Cells were analyzed by flow cytometry (BD Bioscience, San Jose, CA) and results were expressed as fold-change to isotype-matched control Ig staining. For the Live/Dead assay, iECs were collected and stained (LifeTechnologies). Briefly, cells were stained with 2 µl of 50 µM calcein AM and 4 µl of 2 mM ethidium homodimer-1 for 45 min at 4°C. The analysis was performed by flow cytometry (BD Bioscience) and results were expressed as percentage of live cells.
Instrument	FACSCalibur (BD Biosciences)
Software	FlowJo
Cell population abundance	Pure NT-ESC or fibroblast cultures were used.

Gating strategy | Living cells were gated in FSC-SSC plots and mean fluorescence intensity (MFI) was quantified in FL1 (FITC).

☒ Tick this box to confirm that a figure exemplifying the gating strategy is provided in the Supplementary Information.

nature biotechnology

SUPPLEMENTARY INFORMATION

https://doi.org/10.1038/s41587-019-0227-7

In the format provided by the authors and unedited.

De novo mutations in mitochondrial DNA of iPSCs produce immunogenic neoepitopes in mice and humans

Tobias Deuse[1,16], Xiaomeng Hu[1,2,3,16], Sean Agbor-Enoh[4,5], Martina Koch[6], Matthew H. Spitzer[7,8,9], Alessia Gravina[1,3], Malik Alawi[10], Argit Marishta[5], Bjoern Peters[11], Zeynep Kosaloglu-Yalcin[11], Yanqin Yang[5], Raja Rajalingam[12], Dong Wang[1,2,3], Bjoern Nashan[6], Rainer Kiefmann[13], Hermann Reichenspurner[2,3], Hannah Valantine[5], Irving L. Weissman[14] and Sonja Schrepfer[1,2,3,15]*

[1]Department of Surgery, Division of Cardiothoracic Surgery, Transplant and Stem Cell Immunobiology Lab, University of California, San Francisco, San Francisco, CA, USA. [2]Department of Cardiovascular Surgery, University Heart Center Hamburg, Hamburg, Germany. [3]Cardiovascular Research Center Hamburg and German Center for Cardiovascular Research, partner site Hamburg/Kiel/Luebeck, Hamburg, Germany. [4]Division of Pulmonary and Critical Care Medicine, The Johns Hopkins School of Medicine, Baltimore, MD, USA. [5]Laboratory of Transplantation Genomics, Division of Intramural Research, National Heart, Lung, and Blood Institute, Bethesda, MD, USA. [6]Department of Hepatobiliary and Transplant Surgery, University Medical Center Hamburg-Eppendorf, University Transplant Center, Hamburg, Germany. [7]Departments of Otolaryngology, Head and Neck Surgery and Microbiology and Immunology, Helen Diller Family Comprehensive Cancer Center, University of California, San Francisco, San Francisco, CA, USA. [8]Parker Institute for Cancer Immunotherapy, San Francisco, CA, USA. [9]Chan Zuckerberg Biohub, San Francisco, CA, USA. [10]Bioinformatics Core, University Medical Center Hamburg-Eppendorf, Hamburg, Germany. [11]Division of Vaccine Discovery, La Jolla Institute for Allergy and Immunology, La Jolla, CA, USA. [12]Immunogenetics and Transplantation Laboratory, Department of Surgery, University of California, San Francisco, San Francisco, CA, USA. [13]Department of Anaesthesia, University Medical Center Hamburg-Eppendorf, Hamburg, Germany. [14]Department of Developmental Biology, Stanford Institute for Stem Cell Biology and Regenerative Medicine, Stanford University School of Medicine, Stanford, CA, USA. [15]Sana Biotechnology Inc., South San Francisco, CA, USA. [16]These authors contributed equally: Tobias Deuse, Xiaomeng Hu. *e-mail: Sonja.Schrepfer@ucsf.edu

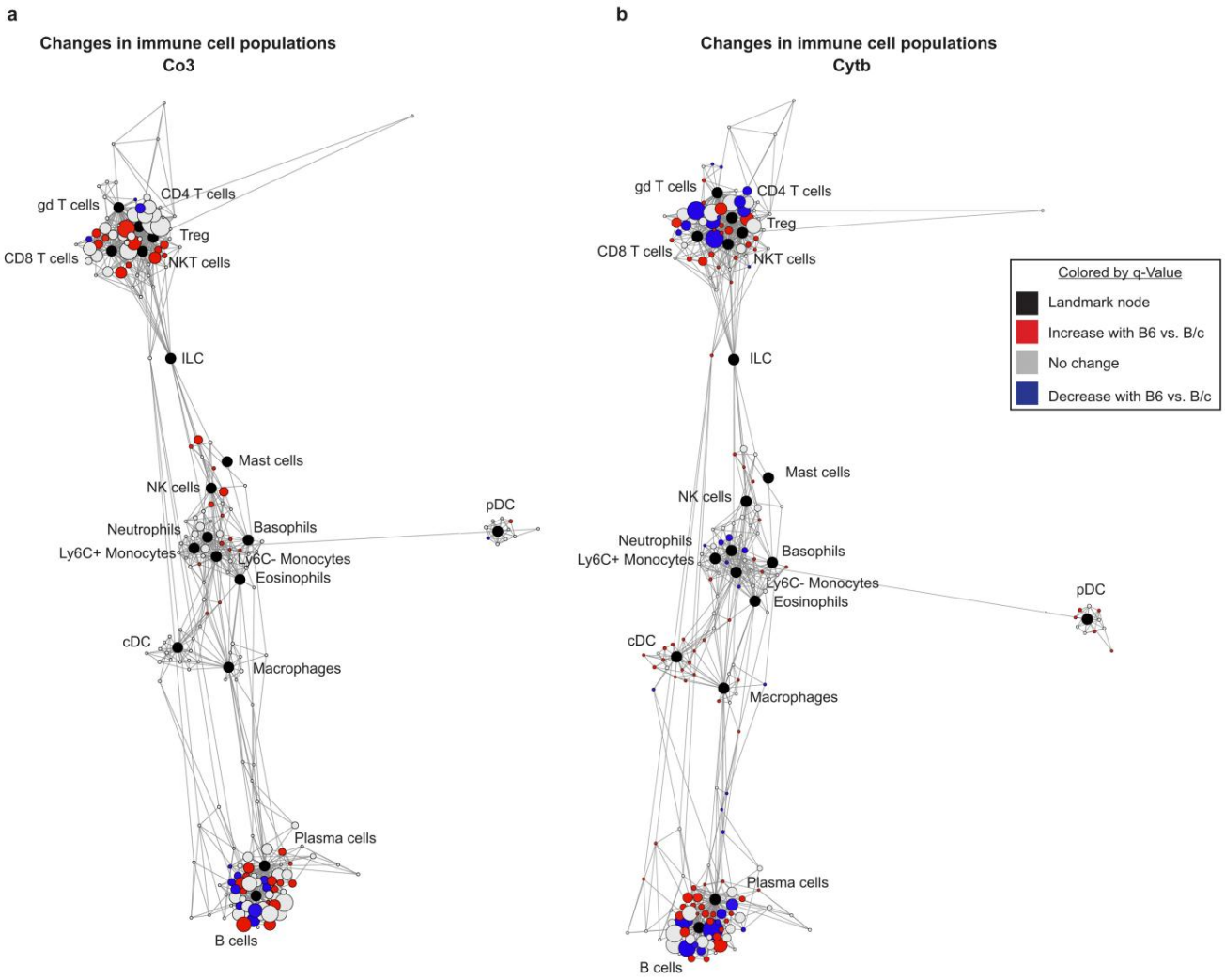

Supplementary Figure 1

System-wide analysis of the immune response by mass cytometry.

a-b, B/c splenocytes from animals receiving syngeneic fibroblasts overexpressing syngeneic B/c or allogeneic B6 Co3 (a) or Cytb proteins (b) were harvested and analyzed by mass cytometry (representative pictures of 6 animals per group). Statistical scaffold analysis was performed on the resulting data to identify immune cell populations of differing frequencies. Immune cell subsets that are significantly increased or decreased in animals receiving B6-overexpressing cells are shown in red and blue, respectively. Landmark cell populations manually identified in the data are shown in black and facilitate interpretation of the map.

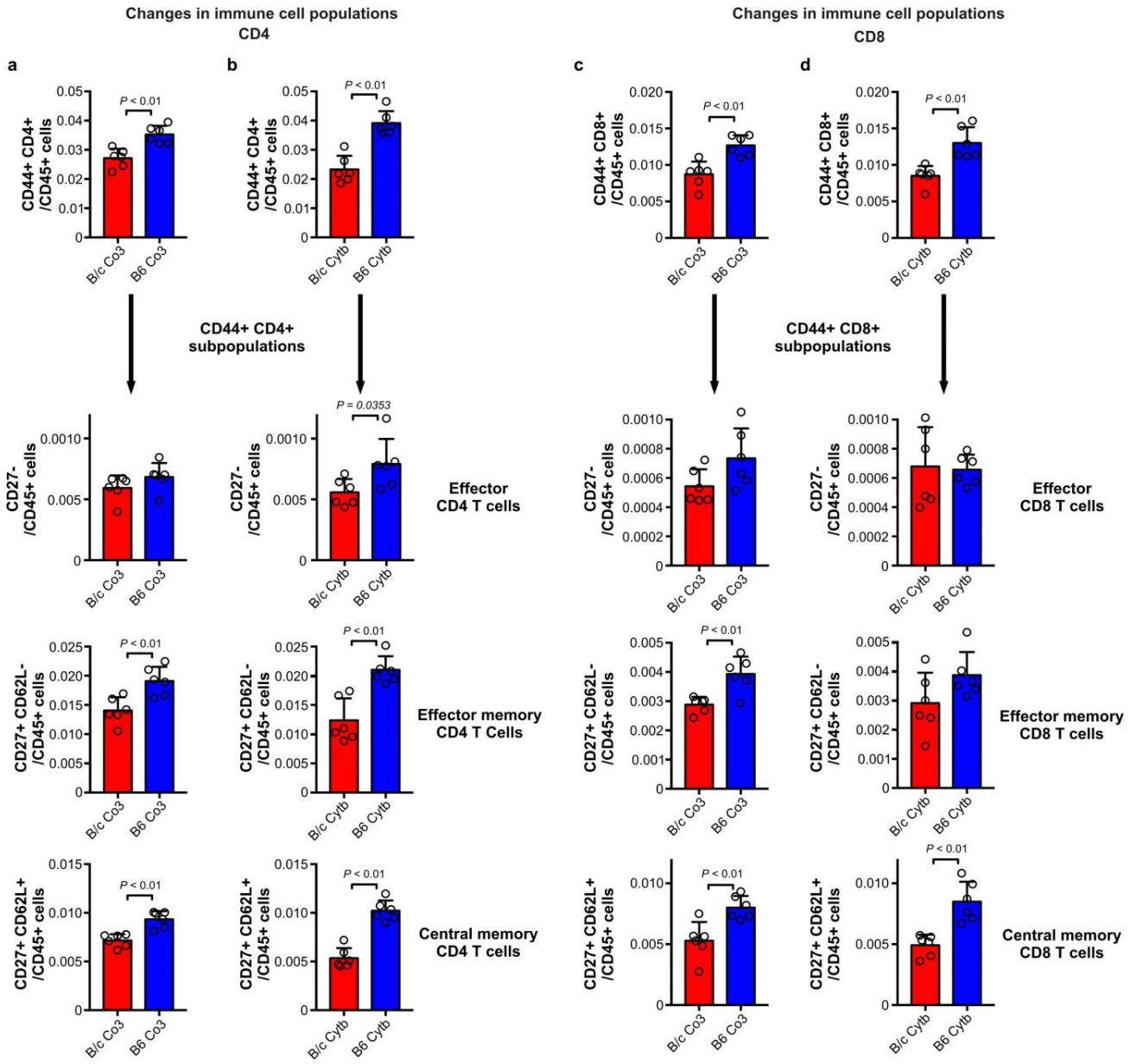

Supplementary Figure 2

Animals challenged with allogeneic proteins have expanded effector / memory T cell populations.

a-d, Animals were immunized with B/c or B6 Co3 proteins (a, c) or Cytb (b, d). Mass cytometry data were analyzed for the frequency of effector / memory CD4 (a, b) and CD8 (c, d) T cell subsets in the spleen (mean ± s.d., 6 animals per group, two-tailed Student's *t*-test). Frequencies of total antigen experienced ($CD44^+$), short-lived effector ($CD45^+CD27^-$), effector memory ($CD45^+CD27^+CD62L^-$), and central memory ($CD45^+CD27^+CD62L^+$) CD4 or CD8 T cells are shown.

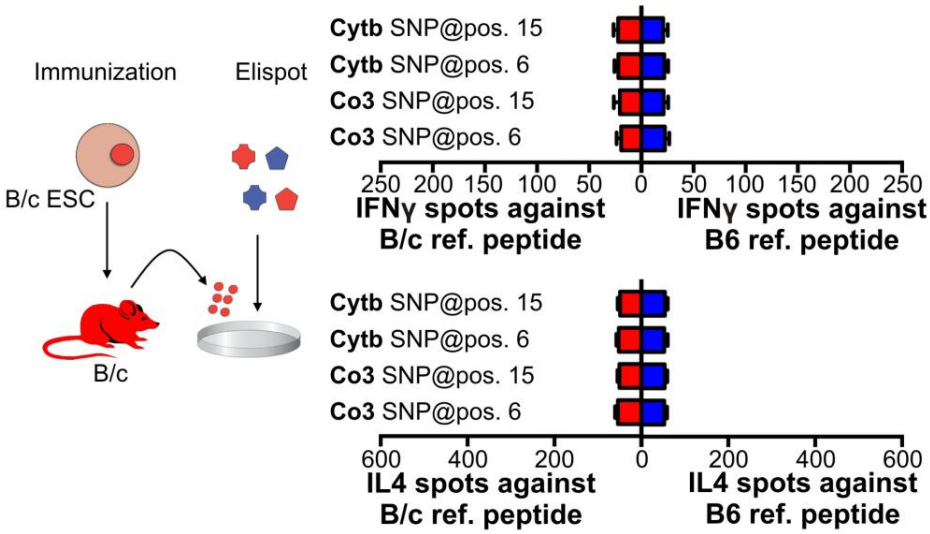

Supplementary Figure 3

There is no cross-reactivity between fetal nuclear gene-derived antigens and the Co3 and Cytb 20mers.

B/c mice were immunized with B/c ESCs, which were suspended in saline and injected into the thigh muscle. After 5 days, Elispot assays were performed with recipient splenocytes to test reactivity against 20mers carrying the B6-specific (blue) or B/c-specific (red) amino acid of the SNP at position 6 or 15 (mean ± s.d., quadruplicates of 4 animals per protein, two-tailed Student's *t*-test).

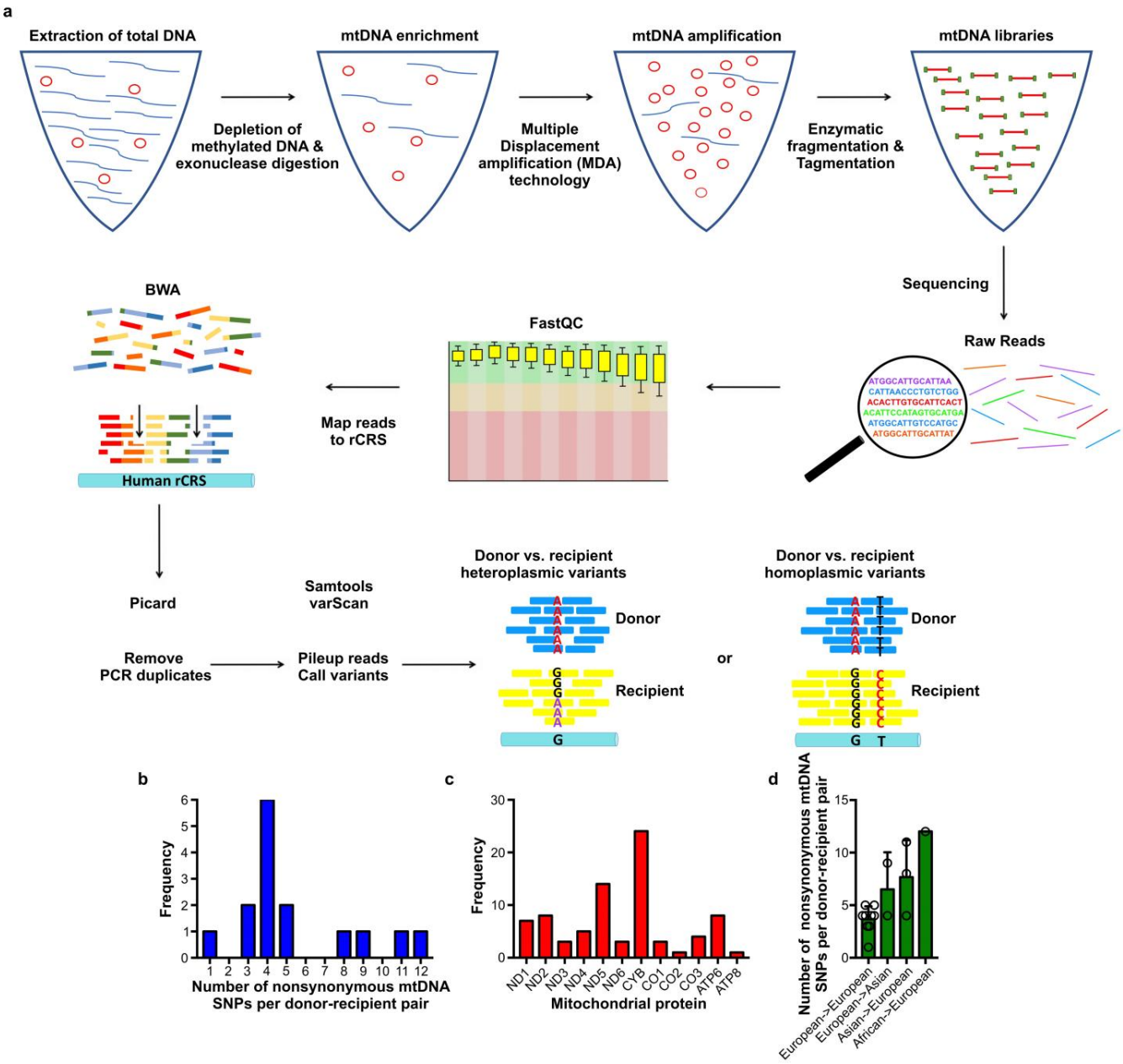

Supplementary Figure 4

mtDNA sequencing of human donor-recipient pairs.

a, Total DNA was extracted from donor tissue and recipient blood. mtDNA was enriched and amplified and mtDNA libraries were created. After sequencing, raw reads underwent quality control and map reads were aligned to human rCRS. After removal of duplicates and pileup of variants, either heteroplasmic or homoplasmic donor-recipient SNP variants were identified. **b**, Of 15 patient pairs, the number of homoplasmic nonsynonymous mtDNA SNPs is shown. **c**, Nonsynonymous homoplasmic SNPs were found at different frequencies in 12 mitochondrial proteins. **d**, The number of nonsynonymous mtDNA SNPs in donor-recipient pairs by ethnic background is shown.

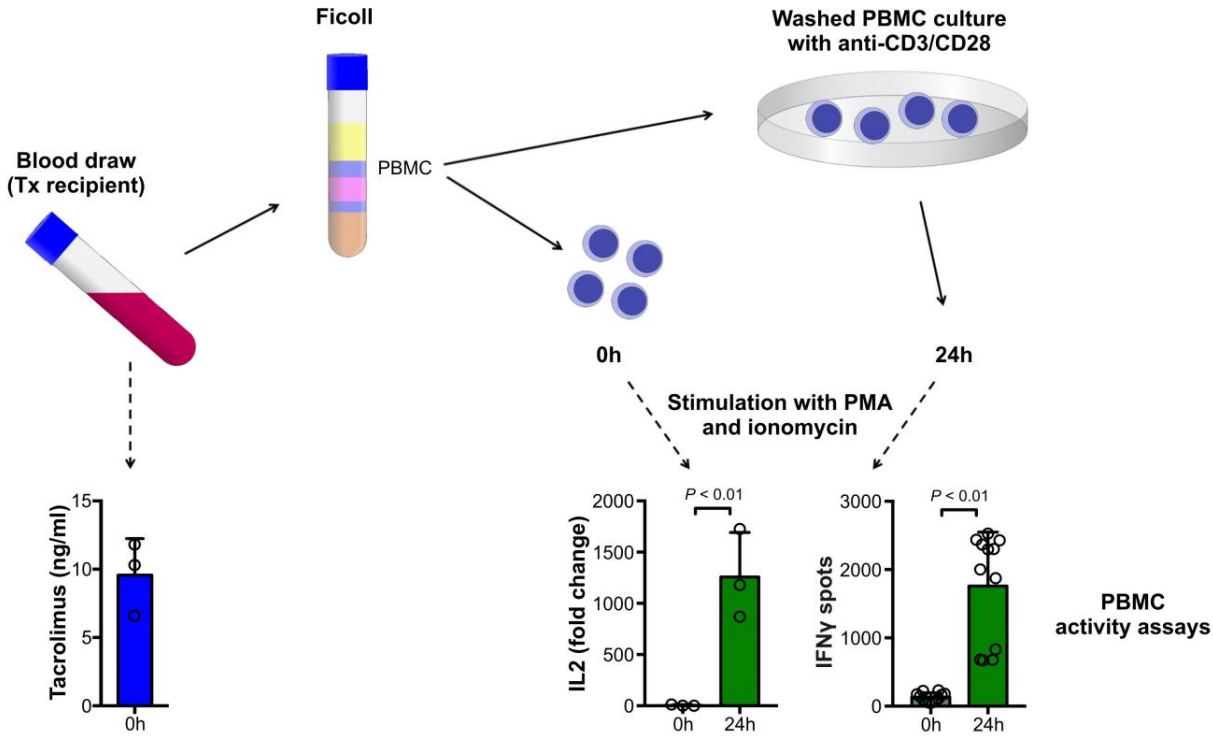

Supplementary Figure 5

In vitro reactivation of PBMCs of immunosuppressed organ recipients.

Blood was drawn from three organ recipients 3 weeks after transplantation. All patients were on a regimen including tacrolimus, mycophenolate mofetil, and steroids with therapeutic tacrolimus trough levels (mean ± s.d., n = 3 patients). PBMCs were isolated using Ficoll gradient centrifugation and one fraction was immediately tested for their immune responsiveness (0 h). Another fraction of PBMCs was washed and cultured in the presence of anti-CD3 and anti-CD28 for 24 h before being tested (24 h). PBMCs were unspecifically stimulated with PMA and ionomycin and their IL2 expression was quantified by PCR (mean ± s.d., n = 3 patients, two-tailed Student's *t*-test) and their IFNγ release by Elispot assays (mean ± s.d., quadruplicates of n = 3 patients, two-tailed Student's *t*-test).

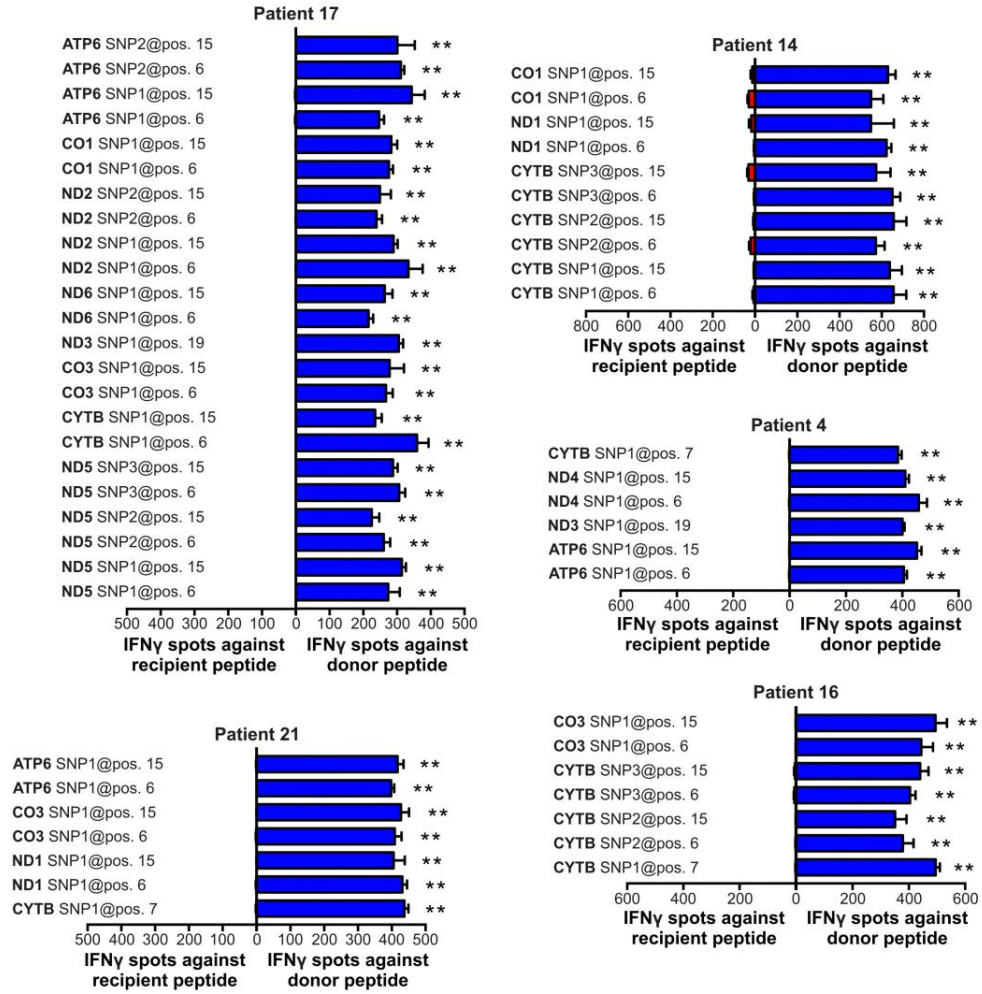

Supplementary Figure 6

Additional patients for the human transplant study.

Five more patients are displayed from the human transplant study outlined in Figure 2 (mean ± s.d., quadruplicates per 20mer and patient, two-tailed Student's *t*-test). Blue shades correspond to donor, red shades to recipient 20mers. ** $P < 0.01$.

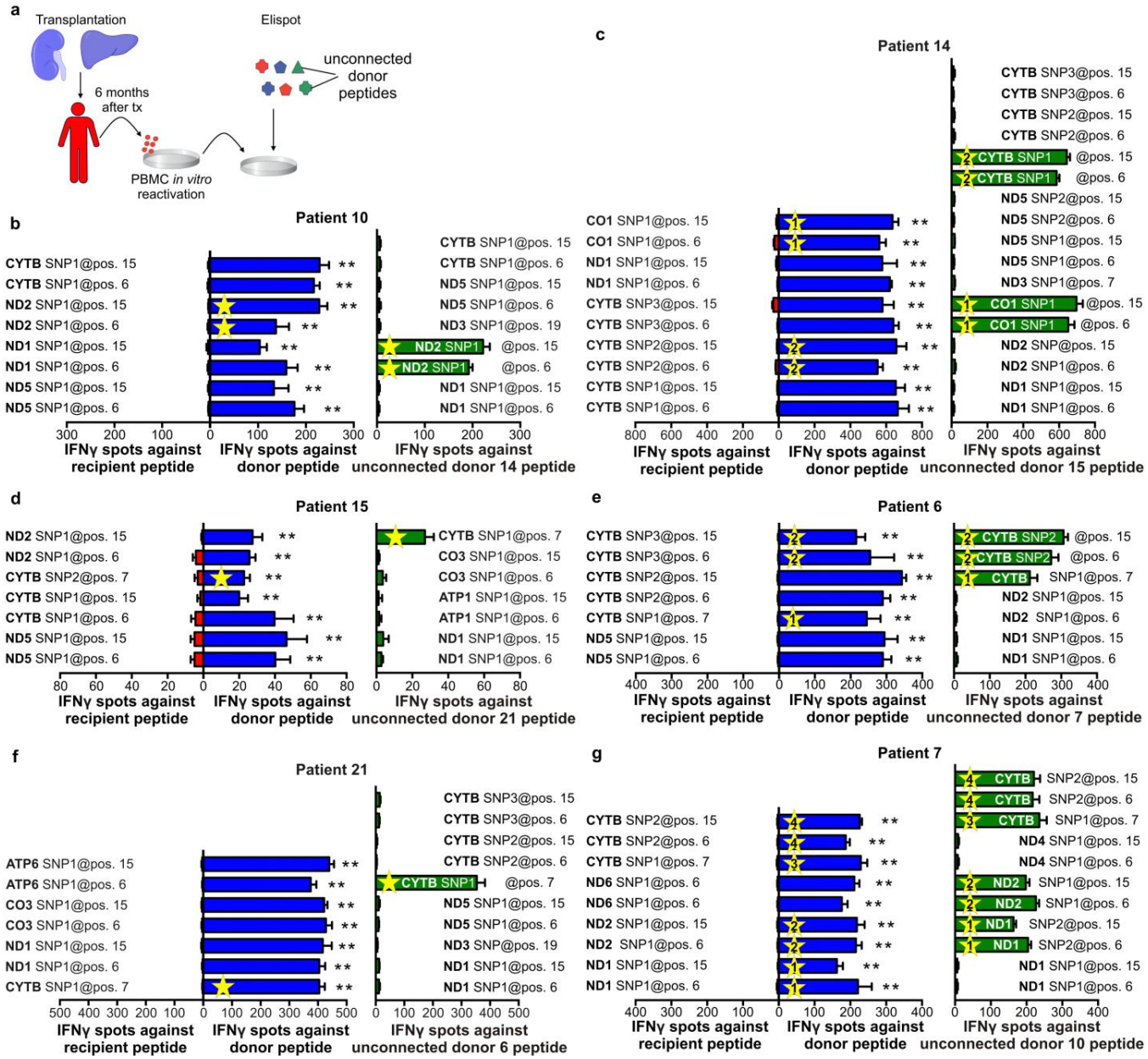

Supplementary Figure 7

Confirmatory patient study on the specificity of the immune response.

Six patients with 4-5 nonsynonymous mtDNA SNPs to their donor were chosen for this study. Blood was drawn 6 months after liver or kidney transplantation and PBMCs underwent *in vitro* reactivation. In Elispot assays, PBMCs were challenged with autologous (red) or two sets of allogeneic 20mers reflecting mtDNA SNPs of their donor (blue) or another unconnected donor (green; mean ± s.d., quadruplicates per 20mer and patient, two-tailed Student's *t*-test). Among the depicted SNPs, yellow asterisks mark SNPs that are identical between the patient's donor and the unconnected donor. ** $P < 0.01$.

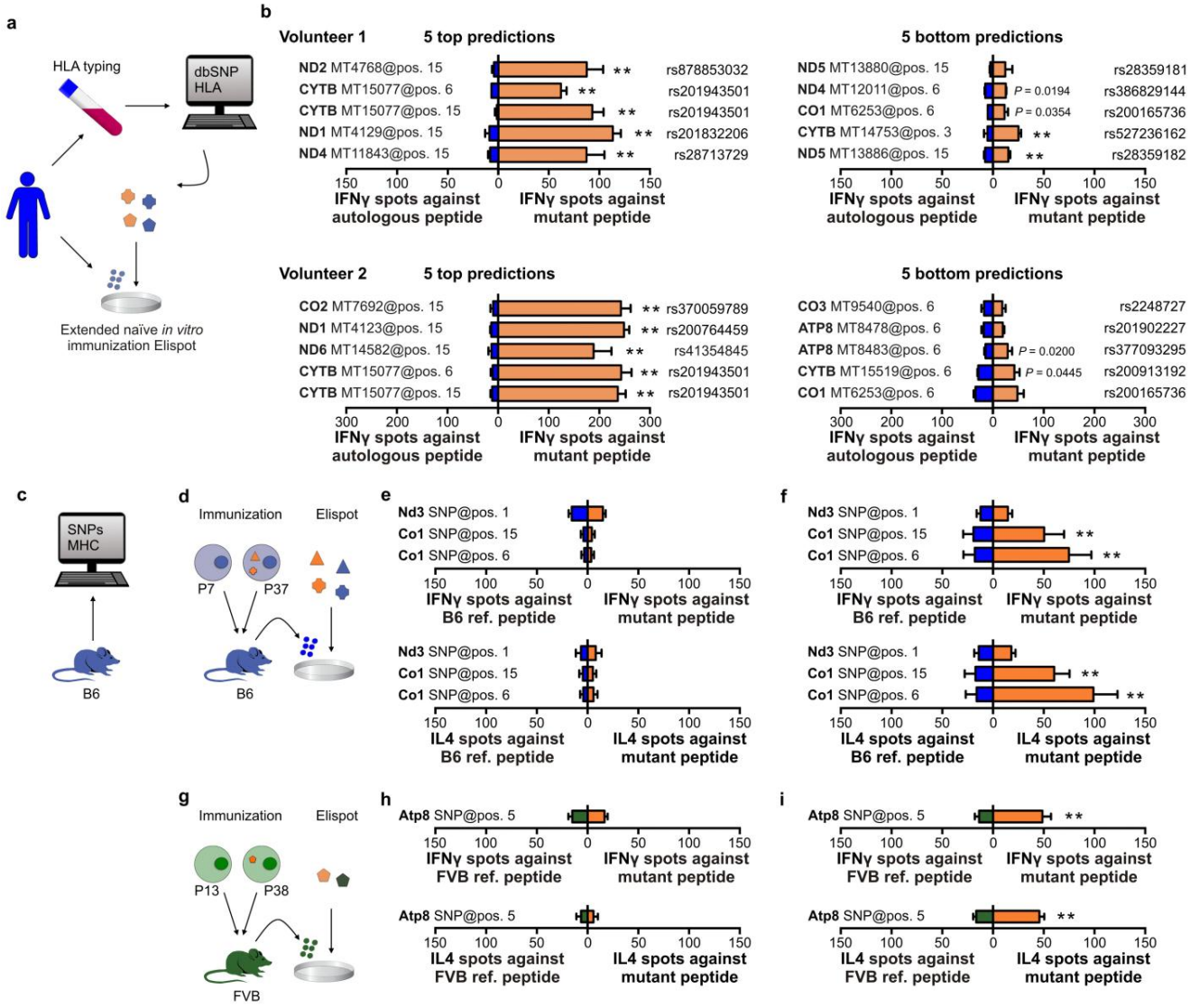

Supplementary Figure 8

In silico antigenicity predictions of human and mouse SNPs.

a, Blood was drawn from two volunteers for 4-digit HLA typing. Using *in silico* prediction models, the top 5 peptides with the highest predicted immunogenicity and bottom 5 SNPs with the lowest predicted immunogenicity from the annotated human SNP library were identified for each volunteer. **b**, 20mers were generated to cover either the mutant or autologous SNP and used in extended naïve *in vitro* immunization Elispot assays with volunteer PBMCs (Volunteer 1: mean ± s.d., triplicates per 20mer, two-tailed Student's *t*-test; Volunteer 2: mean ± s.d., quadruplicates per 20mer, two-tailed Student's *t*-test). Blue shades correspond to autologous, yellow shades to mutant 20mers. **c**, *In silico* predictions for B6 MHC binding was performed for the 3 neoantigenic SNP candidates identified in P37 iPSCs. **d**, B6 mice were immunized with autologous P7 or P37 iPSCs and after 5 days, splenocytes were incubated in Elispot assays with 20mers from the 2 neoantigen candidate SNPs or the B6 reference SNPs. **e**, Elispot assays from mice immunized with P7 iPSCs (mean ± s.d., quadruplicates of 6 animals per 20mer, two-tailed Student's *t*-test). **f**, Elispot assays from mice immunized with P37 iPSCs (mean ± s.d., quadruplicates of 6 animals per 20mer, two-tailed Student's *t*-test). **g**, FVB mice were immunized with autologous P13 or P38 iPSCs and after 5 days, splenocytes were incubated in Elispot assays with 20mers from the neoantigen candidate SNP or the FVB reference SNP. **h**, Elispot assays from mice immunized with P13 iPSCs (mean ± s.d., quadruplicates of 6 animals per 20mer, two-tailed Student's *t*-test). **i**, Elispot assays from mice immunized with P38 iPSCs (mean ± s.d., quadruplicates of 6 animals per 20mer, two-tailed Student's *t*-test). Blue shades correspond to the B6 reference 20mer, green to the FVB reference 20mer, and yellow shades to the neoantigenic 20mer. ** $P < 0.01$.

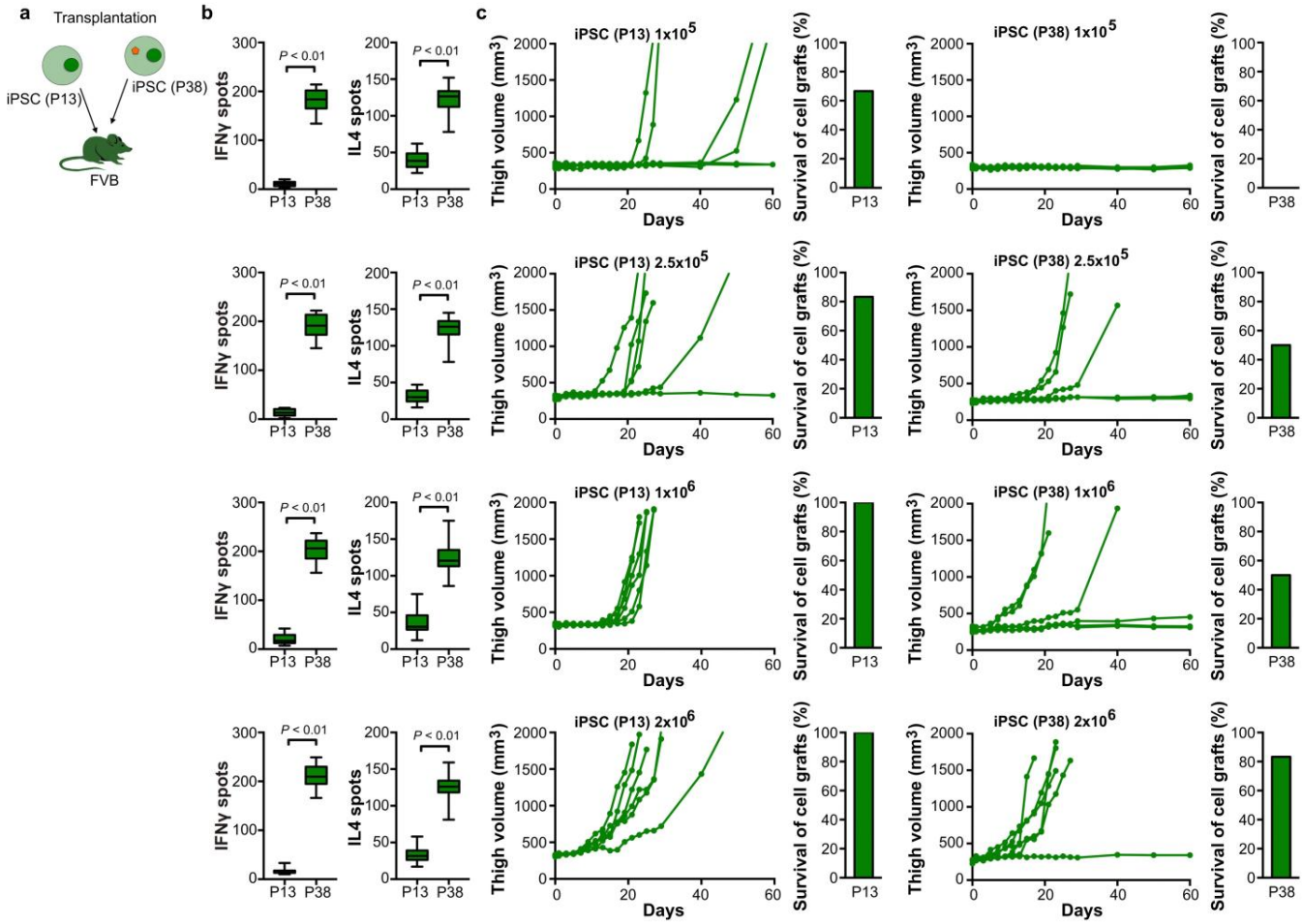

Supplementary Figure 9

Survival of low- and high-passage FVB iPSCs.

a, FVB mice received different cell amounts of autologous low-passage (P13) or high-passage (P38) iPSCs grafts injected into the thigh muscle and were followed for immune response and teratoma development. **b**, After 5 days, splenocytes were recovered for Elispot assays (mean ± s.d., quadruplicates of 6 animals per group, two-tailed Student's *t*-test). **c**, Teratoma growth is depicted for every animal and the percentage of teratoma formation for each group is shown in a separate bar graph (n = 6 per cell amount and iPSC group).

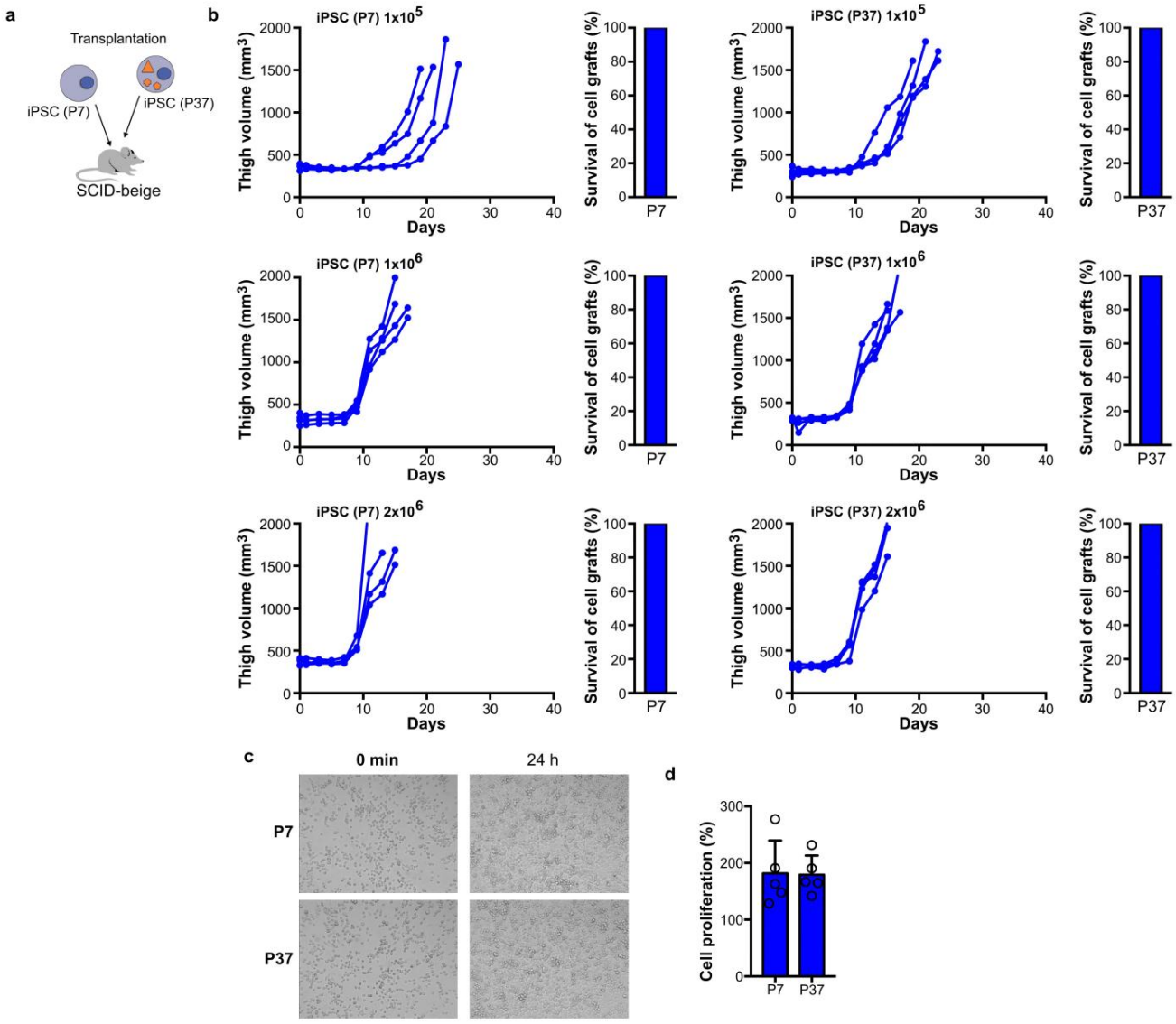

Supplementary Figure 10

Proliferative capacity of B6 iPSCs P7 and P37 *in vivo* and *in vitro*.

a, B6 iPSC grafts from P7 and P37 were injected into the thigh muscle of immunodeficient SCID-beige mice. **b**, Teratoma growth of iPSCs P7 and P37 was followed and the percentage of teratoma formation for each group is shown in a separate bar graph (Individual animals are shown, n = 4 per group). **c**, *In vitro* growth of P7 and P37 iPSC cultures was captured with time-laps life cell imaging and the confluency at 0 min and 24 h is shown (representative pictures of two independent experiments). **d**, The calculated cell proliferation after 24 h is shown (mean ± s.d., 5 replicates per group, two-tailed Student's *t*-test).

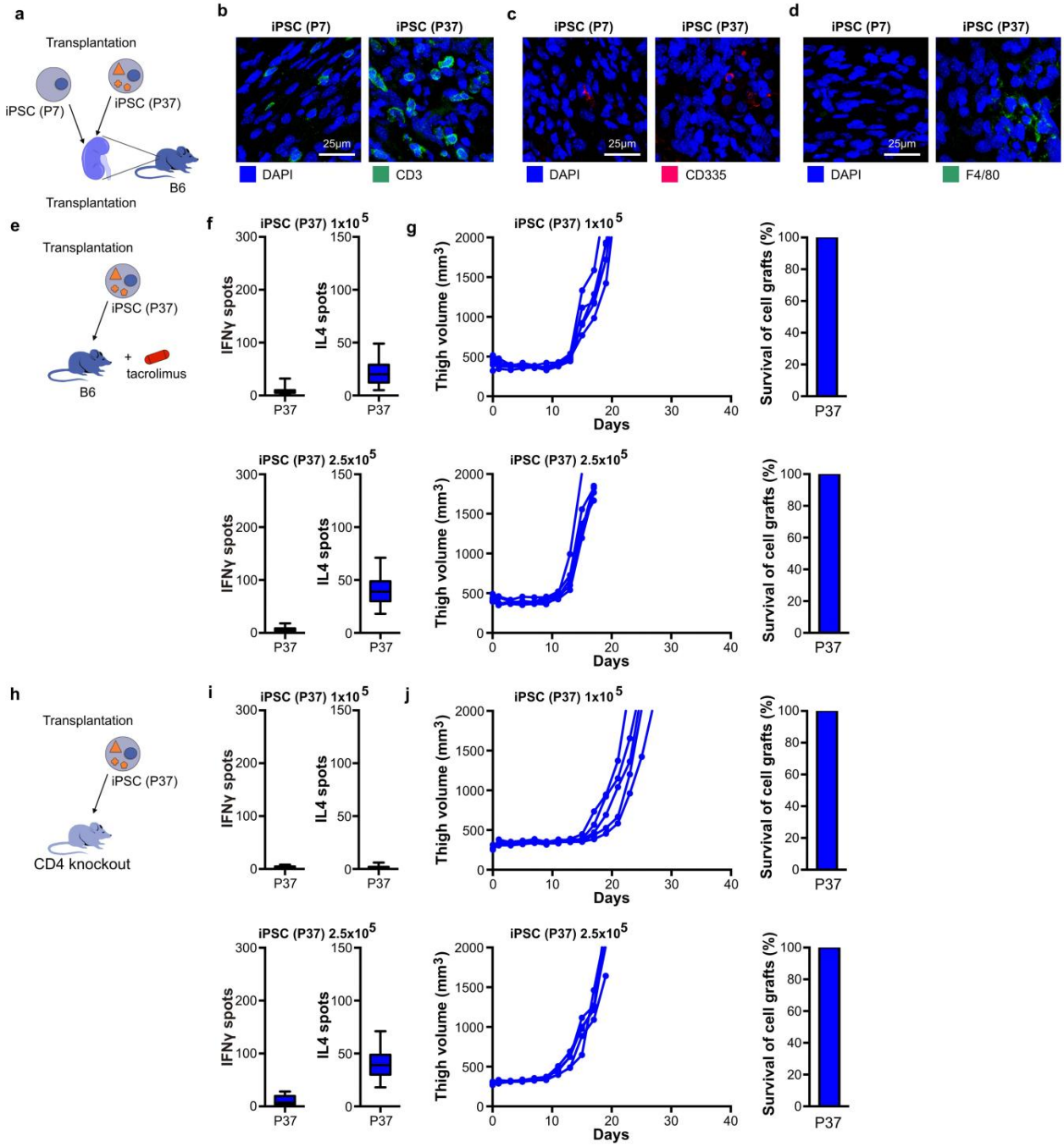

Supplementary Figure 11

The immunogenic nature of B6 iPSC P37 fate after transplantation.

a, iPSC grafts from P7 and P37 were injected below the kidney capsule of syngeneic B6 recipients. **b-d**, Infiltration of P7 and P37 iPSC grafts with $CD3^+$ lymphocytes (b), $CD335^+$ natural killer cells (c), and $F4/80^+$ macrophages (d) by immunofluorescence staining is shown. Scale bar 25 µm. **e**, P37 iPSC grafts at two low cell amounts, which were completely or mostly rejected in immunocompetent B6 mice in Figure 3, were injected into the thigh muscle of B6 recipients immunosuppressed with tacrolimus. **f**, Elispot assays with splenocytes recovered after 5 days are shown (mean ± s.d., quadruplicates of 5 animals per group). **g**, Teratoma growth is depicted for every animal and the percentage of teratoma formation for each group is shown in a separate bar graph (n = 5 animals per group). **h**, P37 iPSC grafts at the same two low cell amounts were then transplanted into immunocompromized CD4 knockout recipients on B6

background. **i**, Elispot assays with splenocytes recovered after 5 days are shown (mean ± s.d., quadruplicates of 5 animals per group). **j**, Teratoma growth is depicted for every animal and the percentage of teratoma formation for each group is shown in a separate bar graph (n = 5 animals per group).

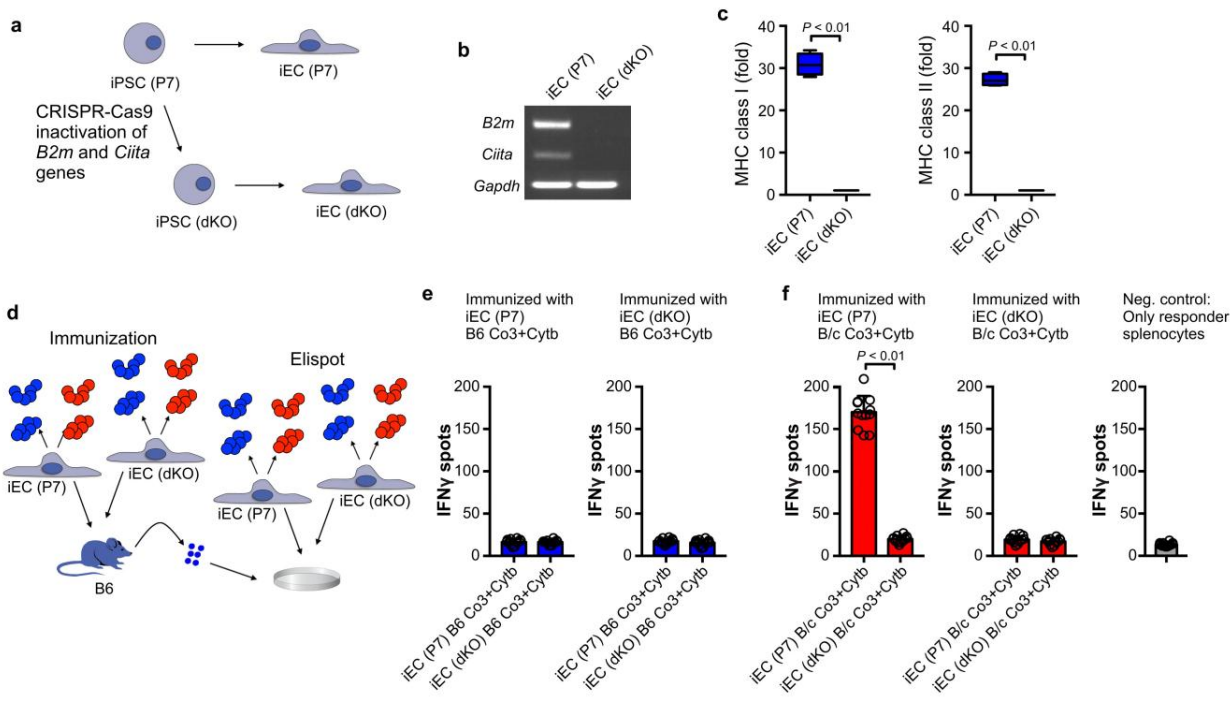

Supplementary Figure 12

Presentation of mtDNA neoantigens via MHC.

a, iPSCs (P7) underwent CRISPR-Cas9 inactivation of the *B2m* and *Ciita* genes to generate double MHC knockout (dKO) iPSCs and iEC (dKO) were differentiated. **b**, The knockouts of *B2m* and *Ciita* in iEC (dKO) were confirmed by PCR (representative gel of two independent experiments). **c**, Surface expression of MHC class I and II was assessed by flow cytometry (mean ± s.d., 4 independent experiments per group, two-tailed Student's *t*-test). **d**, B/6 mice were immunized with either iEC (P7) or iEC (dKO) overexpressing B/c (red) or B6 (blue) Co3 and Cytb. The splenocyte response after 5 days against the same overexpressed proteins in either iEC (P7) or iEC (dKO) was assessed in Elispot assays to determine the mechanistic role of MHC. **e**, Elispot assays of B/6 mice immunized with iEC (P7) or iEC (dKO) overexpressing syngeneic B/6 proteins are shown (mean ± s.d., quadruplicates of 3 animals per group, two-tailed Student's *t*-test). **f**, Elispot assays of B/6 mice immunized with iEC (P7) or iEC (dKO) overexpressing allogeneic B/c proteins are shown. Unstimulated responder splenocytes served a control (mean ± s.d., quadruplicates of 3 animals per group, two-tailed Student's *t*-test).

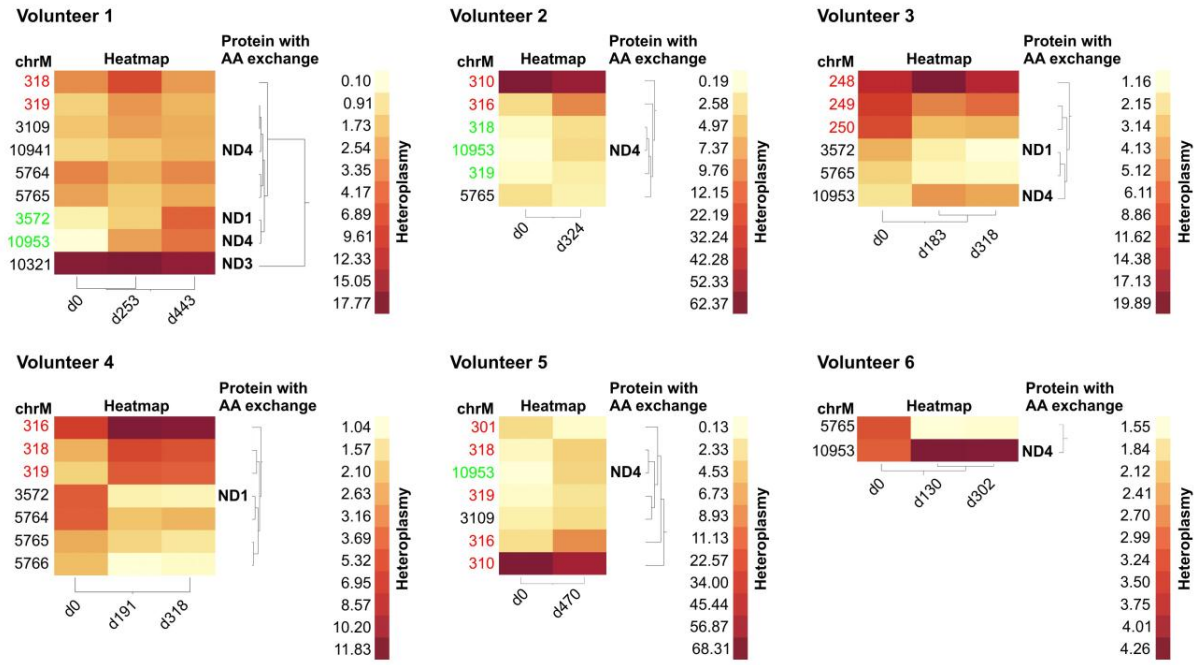

Supplementary Figure 13

Longitudinal mtDNA sequencing of human PBMC SNPs *in vivo*.

PBMCs were repeatedly isolated from 6 volunteers over a minimum of 6 months and mtDNA sequencing was performed. SNPs in the non-coding D-loop are marked in red. SNPs with < 1% heteroplasmy in the first specimen that increased to > 1% in subsequent specimens were considered de novo mutations and are marked in green. SNPs that have been present in the first PBMC specimen and changed their heteroplasmy >1% over time are marked in black. None of the volunteers developed candidate SNPs for neoantigens *in vivo*.

Supplementary Note 1

Mouse iPSC reprograming and modification

Briefly, β2m and Ciita were disrupted consecutively by the transfection of All-In-One (AIO) vectors (GeneArt CRISPR Nuclease Vector Kit, Thermo Fisher Scientific, Waltham, MA) with gene specific CRISPR sequences. Single clones were isolated and expanded to colonies before Sanger sequencing was performed. Using the DNA sequence chromatogram, edited clones were identified through the presence of altered sequence from the CRISPR cleavage site. RT-PCR and FACS analysis were performed to verify the cell knockout.

For RT-PCR, RNA was extracted using the RNeasy Plus Mini Kit (Qiagen, Hikden, Germany) according to the manufactures protocol. Genomic DNA contamination was removed using the gDNA spin column. cDNA was generated using Applied Biosystems High-Capacity cDNA Reverse Transcription kit (Applied Biosystems, Foster City, CA). The following primers were used: mouse MHC class I forward: 5'-AGT GGT GCT GCA GAG CAT TAC AA-3', reverse: 5'-GGT GAC TTC ACC TTT AGA TCT GGG-3', MHC class II forward: 5'-GAT GTG GAA GAC CTG CG-3', reverse: 5'-TGC ATC TTC TGA GGG GTT TC-3' and GapDH forward: 5'-TCA CCA CCA TGG AGA AGG C-3', reverse: 5'-GCT AAG CAG TTG GTG GTG CA-3'. PCRs were performed on Mastercycler nexus (Eppendorf AG, Hamburg, Germany) and the amplification products were visualized by 2% agarose gel electrophoresis (Thermo Fisher Scientific).

For the detection of MHC class I and II surface molecules, cells were plated on gelatin-coated 6-well plates in medium containing 100 ng/ml IFNγ (Peprotech, Rocky Hill, NJ). After harvesting, cells were labeled with antibodies. For MHC class I: PerCP-eFlour710-labeled anti-MHC class I antibody (clone AF6-88.5.5.3, eBioscience, Santa Clara, CA) or PerCP-eFlour710-labeled mouse IgG2b isotype-matched control antibody (clone eB149/10H5, eBioscience). The anti-MHC class I antibody reacts with the H-2Kb MHC class I alloantigen. For MHC class II: PerCP-eFlour710-labeled anti-MHC class II antibody (clone M5/114.15.2, eBioscience) or PerCP-eFlour710-labeled mouse IgG2a isotype-matched control antibody (clone eBM2a, eBioscience). The MHC class II antibody reacts with the mouse MHC class II, both I-A and I-E subregion-encoded glycoproteins. Cells were analyzed by flow cytometry (BD Bioscience, San Jose, CA) and results were expressed as fold-change to isotype-matched control Ig staining.

Pluripotent cells were cultured on MEF in KO DMEM 10829 with 15% KO Serum Replacement, 1% glutamine, 1% MEM-NEAA, 1% pen-strep (all Gibco, Darmstadt, Germany), 0.2% beta-mercaptoethanol, and 100 units LIF (both Millipore, Billerica, MA). Cells were maintained in 10 cm dishes, medium was changed daily, and the cells were passaged every 2-3 days using 0.05% trypsin-EDTA (Gibco). iPSCs were sorted for the mouse pluripotency marker SSEA-1 using antibody-coated magnetic-bead based cell sorting (130-094-530, Miltenyi, Bergisch-Gladbach, Germany).

Supplementary Note 2

Single cell targeted mtDNA sequencing

Single cell analysis was done to determine the distribution of heteroplasmy frequencies at a single cell resolution. We analyzed this in cell line 1 P61 and in one mtDNA position (mtDNA11226). For controls, several positions that showed homoplasmy in bulk culture were added. To validate the PCR primers, we aliquoted known quantities of DNA from bulk iPSC culture and used quantitative PCR to quantitate the DNA of interest; the expected and measured DNA were similar. We then sorted individual cells into individual wells and used the designed PCR primers to amplify both variants of the SNP by PCR. The amplified sequences were used to make libraries that were then sequenced and analyzed. Sequences were aligned to the reference sequence to identify the SNP and the frequency of heteroplasmy was then computed. We only analyzed single cell data in experiments that showed adequate amplification defined as coverage at the position of interest of >150× accompanied by >150× coverage on the bulk DNA sample.

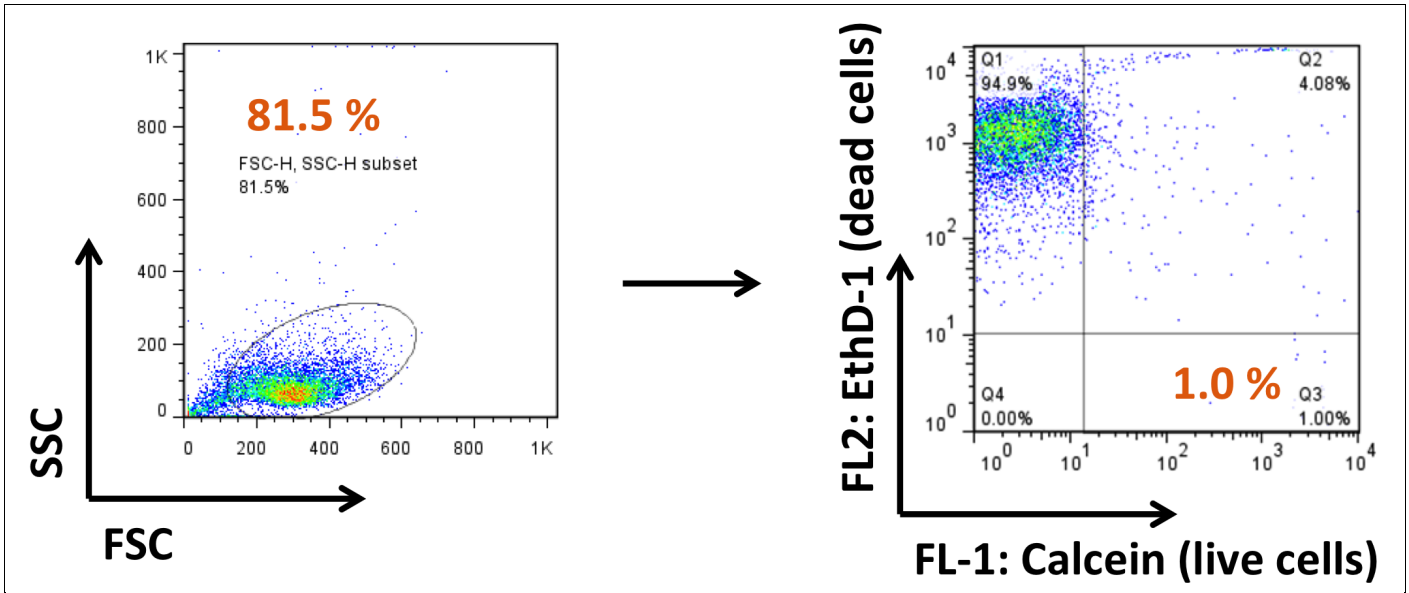

Supplementary Note 3

Example of the flow cytometry gating strategy for the Live/Dead assay.

First gating shows the FSC (forward scatter) and SSC (side scatter) to exclude cellular debris. Cells in FSC-SSC subset were investigated for calcein in channel FL-1 (staining for live cells) and EthD-1 in channel FL-2 (staining for dead cells). Live cells were defined as calcein positive and EthD-1 negative cells. Results were expressed as percentage of live cells.

Supplementary Note 4

Mass cytometry (**cytometry by time of flight, CyTOF)**

A summary of all mass cytometry antibodies, reporter isotopes and concentrations used for analysis can be found in Supplementary Table 18. Primary conjugates of mass cytometry antibodies were prepared using the MaxPAR antibody conjugation kit (Fluidigm, South San Francisco, CA) according to the manufacturer's protocol. Following labeling, antibodies were diluted in Candor PBS Antibody Stabilization solution (Candor Bioscience GmbH, Wangen, Germany) supplemented with 0.1% NaN_3 to between 0.1 and 0.5 mg/ml and stored long-term at 4°C. Each antibody clone and lot was titrated to optimal staining concentrations using primary murine samples. One antibody cocktail was prepared for the staining of all samples for mass cytometry analysis.

Mass-tag cellular barcoding was performed as previously described (Zunder, ER. Nat Protoc 10, 316-333, 2015). Briefly, 1×10^6 cells from each animal were barcoded with distinct combinations of stable Pd isotopes chelated by isothiocyanobenzyl-EDTA in 0.02% saponin in PBS. Samples from any given tissue from one mouse per treatment group were barcoded together, with at least 3 biological replicates per treatment group across different plates. Cells were washed two times in PBS with 0.5% BSA and 0.02% NaN_3 and pooled into a single FACS tube (BD Biosciences). After data collection, each condition was deconvoluted using a single-cell debarcoding algorithm (Zunder, ER. Nat Protoc 10, 316-333, 2015).

Cells were resuspended in PBS with 0.5% BSA and 0.02% NaN_3 and metal-labeled antibodies against CD16/32 were added at 20 µg/ml for 5 min at room temperature on a shaker to block Fc receptors. Surface marker antibodies were then added, yielding 500 µl final reaction volumes and stained at room temperature for 30 min at RT on a shaker. Following staining, cells were washed 2 more times with PBS with 0.5% BSA and 0.02% NaN_3 then permeabilized with 4°C methanol for at 10 min at 4°C. Cells were then washed twice in PBS with 0.5% BSA and 0.02% NaN_3 to remove remaining methanol, and then stained with intracellular antibodies in 500 µl for 30 min on a shaker. Cells were washed twice in PBS with 0.5% BSA and 0.02% NaN_3 and then stained with 1 ml of 1:4000 191/193Ir DNA intercalator (Fluidigm) diluted in PBS with 1.6% PFA overnight. Cells were then washed once with PBS with 0.5% BSA and 0.02% NaN_3 and then two times with double-deionized (dd)H_2O. Care was taken to assure buffers preceding analysis were not contaminated with metals in the mass range above 100 Da. Mass cytometry samples were diluted in (dd)H_2O containing bead standards (see below) to approximately 10^6 cells per ml and then analyzed on a CyTOF^{TM} 2 mass cytometer (Fluidigm) equilibrated with (dd)H_2O. We analyzed $1\text{-}5\times10^5$ cells per animal, consistent with generally accepted practices in the field.

Just before analysis, the stained and intercalated cell pellet was resuspended in (dd)H_2O containing the bead standard at a concentration ranging between 1 and 2×10^4 beads per ml as previously described (Finck, R. Cytometry A 83, 483-494, 2013). The bead standards were prepared immediately before analysis, and the mixture of beads and cells were filtered through a filter cap FACS tube (BD Biosciences). All mass cytometry files were normalized together using the mass cytometry data normalization algorithm (Finck, R. Cytometry A 83, 483-494, 2013), which uses the intensity values of a sliding window of these bead standards to correct for instrument fluctuations over time and between samples.

Total live leukocytes (excluding erythrocytes) were used for all analyses. Cells from all animals were clustered together rather than performing CLARA clustering on each file individually as originally implemented (Spitzer, MH. Science 349, 1259425, 2015). Cells were then deconvolved into their respective samples. Cluster frequencies or the Boolean expression of Ki67 or PD-L1 for each cluster were passed into the Significance Across Microarrays algorithm (Bair, E. PLoS Biol 2, E108, 2004; Bruggner, RV. Proc Natl Acad Sci U S A 111, E2770-2777, 2014), and results were tabulated into the scaffold map files for visualization through the graphical user interface. Cluster frequencies were calculated as a percent of total live leukocytes ($CD45^+$ cells).

Scaffold maps were then generated as previously reported (Spitzer, MH. Science 349, 1259425, 2015). Briefly, we chose the spleen data to spatialize the initial scaffold map because all major, mature immune cell populations are present in that tissue. A graph was constructed by first connecting together the nodes representing the manually gated landmark populations and then connecting to them the nodes representing the cell clusters as well as connecting the clusters to one another. Each node is associated with a vector containing the median marker values of the cells in the cluster (unsupervised nodes) or gated populations (landmark nodes). Edge weights were defined as the cosine similarity between these vectors after comparing the results from the implementation of several distance metrics. Edges of low weight were filtered out. We experimented with different threshold values for the weights and we found values of 0.8 for the initial subgraph of landmark nodes, and 0.7 for the complete graph to produce satisfying results. The graph was then laid out using an in-house R implementation of the ForceAtlas2 algorithm from the graph visualization software Gephi. To overlay the additional samples on the spleen map, the position and identity of the landmark nodes was fixed and the clusters of each sample were connected to the landmark nodes as described above. Once again, the graphs were laid out using ForceAtlas2 but this time only the unsupervised nodes were allowed to move. All analyses were performed using the open source Scaffold maps R package available at github.com/nolanlab/scaffold.

Supplementary Note 5

HLA typing

Genomic DNA was extracted from cell lines using the (QIAamp DNA isolation kit, Qiagen). DNA was quantified with NanoDrop (Thermo Fisher) and adjusted to a concentration of 30 ng/µl. Quality of DNA was assessed by measuring absorbance at A_{230}, A_{260}, and A_{280}. DNA samples were amplified by long-range PCR using the Omixon Holotype HLA genotyping kit, generating full-length gene amplicons for HLA-A, B, C, DRB1, DRB3, DRB4, DRB5, DQA1, DQB1, DPA1, and DPB1 loci. Following PCR, amplicons were cleaned with Exo-SAP (Affymetrix, Santa Clara, CA), quantified with QuantiFluor dsDNA system (Promega, Madison, WI), and normalized to approximately 70 ng/µl.

Sequencing libraries were generated for each sample using the Omixon Holotype HLA Genotyping Kit (Omixon, Budapest, Hungary). In brief, libraries from individual HLA amplicons were prepared by enzymatic fragmentation, end repair, adenylation, and ligation of indexed adaptors. The indexed libraries were pooled and concentrated with Ampure XP beads (Beckman Coulter, Brea, CA) prior to fragment size selection using a PippinPrep™ (Sage Science, Beverly, MA), selecting a range of fragments between 650 and 1300 bp. The size-selected library pool was quantified by quantitative PCR (Kapa Biosystems, Wilmington, MA) and adjusted to 2 nM. The library was then denatured with NaOH and diluted to a final concentration of 8 pM for optimal cluster density and 600 µl was loaded into the MiSeq reagent cartridge (v2 500 cycle kit). The reagent cartridge and flow cell were placed on the Illumina MiSeq (Illumina, San Diego, CA, USA) for cluster generation and 2×250 bp paired-end sequencing. Samples were demultiplexed on the instrument and the resulting FASTQ files were used for further analysis. HLA genotyping was assigned using TwinTM version 2.0.1 (Omixon) and IMGT/HLA database version 3.24.0_2, using 16000 read-pairs.

nature biotechnology

LETTERS

https://doi.org/10.1038/s41587-019-0016-3

Hypoimmunogenic derivatives of induced pluripotent stem cells evade immune rejection in fully immunocompetent allogeneic recipients

Tobias Deuse[1,7], Xiaomeng Hu[1,2,3,7], Alessia Gravina[1], Dong Wang[1,2], Grigol Tediashvili[1,2,3], Chandrav De[4], William O. Thayer[4], Angela Wahl[4], J. Victor Garcia[4], Hermann Reichenspurner[2,3], Mark M. Davis[5], Lewis L. Lanier[6] and Sonja Schrepfer[1*]

Autologous induced pluripotent stem cells (iPSCs) constitute an unlimited cell source for patient-specific cell-based organ repair strategies. However, their generation and subsequent differentiation into specific cells or tissues entail cell line-specific manufacturing challenges and form a lengthy process that precludes acute treatment modalities. These shortcomings could be overcome by using prefabricated allogeneic cell or tissue products, but the vigorous immune response against histo-incompatible cells has prevented the successful implementation of this approach. Here we show that both mouse and human iPSCs lose their immunogenicity when major histocompatibility complex (MHC) class I and II genes are inactivated and CD47 is over-expressed. These hypoimmunogenic iPSCs retain their pluripotent stem cell potential and differentiation capacity. Endothelial cells, smooth muscle cells, and cardiomyocytes derived from hypoimmunogenic mouse or human iPSCs reliably evade immune rejection in fully MHC-mismatched allogeneic recipients and survive long-term without the use of immunosuppression. These findings suggest that hypoimmunogenic cell grafts can be engineered for universal transplantation.

Treatment of heart disease with adult multipotent, bone marrow-derived stem cells has shown marginal efficacy in patients with acute myocardial infarction[1] or chronic ischemic cardiomyopathy[2,3]. This has been attributed to the limited plasticity of adult hematopoietic stem cells, which do not differentiate into cardiomyocytes and thus cannot replace contractile elements[4]. Pluripotent stem cells are more promising cell sources for regenerative strategies as they can produce an unlimited amount of progeny cells that can be differentiated into functional tissue cells. Although reprogramming technology allows the generation of autologous iPSCs for patient-specific treatments, this is laborious, costly, associated with uncertain quality and efficacy of individual cell products and is only practical for chronic diseases[5–7]. Thus, most regenerative approaches relying on autologous iPSC generation have been abandoned. Allogeneic cell therapies targeting large patient populations could be more economically feasible[8,9], but are subject to forceful immune rejection[10]. The use of allogeneic iPSC- or embryonic stem cell (ESC)-based products would require strong immunosuppression.

We envisioned engineering hypoimmunogenic pluripotent stem cells as a source for universally compatible cell or tissue grafts not requiring any immunosuppression. During pregnancy, the maternal immune system is tolerant of allogeneic paternal antigens although it would reject cells from the baby later in life[11]. We examined syncytiotrophoblast cells, which form the interface between maternal blood and fetal tissue, and found low MHC class I and II expression (Supplementary Fig. 1) as well as strong expression of CD47, a ubiquitous membrane protein that can interact with several cell surface receptors to inhibit phagocytosis[12]. We used this knowledge to design hypoimmunogenic mouse iPSCs (miPSCs).

C57BL/6 wild type (WT) miPSCs[13] give rise to classical teratomas with ectodermal, mesodermal and endodermal features in SCID-beige mice (Supplementary Fig. 2). To achieve hypoimmunogenicity, these miPSCs underwent a three-step gene-editing process (Supplementary Fig. 3a). First, CRISPR guide RNAs targeting the coding sequence of the mouse β2-microglobulin (*B2m*) gene were ligated into vectors containing the Cas9 expression cassette and subsequently transfected into miPSCs. B2m is a structural component of MHC class I. Second, $B2m^{-/-}$ miPSCs were transfected with a CRISPR-Cas9 vector targeting *Ciita*, the master regulator of MHC class II molecules[14]. Third, the *Cd47* gene sequence was synthesized and cloned into a lentivirus with blasticidin resistance, which was used to transduce $B2m^{-/-}Ciita^{-/-}$ miPSC clones followed by antibiotic selection and expansion of $B2m^{-/-}Ciita^{-/-}$ *Cd47* transgene (tg)-expressing miPSCs. WT miPSCs had interferon-γ (IFN-γ)-inducible MHC class I surface expression, low but detectable MHC class II expression and negligible Cd47 expression (Supplementary Fig. 3b–d). We confirmed that the miPSC lines we generated lacked MHC class I and II expression, and over-expressed Cd47 roughly 4.5-fold in flow cytometry. All three lines maintained their expression of pluripotency genes (Supplementary Fig. 3e–h).

Next, we transplanted WT miPSCs or engineered miPSCs into syngeneic C57BL/6 ($H2^b$) and allogeneic ($H2^d$) BALB/c recipients without immunosuppression. As expected, WT miPSCs showed

[1]Department of Surgery, Division of Cardiothoracic Surgery, Transplant and Stem Cell Immunobiology-Lab, University of California San Francisco, San Francisco, CA, USA. [2]Department of Cardiovascular Surgery, University Heart Center Hamburg, Hamburg, Germany. [3]Cardiovascular Research Center Hamburg and DZHK (German Center for Cardiovascular Research), Partner Site Hamburg/Kiel/Luebeck, Hamburg, Germany. [4]Division of Infectious Diseases, UNC Center for AIDS Research, University of North Carolina School of Medicine, Chapel Hill, NC, USA. [5]Howard Hughes Medical Institute, Institute for Immunity, Transplantation and Infection, and Department of Microbiology and Immunology, Stanford University School of Medicine, Stanford, CA, USA. [6]Department of Microbiology and Immunology and the Parker Institute for Cancer Immunotherapy, University of California San Francisco, San Francisco, California, USA. [7]These authors contributed equally: Tobias Deuse, Xiaomeng Hu. *e-mail: Sonja.Schrepfer@ucsf.edu

100% teratoma growth in syngeneic recipients, but all cell grafts were rejected in allogeneic BALB/c mice (Fig. 1a,b). After 5 days, splenocytes from allogeneic BALB/c recipients showed a strong IFN-γ and a moderate IL-4 response relative to baseline responder cell activity (not shown); syngeneic mice showed no responsiveness (Fig. 1c). Only allogeneic BALB/c recipients mounted a strong IgM antibody response against the WT miPSCs relative to baseline MFI (not shown) (Fig. 1d). Engineered miPSCs developed comparable teratomas to WT miPSCs in syngeneic recipients, with enhanced survival in allogeneic recipients that depended on their level of hypoimmunogenicity and increased with every engineering step (Supplementary Fig. 4a–h). Our final *B2m*$^{-/-}$*Ciita*$^{-/-}$ Cd47 tg miPSC line showed 100% teratoma formation and induced no IFN-γ or antibody responses (Fig. 1e–h).

We further evaluated the contribution of Cd47 overexpression by comparing *B2m*$^{-/-}$*Ciita*$^{-/-}$ miPSCs to *B2m*$^{-/-}$*Ciita*$^{-/-}$ Cd47 tg miPSCs in natural killer (NK) cell toxicity assays. Gene editing did not enhance the expression of stimulatory ligands for the mouse NK cell NKG2D or NKp46 receptors (Supplementary Fig. 4i), which are constitutively expressed in the NK cell-sensitive target cell line YAC-1[15]. *B2m*$^{-/-}$*Ciita*$^{-/-}$ miPSCs induced IFN-γ release that was significantly elevated when compared to unchallenged NK cells, but lower than IFN-γ release triggered by YAC-1 (Supplementary Fig. 4j). This suggested that Cd47 overexpression completely prevented any miPSC-induced NK cell IFN-γ release in vitro. To further assess innate miPSC clearance in vivo, a 1:1 mixture of CFSE-labeled WT miPSCs and either *B2m*$^{-/-}$*Ciita*$^{-/-}$ miPSCs or *B2m*$^{-/-}$*Ciita*$^{-/-}$ Cd47 tg miPSCs were injected into the innate immune cell-rich peritoneum of syngeneic C57BL/6 mice (Supplementary Fig. 5a). Using a syngeneic host for this assay precluded relevant T cell-mediated cytotoxicity. After 48 h, the peritoneal fluid was aspirated and CFSE-labeled cells were analyzed by flow cytometry. *B2m*$^{-/-}$*Ciita*$^{-/-}$ Cd47 tg miPSCs, but not *B2m*$^{-/-}$*Ciita*$^{-/-}$ miPSCs, were resistant to innate immune clearance and the 1:1 ratio with WT miPSCs could be maintained. We observed the same pattern of cell clearance when mice were pretreated with clodronate to eliminate macrophages (Supplementary Fig. 5b). Notably, a blocking antibody against mouse Cd47 completely abolished the protective effect of Cd47 in macrophage-depleted mice and *B2m*$^{-/-}$*Ciita*$^{-/-}$ Cd47 tg miPSCs were rapidly eliminated (Supplementary Fig. 5c). Collectively, these data suggest an inhibitory effect of Cd47 on NK cells in vivo.

To test whether hypoimmunogenic *B2m*$^{-/-}$*Ciita*$^{-/-}$ Cd47 tg miPSCs could give rise to hypoimmunogenic cardiac tissue, they were differentiated into endothelial cells (miECs), smooth muscle cells (miSMCs) and cardiomyocytes (miCMs) with WT miPSC derivatives serving as controls (Supplementary Fig. 6). All derivatives showed the morphologic appearance, cell marker immunofluorescence and gene expression characteristic of their mature target tissue cell lines, and cultures achieved >90% purity of VE-Cadherin^{+} miECs, Sma^{+} miSMCs and troponin I^{+} miCMs. The expression of MHC class I and II molecules in WT derivatives markedly varied by cell type (Supplementary Fig. 7a–c) but, as expected, miECs had by far the highest expression of IFN-γ induced MHC class I and II, miSMCs had moderate MHC class I and II expression[16] and miCMs had moderate MHC class I but very low MHC class II expression[17]. All *B2m*$^{-/-}$*Ciita*$^{-/-}$ Cd47 tg derivatives appropriately showed a complete lack of MHC class I and II and significantly elevated Cd47 compared to their WT counterparts. None of the *B2m*$^{-/-}$*Ciita*$^{-/-}$ Cd47 tg derivatives showed upregulation of NKG2D or NKp46 ligands (Supplementary Fig. 7d,e).

We next assessed the in vivo immunogenicity of WT and hypoimmunogenic miPSCderivatives. miECs, miSMCs or miCMs derived from WT or *B2m*$^{-/-}$*Ciita*$^{-/-}$ Cd47 tg were transplanted intramuscularly into syngeneic C57BL/6 or allogeneic BALB/c mice and adaptive immune responses were assessed after 5 days. All allogeneic recipients mounted a strong cellular IFN-γ response, as well as a strong IgM antibody response against all differentiated WT cell grafts (Supplementary Fig. 8a–c). In contrast, neither of the corresponding *B2m*$^{-/-}$*Ciita*$^{-/-}$ Cd47 tg derivatives showed detectable increases in IFN-γ Elispot frequencies or IgM antibody production (Supplementary Fig. 8d–f). To assess the efficacy of Cd47 to mitigate the susceptibility to innate immune killing, we performed NK cell Elispot assays with antibody-coated magnetic bead-enriched BALB/c NK cells and *B2m*$^{-/-}$*Ciita*$^{-/-}$ or *B2m*$^{-/-}$*Ciita*$^{-/-}$ Cd47 tg derivatives (Supplementary Fig. 8g–i). While *B2m*$^{-/-}$*Ciita*$^{-/-}$ derivatives triggered NK cell IFN-γ release, none of the *B2m*$^{-/-}$*Ciita*$^{-/-}$ Cd47 tg derivatives produced IFN-γ spot frequencies significantly exceeding those of unchallenged NK cells. Accordingly, in vivo innate immune assays showed rapid clearance of all *B2m*$^{-/-}$*Ciita*$^{-/-}$ derivatives, but confirmed that none of the *B2m*$^{-/-}$*Ciita*$^{-/-}$ Cd47 tg derivatives showed susceptibility to innate elimination (Supplementary Fig. 8j–l). To confirm an inhibitory effect of Cd47 on NK cells, we next performed real-time in vitro killing assays with confluent miECs and highly purified NK cells. Both allogeneic (BALB/c) and syngeneic (C57BL/6) NK cells rapidly killed *B2m*$^{-/-}$*Ciita*$^{-/-}$ miECs, but not WT and *B2m*$^{-/-}$*Ciita*$^{-/-}$ Cd47 tg miECs (Supplementary Fig. 5d,e). However, antibody blocking of mouse Cd47 resulted in the rapid killing of *B2m*$^{-/-}$*Ciita*$^{-/-}$ Cd47 tg miECs (Supplementary Fig. 5f). The effect of CD47 is species-specific as human NK cells rapidly killed both *B2m*$^{-/-}$*Ciita*$^{-/-}$ and *B2m*$^{-/-}$*Ciita*$^{-/-}$ Cd47 tg miECs (Supplementary Fig. 5g).

We next examined survival of WT and hypoimmunogenic miPSC derivates in vivo. WT and *B2m*$^{-/-}$*Ciita*$^{-/-}$ Cd47 tg derivatives were transduced to express firefly luciferase, and Matrigel plugs containing differentiated cells were transplanted into syngeneic C57BL/6 or allogeneic BALB/c mice. All three WT derivatives showed long-term (50 days) survival in syngeneic C57BL/6 recipients, but were rejected in allogeneic mice (Fig. 1i–k). In contrast, all three *B2m*$^{-/-}$*Ciita*$^{-/-}$ Cd47 tg derivatives showed 100% long-term survival in both syngeneic and allogeneic recipients (Fig. 1l–n).

Matrigel plugs containing WT or *B2m*$^{-/-}$*Ciita*$^{-/-}$ Cd47 tg miECs were transplanted into allogeneic BALB/c recipients (Supplementary Fig. 9a). ECs are the most immunogenic cardiac cell type due to their high expression of MHC class I and II, which allows them to function as antigen-presenting cells. We observed infiltrating immune cells containing mostly T and B lymphocytes, but also some NK cells and macrophages in WT miEC plugs. *B2m*$^{-/-}$*Ciita*$^{-/-}$ Cd47 tg miEC-containing plugs had almost no immune cell infiltration (Supplementary Fig. 9b). In the WT plugs, cytokine arrays on day 10 revealed an inflammatory milieu that included upregulated T helper cell (T_h)-1 cytokines (IFN-γ and IL-2) and T_h-2 cytokines (IL-4, IL-5, IL-10 and IL-13). In contrast, in plugs containing *B2m*$^{-/-}$*Ciita*$^{-/-}$ Cd47 tg miECs, the cytokine milieu was very similar to that of cell-free plugs containing only Matrigel, with no indication of immune activation (Supplementary Fig. 9c). Over time, transplanted *B2m*$^{-/-}$*Ciita*$^{-/-}$ Cd47 tg miECs organized in circular structures and formed primitive vessels that contained erythrocytes (Supplementary Fig. 10a). Similarly transplanted *B2m*$^{-/-}$*Ciita*$^{-/-}$ Cd47 tg miSMCs (Supplementary Fig. 10b) or miCMs (Supplementary Fig. 10c) did not form three-dimensional structures, and their in vivo maturation and integration potential in cardiac tissue remains to be studied.

We next applied our engineering strategy to human iPSCs (hiPSCs) using a human episomal iPSC line derived from CD34^{+} cord blood that showed a normal human XX karyotype and features of pluripotency (Supplementary Fig. 11a–c,g–h). The gene-editing process included two steps (Fig. 2a). First, both the human *B2M* and human *CIITA* genes were simultaneously targeted for CRISPR/Cas9-mediated disruption. Second, these edited hiPSCs were transduced with a lentivirus carrying human CD47 complementary DNA with an EFS promotor and puromycin resistance. Antibiotic-resistant *B2M*$^{-/-}$*CIITA*$^{-/-}$ CD47 tg hiPSC colonies maintained their normal

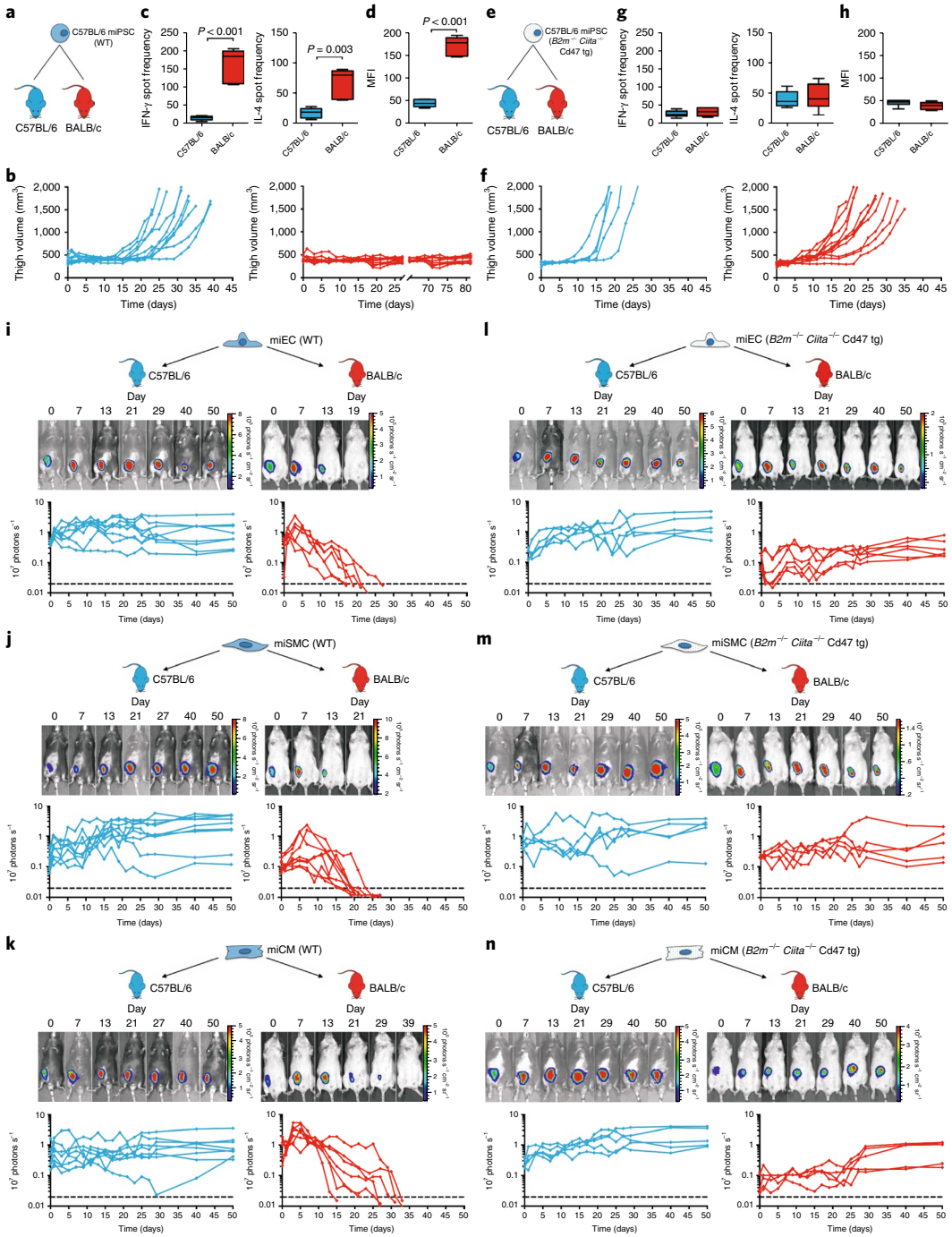

Fig. 1 | Survival of miPSCs and miPSC derivatives. a, WT C57BL/6 miPSCs were injected into the thigh muscle of syngeneic C57BL/6 or allogeneic BALB/c mice. **b**, Teratoma formation was observed by measuring the thigh muscle ($n = 10$ per group). **c**, IFN-γ and IL-4 enzyme-linked immunospots (Elispots) with splenocytes recovered 5 days after the transplantation (box 25th to 75th percentile with median, whiskers min–max, five animals per group, two-tailed Student's *t*-test). **d**, Mean fluorescence imaging (MFI) of IgM binding to WT miPSCs incubated with recipient serum after 5 days (box 25th to 75th percentile with median, whiskers min–max, six animals per group, two-tailed Student's *t*-test). **e**, $B2m^{-/-}Ciita^{-/-}$ Cd47 tg C57BL/6 miPSCs were transplanted into syngeneic C57BL/6 or allogeneic BALB/c recipients. **f**, Thigh volume C57BL/6 ($n = 5$) and BALB/c ($n = 11$) animals. The overall percentage of cell grafts that survived and formed teratomas in BALB/c was 100%. **g**, IFN-γ and IL-4 Elispots with splenocytes recovered 5 days after the transplantation and $B2m^{-/-}Ciita^{-/-}$ Cd47 tg miPSCs stimulator cells (box 25th to 75th percentile with median, whiskers min–max, $n = 6$ per group, two-tailed Student's *t*-test). **h**, MFI of IgM binding to $B2m^{-/-}Ciita^{-/-}$ Cd47 tg miPSCs incubated with recipient serum after 5 days (box 25th to 75th percentile with median, whiskers min–max, six animals per group, two-tailed Student's *t*-test). **i**–**n**, Grafts of Fluc$^+$ C57BL/6 miPSC derivatives in C57BL/6 or BALB/c recipients were longitudinally followed by bioluminescent imaging (BLI). One representative animal is depicted per group and the BLI values of all animals are plotted. All WT miPSC-derived miECs (**i**, eight animals in C57BL/6 and six animals in BALB/c), miSMCs (**j**, nine animals in C57BL/6 and eight animals in BALB/c) and miCMs (**k**, eight animals in C57BL/6 and seven animals in BALB/c) showed long-term survival in syngeneic C57BL/6 recipients but were rejected in allogeneic BALB/c animals. In contrast, all $B2m^{-/-}Ciita^{-/-}$ Cd47 tg miPSC-derived miECs (**l**, five animals in C57BL/6 and six animals in BALB/c), miSMCs (**m**, five animals in C57BL/6 and five animals in BALB/c) and miCMs (**n**, five animals in C57BL/6 and five animals in BALB/c) showed long-term survival in both syngeneic C57BL/6 and allogeneic BALB/c recipients.

human karyotype and pluripotency (Supplementary Fig. 11d–f,i–j) and successful depletion of HLA I and II surface expression, along with overexpression of CD47, was confirmed by flow cytometry (Fig. 2b). Both WT hiPSCs and *B2M*$^{-/-}$*CIITA*$^{-/-}$ CD47 tg hiPSCs were differentiated into endothelial-like cells (hiECs) and cardiomyocyte-like cells (hiCMs) (Fig. 2c). All derivatives showed the morphologic features and protein expression of the differentiated target cells and lost their pluripotency genes (Supplementary Fig. 12a,b). Cultures showed >95% purity for VE-Cadherin^{+} hiECs and troponin I^{+} hiCMs. There were no alterations in the expression of stimulatory NK cell ligands with gene engineering (Supplementary Fig. 12c–i). WT hiECs and hiCMs upregulated IFN-γ induced HLA I expression roughly three- and two-fold, respectively, compared to WT hiPSCs and hiECs also showed roughly 11-fold elevated HLA II (Fig. 2d–e). *B2M*$^{-/-}$*CIITA*$^{-/-}$ CD47 tg hiECs and hiCMs exhibited HLA I and II depletion and significant CD47 upregulation compared to their WT counterparts.

We next performed transplant studies in humanized CD34^{+} hematopoietic stem cell-engrafted NSG-SGM3 mice[18], which were allogeneic to the hiPSC, hiEC and hiCM grafts. Since no syngeneic controls are available in this humanized mouse model, background measurements were collected in naïve mice. After 5 days, recipients of WT hiPSCs (Fig. 2f) showed a high splenocyte IFN-γ spot frequency (Fig. 2g) and elevated IgM levels (Fig. 2h). Recipients of *B2M*$^{-/-}$*CIITA*$^{-/-}$ CD47 tg hiPSCs did not mount any detectable cellular IFN-γ response or antibody response. NK cell activation was assessed using in vitro incubation with human enriched CD56^{+} NK cells. *B2M*$^{-/-}$*CIITA*$^{-/-}$ hiPSCs resulted in an IFN-γ release reaching roughly one-third of the spot frequency of the highly NK cell susceptible K562 line, whereas *B2M*$^{-/-}$*CIITA*$^{-/-}$ CD47 tg hiPSCs did not provoke any measurable response (Fig. 2i). The allogeneic transplantation of WT hiECs (Fig. 2j) and WT hiCMs (Fig. 2n) resulted in strong systemic IFN-γ reactions (Fig. 2k,o) and IgM antibody increases (Fig. 2l,p) of similar intensity as WT hiPSCs, whereas hypoimmunogenic hiECs and hiCMs did not induce any cellular or humoral immune response. Moreover, in vitro, hypoimmunogenic derivatives did not trigger NK cell activation (Fig. 2m, q) or NK cell killing (Supplementary Fig. 5h). As with the miPSCs, a blocking antibody specific for human CD47 completely abolished NK cell protection of *B2M*$^{-/-}$*CIITA*$^{-/-}$ CD47 tg hiPSCs (Supplementary Fig. 5i).

We also assessed the survival of hiPSCs, as well as their derivatives in allogeneic humanized NSG-SGM3 mice. All cell lines were transduced to express Fluc to enable tracking by BLI. There was no significant difference in HLA-A mismatch between groups (Supplementary Fig. 12j). As expected, all WT hiPSC grafts in Matrigel plugs underwent rejection (Fig. 3a) and all *B2M*$^{-/-}$*CIITA*$^{-/-}$ CD47 tg hiPSCs formed teratomas. Similarly, WT hiECs (Fig. 3b) and WT hiCMs (Fig. 3c) were rejected, although at slightly slower rate than in the corresponding miPSC derivative experiments. This difference may be based on the reduced number, diversity and function of human immune cells in mouse recipients[19], although the triple transgenic NSG-SGM3 mice specifically express human cytokines[20] to minimize these limitations. All *B2M*$^{-/-}$*CIITA*$^{-/-}$ CD47 tg hiEC and hiCM grafts showed long-term survival (50 days) and stable BLI signal levels over time. The hiECs gradually organized into structures resembling primitive vascular structures, which occasionally contained erythrocytes, and the hiCMs acquired a limited polarized architecture (Fig. 3d,e).

hiECs, the most immunogenic derivatives, were further tested in the humanized BLT mouse model. BLT humanized mice are bioengineered by implantation of human fetal liver and thymic tissue under the kidney capsule followed by intravenous transplantation with autologous CD34^{+} HSCs[21] (Fig. 3f). This allows for T cell maturation in human thymic tissue and permits HLA restricted T cell responses. WT hiEC grafts in Matrigel plugs triggered a roughly 40% stronger IFN-γ response but 40% weaker IgM antibody response than in the previous NSG-SGM3 mice. No measurable immune activation was detected in recipients of *B2M*$^{-/-}$*CIITA*$^{-/-}$ CD47 tg hiEC grafts (Fig. 3g,h). All WT hiEC grafts underwent rapid rejection while four out of five *B2M*$^{-/-}$*CIITA*$^{-/-}$ CD47 tg hiEC grafts achieved survival (Fig. 3i). We assume a non-immune-related reason for the failure of the fifth graft since no immune activation could be detected in this specific recipient. We thus demonstrated that the combination of MHC class I and II depletion and CD47 overexpression renders both mouse and human stem cells, as well as their differentiated derivatives, hypoimmunogenic. In the models studied here, engineered differentiated derivatives achieved long-term survival in fully allogeneic hosts without any immunosuppression and retained basic cell-specific features after transplantation.

The initial concept of hypoimmunogenic pluripotent stem cells was based on an MHC class I knockdown and showed encouraging early results[22]. However, according to the 'missing-self theory', MHC class I-deficient mouse and human PSCs become susceptible to NK

Fig. 2 | Immune response against hiPSC derivatives. a, WT hiPSCs first underwent *B2M* and *CIITA* gene disruption and then CD47 transgene overexpression **b**, Gene editing of hiPSCs was confirmed by flow cytometry (box 25th to 75th percentile with median, whiskers min–max, four independent experiments per graph, analysis of variance (ANOVA) with Bonferroni's post-hoc test). **c**, WT and *B2M*$^{-/-}$*CIITA*$^{-/-}$ CD47 tg hiPSCs were differentiated into both hiECs and hiCMs. **d**–**e**, The immune phenotype of WT and *B2M*$^{-/-}$*CIITA*$^{-/-}$ CD47 tg hiECs (**d**) and hiCMs (**e**) is shown (box 25th to 75th percentile with median, whiskers min–max, four independent experiments per graph, two-tailed Student's *t*-test). **f**, WT or *B2M*$^{-/-}$*CIITA*$^{-/-}$ CD47 tg hiPSC grafts were injected into allogeneic humanized NSG-SGM3 mice. **g**, IFN-γ Elispots were performed after 5 days (mean ± s.d., $n = 7$ per group, two-tailed Student's *t*-test), the background spot frequency in naïve mice is shown (mean ± s.d., four animals per group, two-tailed Student's *t*-test). **h**, MFI of IgM binding to either hiPSC incubated with recipient serum after 5 days (mean ± s.d., five animals per group, two-tailed Student's *t*-test), the background fluorescence in naïve mice is shown (mean ± s.d., three animals per group, Student's *t*-test). **i**, IFN-γ Elispots with human NK cells were performed with *B2M*$^{-/-}$*CIITA*$^{-/-}$ hiPSC or *B2M*$^{-/-}$*CIITA*$^{-/-}$ CD47 tg hiPSC (box 25th to 75th percentile with median, whiskers min–max, six independent experiments, ANOVA with Bonferroni's post-hoc test). **j**, WT or *B2M*$^{-/-}$*CIITA*$^{-/-}$ CD47 tg hiEC grafts were injected into allogeneic humanized NSG-SGM3 mice. **k**, IFN-γ Elispots were performed after 5 days (mean ± s.d., three animals per group, two-tailed Student's *t*-test), the background spot frequency in naïve mice is shown (mean ± s.d., four animals per group, two-tailed Student's *t*-test). **l**, MFI of IgM binding to either hiEC incubated with recipient serum after 5 days (mean ± s.d., three animals per group, two-tailed Student's *t*-test), the background fluorescence in naïve mice is shown (mean ± s.d., three animals per group, Student's *t*-test). **m**, IFN-γ Elispots with human NK cells were performed with *B2M*$^{-/-}$*CIITA*$^{-/-}$ hiECs or *B2M*$^{-/-}$*CIITA*$^{-/-}$ CD47 tg hiECs (box 25th to 75th percentile with median, whiskers min–max, six independent experiments, ANOVA with Bonferroni's post-hoc test). **n**, WT or *B2M*$^{-/-}$*CIITA*$^{-/-}$ CD47 tg hiCM grafts were injected into allogeneic humanized NSG-SGM3 mice. **o**, IFN-γ Elispots were performed after 5 days (mean ± s.d., three animals per group, two-tailed Student's *t*-test), the background spot frequency in naïve mice is shown (mean ± s.d., four animals per group, two-tailed Student's *t*-test). **p**, MFI of IgM binding to either hiCM incubated with recipient serum after 5 days (mean ± s.d., three animals per group, two-tailed Student's *t*-test), the background fluorescence in naïve mice is shown (mean ± s.d., three animals per group, Student's *t*-test). **q**, IFN-γ Elispots with human NK cells were performed with *B2M*$^{-/-}$*CIITA*$^{-/-}$ hiCMs or *B2M*$^{-/-}$*CIITA*$^{-/-}$ CD47 tg hiCMs (box 25th to 75th percentile with median, whiskers min–max, six independent experiments, ANOVA with Bonferroni's post-hoc test).

cell killing[23–25]. Although isolated expression of HLA-E[26] or HLA-G[27] in human pluripotent stem cells has been used to mitigate NK cell cytotoxicity, we observed that CD47 is a very effective non-MHC ligand to silence all innate immune responses. However, cells eluding immune monitoring may pose the long-term risks of uncontrollable malignant transformation or impaired virus clearance, although for the latter alternative mechanisms have been shown[28]. Inducible kill switches could enhance their overall safety.

The ability to generate substantial amounts of cardiac tissue from allogeneic iPSC-derived CMs has been well demonstrated in macaques[29]. However, the amounts of toxic immunosuppressive drugs required to achieve allogeneic cell survival pose a major

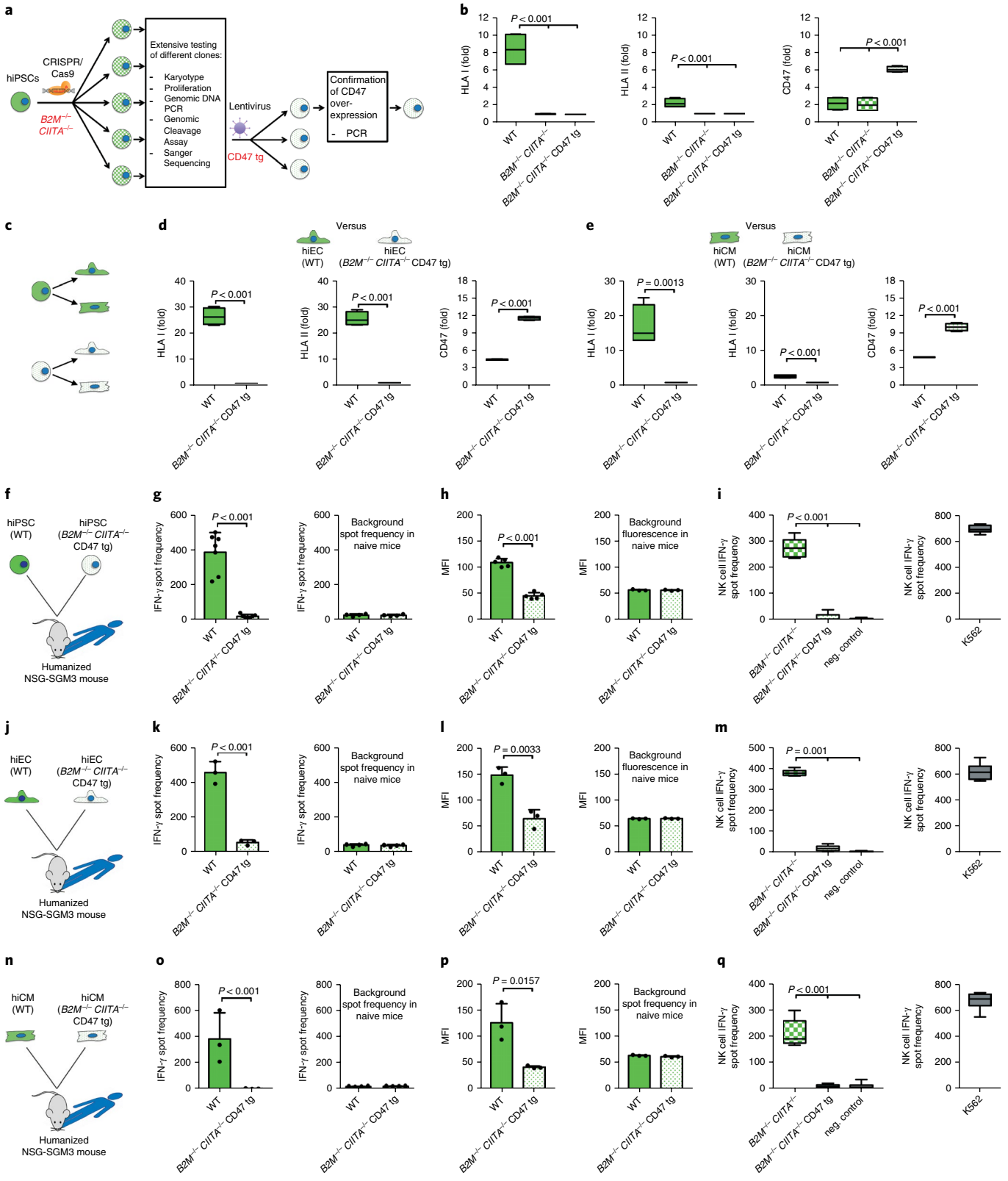

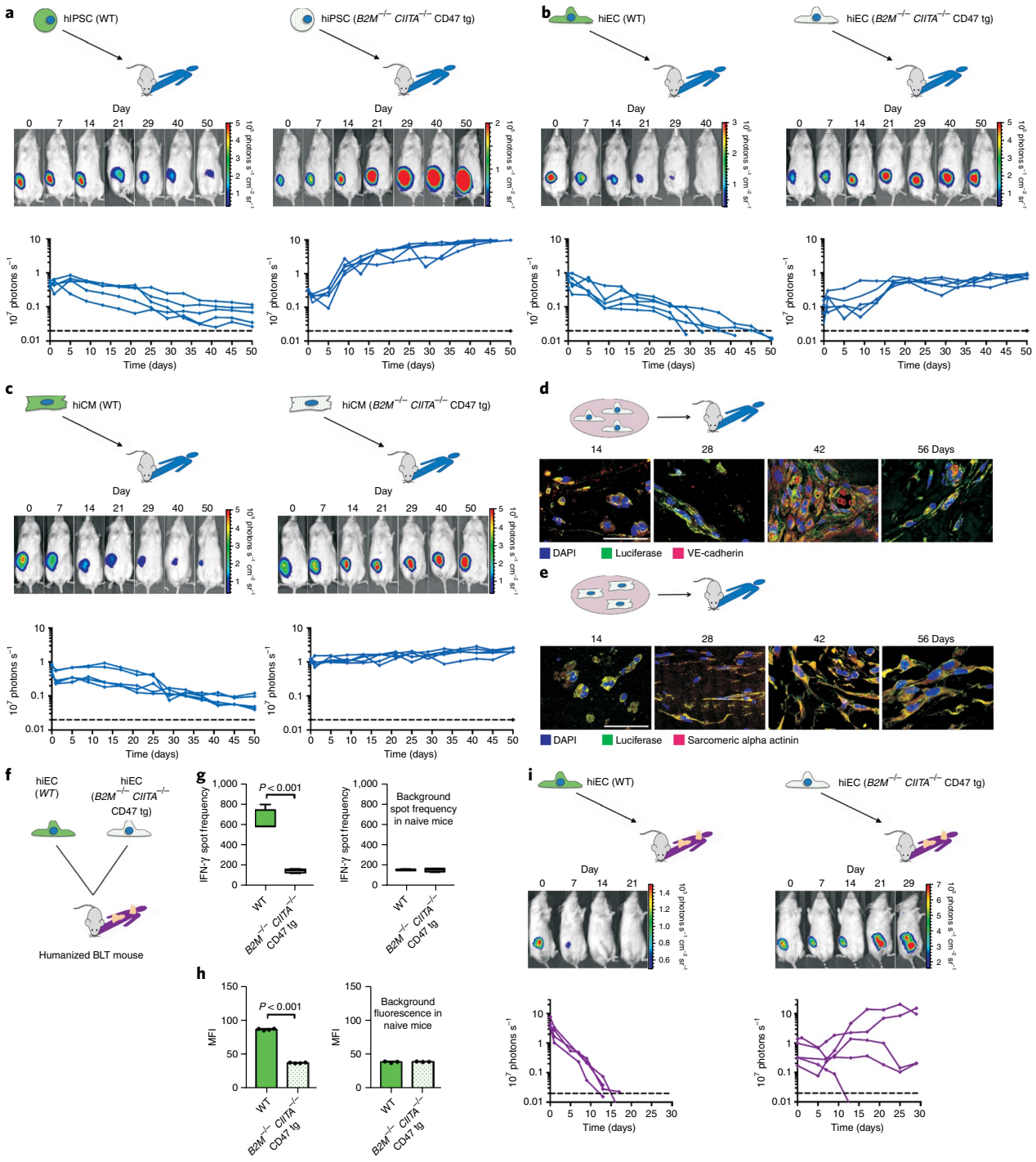

Fig. 3 | Survival of hiPSCs and hiPSC derivatives in allogeneic hosts. Grafts of Fluc$^+$ WT or *B2M*$^{-/-}$*CIITA*$^{-/-}$ CD47 tg hiPSCs, hiECs and hiCMs were transplanted into allogeneic humanized mice (NSG-SGM3 mice in **a**–**e**, BLT mice in **f**–**i**) and were longitudinally followed by BLI. One representative animal is depicted per group and the BLI values of all animals are plotted. **a**, BLI signals over time of WT and *B2M*$^{-/-}$*CIITA*$^{-/-}$ CD47 tg hiPSC grafts ($n = 5$ per group). **b**, WT and *B2M*$^{-/-}$*CIITA*$^{-/-}$ CD47 tg hiECs were transplanted as in **a** ($n = 5$ per group). **c**, WT and *B2M*$^{-/-}$*CIITA*$^{-/-}$ CD47 tg hiCMs ($n = 5$). **d**, *B2M*$^{-/-}$*CIITA*$^{-/-}$ CD47 tg hiECs started to organize into a more complex structure, which included primitive vascular structures (representative pictures of three independent experiments). Scale bar, 50 µm. **e**, The *B2M*$^{-/-}$*CIITA*$^{-/-}$ CD47 tg hiCMs began to organize into a more polarized framework and maintained their sarcomeric alpha-actinin cytoskeletal structure typical of cardiomyocytes (representative pictures of three independent experiments). Scale bar, 50 µm. **f**, WT or *B2M*$^{-/-}$*CIITA*$^{-/-}$ CD47 tg hiECs were transplanted into allogeneic humanized BLT mice. **g**, IFN-γ Elispots were performed after 5 days (box 25th to 75th percentile with median, whiskers min–max, four animals per group, two-tailed Student's *t*-test), the background spot frequency in naïve mice is shown. **h**, MFI of IgM binding to either hiEC incubated with recipient serum after 5 days (mean ± s.d., four animals per group, two-tailed Student's *t*-test), the background fluorescence in naïve mice is shown (mean ± s.d., three animals per group, two-tailed Student's *t*-test). **i**, Grafts of Fluc$^+$ WT or *B2M*$^{-/-}$*CIITA*$^{-/-}$ CD47 tg hiECs were transplanted into allogeneic humanized BLT mice and were longitudinally followed by BLI. All WT hiEC grafts were rejected within roughly 14 days (four animals). Four of the five *B2M*$^{-/-}$*CIITA*$^{-/-}$ CD47 tg hiEC grafts permanently survived, the one failure is believed not to be immune-mediated (five animals).

hurdle for clinical use. Even with fully MHC class I- and II-matched allogeneic iPSC-derived CM grafts, macaque recipients required substantial and highly toxic immunosuppression to prevent cell rejection[29,30]. Thus, the generation of universal hypoimmunogenic iPSCs that can be differentiated into the main components of cardiac tissue and achieve long-term survival in a fully allogeneic recipient without any immunosuppression may help to develop universal cell products to treat heart failure.

Online content

Any methods, additional references, Nature Research reporting summaries, source data, statements of data availability and associated accession codes are available at https://doi.org/10.1038/s41587-019-0016-3.

Received: 23 April 2018; Accepted: 28 December 2018;
Published online: 18 February 2019

References

1. Gyongyosi, M. et al. Meta-analysis of cell-based CaRdiac stUdiEs (ACCRUE) in patients with acute myocardial infarction based on individual patient data. *Circ. Res.* **116**, 1346–1360 (2015).
2. Fisher, S. A., Doree, C., Mathur, A. & Martin-Rendon, E. Meta-analysis of cell therapy trials for patients with heart failure. *Circ. Res.* **116**, 1361–1377 (2015).
3. Kandala, J. et al. Meta-analysis of stem cell therapy in chronic ischemic cardiomyopathy. *Am. J. Cardiol.* **112**, 217–225 (2013).
4. Fernandez-Aviles, F. et al. Global position paper on cardiovascular regenerative medicine. *Eur. Heart J.* **38**, 2532–2546 (2017).
5. Lipsitz, Y. Y., Timmins, N. E. & Zandstra, P. W. Quality cell therapy manufacturing by design. *Nat. Biotechnol.* **34**, 393–400 (2016).
6. Blair, N. F. & Barker, R. A. Making it personal: the prospects for autologous pluripotent stem cell-derived therapies. *Regen. Med.* **11**, 423–425 (2016).
7. Chakradhar, S. An eye to the future: researchers debate best path for stem cell-derived therapies. *Nat. Med.* **22**, 116–119 (2016).
8. Smith, D. M. Assessing commercial opportunities for autologous and allogeneic cell-based products. *Regen. Med.* **7**, 721–732 (2012).
9. Lipsitz, Y. Y., Bedford, P., Davies, A. H., Timmins, N. E. & Zandstra, P. W. Achieving efficient manufacturing and quality assurance through synthetic cell therapy design. *Cell. Stem. Cell.* **20**, 13–17 (2017).
10. van Berlo, J. H. & Molkentin, J. D. An emerging consensus on cardiac regeneration. *Nat. Med.* **20**, 1386–1393 (2014).
11. Arck, P. C. & Hecher, K. Fetomaternal immune cross-talk and its consequences for maternal and offspring's health. *Nat. Med.* **19**, 548–556 (2013).
12. Jaiswal, S. et al. CD47 is upregulated on circulating hematopoietic stem cells and leukemia cells to avoid phagocytosis. *Cell* **138**, 271–285 (2009).
13. Diecke, S. et al. Novel codon-optimized mini-intronic plasmid for efficient, inexpensive, and xeno-free induction of pluripotency. *Sci. Rep.* **5**, 8081 (2015).
14. Chang, C. H., Fontes, J. D., Peterlin, M. & Flavell, R. A. Class II transactivator (CIITA) is sufficient for the inducible expression of major histocompatibility complex class II genes. *J. Exp. Med.* **180**, 1367–1374 (1994).
15. Elsner, L. et al. The heat shock protein HSP70 promotes mouse NK cell activity against tumors that express inducible NKG2D ligands. *J. Immunol.* **179**, 5523–5533 (2007).
16. Maddaluno, M. et al. Murine aortic smooth muscle cells acquire, though fail to present exogenous protein antigens on major histocompatibility complex class II molecules. *Biomed. Res. Int.* **2014**, 949845 (2014).
17. Didie, M., Galla, S., Muppala, V., Dressel, R. & Zimmermann, W. H. Immunological properties of murine parthenogenetic stem cell-derived cardiomyocytes and engineered heart muscle. *Front. Immunol.* **8**, 955 (2017).
18. Wunderlich, M. et al. AML xenograft efficiency is significantly improved in NOD/SCID-IL2RG mice constitutively expressing human SCF, GM-CSF and IL-3. *Leukemia* **24**, 1785–1788 (2010).
19. Shultz, L. D., Ishikawa, F. & Greiner, D. L. Humanized mice in translational biomedical research. *Nat. Rev. Immunol.* **7**, 118–130 (2007).
20. Billerbeck, E. et al. Development of human CD4+ FoxP3+ regulatory T cells in human stem cell factor-, granulocyte-macrophage colony-stimulating factor-, and interleukin-3-expressing NOD-SCID IL2Rgamma(null) humanized mice. *Blood* **117**, 3076–3086 (2011).
21. Melkus, M. W. et al. Humanized mice mount specific adaptive and innate immune responses to EBV and TSST-1. *Nat. Med.* **12**, 1316–1322 (2006).
22. Deuse, T. et al. Human leukocyte antigen I knockdown human embryonic stem cells induce host ignorance and achieve prolonged xenogeneic survival. *Circulation* **124**, S3–S9 (2011).
23. Wang, D., Quan, Y., Yan, Q., Morales, J. E. & Wetsel, R. A. Targeted disruption of the beta2-microglobulin gene minimizes the immunogenicity of human embryonic stem cells. *Stem Cells Transl. Med.* **4**, 1234–1245 (2015).
24. Dressel, R. et al. Pluripotent stem cells are highly susceptible targets for syngeneic, allogeneic, and xenogeneic natural killer cells. *FASEB J.* **24**, 2164–2177 (2010).
25. Kruse, V. et al. Human induced pluripotent stem cells are targets for allogeneic and autologous natural killer (NK) cells and killing is partly mediated by the activating NK Receptor DNAM-1. *PLoS ONE* **10**, e0125544 (2015).
26. Gornalusse, G. G. et al. HLA-E-expressing pluripotent stem cells escape allogeneic responses and lysis by NK cells. *Nat. Biotechnol.* **35**, 765–772 (2017).
27. Zhao, L., Teklemariam, T. & Hantash, B. M. Heterelogous expression of mutated HLA-G decreases immunogenicity of human embryonic stem cells and their epidermal derivatives. *Stem Cell Res.* **13**, 342–354 (2014).
28. Hou, S., Doherty, P. C., Zijlstra, M., Jaenisch, R. & Katz, J. M. Delayed clearance of Sendai virus in mice lacking class I MHC-restricted CD8+ T cells. *J. Immunol.* **149**, 1319–1325 (1992).
29. Shiba, Y. et al. Allogeneic transplantation of iPS cell-derived cardiomyocytes regenerates primate hearts. *Nature* **538**, 388–391 (2016).
30. Kawamura, T. et al. Cardiomyocytes derived from MHC-homozygous induced pluripotent stem cells exhibit reduced allogeneic immunogenicity in MHC-matched non-human primates. *Stem Cell Rep.* **6**, 312–320 (2016).

Acknowledgements

We thank C. Pahrmann for cell culture work, imaging experiments and overall assistance and L. Li for his assistance. The in vivo BLI experiments were performed at the UCSF Pre-clinical Therapeutics Core (A. Fries; with special thanks to B.C. Hann). Special thanks go to J. Wu (Stanford Cardiovascular Institute, Stanford University School of Medicine) for providing the miPSCs and the help of his laboratory with developing the protocol for hiPSC differentiation into cardiomyocytes. We thank J.-F. Garcia-Gomez (City of Hope, Duarte) for the HLA typing of humanized BLT mice. We also thank E. Maltepe and H. Pektas for providing the syncytiotrophoblast cells. D.W. was supported by the Max Kade Foundation. A.W. received funding from the National Institutes of Health (grant AI123010). J.V.G. received funding from the National Institutes of Health (AI111899 and MH108179). The cardiomyocyte research was partly made possible by a grant from the California Institute for Regenerative Medicine (Grant Number DISC1-09984). Research related to cardiomyocyte immunobiology reported in this publication was supported by National Heart, Lung, and Blood Institute of the National Institutes of Health under award number R01HL140236. L.L.L. is an American Cancer Society Professor funded by NIH AI068129 and in part by the Parker Institute for Cancer Immunotherapy. S.S. and T.D. received funding for the cardiomyocyte research from the California Institute for Regenerative Medicine (Grant Number DISC1-09984) and for the immunobiology work from the National Heart, Lung, and Blood Institute of the National Institutes of Health under award number R01HL140236. The contents of this publication are solely the responsibility of the authors and do not necessarily represent the official views of the NIH, CIRM and other agencies of the State of California.

Author contributions

T.D. and S.S. designed the experiments, supervised the project, and wrote the manuscript. X.H. performed the adaptive and innate immunobiology experiments, molecular biology and imaging studies and cell culture work and analyzed the data. A.G. performed imaging studies and analyzed the data. D.W. performed the in vivo and immunofluorescence imaging studies (confocal microscopy) and histopathology. G.T. performed imaging studies and cell injections. C.D. and W.O.T. generated BLT mice and performed the BLT imaging experiments. A.W. and J.V.G. designed and supervised the experiments using BLT mice. W.O.T. and C.D. performed the experiments using BLT mice. H.R., M.M.D. and L.L.L. gave technical support and conceptual advice. All authors contributed to editing the manuscript.

Competing interests

The authors declare no competing interests.

Additional information

Supplementary information is available for this paper at https://doi.org/10.1038/s41587-019-0016-3.

Reprints and permissions information is available at www.nature.com/reprints.

Correspondence and requests for materials should be addressed to S.S.

Publisher's note: Springer Nature remains neutral with regard to jurisdictional claims in published maps and institutional affiliations.

Methods

Syncytiotrophoblast cells of mouse placenta. On isolated mouse syncytiotrophoblast cells, expression of MHC class I, MHC class II and Cd47 was performed using PCR. RNA was isolated with the RNeasy Plus Mini kit (Qiagen) according to the manufacturer's protocol. RT–PCR was performed to generate the cDNA (Applied Biosystems). The following primers were used: mouse MHC class I: 5′-AGTGGTGCTGCAGAGCATTACAA-3′, reverse: 5′-GGTGACTTCACCTTTAGATCTGGG-3′, MHC class II forward: 5′-GATGTGGAAGACCTGCG-3′, reverse: 5′-TGCATCTTCTGAGGGGTTTC-3′; mouse Cd47 forward: 5′-GGCGCAAAGCACCGAAGAAATGTT-3′, reverse: 5′-CCATGGCATCGCGCTTATCCATTT-3′. PCRs were performed on Mastercycler nexus (Eppendorf) and the amplification products were visualized by 2% agarose gel electrophoresis (Thermo Fisher).

Derivation of mouse iPSCs. Mouse tail tip fibroblasts of mice were dissociated and isolated with collagenase type IV (Life Technologies) and maintained with Dulbecco's modified Eagle medium (DMEM) containing 10% fetal bovine serum (FBS), 1% glutamine, 4.5 g l^{-1} glucose, 100 U ml^{-1} penicillin, and 100 µg ml^{-1} streptomycin (pen-strep) at 37 °C, 20% O_2, and 5% CO_2 in a humidified incubator. 1×10^6 mouse fibroblasts were then re-programmed using a mini-intronic plasmid carrying sequences of Oct4, Klf4, Sox2 and c-Myc as well as short hairpin RNA against p53 (10–12 µM of DNA) using the Neon Transfection system[13]. After transfection, fibroblasts were plated on mitomycin-inhibited CF1 mouse embryonic fibroblasts (MEF, Applied Stemcell) and kept in fibroblast media with the addition of sodium butyrate (0.2 mM) and 50 µg ml^{-1} ascorbic acid. When ESC-like colonies appeared, media was changed to mouse iPSC media containing DMEM + GlutaMax 31966 (Gibco) with 10% heat-inactivated fetal calf sera (FCS hi), 1% MEM-NEAA and 1% pen-strep (all Gibco). With every passage, the iPSCs were sorted for the mouse pluripotency marker SSEA-1 using antibody-coated magnetic bead based cell sorting.

Mouse iPSC culture. After the MEF feeder cells attached and were 100% confluent, miPSCs were grown on MEF in knockout DMEM 10829 with 15% knockout Serum Replacement, 1% glutamine, 1% MEM-NEAA, 1% pen-strep (all Gibco), 0.2% beta-mercaptoethanol and 100 units LIF (both Millipore). Cells were maintained in 10 cm dishes, medium was changed daily and the cells were passaged every 2–3 days using 0.05% trypsin-EDTA (Gibco). miPSCs were cultured on gelatin (Millipore) without feeders before experiments using the standard media. Cell cultures were regularly screened for mycoplasma infections using the MycoAlert Kit (Lonza).

Pluripotency analysis by RT–PCR and immunofluorescence. miPSC were plated in confocal dishes (MatTek) for immunofluorescence analysis 48 h after plating using the miPSC Characterization kit (Applied Stemcell). Briefly, cells were fixed, permeabilized, and stained overnight at 4 °C with the primary antibodies for Sox2, SSEA-1 and Oct4. After several washes the cells were incubated with a secondary antibody and DNA staining solution. Alkaline phosphatase activity assay was performed (Applied Stemcell). Stained cells were imaged using a fluorescent microscope.

For RT–PCR, RNA was extracted using the RNeasy Plus Mini Kit (Qiagen). Genomic DNA contamination was removed using the gDNA spin column. cDNA was generated using Applied Biosystems High-Capacity cDNA Reverse Transcription kit. Gene-specific primers of the miPSC Characterization Kit (Applied Stemcell) were used to amplify target sequences. Actin was used as housekeeping gene, which encodes a cellular cytoskeleton protein. PCR reactions were performed on Mastercycler nexus (Eppendorf) and visualized on 2% agarose gels.

Pluripotency analysis by in vivo teratoma assay. Ten million miPSCs were injected intramuscular into the hind limb of immunodeficient SCID-beige mice and teratoma development was observed within 14 days. Teratomas were recovered and fixed in 4% paraformaldehyde in PBS, dehydrated, embedded in paraffin, and cut into sections of 5 µm thickness. For histopathology, sections were rehydrated and stained with hematoxylin and eosin (Carl Roth). Images were taken with an inverted light microscope.

Immunofluorescence staining demonstrated differentiation into ectodermal, mesodermal, and endodermal cells using antibodies against brachyury (ab20680, Abcam), cytokeratin 8 (ab 192467) and GFAP (GA5, Cell Signaling). For visualization, secondary antibodies conjugated with Alexa Fluor 555, 488 and 647 (all Invitrogen) were used, respectively. Cell nuclei were counterstained with 4,6-diamidino-2-phenylindole (DAPI) and imaging was performed with a Leica SP5 laser confocal microscope (Leica).

Gene editing of mouse iPSCs. miPSCs underwent three gene-modification steps. First, CRISPR guides targeting the coding sequence of mouse *B2m* gene were annealed and ligated into vectors containing the Cas9 expression cassette. Transfected miPSCs were dissociated to single cells, expanded to colonies, sequenced and tested for homogeneity. Second, these *B2m*$^{-/-}$ miPSCs were transfected with vectors containing CRISPR guides targeting *Ciita*. Expanded single cell colonies were sequenced and *B2m*$^{-/-}$*Ciita*$^{-/-}$ clones were identified through the presence of aberrant sequence from the CRISPR cleavage site. Third, the *Cd47* gene sequence was synthesized and the DNA was cloned into a lentiviral with blasticidin resistance. *B2m*$^{-/-}$*Ciita*$^{-/-}$ miPSCs were transduced with the resulting lentivirus and grown in the presence of blasticidin. Antibiotic-selected pools were tested for Cd47 overexpression and *B2m*$^{-/-}$*Ciita*$^{-/-}$ Cd47 tg miPSCs were expanded.

Generation of *B2m*$^{-/-}$ miPSCs. CRIPSR technology was used for disruption of the *B2m* gene. For targeting the coding sequence of mouse *B2m* gene, the CRISPR sequence 5′-TTCGGCTTCCCATTCTCCGG(TGG)-3′ was annealed and ligated into the All-In-One (AIO) vectors containing the Cas9 expression cassette as per the kit's instructions (GeneArt CRISPR Nuclease Vector Kit, Thermo Fisher). miPSC were transfected with the AIO vectors using Neon electroporation with two 1,200 V pulses of 20 ms duration. The transfected iPSC cultures were dissociated to single cells using 0.05% trypsin (Gibco) and then sorted with FACSAria cell sorter (BD Bioscience) for removing doublets and debris by selective gating on forward and side light scatter properties. Single cells were expanded to full-size colonies and tested for CRISPR editing by screening for the presence of the altered sequence from the CRISPR cleavage site. Briefly, the target sequence was amplified via PCR using AmpliTaq Gold Master Mix (Applied Biosystems) and the primers B2m gDNA forward: 5′-CTGGATCAGACATATGTGTTGGGA-3′, reverse: 5′-GCAAAGCAGTTTTAAGTCCACACAG-3′. After cleanup of the obtained PCR product (PureLink Pro 96 PCR Purification Kit, Thermo Fisher), Sanger sequencing was performed. The Ion Personal Genome Machine (PGM) Sequencing was used for the identification of the homogeneity, through sequencing of a PCR amplified 250 base pair region of the *B2m* gene using primers B2m gDNA PGM forward: 5′-TTTTCAAAATGTGGGTAGACTTTGG-3′ and reverse: 5′-GGATTTCAATGTGAGGCGGGT-3′. The PCR product was purified as described above and prepared using the Ion PGM Hi-Q Template Kit (Thermo Fisher). Experiments were performed on the Ion PGM System with the Ion 318 Chip Kit v.2 (Thermo Fisher).

Generation of *B2m*$^{-/-}$*Ciita*$^{-/-}$ miPSCs. CRIPSR technology was used for the further disruption of the *Ciita* gene. For targeting the coding sequence of mouse *Ciita* gene, the CRISPR sequence 5'- GGTCCATCTGGTCATAGAGG (CGG)-3′ was annealed and ligated into the All-In-One (AIO) vectors containing the Cas9 expression cassette as per the kit's instructions (GeneArt CRISPR Nuclease Vector Kit, Thermo Fisher). miPSC were transfected with the AIO vectors using the same condition for *B2m* disruption. The transfected miPSC cultures were dissociated to single cells using 0.05% trypsin (Gibco) and then sorted with FACSAria cell sorter (BD Bioscience) for removing doublets and debris by selective gating on forward and side light scatter properties. Single cells were expanded to full-size colonies and tested for CRISPR editing by screening for the presence of an altered sequence from the CRISPR cleavage site. Briefly, the target sequence was amplified via PCR using AmpliTaq Gold Master Mix (Applied Biosystems) and the primers Ciita gDNA forward: 5′-CCCCCAGAACGATGAGCTT-3′, reverse: 5′-TGCAGAAGTCCTGAGAAGGCC-3′. After cleanup of the obtained PCR product (PureLink Pro 96 PCR Purification Kit, Thermo Fisher), Sanger sequencing was performed. Using the DNA sequence chromatogram, edited clones were then identified through the presence of altered sequence from the CRISPR cleavage site. Indel size was calculated using the TIDE tool. PCR and ICC were performed again to verify the pluripotency status of the cells.

Generation of *B2m*$^{-/-}$*Ciita*$^{-/-}$ Cd47 tg miPSCs. Cd47 transgene overexpression was generated using lentivirus-mediated delivery of a Cd47-expressing vector containing the antibiotic resistance cassette blasticidin. The Cd47 cDNA was synthesized and cloned into the lentiviral plasmid pLenti6/V5 (Thermo Fisher) with a blasticidin resistance. Sanger sequencing was performed to verify that no mutation had occurred. Lentivirus generation was performed with a stock titer of 1×10^7 TU per ml. The transduction was performed into 2×10^5 *B2m*$^{-/-}$*Ciita*$^{-/-}$ miPSCs, grown on blasticidin-resistant MEF cells for 72 h with a MOI ratio of 1:10 followed by antibiotic selection with 12.5 µg ml^{-1} blasticidin for 7 days. Antibiotic-selected pools were tested by RT–quantitative PCR amplification of Cd47 mRNA and flow cytometry detection of Cd47 on the surface of the cells. After the confirmation of Cd47, cells were expanded and validated by running pluripotency assays.

Transduction to express firefly luciferase. iPSCs were transduced to express Fluc. One hundred thousand miPSCs were plated in one gelatin-coated six-well plates and incubated overnight at 37 °C at 5% CO_2. The next day, media was changed and one vial of Fluc lentiviral particles expressing luciferase II gene under re-engineered EF1a promotor (GenTarget) was added to 1.5 ml media. After 36 h, 1 ml of cell media was added. After further 24 h, complete media change was performed. After 2 days, luciferase expression was confirmed by adding D-luciferin (Promega). Signals were quantified with IVIS 200 (Perkin Elmer) in maximum photons s^{-1} cm^{-2} sr^{-1}

Karyotyping. Cell collection, slide preparation and G-banded karyotyping were performed using standard cytogenetics protocols optimized for human pluripotent

cells. Cells were incubated with ethidium bromide and colcemid (Gibco) and then trypsinized to detach the cells from the plate. The cells were placed in hypotonic solution (0.075 M potassium chloride, 0.559 g KCl in 100 ml water, Millipore), followed by fixation. Metaphase cell preparations were stained with Leishman's stain. Karyotype analysis consisted of chromosomes counted in twenty cells with band-by-band analysis of eight cells.

Mice. BALB/c (BALB/cAnNCrl, $H2^d$), C57BL/6 (C57BL/6 J, $H2^b$) and SCID-beige (CBySmn.CB17-Prkdcscid/J) (all 6–12 weeks) were used as recipients for different assays. The number of animals per experimental group is presented in each figure. Mice were purchased from Charles River Laboratories (Sulzfeld) and received humane care in compliance with the Guide for the Principles of Laboratory Animals. Animal experiments were approved by the Hamburg 'Amt für Gesundheit und Verbraucherschutz' or the University of California San Francisco (UCSF) Institutional Animal Care and Use Committee and performed according to local and EU guidelines.

Teratoma assays to study miPSC survival in vivo. Six-to-eight-week-old syngeneic or allogeneic mice were used for transplantation of WT miPSCs or hypoimmunogenic miPSCs. Two million cells were injected in 60 µl saline into the right thigh muscle of the mice. Tumor growth was measured with a caliper every other day until day 30 and from day 30 to day 80 every tenth day. They were killed after development of tumors larger than 1.5 cm^3 or following an observation period of 80 days.

Derivation and characterization of miPSC-derived endothelial cells (miECs). miPSC were plated on gelatin in six-well plates and maintained in mouse iPSC media. After the cells reached 60% confluency, the differentiation was started and media was changed to RPMI-1640 containing 2% B-27 minus Insulin (both Gibco) and 5 µM CHIR-99021 (Selleckchem). On day 2, the media was changed to reduced media: RPMI-1640 containing 2% B-27 minus Insulin (both Gibco) and 2 µM CHIR-99021 (Selleckchem). From day 4 to day 7, cells were exposed to RPMI-1640 EC media, RPMI-1640 containing 2% B-27 minus Insulin plus 50 ng ml^{-1} mouse vascular endothelial growth factor (mVEGF; R&D Systems), 10 ng ml^{-1} mouse fibroblast growth factor basic (mFGFb; R&D Systems), 10 µM Y-27632 (Sigma-Aldrich) and 1 µM SB 431542 (Sigma-Aldrich). Endothelial cell clusters were visible from day 7 and cells were maintained in EGM-2 SingleQuots media (Lonza) plus 10% FCS hi (Gibco), 25 ng ml^{-1} mVEGF, 2 ng ml^{-1} mFGFb, 10 µM Y-27632 (Sigma-Aldrich) and 1 µM SB 431542. The differentiation process was completed after 21 days and undifferentiated cells detached during the differentiation process. For purification, cells went through magnetic-activated cell separation (MACS) purification according the manufacturer's protocol using anti-CD15 mAb-coated magnetic microbeads (Miltenyi) for negative selection.

The highly purified miECs in the flow-through were cultured in EGM-2 SingleQuots media plus supplements and 10% FCS hi. TrypLE was used for splitting the cells 1:3 every 3–4 days. Their phenotype was confirmed by immunofluorescence for CD31 (ab28364, Abcam) and VE-Cadherin (sc-6458, Santa Cruz Biotechnology). Briefly, cells were fixed with 4% paraformaldehyde in PBS for 15 min. Cell membranes were permeabilized with Permeabilization solution (ASB-0102, Applied StemCell), followed by Blocking solution (ASB-0103, Applied StemCell) and incubation with the primary antibodies. For visualization, cells were incubated with secondary antibody conjugated with AF488 or AF555 (Invitrogen). After nuclei staining with DAPI, images were obtained and analyzed with a Leica SP5 laser confocal microscope (Leica).

Tube formation assay was performed for miEC characterization: 2.5×10^5 miECs were stained with 5 µM CFSE and 0.1 µg ml^{-1} Hoechst (both Thermo Fisher) for 10 min at room temperature and plated on 10 mg ml^{-1} undiluted Matrigel (356231, Corning) in 24-well plates. After 48 h, tube formations were visualized by immunofluorescence. PCR was performed as described above. The following primers were used: VE-Cadherin forward: 5′-GGATGCAGAGGCTCACAGAG-3′, reverse: 5′-CTGGCGGTTCACGTTGGACT-3′.

Derivation and characterization of miPSC-derived smooth muscle cells (miSMCs). The resuspended miPSCs were cultivated on six-well, 0.1% gelatin-coated plastic petri dishes (Falcon, Becton–Dickinson) at 2×10^6 cells per well at 37 °C, 5% CO_2 in 2 ml of differentiation medium with the presence of 10 µM all-trans-retinoic acid. The differentiation medium was made of DMEM, 15% FCS, 2 mM L-glutamine, 1 mM methyl thioglycolate (MTG) (Sigma-Aldrich), 1% non-essential amino acids and pen-strep. The culture was continued for 10 days with daily media changes. Starting from the 11th day, the differentiation medium was replaced by serum-free culture medium, which was composed of knock-out DMEM, 15% knock-out serum replacement, 2 mM L-glutamine, 1 mM MTG, 1% non-essential amino acids and pen-strep. The cultures were continued for another 10 days with daily change of the serum-free medium. For purification, cells were enriched according the manufacturer's protocol using anti-CD15 mAb-coated magnetic microbeads (Miltenyi) for negative selection. The flow-through containing enriched miSMCs were cultured in RMPI-1640 Glutamax plus 20% FCS hi and 1% pen-strep (all Gibco). Their phenotype was confirmed by immunofluorescence and PCR for both Sma and Sm22.

Immunofluorescence staining was performed as described above. Primary antibodies were used against smooth muscle actin (ab21027, Abcam) and sm22 (ab14106, Abcam), followed by the corresponding secondary antibody conjugated with AF488 or AF555 (Invitrogen).

PCR was performed as described above. The following primers were used: SMA forward: 5′-CGGCTTCGCTGGTGATGAT-3′, reverse: 5′-CATTCCAACCATTACTCCCTGAT-3′; SM22 forward: 5′-AACAGCCTGTACCCTGATGG-3′, reverse: 5′-CGGTAGTGCCCATCATTCTT-3′.

Derivation and characterization of miPSC-derived cardiomyocytes (miCMs). Before differentiation, miPSCs were passaged two times on gelatin-coated flasks to remove the feeder cells. At day 0, differentiation was started with 80,000 cells per ml in IMEM/Ham's F12 (3/1, both Corning) +0.5% N2-Supplement, 1% B27 retinoic acid, 0.05% BSA, 1% pen-strep, 1% glutamine (Gibco), 5 mg ml^{-1} ascorbic acid and 40 ng ml^{-1} MTG (both Sigma-Aldrich) for 2 days in uncoated 10 cm plates. At day 2, cells were transferred in IMEM/Ham's F12 (3/1, both Corning) with 0.5% N2-Supplement, 1% B27 retinoic acid, 0.05% BSA, 1% pen-strep, 1% glutamine (all Gibco), 5 mg ml^{-1} ascorbic acid and 40 ng ml^{-1} MTG (Sigma-Aldrich) for 2 days in uncoated 10 cm plates. On day 4, cells were plated in gelatin-coated six-well plates in SP34 media containing 1% glutamine, 50 µg ml^{-1} ascorbic acid, 5 ng ml^{-1} VEGF, 500 µg ml^{-1} hFGFb and 25 ng ml^{-1} hFGF10 (R&D Systems). Media was changed on day 7 to SP34 media containing 1% glutamine and 50 µg ml^{-1} ascorbic acid and was changed every other day. Beating of cells started around days 11–14 and demonstrated their function.

For enrichment, cells separated by MACS according the manufacturer's protocol using anti-CD15 mAb-coated magnetic microbeads (Miltenyi) for negative selection. The flow-through containing enriched miCMs were replated and used for different assays.

Immunofluorescence staining was performed as described above to confirm their phenotype. Primary antibodies were used against α-sarcomeric actinin (EA-53, Abcam) or troponin I (ab47003, Abcam) followed by the corresponding secondary antibody conjugated with AF488 or AF555 (Invitrogen).

PCR for Gata4 forward: 5′-CTGTCATCTCACTATGGGCA-3′, reverse: 5′-CCAAGTCCGAGCAGGAATTT-3′ and Mhy6 forward: 5′-ATCATTCCCAACGAGCGAAAG-3′, reverse: 5′-AAGTCCCCATAGAGAATGCGG-3′ was performed as described above.

Flow cytometry analysis. For the detection of MHC class I and II surface molecules on miPSCs, miECs, miSMCs and miCMs, cells were plated on gelatin-coated six-well plates in medium containing 100 ng ml^{-1} of IFN-γ. After collection, cells were labeled with antibodies. For MHC class I: PerCP-eFlour710-labeled anti-MHC class I antibody (clone AF6-88.5.5.3, eBioscience) or PerCP-eFlour710-labeled mouse IgG2b isotype-matched control antibody (clone eB149/10H5, eBioscience). The anti-MHC class I antibody reacts with the $H\text{-}2K^b$ MHC class I alloantigen. For MHC class II: PerCP-eFlour710-labeled anti-MHC class II antibody (clone M5/114.15.2, eBioscience) or PerCP-eFlour710-labeled mouse IgG2a isotype-matched control antibody (clone eBM2a, eBioscience). The MHC class II antibody reacts with the mouse MHC class II, both I-A and I-E subregion-encoded glycoproteins. Cd47: Alexa Fluor 647-labeled anti-mouse Cd47 antibody (clone miap301, BD Biosciences) or Alexa Fluor 647-labeled mouse IgG2a isotype-matched control antibody (clone R35-95, BD Biosciences). The anti-Cd47 antibody specifically binds to the extracellular domain of mouse Cd47, also known as Integrin-Associated Protein. Cells were analyzed by flow cytometry (BD Bioscience) and results were expressed as fold change to isotype-matched control Ig staining.

For the assessment of purity of miPSC derivatives, antibodies against SSEA-1 (Thermo Fisher), VE-Cadherin (Sigma), SMA (Abcam) and Troponin I (Santa Cruz) were used. The miECs, miSMCs and miCMs were generated with a purity of >90%.

Elispot assays. For uni-directional Elispot assays, recipient splenocytes were isolated from spleen 5 days after cell injection and used as responder cells. Donor cells were mitomycin-treated (50 µg ml^{-1} for 30 min) and used as stimulator cells. One hundred thousand stimulator cells were incubated with 1×10^6 recipient responder splenocytes for 24 h and IFN-γ and IL-4 spot frequencies were enumerated using an Elispot plate reader.

Donor-specific antibodies. Sera from recipient mice were de-complemented by heating to 56 °C for 30 min. Equal amounts of sera and cell suspensions (5×10^6 ml) were incubated for 45 min at 4 °C. Cells were labeled with FITC-conjugated goat anti-mouse IgM (Sigma-Aldrich) and analyzed by flow cytometry (BD Bioscience).

Mouse NK cell Elispot assays in vitro. NK cells were isolated from fresh BALB/c spleen 18 h after poly I:C injection (150 ng poly I:C in 200 µl sterile saline, intraperitoneally, Sigma-Aldrich). After red cell lysis, cells were purified by anti-CD49b mAb-coated magnetic bead-sorting and were used as responder cells. This cell population was >99% CD3- and contains NK cells (>90%) and other cells including myeloid cells (<10%). Using the Elispot principle, NK cells were

co-cultured with *B2m*$^{-/-}$*Ciita*$^{-/-}$ or *B2m*$^{-/-}$*Ciita*$^{-/-}$ Cd47 tg miPSCs in the presence of IL-2 (1 ng ml^{-1}, Peprotech) and their IFN-γ release was measured. YAC-1 cells (Sigma-Aldrich) served as positive control. Mitomycin-treated (50 µg ml^{-1} for 30 min) stimulator cells were incubated with NK cells (1:1) for 24 h and IFN-γ spot frequencies were enumerated using an Elispot plate reader.

Mouse in vivo innate cytotoxicity assay. Five million WT miPSCs and 5×10^6 *B2m*$^{-/-}$*Ciita*$^{-/-}$ miPSCs or 5×10^6 *B2m*$^{-/-}$*Ciita*$^{-/-}$ Cd47 tg miPSCs were mixed and stained with 5 µM CFSE. Cells in saline with IL-2 (1 ng ml^{-1}, Peprotech) were injected intraperitoneally into syngeneic C57BL/6 mice. After 48 h, cells were collected from the abdomen and stained with PerCP-eFlour710 labeled anti-MHC class I mAb for 45 min at 4 °C. The CFSE-positive and MHC class I-negative population was analyzed by flow cytometry (BD Bioscience) and compared between the WT and the engineered miPSC group. The assay was performed with miPSCs, miECs, miSMCs and miCMs. Some animals were pretreated with clodronate (200 µl intraperitoneally 3 days before the experiment; Liposoma) to eliminate macrophages and make the assay more specific for NK cells. Some animals were pretreated with in vivo Cd47-blocking antibody (BE0270, 100 µg intraperitoneally, 7 days and 3 days before the experiment; BioXCell) to eliminate Cd47.

NK cell stimulatory ligands. For the detection of NK cell stimulatory ligands on miPSCs, miECs, miSMCs and miCMs, cells were blocked with mouse FcR blocking reagent (Miltenyi) according to manufacturer's protocol. WT cells, *B2m*$^{-/-}$*Ciita*$^{-/-}$ cells and *B2m*$^{-/-}$*Ciita*$^{-/-}$ Cd47 tg cells were then incubated with the recombinant mouse NKp46 or NKG2D human Fc chimera protein or the recombinant control IgG1 Fc protein (R&D systems) for 45 min at 4 °C. FITC-conjugated anti-human IgG1 antibody (Invitrogen) served as secondary antibody. YAC-1 cells were used as positive control. Data analysis was carried out using flow cytometry (BD Bioscience) and FlowJo software, and results were expressed as fold change to the isotype-matched control Fc fusion protein.

Survival analysis of differentiated derivatives using BLI. For BLI, D-luciferin firefly potassium salt (375 mg kg^{-1}; Biosynth) was dissolved in PBS (pH 7.4) (Gibco, Invitrogen) and was injected intraperitoneally (250 µl per mouse) into anesthetized mice. Animals were imaged using the IVIS 200 system (Xenogen). Region of interest (ROI) bioluminescence was quantified in units of maximum photons per second per centimeter square per steradian (p s^{-1} cm^{-2} sr^{-1}). The maximum signal from an ROI was measured using Living Image software (MediaCybernetics). Mice were monitored on day 0, day 1 and every other day until day 30 and every 10 days afterwards.

Matrigel plugs: cell morphology for miECs, miSMCs or miCMs. Eight hundred thousand *B2m*$^{-/-}$*Ciita*$^{-/-}$ Cd47 tg miECs, miSMCs or miCMs in 1:1 diluted Matrigel (Corning) were injected into allogeneic BALB/c mice. Matrigel plugs were recovered after 1, 2, 3, 4, 5, 6 and 8 weeks and fixed in 4% paraformaldehyde in PBS with 1% glutaraldehyde for 24 h. Samples were dehydrated, embedded in paraffin and cut into sections of 5 µm thickness. For histopathology, sections were stained with hematoxylin and eosin (Carl Roth) and images taken with an inverted light microscope. Origin of cells was demonstrated with immunofluorescence staining. Sections were rehydrated, and underwent antigen retrieval and blocking. Samples were incubated with antibodies against luciferase (ab21176), SMA (ab21027, Abcam), VE-Cadherin (SC-6458) or α-sarcomeric actinin (EA-53, Abcam) and a corresponding secondary antibody conjugated with AF488 or AF555 (Invitrogen). Cell nuclei were counterstained with DAPI and images taken with a Leica SP5 laser confocal microscope (Leica).

For co-staining experiments of miECs and immune cells, primary antibodies were used against VE-Cadherin (SC-6458, Sigma) and CD3 (ab16669, Abcam), followed by the corresponding secondary antibody conjugated with AF488 or AF555 (Invitrogen).

Generation of human iPSCs (hiPSCs). The Human Episomal iPSC Line was derived from CD34$^+$ cord blood using a three-plasmid, seven-factor (SOKMNLT; SOX2, OCT4 (POU5F1), KLF4, MYC, NANOG, LIN28 and SV40L T antigen) EBNA-based episomal system by Thermo Scientific. This cell line has been shown to be free of all reprogramming genes. These hiPSCs have a normal XX karyotype and endogenous expression of pluripotent markers including Oct4, SOX2 and NANOG (as shown by RT–PCR) and OCT4, SSEA4, TRA-1-60 and TRA-1-81 (as shown by immunofluorescence).

Gene editing of hiPSC. hiPSC underwent two gene-modification steps. In the first step, CRISPR technology was used for a combined targeting of the coding sequence of human *B2M* gene with the CRISPR sequence 5′- CGTGAGTAAACCTGAATCTT-3′ and the coding sequence of human *CIITA* gene with the CRISPR sequence 5′-GATATTGGCATAAGCCTCCC-3′. Linearized CRISPR sequence with T7 promoter were used to synthesize gRNA as per the kit's instructions (MEGAshortscript T7 Transcription Kit, Thermo Fisher). The obtained in vitro transcription (IVT) gRNA was then purified via the MEGAclear Transcription Clean-Up Kit. For IVT gRNA delivery, cells were electroporated with 300 ng IVT gRNA using a Neon electroporation system and the conditions 1,200 V, 30 ms, 1 pulse into hiPSC stably expressing Cas9. After electroporation, edited hiPSC were expanded for single cell seeding: hiPSC cultures were dissociated into single cells using TrypLE Express (Gibco) and stained with Alexa Fluor 488-conjugated anti-TRA-160 mAb and propidium iodide. A FACSAria II cell sorter (BD Biosciences) was used for the sorting and doublets and debris were excluded from seeding by selective gating on forward and side light scatter properties. Viable pluripotent cells were selected on the absence of propidium iodide and presence of Tra1-60 staining. Single cells were then expanded into full-size colonies, after which the colonies were tested for CRISPR editing by sequencing. CRISPR-mediated cleavage was assessed using the GeneArt Genomic Cleavage Detection Kit (Thermo Fisher) for testing of the initial edited pools. For screening of the isolated clones, genomic DNA was isolated from 1×10^6 hiPSCs and the *B2M* and *CIITA* genomic DNA regions were PCR amplified using AmpliTaq Gold 360 Master Mix and the primer sets forward: 5′-TGGGGCCAAATCATGTAGACTC -3′ and reverse: 5′-TCAGTGGGGGTGAATTCAGTGT-3′ for *B2M* as well as forward: 5′-CTTAACAGCGATGCTGACCCC-3′ and reverse: 5′-TGGCCTCCATCTCCCCTCTCTT-3′ for *CIITA*. For TIDE analysis, the obtained PCR product was cleaned up (PureLink PCR Purification Kit, Thermo Fisher) and Sanger sequencing was performed for the prediction of indel frequency. After the confirmation of *B2M* and *CIITA* disruption, cells were further characterized through karyotype analysis and the TaqMan hiPSC Scorecard Panel (Thermo Fisher). The hiPSCs were found to be pluripotent and maintained a normal (46,XX) karyotype during the genome editing process.

In the second step, the CD47 cDNA was synthesized and the DNA was cloned into a lentiviral plasmid with an EFS promotor and puromycin resistance cassette. Cells were transduced with lentiviral stocks and 8 µg ml^{-1} of Polybrene (Thermo Fisher). Media was changed daily after transduction. Three days after transduction, cells were expanded and selected with 0.5 µg ml^{-1} of puromycin. After 5 days of antibiotic selection, antibiotic-resistant colonies emerged and were further expanded to generate stable pools. The expression of CD47 transcripts was confirmed by quantitative PCR. Pluripotency assay (TaqMan hPSC Scorecard Panel, Thermo Fisher) and karyotyping was performed again to verify the pluripotent status of the cells.

Teratoma assays to study iPSC survival in vivo. Six to eight week-old immunodeficient SCID-beige mice were used for transplantation of WT hiPSC or *B2M*$^{-/-}$*CIITA*$^{-/-}$ CD47 tg hiPSCs. Here 1×10^7cells were resuspended in 100 µl saline solution and injected into the right thigh muscle of the mice. Teratomas were recovered, fixed in 4% paraformaldehyde, dehydrated, embedded in paraffin and cut into sections of 5 µm thickness. For histopathology, sections were rehydrated and stained with hematoxylin and eosin. Images were taken with an inverted light microscope. For immunofluorescence, slides underwent heat-induced antigen retrieval in a steamer with Dako antigen-retrieval solution (Dako), followed by antigen blocking with Image-iT FX signal enhancer solution (Invitrogen). Tissue sections were incubated with a primary antibody against brachyury (Ab20680, Abcam), followed by a goat anti-rabbit IgG secondary antibody conjugated with Alexa Fluor 555 (Invitrogen). Subsequently, sections were incubated with primary antibodies against cytokeratin 8 (EP1628Y, Abcam) and GFAP (GA5, Cell Signaling) conjugated with AF488 or AF647, respectively. DAPI was used to counterstain cell nuclei and images were acquired with a Leica SP5 laser confocal microscope (Leica).

Pluripotency analysis by RT–PCR and immunofluorescence. hiPSCs were plated in confocal dishes (MatTek) for immunofluorescence analysis 48 h after plating using the hiPSC Characterization Kit (Applied Stem Cell). Briefly, cells were fixed, permeabilized and stained overnight at 4 °C with the primary antibodies for OCT4, SOX2, SSEA4, TRA-1-60 and TRA-1-81 (Applied Stem Cell). After several washes, the cells were incubated with a secondary antibody and DNA staining solution. Alkaline phosphatase activity assay was performed (Applied Stem Cell). Stained cells were imaged using a fluorescent microscope.

For RT–PCR, RNA was extracted using the RNeasy Plus Mini Kit (Qiagen). Genomic DNA contamination was removed using the gDNA spin column. cDNA was generated using Applied Biosystems High-Capacity cDNA Reverse Transcription Kit. Gene-specific primers of the hiPSC Characterization Kit (Applied Stem Cell) were used to amplify target sequences Actin was used as housekeeping gene. PCR reactions were performed on Mastercycler nexus (Eppendorf) and visualized on 2% agarose gels.

Humanized mice. Humanized NSG-SGM3 mice (18–30 weeks) were purchased from Jackson Laboratories. Human CD34$^+$ hematopoietic stem cell-engrafted NSG-SGM3 mice develop multi-lineage human immune cells, and demonstrate a functional human immune system displaying T cell-dependent immune responses with no donor cell immune reactivity towards the host. Animals were randomly assigned to experimental groups. The percentage of CD3$^+$ cells among the human CD45$^+$ cell population was assessed in every animal and CD3 percentages were never significantly different between WT and *B2M*$^{-/-}$*CIITA*$^{-/-}$ CD47 tg groups (Supplementary Fig. 13a). The number of animals per

experimental group is presented in each figure. All humanized NSG-SGM3 mice were HLA-A typed and the number of mismatches to the cell graft calculated (Supplementary Fig. 13b). In the Elispot assays with hiPSCs, there were 1.6 ± 0.5 and 1.7 ± 0.5 ($P = 0.61$), with hiCMs 1.3 ± 0.6 and 1.3 ± 0.6 ($P = 1$) mismatches for WT and *B2M*$^{-/-}$*CIITA*$^{-/-}$ CD47 tg, respectively, and in the hiEC groups there were always two mismatches. The mismatches for the BLI experiments are shown in Supplementary Fig. 10j.

All BLT mice were approved by the University of North Carolina at Chapel Hill Institutional Animal Care and Use Committee and were generated with the same human tissue using NSG mice (NOD.Cg-*Prkdc*^{scid} *Il2rg*^{tm1Wjl}/SzJ, Jackson Laboratories) and there were five out of six HLA class I and 4 out of 4 class II mismatches to the transplanted hiPSCs or derivatives. The percentage of CD3$^+$ cells among the human CD45$^+$ cell population was never significantly different between WT and *B2M*$^{-/-}$*CIITA*$^{-/-}$ CD47 tg groups (Supplementary Fig. 13c). The percentage of CD3$^+$ cells among the human CD45$^+$ cell population was typically in the 15–65% range.

Human iPSC differentiation into hiECs. hiPSC were plated on diluted Matrigel (356231, Corning) in six-well plates and maintained in Essential 8 Flex media (Thermo Fisher). The differentiation was started at 60% confluency and media was changed to RPMI-1640 containing 2% B-27 minus insulin (both Gibco) and 5 µM CHIR-99021 (Selleckchem). On day 2, the media was changed to reduced media: RPMI-1640 containing 2% B-27 minus insulin (Gibco) and 2 µM CHIR-99021 (Selleckchem). From day 4 to 7, cells were exposed to RPMI-1640 EC media, RPMI-1640 containing 2% B-27 minus insulin plus 50 ng ml^{-1} human vascular endothelial growth factor (VEGF; R&D Systems), 10 ng ml^{-1} human fibroblast growth factor basic (FGFb; R&D Systems), 10 µM Y-27632 (Sigma-Aldrich), and 1 µM SB 431542 (Sigma-Aldrich). Endothelial cell clusters were visible from day 7 and cells were maintained in EGM-2 SingleQuots media (Lonza) plus 10% FCS hi (Gibco), 25 ng ml^{-1} VEGF, 2 ng ml^{-1} FGFb, 10 µM Y-27632 (Sigma-Aldrich) and 1 µM SB 431542 (Sigma-Aldrich). The differentiation process was completed after 14 days und undifferentiated cells detached during the differentiation process. For purification, cells were treated with 20 µM PluriSln-1 (StemCell Technologies) for 48 h. The highly purified ECs were cultured in EGM-2 SingleQuots media (Lonza) plus supplements and 10% FCS hi (Gibco). TrypLE Express was used for passaging the cells 1:3 every 3–4 days.

Immunofluorescence staining was performed as described above to confirm their phenotype. Primary antibodies were used against CD31 (ab28364, Abcam) and VE-Cadherin (sc-6458, Santa Cruz Biotechnology), followed by the corresponding secondary antibody conjugated with AF488 or AF555 (Invitrogen). Cell nuclei were stained with DAPI. Imaging was performed using a Leica SP5 laser confocal microscope (Leica).

PCR for VE-Cadherin (forward: 5′-AAGATGCAGAGGCTCATG-3′, reverse: 5′-CATGAGCCTCTGCATCTT-3′) was performed as described above.

Human iPSC differentiation into hiCMs. hiPSCs were plated on diluted Matrigel (356231, Corning) in six-well plates and maintained in Essential 8 Flex media (Thermo Fisher). Differentiation was started at 90% confluency, and media was changed to 5 ml of RPMI-1640 containing 2% B-27 minus Insulin (Gibco) and 6 µM CHIR-99021 (Selleckchem). After 2 days, media was changed to RPMI-1640 containing 2% B-27 minus insulin without CHIR. On day 3, 5 µl IWR1 was added to the media for two further days. At day 5, the media was changed back to RPMI-1640 containing 2% B-27 minus insulin medium and left for 48 h. At day 7, media was changed to RPMI-1640 containing B27 plus insulin (Gibco) and replaced every 3 days thereafter with the same media. Spontaneous beating of cardiomyocytes was first visible around day 10. Purification of cardiomyocytes was performed on day 10 post-differentiation. Briefly, media was changed to low glucose media and maintained for 3 days. At day 13, media was changed back to RPMI-1640 containing B27 plus insulin. This procedure was repeated on day 14.

Immunofluorescence staining was performed as described above to confirm their phenotype. Primary antibodies were used against α-sarcomeric actinin (EA-53, Abcam) and troponin I (ab47003, Abcam), followed by the corresponding secondary antibody conjugated with AF488 or AF555 (Invitrogen). Cell nuclei were stained with DAPI. Imaging was performed using a Leica SP5 laser confocal microscope (Leica).

PCR for troponin (cTNT, forward: 5′-GAGGCACCAAGTTGGGCATGAACG A-3′, reverse: 5′-GGCAGCGGAAGAGGATGCTGAA′) was performed as described above.

Flow cytometry analysis. Human iPSCs, iCMs and iECs were plated in six-well plates in medium containing 100 ng ml^{-1} of IFN-γ. Cells were harvested and labeled with antibodies. APC-conjugated anti-HLA-A,B,C antibody (clone G46_2.6,BD Biosciences) or APC-conjugated IgG1 isotype-matched control antibody (clone MOPC-21,BD Biosciences). Alexa-flour647-labeled anti-HLA-DR,DP,DQ antibody (clone Tu3a, BD Biosciences) or Alexa-flour647-labeled IgG2a isotype-matched control antibody (clone G155-178, BD Biosciences). PerCP-Cy5-conjugated anti-CD47 (clone B6H12, BD Biosciences) or PerCP-Cy5-conjugated IgG1 isotype-matched control antibody (clone MOPC-21, BD Biosciences). Results were expressed as fold change to isotype-matched control Ig staining.

For the assessment of purity of hiPSC derivatives, antibodies against TRA-1-60 (Thermo Fisher), VE-Cadherin (Santa Cruz) and Troponin I (Santa Cruz) were used. The hiECs and hiCMs were generated with a purity of >95%.

Human NK cell Elispot assays. Human NK cells were co-cultured with *B2M*$^{-/-}$*CIITA*$^{-/-}$ or *B2M*$^{-/-}$*CIITA*$^{-/-}$ CD47 tg hiPSC and their IFN-γ release was measured. Human NK cells were purchased from StemCell Technologies and were >99% CD3- and 95% CD56$^+$. Flow cytometry revealed >95% NK cells and <5% other cells including myeloid cells. Donor cells were mitomycin-treated and used as stimulator cells. K562 cells (Sigma-Aldrich) served as positive control. Stimulator cells were incubated with NK cells (1:1) in RPMI-1640 containing 1% pen-strep and 1 ng ml^{-1} human IL-2 (Peprotech) for 24 h and IFN-γ spot frequencies were enumerated using an Elispot plate reader.

T cell Elispot using humanized mice. For uni-directional Elispot assays, recipient splenocytes were isolated from humanized mice 5 days after cell injection and used as responder cells. Cells were incubated for 24 h in vitro with 1 µg ml^{-1} anti-CD3 and 1 µg ml^{-1} anti-CD28 before plated for Elispot Assay. Donor cells were mitomycin-treated (50 µg ml^{-1} for 30 min) and used as stimulator cells. One hundred thousand stimulator cells were incubated with 1×10^6 recipient responder splenocytes for 48 h and IFN-γ and IL-5 spot frequencies were enumerated using an Elispot plate reader.

DSA. Sera from recipient mice were de-complemented by heating to 56 °C for 30 min. Equal amounts of sera and cell suspensions (5×10^6 per ml) were incubated for 45 min at 4 °C. Cells were labeled with FITC-conjugated goat anti-human IgM (BD Bioscience) and analyzed by flow cytometry (BD Bioscience).

Matrigel plugs: cell morphology. One million *B2M*$^{-/-}$*CIITA*$^{-/-}$ CD47 tg hiECs or hiCMs in 1:1 pro survival scaffold, consisting of 50% (vol/vol) Matrigel (Corning), 100 µM ZVAD (Millipore), 50 nM Bcl-Xl BH4 (Millipore), 200 nM cyclosporine A (Sigma-Aldrich), 100 ng ml^{-1} IGF-1 (Peprotech) and 50 µM Pinacidil (Sigma-Aldrich) were injected into humanized NSG-SGM3 mice. Matrigel plugs were recovered after 2, 4, 6 and 8 weeks, fixed in 4% paraformaldehyde in PBS with 1% glutaraldehyde, dehydrated and embedded in paraffin. Sections of 5 µm thickness were cut. For immunofluorescence, sections were rehydrated and underwent antigen retrieval, followed by antigen blocking. After incubation with a primary antibody against luciferase (ab21176), VE-Cadherin (SC-6458) or α-sarcomeric actinin (EA-53, Abcam), sections were incubated with a corresponding secondary antibody conjugated with AF488 or AF555 (Invitrogen). DAPI was used to counterstain cell nuclei and images were obtained with a Leica SP5 laser confocal microscope (Leica).

BLI. For BLI, D-luciferin firefly potassium salt (375 mg kg^{-1}) (Biosynth) dissolved in sterile PBS (pH 7.4) (Gibco, Invitrogen) was injected intraperitoneally (250 µl per mouse) into anesthetized mice. Animals were imaged using the ami HT (Spectral Instruments Imaging) ROI bioluminescence was quantified in units of maximum photons per second per centimeter square per steradian (p s^{-1} cm^{-2} sr^{-1}). The maximum signal from an ROI was measured using Living Image software (MediaCybernetics). Humanized mice were injected with 5×10^5 or 1×10^6 cells in pro survival scaffold as described above. Mice were monitored on day 0, day 1 and every 4 days until cells were rejected or up to 50 days.

In vitro NK cell killing. Mouse NK cells were isolated from fresh BALB/c or C57BL/6 spleens 18 h after poly I:C injection (100 µg intraperitoneally). After red cell lysis, NK cells were purified with MagniSort Mouse NK cell Enrichment Kit (Invitrogen), followed by CD49b MACS-sorting (Miltenyi). This cell population was highly selected for NK cells with a purity of >9%. Human NK cells from PBMCs were purchased from StemCell Technologies containing >99% NK cells.

NK cell killing assays were performed on the XCelligence SP platform (ACEA BioSciences). 96-well E-plates (ACEA BioSciences) were coated with collagen (Sigma-Aldrich) and 4×10^5 WT, *B2m*$^{-/-}$*Ciita*$^{-/-}$, or *B2m*$^{-/-}$*Ciita*$^{-/-}$ Cd47 tg miECs or WT, *B2M*$^{-/-}$*CIITA*$^{-/-}$ or *B2M*$^{-/-}$*CIITA*$^{-/-}$ CD47 tg hiECs were plated in 100 µl cell-specific media containing 1 ng ml^{-1} mouse or human IL-2 (Peprotech). After the Cell Index value reached 0.7, NK cells were added with an effector cell / target cell (E/T) ratio of 0.5/1, 0.8/1 or 1/1. As a negative control, cell treated with 2% Triton X100 was used. Some wells were pretreated with mouse Cd47 or human CD47-blocking antibody (BioXCell) with 10 µg ml^{-1} media for 2 h. Data were standardized and analyzed with the RTCA software (ACEA).

NK cell stimulatory ligands. For the detection of NKG2D, NKp80, NKp46, NKp44 and NKp30 on hiPSCs, hiECs and hiCMs, cells were plated on gelatin-coated six-well plates. K562 cells were plated in six-well plates as suspension cells. After harvesting, cells were blocked with human FcR blocking reagent (Miltenyi) according to manufacturer's protocol. Cells were labeled with recombinant human NKG2D, Nkp80, Nkp46, Nkp44 or Nkp30 Fc chimera proteins or the recombinant control IgG1 Fc protein (all R&D Systems) for 45 min at 4 °C, followed by the secondary antibody IgG1 conjugated with FITC (Invitrogen). Data analysis was

carried out by Flow Cytometry (BD Bioscience) and results were expressed as fold change to isotype control.

Statistics. All data are expressed as mean ± s.d. or in box blot graphs showing the median and the minimum to maximum range. Intergroup differences were appropriately assessed by either an unpaired Student's *t*-test or a one-way ANOVA with Bonferroni's post-hoc test. Further information on experimental design and reagents is available in the Nature Research Reporting Summary linked to this article.

Reporting Summary. Further information on research design is available in the Nature Research Reporting Summary linked to this article.

Data availability

All data supporting the findings of this study are available in the paper and its Supplementary Information files.

nature research

Corresponding author(s): Sonja Schrepfer

☐ Initial submission ☐ Revised version ☒ Final submission

Life Sciences Reporting Summary

Nature Research wishes to improve the reproducibility of the work that we publish. This form is intended for publication with all accepted life science papers and provides structure for consistency and transparency in reporting. Every life science submission will use this form; some list items might not apply to an individual manuscript, but all fields must be completed for clarity.

For further information on the points included in this form, see Reporting Life Sciences Research. For further information on Nature Research policies, including our data availability policy, see Authors & Referees and the Editorial Policy Checklist.

Experimental design

1. Sample size

Describe how sample size was determined.

The sample size for the in vivo studies to achieve statistical significance was not calculated before the studies as the survival of the hypo-cells in the different models was unknown prior. It was reasoned that 5-10 mice per group in individual experiments would indicate valid efficacy. Sample sizes in vitro were determined by three or more samples for comparisons between one or multiple groups, followed by the statistical test. Again, the sample size to achieve statistical significance was not calculated before the studies for the reason described above.

2. Data exclusions

Describe any data exclusions.

No pre-established data exclusion method was used.

3. Replication

Describe whether the experimental findings were reliably reproduced.

The experimental findings can be reliably reproduced. Some key data generated by one co-author were repeated by other co-authors.

4. Randomization

Describe how samples/organisms/participants were allocated into experimental groups.

All samples were number coded until the readout was finalized. The numbers were assigned prior to the experiment and determined the group/ treatment/ condition. Animals were number coded and assigned to a group prior to the surgical procedure.

5. Blinding

Describe whether the investigators were blinded to group allocation during data collection and/or analysis.

Group allocation for cell transplantations were performed by blinded investigators. For in vivo imaging and teratoma measurement, the investigators doing the readouts (Core Facility) were not blinded, but not familiar with the experimental setup of this study. For immunofluorescent images, the animal group that each cell type belonged to was unknown at the time to the individual doing the imaging.

Note: all studies involving animals and/or human research participants must disclose whether blinding and randomization were used.

6. Statistical parameters

For all figures and tables that use statistical methods, confirm that the following items are present in relevant figure legends (or in the Methods section if additional space is needed).

n/a	Confirmed
☐	☒ The exact sample size (*n*) for each experimental group/condition, given as a discrete number and unit of measurement (animals, litters, cultures, etc.)
☐	☒ A description of how samples were collected, noting whether measurements were taken from distinct samples or whether the same sample was measured repeatedly
☐	☒ A statement indicating how many times each experiment was replicated
☐	☒ The statistical test(s) used and whether they are one- or two-sided (note: only common tests should be described solely by name; more complex techniques should be described in the Methods section)
☐	☒ A description of any assumptions or corrections, such as an adjustment for multiple comparisons
☐	☒ The test results (e.g. *P* values) given as exact values whenever possible and with confidence intervals noted
☐	☒ A clear description of statistics including central tendency (e.g. median, mean) and variation (e.g. standard deviation, interquartile range)
☐	☒ Clearly defined error bars

See the web collection on statistics for biologists for further resources and guidance.

Software

Policy information about availability of computer code

7. Software

Describe the software used to analyze the data in this study.	FlowJo7 was used to analyze flow cytometric data. Prism7 or Excel 2010 was used for graphing and statistical analysis. LivingImage3.1 was used for quantification of bioluminescence imaging. Elispots were enumerated by Immunospot software.

For manuscripts utilizing custom algorithms or software that are central to the paper but not yet described in the published literature, software must be made available to editors and reviewers upon request. We strongly encourage code deposition in a community repository (e.g. GitHub). *Nature Methods* guidance for providing algorithms and software for publication provides further information on this topic.

Materials and reagents

Policy information about availability of materials

8. Materials availability

Indicate whether there are restrictions on availability of unique materials or if these materials are only available for distribution by a for-profit company.	No restriction. Standard MTA needed.

9. Antibodies

Describe the antibodies used and how they were validated for use in the system under study (i.e. assay and species).

The following antibodies were used for immunostaining: brachyury (polyclonal, catalog# ab20680, Abcam), cytokeratin 8 (clone: EP1628Y, AF488, catalog#ab192467), GFAP (clone: GA5, catalog#3670, Cell Signaling), CD31 (polyclonal, catalog # ab28364, abcam), Ve-Cadherin (polyclonal, catalog# sc-6458, Santa Cruz Biotechnology), smooth muscle actin (polyclonal, catalog #ab21027, Abcam), sm22 (polyclonal, catalog #ab14106, Abcam), α-sarcomeric actinin (clone: EA-53, catalog# ab9465, Abcam), troponin I (polyclonal, catalog #ab47003, Abcam), luciferase (polyclonal, catalog #ab21176, abcam), CD3 (clone: SP7, catalog #ab16669, abcam). Following corresponding Secondary antibodies were used: donkey-anti-mouse IgG (polyclonal, AF555, catalog #A31570, Invitrogen), donkey-anti-mouse IgG (polyclonal, AF488, catalog #A21202, Invitrogen), donkey-anti-rabbit IgG (polyclonal, AF555, catalog #A31572, Invitrogen), donkey-anti-rabbit IgG (polyclonal, AF488, catalog #A21206, Invitrogen), goat-anti-rabbit IgG (polyclonal, AF555, catalog #A21430, Invitrogen), goat-anti-rabbit IgG (polyclonal, AF488, catalog #A11070, Invitrogen), goat-anti-mouse IgG (polyclonal, AF488, catalog #A11017, Invitrogen).

For Flow cytometry analysis: MHC class I (clone AF6-88.5.5.3, PerCP-eFlour710,catalog#46-5958-82, eBioscience), MHC class II (clone: M5/114.15.2, PerCP-eFlour710, catalog#46-5321-82, eBioscience) Cd47 (clone: miap301, Alexa Fluor 647, catalog #563584, BD Biosciences), TRA-160 (clone XXX,) HLA-A,B,C (clone G46_2.6, APC, catalog #562006, BD Biosciences), HLA-DR,DP,DQ (clone Tu3a, AF647, catalog #563591, BD Biosciences), CD47 (clone B6H12, PerCP-Cy5, catalog #561261, BD Biosciences), VE-Cadherin (clone F-8, catalog #SC-9989, Santa Cruz Biotechnology), smooth muscle actin (polyclonal, catalog #ab5694, Abcam) and troponin I (clone CT3, PE, catalog #sc-20025, Santa Cruz).

For NK-stimulation assays: NKG2D (catalog #1299-NK-050, R&D Systems), Nkp80 (catalog #1900-NK-050, R&D Systems), Nkp46 (catalog #1850-NK-025, R&D Systems), Nkp44 (catalog #2249-NK-050, R&D Systems), or Nkp30 (catalog #1849-NK-025, R&D Systems).

Characterization of human pluripotent stem cells were conducted using the Applied stem cell Human ES/iPS Cell Characterization Kit (ASK-3006). Mouse pluripotent stem cells were characterized by Applied stem cell Mouse ES/iPS Cell Characterization Kit (ASK-3005). For cell selection TRA-1-60 Alexa Fluor™ 488 Conjugate Kit for Live Cell Imaging (A25618, Invitrogen) was used.

10. Eukaryotic cell lines

a. State the source of each eukaryotic cell line used.

The Human Episomal iPSC Line was purchased from Thermo Fisher Scientific (Waltham, MA). Mouse iPSCs were reprogramed from C57BL/6 mice. Mouse YAC-1 and human K-562 were purchased from ATCC (Manassas, VA) and used as controls in appropriate NK cell assays. Irradiated CF1 Mouse Embryonic Fibroblasts (MEFs) were used as feeder cells for mouse iPSCs and purchased from Thermo Fisher Scientific.

b. Describe the method of cell line authentication used.

None of the cell lines used have been authenticated.

c. Report whether the cell lines were tested for mycoplasma contamination.

All cell lines were tested and negative for mycoplasma contamination using the Universal Mycoplasma test kit from ATCC.

d. If any of the cell lines used are listed in the database of commonly misidentified cell lines maintained by ICLAC, provide a scientific rationale for their use.

No commonly misidentified cell lines were used.

Animals and human research participants

Policy information about studies involving animals; when reporting animal research, follow the ARRIVE guidelines

11. Description of research animals

Provide details on animals and/or animal-derived materials used in the study.	Male C57BL/6J, BALB/cAnNCrl, SCID-beige (CBySmn.CB17-Prkdcscid/J) and NSG (NOD.Cg-Prkdc-scid IL2rg-tm1Wjl/SzJ mice 6-12 weeks of age and humanized NSG-SGM3 mice 18-30 weeks were purchased from Jackson Laboratories (Bar Harbor, Maine, USA). All mice were maintained in pathogen-free, ventilated cages with irradiated food and autoclaved water at the University of California San Francisco (UCSF) or at the University Hamburg (HH). Experimental procedures were approved by the Institutional Animal Care and Use Committee (IACUC) at UCSF or the "Amt fuer Gesundheit und Verbraucherschutz" at HH. Mice were monitored daily and euthanized by CO2 asphyxiation and cervical dislocation prior to any signs of distress. BLT mice were generated at the University of North Carolina (UNC) and were approved by the local IACUC at UNC.

Policy information about studies involving human research participants

12. Description of human research participants

Describe the covariate-relevant population characteristics of the human research participants.	The study did not involve human subjects.

nature biotechnology

SUPPLEMENTARY INFORMATION

https://doi.org/10.1038/s41587-019-0016-3

In the format provided by the authors and unedited.

Hypoimmunogenic derivatives of induced pluripotent stem cells evade immune rejection in fully immunocompetent allogeneic recipients

Tobias Deuse[1,7], Xiaomeng Hu[1,2,3,7], Alessia Gravina[1], Dong Wang[1,2], Grigol Tediashvili[1,2,3], Chandrav De[4], William O. Thayer[4], Angela Wahl[4], J. Victor Garcia[4], Hermann Reichenspurner[2,3], Mark M. Davis[5], Lewis L. Lanier[6] and Sonja Schrepfer[1]*

[1]Department of Surgery, Division of Cardiothoracic Surgery, Transplant and Stem Cell Immunobiology-Lab, University of California San Francisco, San Francisco, CA, USA. [2]Department of Cardiovascular Surgery, University Heart Center Hamburg, Hamburg, Germany. [3]Cardiovascular Research Center Hamburg and DZHK (German Center for Cardiovascular Research), Partner Site Hamburg/Kiel/Luebeck, Hamburg, Germany. [4]Division of Infectious Diseases, UNC Center for AIDS Research, University of North Carolina School of Medicine, Chapel Hill, NC, USA. [5]Howard Hughes Medical Institute, Institute for Immunity, Transplantation and Infection, and Department of Microbiology and Immunology, Stanford University School of Medicine, Stanford, CA, USA. [6]Department of Microbiology and Immunology and the Parker Institute for Cancer Immunotherapy, University of California San Francisco, San Francisco, California, USA. [7]These authors contributed equally: Tobias Deuse, Xiaomeng Hu. *e-mail: Sonja.Schrepfer@ucsf.edu

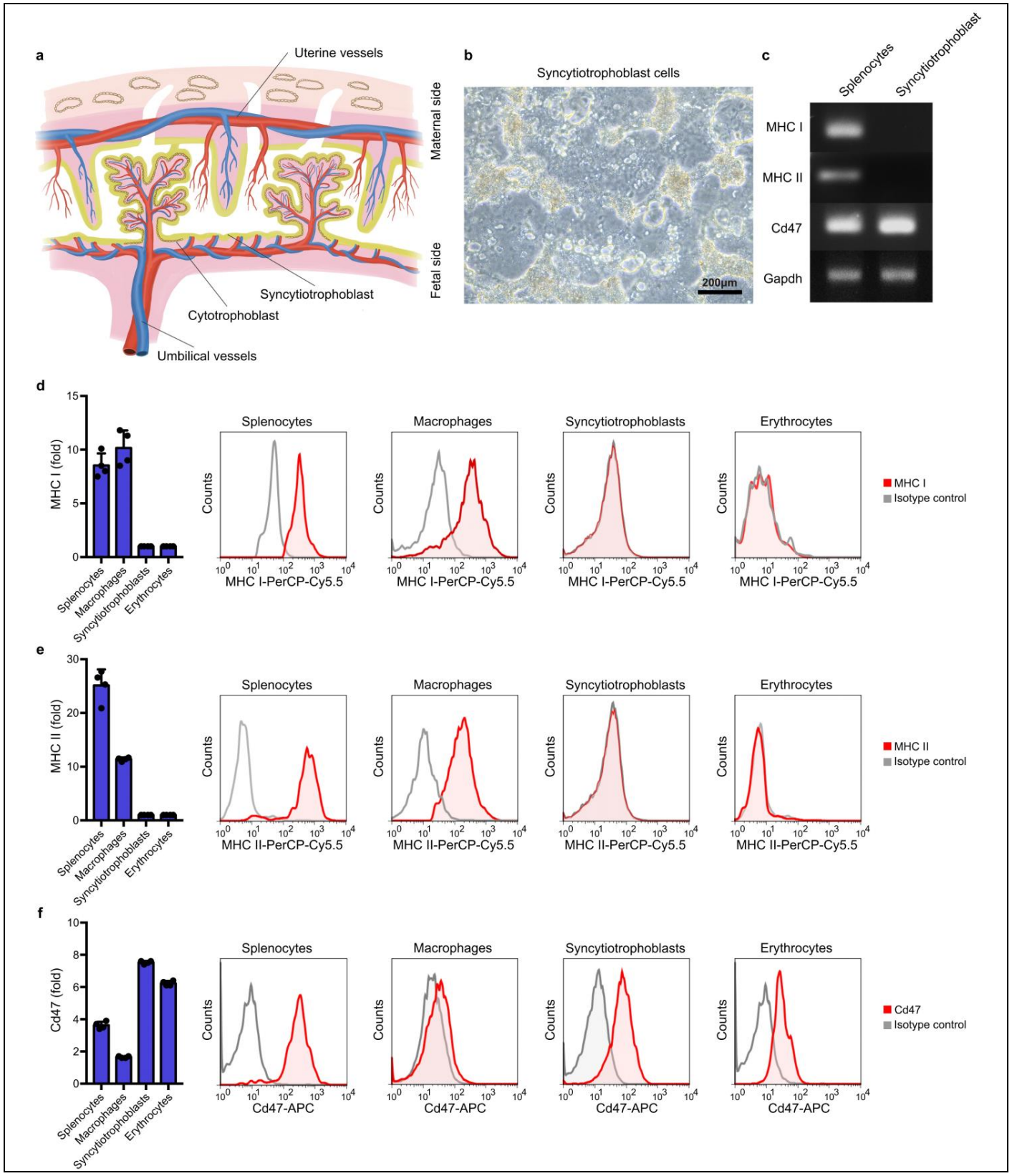
a
Uterine vessels
Maternal side
Fetal side
Syncytiotrophoblast
Cytotrophoblast
Umbilical vessels
b
Syncytiotrophoblast cells
200μm
c
Splenocytes
Syncytiotrophoblast
MHC I
MHC II
Cd47
Gapdh
d
MHC I (fold)
Splenocytes
Macrophages
Syncytiotrophoblasts
Erythrocytes
Counts
MHC I-PerCP-Cy5.5
MHC I
Isotype control
e
MHC II (fold)
MHC II-PerCP-Cy5.5
MHC II
Isotype control
f
Cd47 (fold)
Cd47-APC
Cd47
Isotype control

Supplementary Figure 1

The immune phenotype of syncytiotrophoblast cells.

a, The syncytiotrophoblast is the immediate interface between maternal blood and the fetal side of the placenta. **b**, Mouse syncytiotrophoblast cells were isolated and cultured (representative picture of two independent experiments). **c**, RT-PCR showed depleted MHC class I and II expression, but positive Cd47 expression (representative gel of three independent experiments). **d-f**, The surface expression of MHC class I (d), MHC class II (e), and Cd47 (f) was assessed by flow cytometry (mean ±s.d., 4 independent experiments per group). Representative histograms are shown.

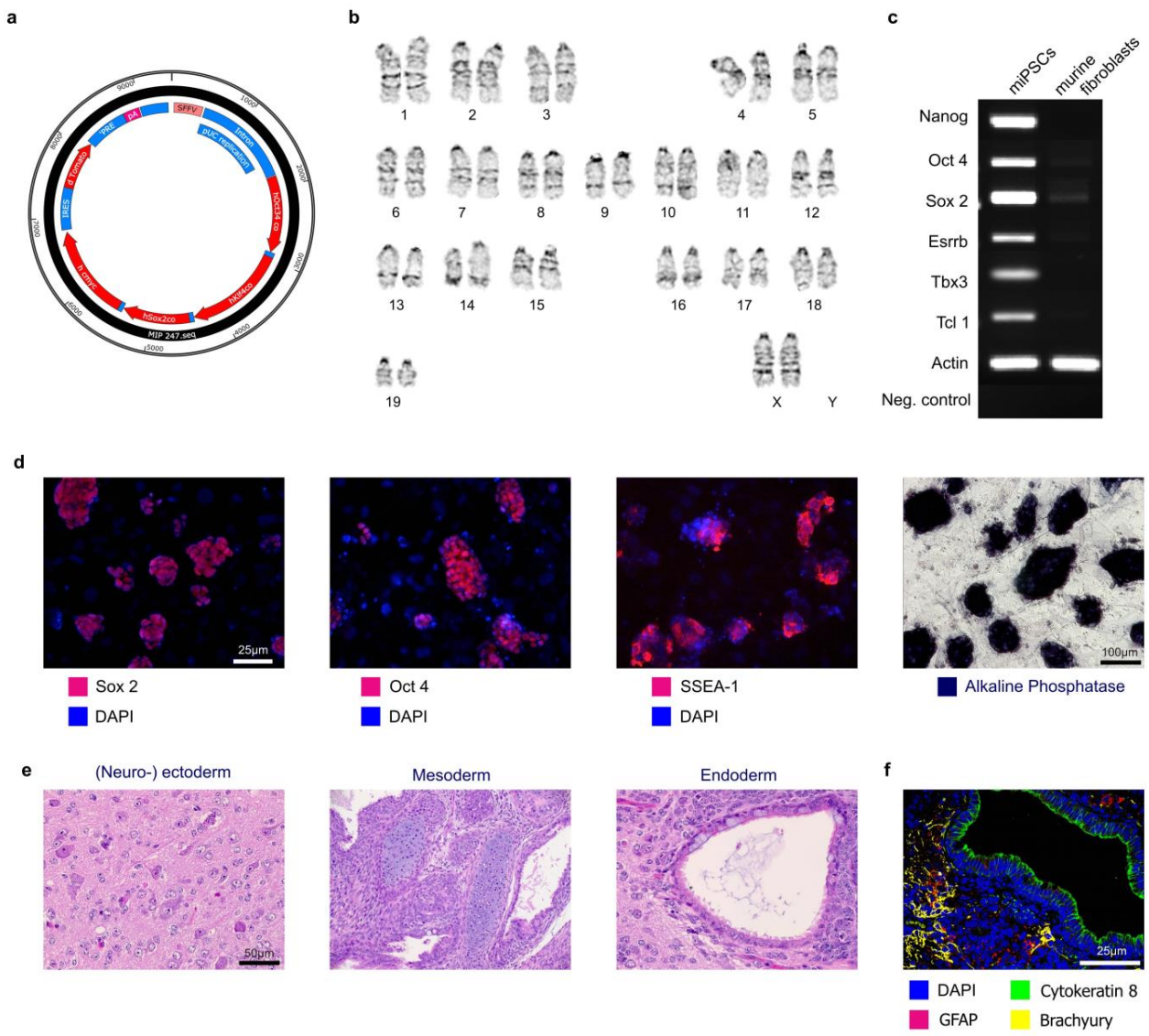

Supplementary Figure 2

The generation of miPSCs.

a, Mouse tail tip fibroblasts were re-programmed using a plasmid expressing the four re-programming factors Oct4, KLF4, Sox2, and c-Myc. **b**, The miPSCs showed a normal 40, XX mouse karyotype in one analysis. **c**, miPSCs showed the typical gene expression profile of pluripotent stem cells (representative gel of two independent experiments). **d**, In immunofluorescence, miPSC cultures were positive for Sox2, Oct4, SSEA-1, and alkaline phosphatase (representative pictures of three independent experiments). **e**, When transplanted into immunodeficient SCID-beige mice, they formed teratomas containing (neuro-) ectoderm, mesoderm, and endoderm (representative pictures of three independent experiments). **f**, Endodermal (cytokeratin 8), mesodermal (brachyury), and ectodermal (GFAP) lineages were demonstrated by confocal immunofluorescence microscopy (representative pictures of three independent experiments).

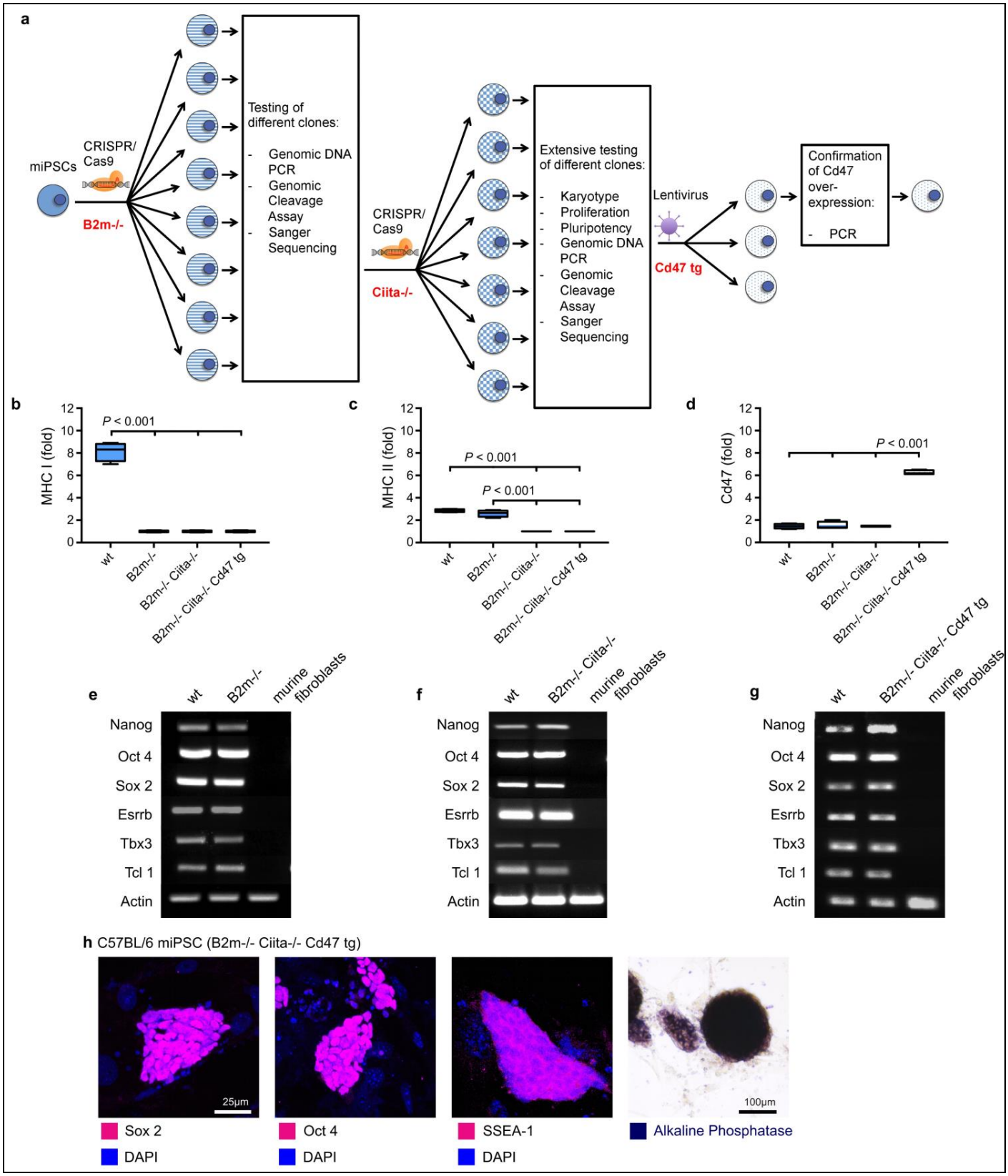
a
miPSCs
CRISPR/
Cas9
B2m-/-
Testing of
different clones:
- Genomic DNA
PCR
- Genomic
Cleavage
Assay
- Sanger
Sequencing
CRISPR/
Cas9
Ciita-/-
Extensive testing
of different clones:
- Karyotype
- Proliferation
- Pluripotency
- Genomic DNA
PCR
- Genomic
Cleavage
Assay
- Sanger
Sequencing
Lentivirus
Cd47 tg
Confirmation
of Cd47
over-
expression:
- PCR
b
MHC I (fold)
P < 0.001
wt
B2m-/-
B2m-/- Ciita-/-
B2m-/- Ciita-/- Cd47 tg
c
MHC II (fold)
P < 0.001
P < 0.001
d
Cd47 (fold)
P < 0.001
e
wt
B2m-/-
murine
fibroblasts
Nanog
Oct 4
Sox 2
Esrrb
Tbx3
Tcl 1
Actin
f
wt
B2m-/- Ciita-/-
murine
fibroblasts
g
wt
B2m-/- Ciita-/- Cd47 tg
murine
fibroblasts
h C57BL/6 miPSC (B2m-/- Ciita-/- Cd47 tg)
25µm
100µm
Sox 2
DAPI
Oct 4
DAPI
SSEA-1
DAPI
Alkaline Phosphatase

Supplementary Figure 3

Immune phenotype and pluripotency of engineered miPSCs.

a, Mouse iPSCs underwent three editing steps to disrupt *B2m*, *Ciita*, and over-express Cd47 to achieve a hypo-immunogenic phenotype. Every step included rigorous testing for quality control. **b-d**, MHC class I (b), MHC class II (c), and Cd47 expression (d) by flow cytometry is shown for each engineering step, confirming successful gene editing (box 25th to 75th percentile with median, whiskers min-max, 4 independent experiments per graph, ANOVA with Bonferroni's post-hoc test). **e-g**, During the engineering process, all edited miPSCs maintained expression of the pluripotent gene expression signature (representative gel of two independent PCR experiments). **h**, *B2m*$^{-/-}$*Ciita*$^{-/-}$ Cd47 tg miPSCs exhibited Sox2, Oct4, and SSEA-1 expression in confocal immunofluorescence stainings, as well as alkaline phosphatase in immunohistochemistry (representative pictures of three independent experiments).

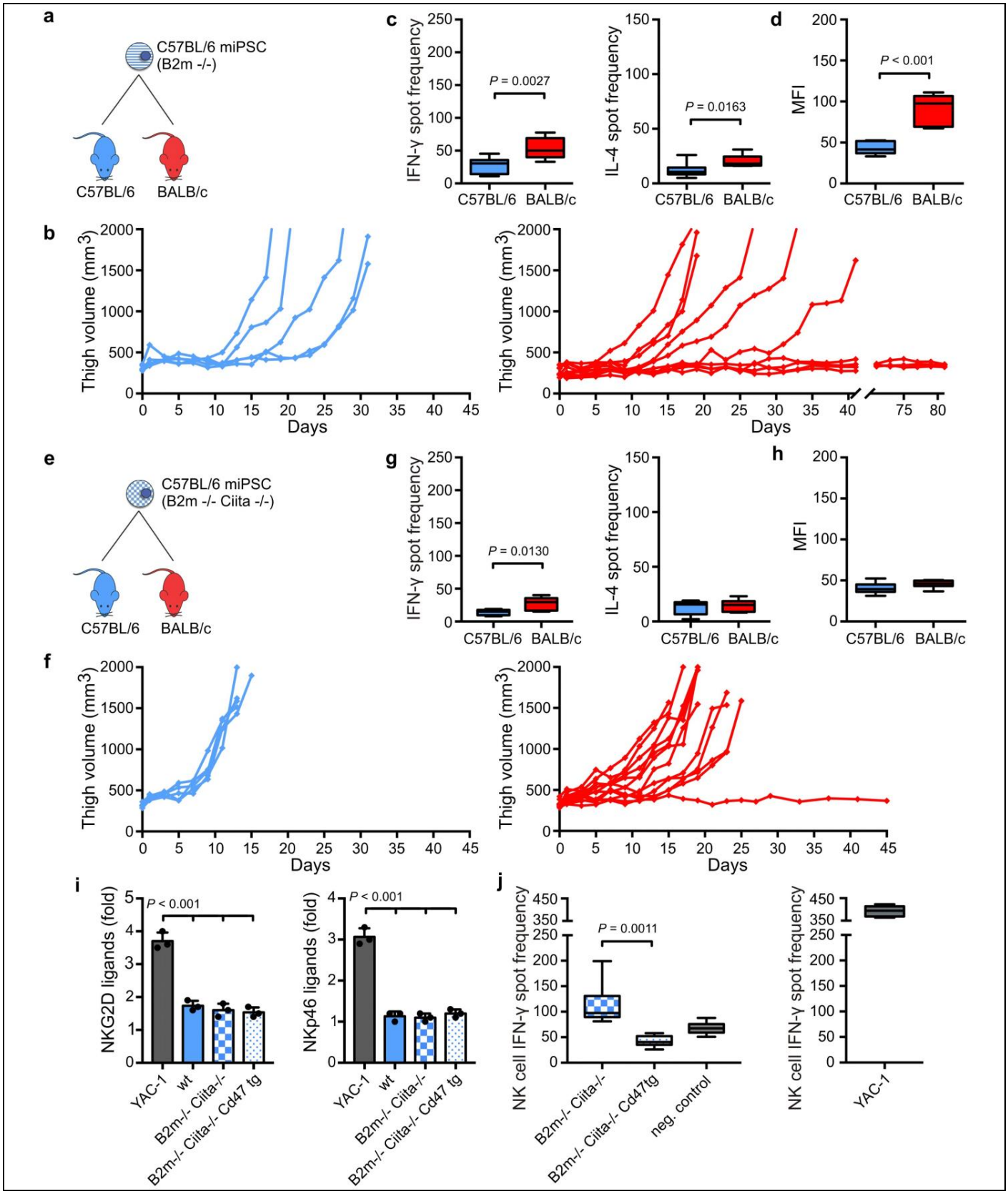
a
C57BL/6 miPSC
(B2m -/-)
C57BL/6
BALB/c
c
IFN-γ spot frequency
P = 0.0027
C57BL/6
BALB/c
IL-4 spot frequency
P = 0.0163
C57BL/6
BALB/c
d
MFI
P < 0.001
C57BL/6
BALB/c
b
Thigh volume (mm3)
Days
Thigh volume (mm3)
Days
e
C57BL/6 miPSC
(B2m -/- Ciita -/-)
C57BL/6
BALB/c
g
IFN-γ spot frequency
P = 0.0130
C57BL/6
BALB/c
IL-4 spot frequency
C57BL/6
BALB/c
h
MFI
C57BL/6
BALB/c
f
Thigh volume (mm3)
Days
Thigh volume (mm3)
Days
i
NKG2D ligands (fold)
P < 0.001
YAC-1
wt
B2m-/- Ciita-/-
B2m-/- Ciita-/- Cd47 tg
NKp46 ligands (fold)
P < 0.001
YAC-1
wt
B2m-/- Ciita-/-
B2m-/- Ciita-/- Cd47 tg
j
NK cell IFN-γ spot frequency
P = 0.0011
B2m-/- Ciita-/-
B2m-/- Ciita-/- Cd47tg
neg. control
NK cell IFN-γ spot frequency
YAC-1

Supplementary Figure 4

Survival of gene-engineered miPSCs.

a, C57BL/6 *B2m*$^{-/-}$ miPSCs were transplanted into either syngeneic C57BL/6 (blue) mice or allogeneic (red) BALB/c mice. **b,** The thigh volume of all five C57BL/6 and ten BALB/c animals is shown over time. The overall percentage of cell grafts that survived and formed teratomas in BALB/c was 60%. **c**, IFN-γ Elispots and IL-4 Elispots are shown with splenocytes recovered 5 days after the transplantation and *B2m*$^{-/-}$ miPSCs stimulator cells (box 25th to 75th percentile with median, whiskers min-max, 8 animals per group, two-tailed Student's t-test). **d**, Mean fluorescence (MFI) of IgM binding to *B2m*$^{-/-}$ miPSCs incubated with recipient serum after 5 days (box 25th to 75th percentile with median, whiskers min-max, 6 animals per group, two-tailed Student's t-test). **e**, C57BL/6 *B2m*$^{-/-}$*Ciita*$^{-/-}$ miPSCs were transplanted into syngeneic C57BL/6 or allogeneic BALB/c mice. **f**, The thigh volume of all 5 C57BL/6 and 12 BALB/c animals is shown over time. The overall percentage of cell grafts that survived and formed teratomas in BALB/c was 91.7%. **g**, IFN-γ Elispots and IL-4 Elispots are shown with splenocytes recovered 5 days after the transplantation and *B2m*$^{-/-}$*Ciita*$^{-/-}$ miPSCs stimulator cells (box 25th to 75th percentile with median, whiskers min-max, 6 animals per group, two-tailed Student's t-test). **h**, Mean fluorescence (MFI) of IgM binding to *B2m*$^{-/-}$*Ciita*$^{-/-}$ miPSCs incubated with recipient serum after 5 days (box 25th to 75th percentile with median, whiskers min-max, 6 animals per group, two-tailed Student's t-test). **i**, The expression of stimulatory NKG2D ligands and NKp46 ligands on miPSC lines and YAC-1 was assessed using receptor Fc chimera proteins in flow cytometry (mean ± s.d., 3 independent experiments per group, ANOVA with Bonferroni's post-hoc test). **j**, IFN-γ spot frequencies of miPSC lines and YAC-1 in Elispot assays with BALB/c NK cells (box 25th to 75th percentile with median, whiskers min-max, 6 independent experiments, ANOVA with Bonferroni's post-hoc test).

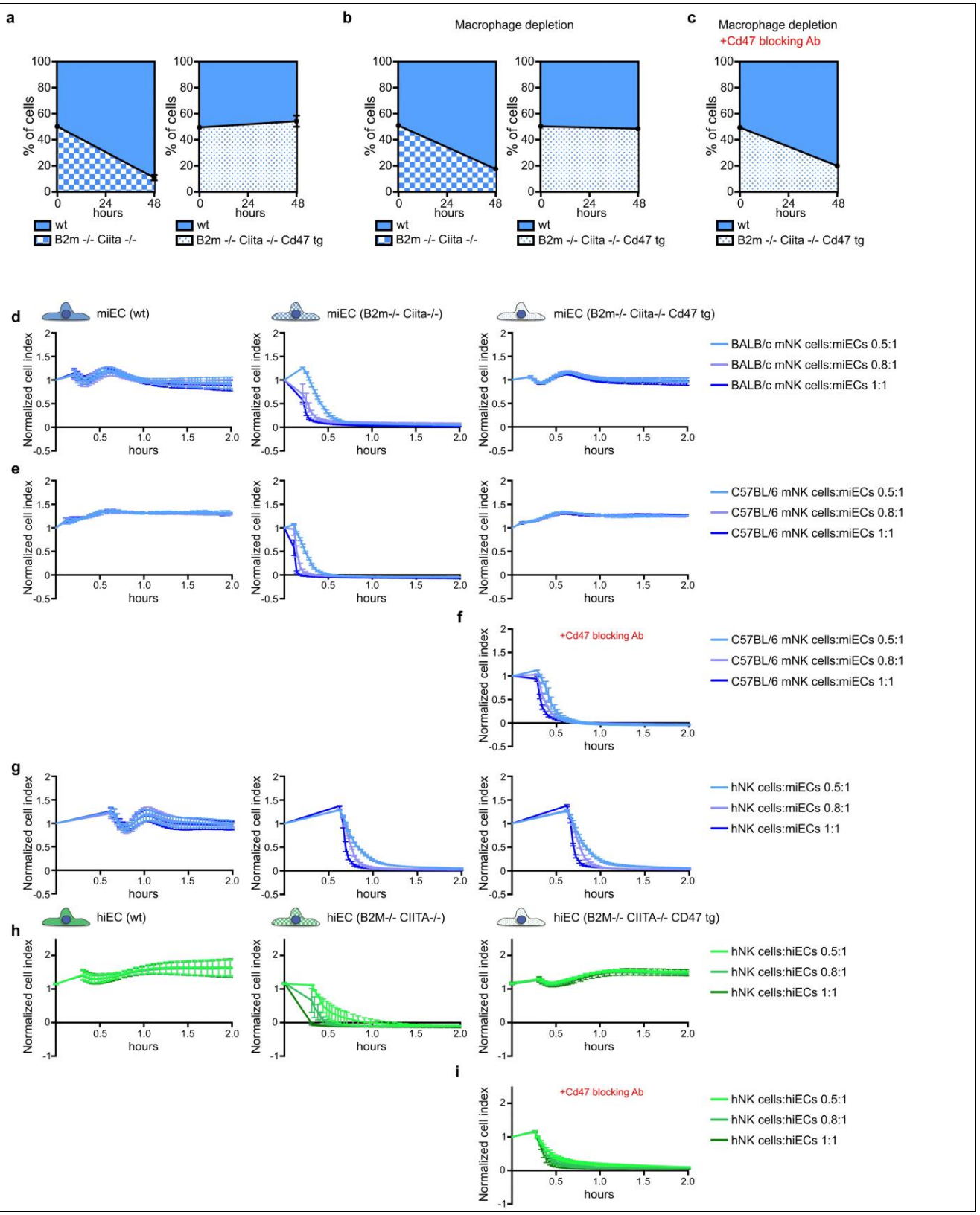
a
b
c
Macrophage depletion
Macrophage depletion
+Cd47 blocking Ab
% of cells
hours
wt
B2m -/- Ciita -/-
B2m -/- Ciita -/- Cd47 tg
d
miEC (wt)
miEC (B2m-/- Ciita-/-)
miEC (B2m-/- Ciita-/- Cd47 tg)
Normalized cell index
BALB/c mNK cells:miECs 0.5:1
BALB/c mNK cells:miECs 0.8:1
BALB/c mNK cells:miECs 1:1
e
C57BL/6 mNK cells:miECs 0.5:1
C57BL/6 mNK cells:miECs 0.8:1
C57BL/6 mNK cells:miECs 1:1
f
+Cd47 blocking Ab
g
hNK cells:miECs 0.5:1
hNK cells:miECs 0.8:1
hNK cells:miECs 1:1
h
hiEC (wt)
hiEC (B2M-/- CIITA-/-)
hiEC (B2M-/- CIITA-/- CD47 tg)
i

Supplementary Figure 5

Interaction between CD47 and NK cells.

a, *In vivo* innate immune clearance was assessed by injecting a 1 : 1 mixture of CFSE-labeled wt miPSCs and either *B2m*$^{-/-}$*Ciita*$^{-/-}$ or *B2m*$^{-/-}$*Ciita*$^{-/-}$ Cd47 tg miPSCs into the peritoneum of syngeneic C57BL/6 mice. After 48 h, CSFE-labeled peritoneal miPSCs were recovered and the percentages of both fractions assessed by flow cytometry (mean ± s.d., 4 animals per group). While *B2m*$^{-/-}$*Ciita*$^{-/-}$ miPSCs were rapidly cleared, *B2m*$^{-/-}$*Ciita*$^{-/-}$ Cd47 tg miPSCs were spared. **b**, Mice were pre-treated with clodronate to deplete macrophages, making this model more specific to NK cell killing and again only *B2m*$^{-/-}$*Ciita*$^{-/-}$ Cd47 tg miPSCs were spared from NK cell killing (mean ± s.d., 4 animals per group). **c**, When a Cd47 blocking antibody was co-injected into the peritoneum, the protection was abolished and *B2m*$^{-/-}$*Ciita*$^{-/-}$ Cd47 tg miPSCs were killed (mean ± s.d., 4 animals per group). **d**, *In vitro* real-time NK cell killing was assessed on confluent wt, *B2m*$^{-/-}$*Ciita*$^{-/-}$, and *B2m*$^{-/-}$*Ciita*$^{-/-}$ Cd47 tg miECs in three different effector : target cell ratios. Using allogeneic BALB/c mouse NK (mNK) cells, *B2m*$^{-/-}$*Ciita*$^{-/-}$ miECs were rapidly killed, and wt and *B2m*$^{-/-}$*Ciita*$^{-/-}$ Cd47 tg miECs permanently survived (mean ± s.d., 3 independent experiments per group). **e**, Similarly, using syngeneic C57BL/6 mNK cells, *B2m*$^{-/-}$*Ciita*$^{-/-}$ miECs were rapidly killed, and wt and *B2m*$^{-/-}$*Ciita*$^{-/-}$ Cd47 tg miECs permanently survived (mean ± s.d., 3 independent experiments per group). **f**, When a Cd47 blocking antibody was added to syngeneic C57BL/6 mNK cells, *B2m*$^{-/-}$*Ciita*$^{-/-}$ Cd47 tg miECs were swiftly killed (mean ± s.d., 3 independent experiments per group). **g**, When human NK (hNK) cells were used, both *B2m*$^{-/-}$*Ciita*$^{-/-}$ and *B2m*$^{-/-}$*Ciita*$^{-/-}$ Cd47 tg miECs were rapidly killed (mean ± s.d., 3 independent experiments per group). **h**, When hNK cells were used with human wt, *B2M*$^{-/-}$*CIITA*$^{-/-}$, and *B2M*$^{-/-}$*CIITA*$^{-/-}$ CD47 tg hiECs, only *B2M*$^{-/-}$*CIITA*$^{-/-}$ hiECs were rapidly killed and wt and *B2M*$^{-/-}$*CIITA*$^{-/-}$ CD47 tg hiECs were spared (mean ± s.d., 3 independent experiments per group). **i**, With a CD47 blocking antibody, *B2M*$^{-/-}$*CIITA*$^{-/-}$ CD47 tg hiECs were then swiftly killed (mean ± s.d., 3 independent experiments per group).

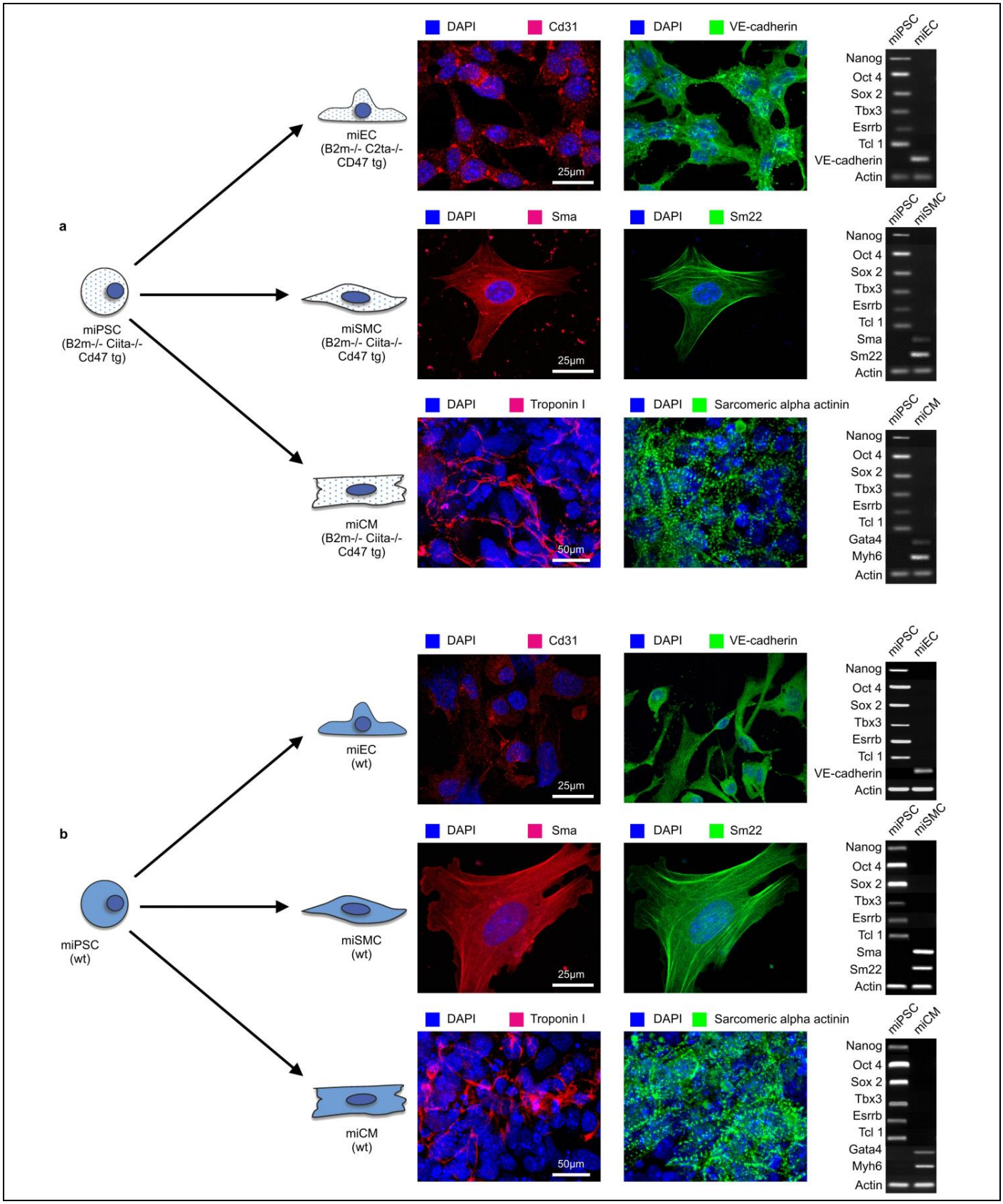
a
miPSC
(B2m-/- Ciita-/-
Cd47 tg)
miEC
(B2m-/- C2ta-/-
CD47 tg)
miSMC
(B2m-/- Ciita-/-
Cd47 tg)
miCM
(B2m-/- Ciita-/-
Cd47 tg)
DAPI
Cd31
VE-cadherin
Sma
Sm22
Troponin I
Sarcomeric alpha actinin
25µm
50µm
miPSC
miEC
miSMC
miCM
Nanog
Oct 4
Sox 2
Tbx3
Esrrb
Tcl 1
VE-cadherin
Sma
Sm22
Gata4
Myh6
Actin
b
miPSC
(wt)
miEC
(wt)
miSMC
(wt)
miCM
(wt)

Supplementary Figure 6

Differentiation of miPSCs into miECs, miSMCs and miCMs.

a-b, *B2m*$^{-/-}$*Ciita*$^{-/-}$ Cd47 tg miPSCs (a) and wt miPSCs (b) were successfully differentiated into corresponding miEC, miSMC, and miCM derivatives (representative pictures of three independent experiments). miECs were positive for Cd31 and VE-cadherin, miSMCs were positive for Sma and Sm22, miCMs were positive for Troponin I and Sarcomeric alpha-actinin by confocal immunofluorescence. All derivatives lost their expression of pluripotency genes (representative pictures of two independent PCR experiments).

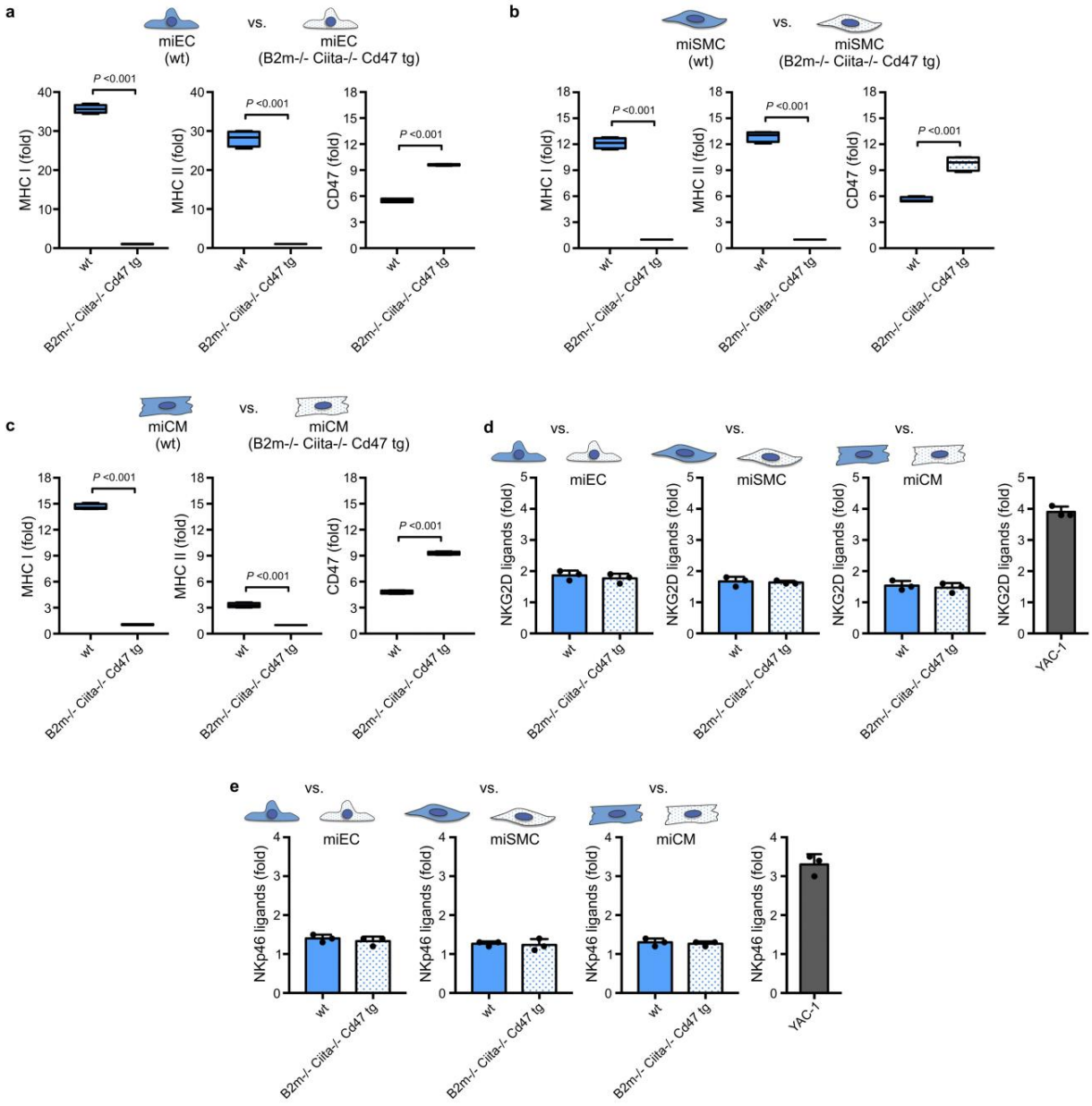

Supplementary Figure 7

Immune phenotype of wt and engineered miPSC derivatives.

a, wt miECs showed high MHC class I and MHC class II expression, while *B2m*$^{-/-}$*Ciita*$^{-/-}$ Cd47 tg miECs were MHC class I and MHC class II depleted and showed increased Cd47 expression (box 25th to 75th percentile with median, whiskers min-max, 4 independent experiments per graph, two-tailed Student's t-test). **b**, wt miSMCs showed moderate MHC class I and MHC class II expression, while *B2m*$^{-/-}$*Ciita*$^{-/-}$ Cd47 tg miSMCs were MHC class I and MHC class II depleted and showed increased Cd47 expression (box 25th to 75th percentile with median, whiskers min-max, 4 independent experiments per graph, two-tailed Student's t-test). **c**, wt miCMs showed moderate MHC class I and low MHC class II expression; *B2m*$^{-/-}$*Ciita*$^{-/-}$ Cd47 tg miCMs were MHC class I and MHC class II depleted and showed increased Cd47 expression (box 25th to 75th percentile with median, whiskers min-max, 4 independent experiments per graph, two-tailed Student's t-test). **d-e**, The expression of stimulatory NKG2D ligands (d) and NKp46 ligands (e) on wt and *B2m*$^{-/-}$*Ciita*$^{-/-}$ Cd47 tg miECs, miSMCs, miCMs, and YAC-1 was assessed using receptor Fc chimera proteins in flow cytometry (mean ± s.d., 3 independent experiments per group, two-tailed Student's t-test).

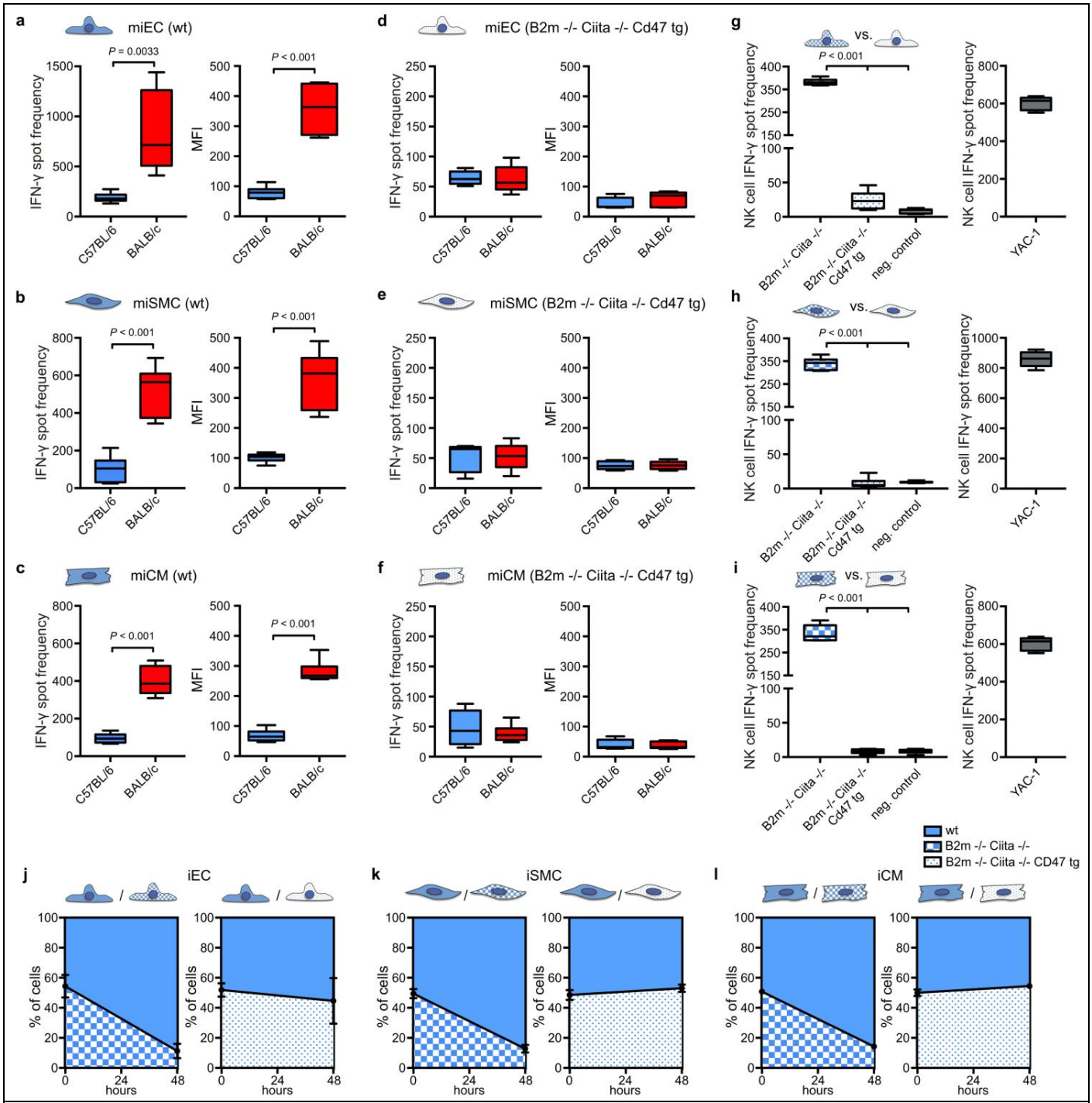

Supplementary Figure 8

Immune response against miPSC derivatives.

a-c, Five days after the injection of wt miPSC-derived miECs (a), miSMCs (b), or miCMs (c) into C57BL/6 or BALB/c recipients, splenocytes were recovered for IFN-γ Elispot assays (box 25th to 75th percentile with median, whiskers min-max, 6 animals per group, two-tailed Student's t-test). The IFN-γ response was vastly stronger in all allogeneic recipients. Mean fluorescence (MFI) of IgM binding to wt miPSC-derived miECs (a), miSMCs (b), and miCMs (c), incubated with recipient serum after 5 days (box 25th to 75th percentile

with median, whiskers min-max, 6 animals per group, two-tailed Student's t-test). There was a markedly stronger IgM response in all allogeneic recipients. **d-f**, Similarly, *B2m*$^{-/-}$*Ciita*$^{-/-}$ Cd47 tg miPSC-derived miECs (d), miSMCs (e), or miCMs (f) were injected into C57BL/6 or BALB/c recipients and IFN-γ Elispots were performed after 5 days (box 25th to 75th percentile with median, whiskers min-max, 6 animals per group, two-tailed Student's t-test). Mean fluorescence (MFI) of IgM binding to *B2m*$^{-/-}$*Ciita*$^{-/-}$ Cd47 tg miPSC-derived miECs (d), miSMCs (e), and miCMs (f), incubated with recipient serum after 5 days (box 25th to 75th percentile with median, whiskers min-max, 6 animals per group, two-tailed Student's t-test). There was no measurable IFN-γ response or IgM response in allogeneic recipients. **g-i**, To assess the inhibitory effect of Cd47 over-expression on NK cell killing, IFN-γ Elispots with NK cells were performed with miECs (g), miSMCs (h), or miCMs (i) derived from *B2m*$^{-/-}$*Ciita*$^{-/-}$ miPSC or *B2m*$^{-/-}$*Ciita*$^{-/-}$ Cd47 tg miPSC (box 25th to 75th percentile with median, whiskers min-max, 6 independent experiments, ANOVA with Bonferroni's post-hoc test) Only derivatives from *B2m*$^{-/-}$*Ciita*$^{-/-}$ miPSC were susceptible for NK cell killing. **j-l**, *In vivo* innate immune clearance was assessed by injecting a 1 : 1 mixture of wt derivative engineered derivative into the peritoneum of C57BL/6 mice. After 48 h, peritoneal miECs (j), miSMCs (k), and miCMs (l) were recovered and the percentage assessed by flow cytometry (mean ± s.d., 4 animals per group).

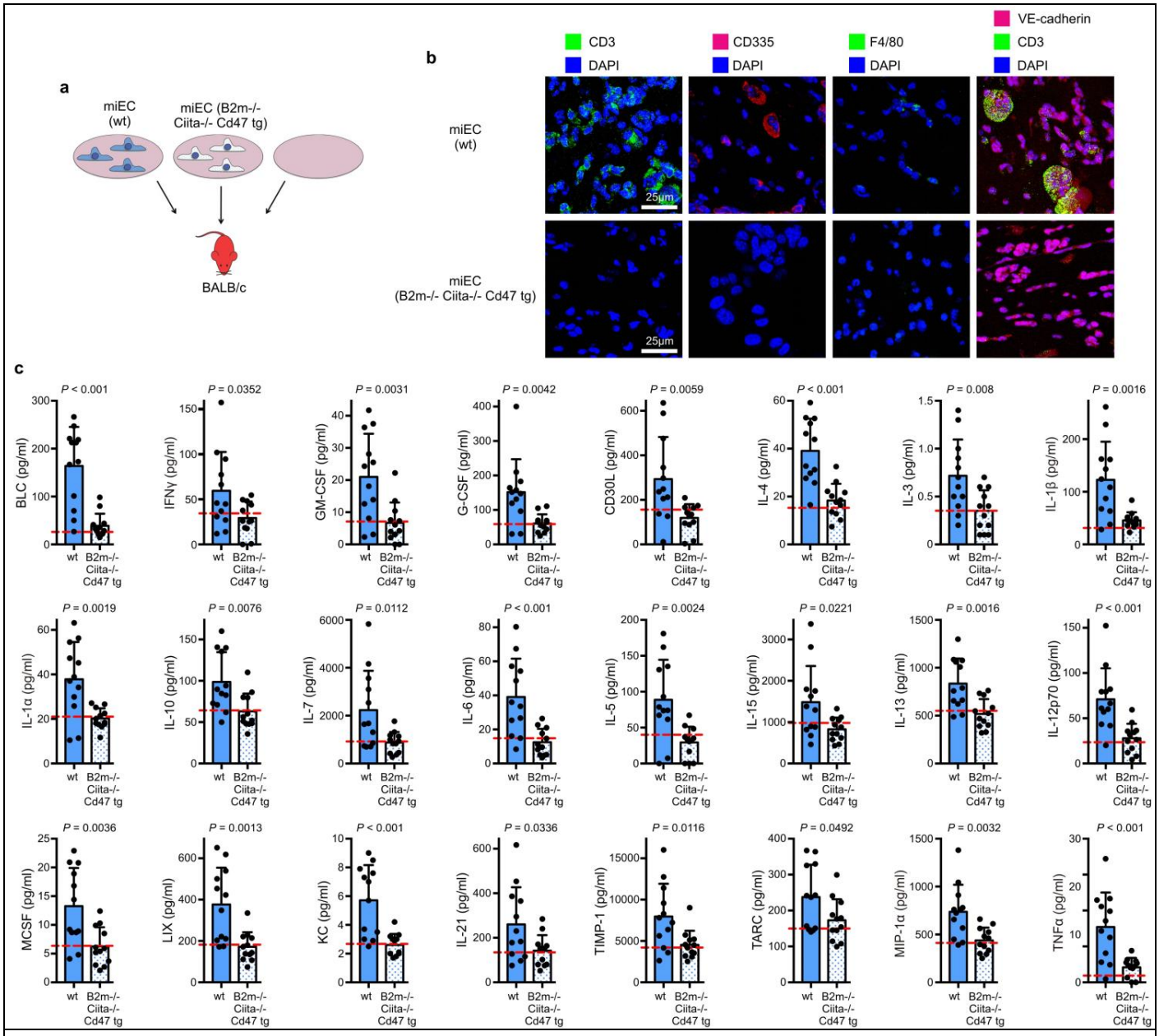

Supplementary Figure 9

Immune cell infiltration and cytokine expression in miEC grafts.

a, Matrigel plugs containing either wt miECs or *B2m*$^{-/-}$*Ciita*$^{-/-}$ Cd47 tg miECs were implanted in allogeneic BALB/c recipients. Cell-free matrigel plugs served as controls. **b**, Immunofluorescence stainings detected immune cell infiltration in wt iEC-plaques containing CD3^{+} T lymphocytes, CD335^{+} NK cells, and sparse F4/80^{+} macrophages. Co-staining of CD3 and VE-cadherin confirmed CD3^{+} lymphocyte infiltration in EC grafts in the wt group. Practically no immune cells were found in plugs containing *B2m*$^{-/-}$*Ciita*$^{-/-}$ Cd47 tg miECs (representative pictures of three independent experiments). **c**, The cytokine profile in wt miEC plugs was shifted towards a pro-inflammatory milieu. Multiple significantly up-regulated cytokines were typical of activated cytotoxic CD8^{+} T cells, CD4^{+} T helper-1 cells, and CD4^{+} T helper-2 cells, as well as macrophages (mean ± s.d., 12 animals per group, two-tailed Student's t-test; dashed red lines show levels of cell-free matrigel).

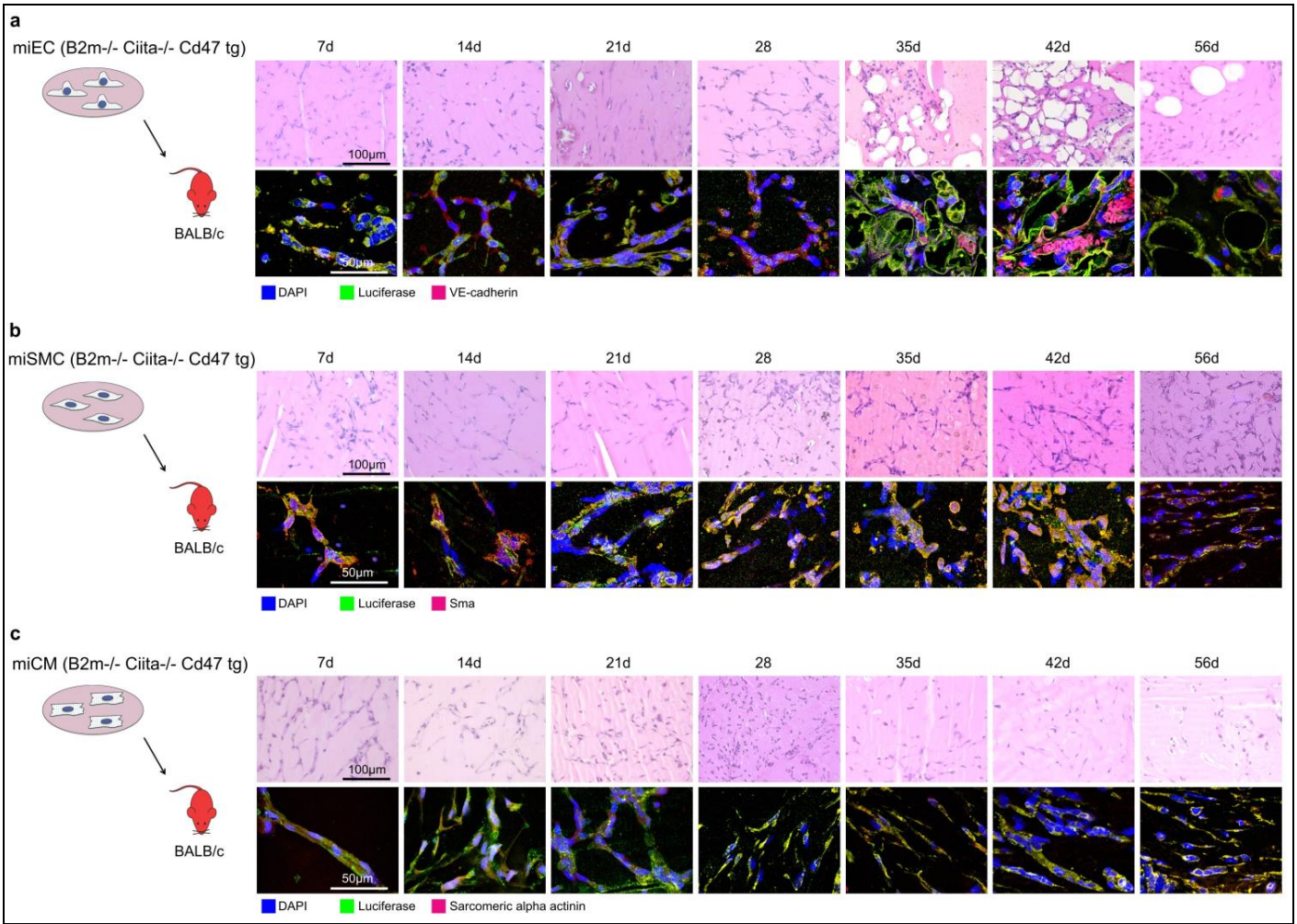

Supplementary Figure 10

Morphology of transplanted *B2m*$^{-/-}$*Ciita*$^{-/-}$ Cd47 tg miPSC derivatives in allogeneic hosts.

a-c, *B2m*$^{-/-}$*Ciita*$^{-/-}$ Cd47 tg miEC (a), miSMC (b), or miCM (c) grafts in matrigel were transplanted subcutaneously into allogeneic BALB/c mice to investigate whether these hypo-immunogenic derivatives further mature *in vivo* or change their morphology over time in allogeneic recipients. Matrigel plugs were recovered after different time points for hematoxylin and eosin and immunofluorescence stainings (representative pictures of two independent experiments). Transplanted miECs started to organize in circular structures around day 14 and formed primitive vessels that contained erythrocytes around day 35 (a). Transplanted miSMCs (b) maintained their typical spindle-shape appearance and loose arrangement, whereas miCMs retained their immature round progenitor morphology (c). Both latter cell types did not show a higher degree of three-dimensional organization, which may be attributed to the lack of mechanical stimulus necessary for maturation of any type of muscle cell.

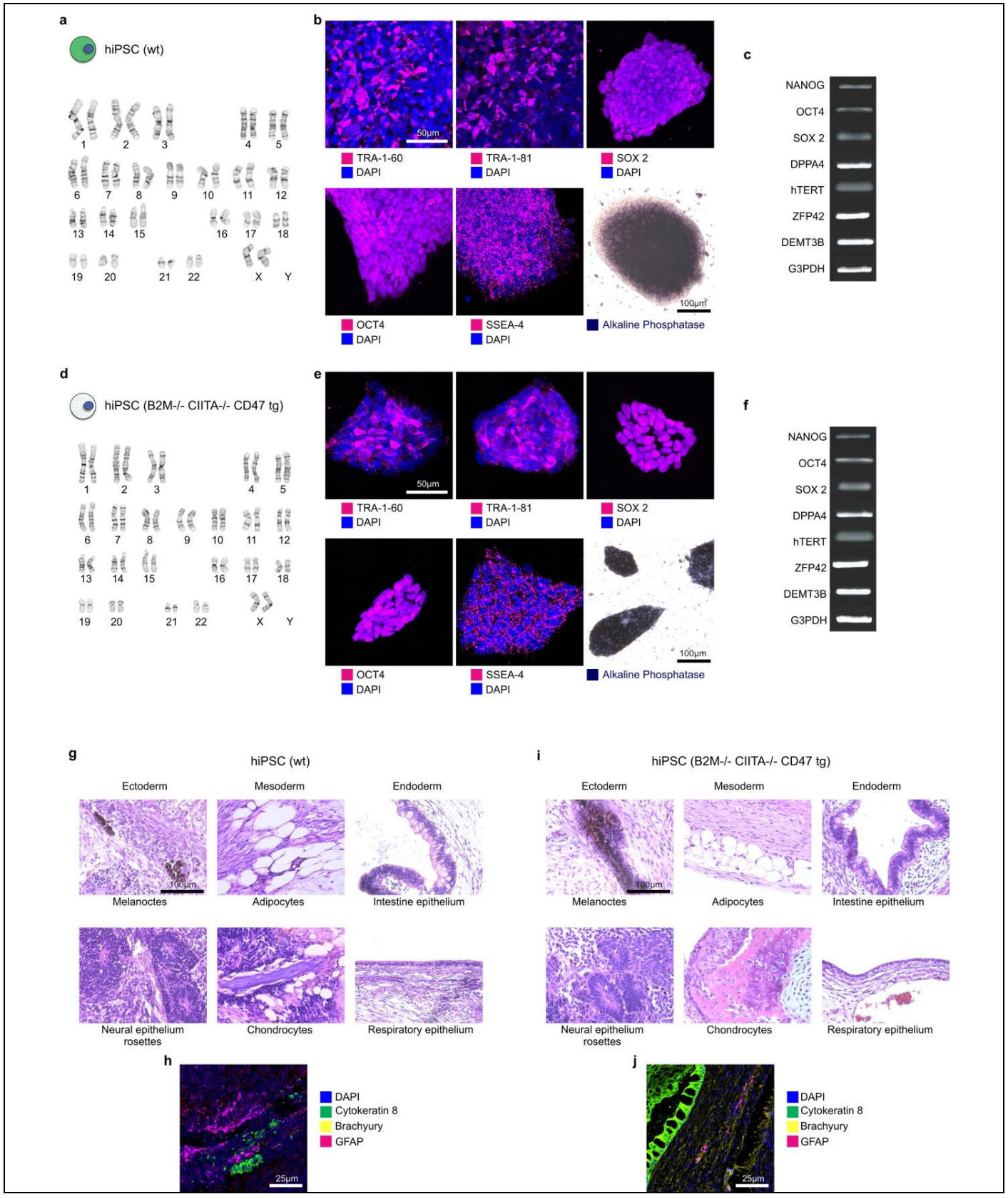
a
hiPSC (wt)
1 2 3 4 5
6 7 8 9 10 11 12
13 14 15 16 17 18
19 20 21 22 X Y
b
50µm
TRA-1-60
DAPI
TRA-1-81
DAPI
SOX 2
DAPI
OCT4
DAPI
SSEA-4
DAPI
100µm
Alkaline Phosphatase
c
NANOG
OCT4
SOX 2
DPPA4
hTERT
ZFP42
DEMT3B
G3PDH
d
hiPSC (B2M-/- CIITA-/- CD47 tg)
1 2 3 4 5
6 7 8 9 10 11 12
13 14 15 16 17 18
19 20 21 22 X Y
e
50µm
TRA-1-60
DAPI
TRA-1-81
DAPI
SOX 2
DAPI
OCT4
DAPI
SSEA-4
DAPI
100µm
Alkaline Phosphatase
f
NANOG
OCT4
SOX 2
DPPA4
hTERT
ZFP42
DEMT3B
G3PDH
g
hiPSC (wt)
Ectoderm
Mesoderm
Endoderm
100µm
Melanoctes
Adipocytes
Intestine epithelium
Neural epithelium rosettes
Chondrocytes
Respiratory epithelium
i
hiPSC (B2M-/- CIITA-/- CD47 tg)
Ectoderm
Mesoderm
Endoderm
100µm
Melanoctes
Adipocytes
Intestine epithelium
Neural epithelium rosettes
Chondrocytes
Respiratory epithelium
h
25µm
DAPI
Cytokeratin 8
Brachyury
GFAP
j
25µm
DAPI
Cytokeratin 8
Brachyury
GFAP

Supplementary Figure 11

Pluripotency of wt and *B2M*$^{-/-}$*CIITA*$^{-/-}$ CD47 tg hiPSCs.

a, wt hiPSCs showed a normal human 46, XX karyotype in one analysis. **b**, wt hiPSCs were positive for TRA-1-60, TRA-1-81, SOX 2, OCT4, and SSEA-4 in confocal immunofluorescence and positive for alkaline phosphatase in immunohistochemistry (representative pictures of three independent experiments). **c**, wt hiPSCs expressed typical pluripotency genes (representative gel of two independent PCR experiments). **d**, *B2M*$^{-/-}$*CIITA*$^{-/-}$ *CD47* tg hiPSCs maintained the normal human 46, XX karyotype in one analysis. **e**, *B2M*$^{-/-}$*CIITA*$^{-/-}$ *CD47* tg hiPSCs were also positive for TRA-1-60, TRA-1-81, SOX 2, OCT4, and SSEA-4 in confocal immunofluorescence and positive for alkaline phosphatase in immunohistochemistry (representative pictures of three independent experiments). **f**, *B2M*$^{-/-}$*CIITA*$^{-/-}$ *CD47* tg hiPSCs continued to express the typical pluripotency genes (representative gel of two independent PCR experiments). **g-j**, wt hiPSCs (g, h) and B2M-/- CIITA-/- CD47 tg hiPSCs (i, j) gave rise to cell types of all 3 germ layers after transplantation into SCID-beige mice. Endodermal (cytokeratin 8), mesodermal (brachyury), and ectodermal lineages (GFAP) were also demonstrated by confocal immunofluorescence microscopy (representative pictures of three independent experiments).

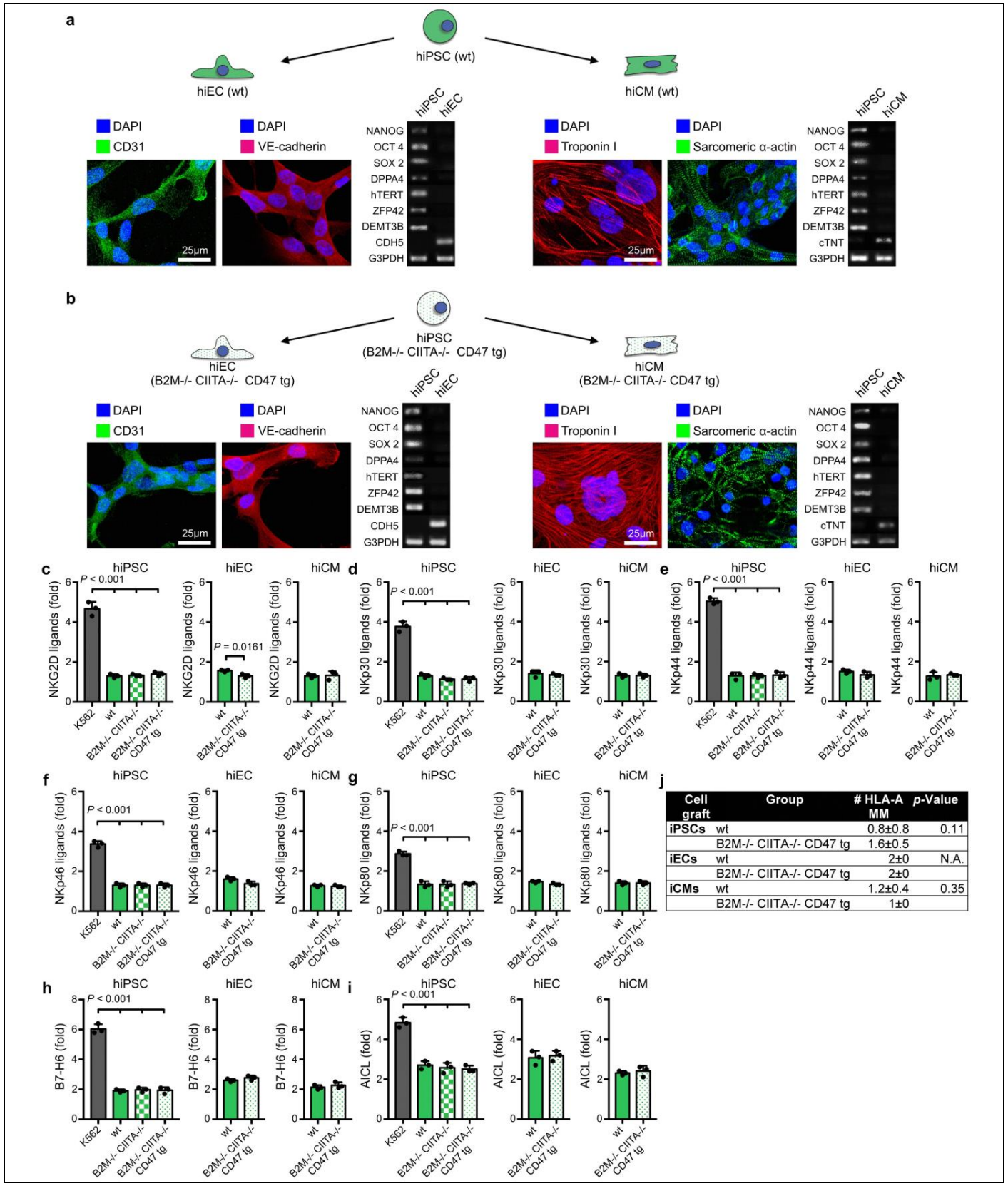

j

Cell graft	Group	# HLA-A MM	*p*-Value
iPSCs	wt	0.8±0.8	0.11
	B2M-/- CIITA-/- CD47 tg	1.6±0.5	
iECs	wt	2±0	N.A.
	B2M-/- CIITA-/- CD47 tg	2±0	
iCMs	wt	1.2±0.4	0.35
	B2M-/- CIITA-/- CD47 tg	1±0	

Supplementary Figure 12

Differentiation of hiPSCs into hiECs and hiCMs.

a-b, wt hiPSCs (a) and *B2M*$^{-/-}$*CIITA*$^{-/-}$ *CD47* tg hiPSCs (b) were successfully differentiated into corresponding miEC and miCM derivatives (representative pictures of three independent experiments). miECs were positive for CD31 and VE-cadherin and miCMs were positive for Troponin I and Sarcomeric alpha-actinin by confocal immunofluorescence. All derivatives lost their expression of pluripotency genes (representative pictures of two independent experiments). **c-g**, The expression of stimulatory NK cell ligands was assessed on hiPSCs and their derivatives using receptor Fc chimera proteins in flow cytometry (mean ± s.d., 3 independent experiments per group, ANOVA with Bonferroni's post-hoc test (hiPSCs) or two-tailed Student's t-test (hiECs and hiCMs)). Ligands for NKG2D (c), NKp30 (d), NKp44 (e), NKp46 (f), and NKp80 (g) were compared between wt and engineered hiPSCs, hiECs, hiCMs, and K562. **h-i**, The expression of specific human natural cytotoxicity receptor ligands was evaluated by flow cytometry (mean ± s.d., 3 independent experiments per group, ANOVA with Bonferroni's post-hoc test (hiPSCs) or two-tailed Student's t-test (hiECs and hiCMs)). Surface expression of B7-H6 (h), and AICL (i) was compared between wt and engineered hiPSCs and derivatives, and K562. **j**, The HLA-A mismatches in transplant experiments with wt and *B2M*$^{-/-}$*CIITA*$^{-/-}$ *CD47* tg hiPSCs, hiECs, and hiCMs in allogeneic humanized NSG-HGM3 recipients (mean ± s.d., 5 animals per group, two-tailed Student's t-test).

a

Assay	Cell graft	Group	CD3% of hCD45	*p*-Value
Elispot	iPSCs	wt	38±35	0.31
		B2M-/- CIITA-/- CD47 tg	57±31	
	iECs	wt	22±13	0.22
		B2M-/- CIITA-/- CD47 tg	63±48	
	iCMs	wt	25±22	0.96
		B2M-/- CIITA-/- CD47 tg	26±29	
BLI	iPSCs	wt	17±10	0.19
		B2M-/- CIITA-/- CD47 tg	38±32	
	iECs	wt	52±28	0.25
		B2M-/- CIITA-/- CD47 tg	34±18	
	iCMs	wt	18±12	0.56
		B2M-/- CIITA-/- CD47 tg	15±3	

b

Experiments with NSG-SGM3 mice				
Assay	Group	Recipient HLA-A		# HLA-A MM to cell graft
Elispot iPSCs	wt	A*03:01	A*68:01	2
	wt	A*03:01	A*68:01	2
	wt	A*24:02	A*32:01	2
	wt	A*24:02	A*32:01	2
	wt	A*01:01	A*32:01	1
	wt	A*01:01	A*32:01	1
	wt	A*01:01	A*32:01	1
	B2M-/- CIITA-/- CD47 tg	A*03:01	A*68:01	2
	B2M-/- CIITA-/- CD47 tg	A*02:01	A*29:02	2
	B2M-/- CIITA-/- CD47 tg	A*24:02	A*32:01	2
	B2M-/- CIITA-/- CD47 tg	A*24:02	A*32:01	2
	B2M-/- CIITA-/- CD47 tg	A*01:01	A*30:02	1
	B2M-/- CIITA-/- CD47 tg	A*01:01	A*30:02	1
	B2M-/- CIITA-/- CD47 tg	A*32:01	A*66:01	2
Elispot CMs	wt	A*24:02	A*32:01	2
	wt	A*01:01	A*32:01	1
	wt	A*01:01	A*32:01	1
	B2M-/- CIITA-/- CD47 tg	A*24:02	A*32:01	2
	B2M-/- CIITA-/- CD47 tg	A*01:01	A*32:01	1
	B2M-/- CIITA-/- CD47 tg	A*01:01	A*32:01	1
Elispot Ecs	wt	A*24:02	A*25:01	2
	wt	A*24:02	A*25:01	2
	wt	A*24:02	A*25:01	2
	B2M-/- CIITA-/- CD47 tg	A*24:02	A*25:01	2
	B2M-/- CIITA-/- CD47 tg	A*03:01	A*68:01	2
	B2M-/- CIITA-/- CD47 tg	A*11:01	A*23:01	2
BLI_iPSC	wt	A*01:01	A*02:01	0
	wt	A*01:01	A*02:01	0
	wt	A*02:01	A*24:02	1
	wt	A*02:01	A*24:02	1
	wt	A*30:01	A*30:02	2
	B2M-/- CIITA-/- CD47 tg	A*24:02	A*32:01	2
	B2M-/- CIITA-/- CD47 tg	A*01:01	A*32:01	1
	B2M-/- CIITA-/- CD47 tg	A*01:01	A*32:01	1
	B2M-/- CIITA-/- CD47 tg	A*11:01	A*25:01	2
	B2M-/- CIITA-/- CD47 tg	A*11:01	A*25:01	2
BLI_EC	wt	A*11:01	A*25:01	2
	wt	A*11:01	A*25:01	2
	wt	A*11:01	A*25:01	2
	wt	A*11:01	A*25:01	2
	wt	A*11:01	A*25:01	2
	B2M-/- CIITA-/- CD47 tg	A*11:01	A*25:01	2
	B2M-/- CIITA-/- CD47 tg	A*11:01	A*25:01	2
	B2M-/- CIITA-/- CD47 tg	A*11:01	A*25:01	2
	B2M-/- CIITA-/- CD47 tg	A*11:01	A*25:01	2
	B2M-/- CIITA-/- CD47 tg	A*11:01	A*25:01	2
BLI_CM	wt	A*24:02	A*32:01	2
	wt	A*01:01	A*32:01	1
	wt	A*01:01	A*03:01	1
	wt	A*01:01	A*03:01	1
	wt	A*01:01	A*03:01	1
	B2M-/- CIITA-/- CD47 tg	A*01:01	A*03:01	1
	B2M-/- CIITA-/- CD47 tg	A*01:01	A*03:01	1
	B2M-/- CIITA-/- CD47 tg	A*01:01	A*03:01	1
	B2M-/- CIITA-/- CD47 tg	A*01:01	A*03:01	1
	B2M-/- CIITA-/- CD47 tg	A*01:01	A*03:01	1

c

Assay	Cell graft	Group	CD3% of hCD45	*p*-Value
Elispot	iECs	wt	48±18	0.70
		B2M-/- CIITA-/- CD47 tg	53±16	
BLI	iECs	wt	57±9	0.95
		B2M-/- CIITA-/- CD47 tg	58±8	

Supplementary Figure 13

CD3 reconstitution and HLA matching in humanized mice.

a, Percentage of $CD3^+$ cells among the reconstituted human $CD45^+$ cell population in NSG-SGM3 mice receiving hiPSC grafts (n=7 per group), hiEC grafts (n=3 per group), or hiCM grafts (n=3 per group) in the Elispot groups or hiPSC grafts, hiEC grafts, or hiCM grafts (n=5 per group) in the BLI groups (mean ± s.d., two-tailed Student's t-test). **b**, All NSG-SGM3 mice were typed for HLA-A and the number of HLA-A mismatches (MM) was calculated for every single animal used in this study. 2 MM are coded in red, 1 MM in orange, and zero MM in green. **c**, Percentage of $CD3^+$ cells among the reconstituted human $CD45^+$ cell population in BLT mice receiving iEC grafts in the Elispot groups (n=4 per group) or BLI groups (n=5) (mean ± s.d., two-tailed Student's t-test).